Synthetic membrane performance modification by selective species adsorption

Argyle, Iain

Award date:
2015

Awarding institution:
University of Bath

Synthetic membrane performance modification by selective species adsorption

Iain S. Argyle

A thesis submitted for the degree of Doctor of Philosophy

University of Bath

Department of Chemical Engineering

June 2015

I. Declaration of Authorship

This is all my own work except where I have indicated via references or other forms of acknowledgement.

Signature:

Date:

II. Acknowledgements

My profound gratitude goes to Dr. Mike Bird, who was firstly my undergraduate lecturer, and then Ph.D supervisor. He has provided me with the necessary expertise, tools and resources to complete this work. The time he has spent with me in meetings, both scheduled and impromptu, has been tremendously generous. Above all he has questioned my work and provided insight into my findings. For all of this I am eternally grateful.

Gratitude is also extended to the community of students, researchers, academics, technical and support staff in the department at Bath, as well as neighbouring departments and other universities in which I have worked.

Additional thanks go to:

Dr. Arto Pihlajamäki of Lappeenranta University of Technology, Lappeenranta, Finland for allowing me to carry out zeta potential measurements and provide insight into the results obtained.

Dr. Chris Wright and Dr. Lydia Powell of Swansea University for allowing me access to the tools at the College of Engineering and Centre for NanoHealth in which atomic force microscopy was performed.

Dr. Frank Lipnizki of Alfa Laval, Copenhagen for kindly providing all membranes used in this work.

Dr. Tim Bond, Dr. Huafu Wang, and Mr. Wycliff Odoyo of James Finlay Ltd, London for providing spray-dried black tea powder and analytical equipment, and bringing invaluable commercial relevance to the project.

The EPSRC for providing the funding for the DTA studentship which funded this work.

III. Abstract

The efficiency of membrane processes in the food industry is largely reliant on minimising fouling, optimising hydrodynamic conditions, improving cleaning, or developing specialised membranes for a given purpose. A different strategy is to make an intuitive physical or chemical modification to readily available membranes.

Presented here are experimental findings relating to the modification of commercial polysulfone (PS) membranes of varying nominal molecular weight cut-off (nMWCO) by primary alcohols using both a static and dynamic treatment methodology. Furthermore, an assessment of their performance is made by analysis of ultrafiltration (UF) experiments of model solutions, as well as an industrially relevant food stuff - black tea, for the purpose of haze removal. Previous research into black tea filtration showed that it's fouling and rejection could be influenced strongly by membrane material and surface chemical aspects. This led to the hypothesis that modifying membranes with alcohols would aid in improving aspects of black tea UF.

Modification of 25, 50, and 100 kDa membranes by primary alcohols (with the majority of focus on ethanol treatment) was found to dramatically increase membrane water flux after both 90 minutes of continuous alcohol permeation and 24 hours of treatment in a static environment. The effects on surface characteristics were equally as pronounced. Hydrophobicity of membranes was increased, and control membrane negative ζ potential was neutralised, indicating that selectivity and fouling propensity would be altered. Further characterisation of the membranes revealed that there was an enhancement in glycerol preservative removal from the membranes, and that pore forming agents used in membrane casting were being leached out. Additionally, macroscopic swelling caused expansion of the porous matrix as confirmed by dimensional and porosimetric measurements, a relaxation of the membrane active layer, and an elastic modulus decrease of active layer as measured by atomic force microscopy (AFM).

For model protein dead-end filtration, the process duration for de-watering of a fixed amount of bovine serum albumin (BSA) solution was reduced, proving that flux uplifts were translated to the filtration environment. No differences in rejection of both β-lactoglobulin and BSA were observed. Sorption of protein was shown to be greater as deduced from adsorptive fouling measurements, which prompted an investigation into specific membrane-foulant interactions. AFM performed with a BSA-functionalised colloidal probe indicated that adherence of protein to treated membranes was indeed increased. This was caused by both a decrease in charge, which promoted deposition, and an increase in hydrophobicity, giving rise to additional hydrophobic interactions probably with the secondary protein structure.

During filtration of black tea, flux improvements for treated membranes were observed over untreated membranes in the pressure controlled region of the generalised transmembrane pressure–flux relationship. Typically the rejection of solids and polyphenols for UF membranes was disproportional; the membrane in effect, stripping

some polyphenols from the tea. In addition, solids transmission increased, though less so than the transmission of polyphenols. The disproportional increase in polyphenols transmission was attributed to the reduced surface charge of the membranes; the polyphenolic anions experiencing less repulsion from the membrane surface. This was reinforced by colour measurements which showed increased redness (an indicator of higher key polyphenols concentrations in tea).

These findings were then applied under a constant dilution diafiltration regime to demonstrate the mitigation of polyphenols loss in a process simulation setting. It was found that ethanol treatment could improve yield of tea solids or use of untreated membranes gave way to stream fractionation. Also discussed is the potential treatment of waste streams based on the accumulation of polyphenols in the retentate side of the membrane process.

An investigation into the longevity of alcohol treatment whilst filtering black tea over multiple cycles has been carried out. This investigation looked at 4/5 foul-clean cycles, and showed that some of the initial modifications made to the membrane such as increased PWF were apparent after fouling and cleaning with caustic solutions. Also, untreated membranes showed moderate cycle on cycle increases in performance (polyphenols transmission and flux) over multiple cycles, whereas treated membrane showed a decline from the first filtration cycle onwards. This indicated that whilst some modifications to membranes may be permanent, some may simply be an accelerated result of what may occur 'naturally' over multiple foul-clean cycles, regardless of ethanol treatment.

Finally, an investigation into the merits of using microfiltration (MF) for black tea haze removal was made using three commercial polysulfone MF membranes with 0.5, 0.9 and 1.5 μm nominal pore sizes. This enabled a comparison of processing methods and showed that whilst UF was efficient in haze removal, MF could also be implemented to remove and prevent haze reformation at feed concentrations far in excess of those possible in UF. Fluxes were typically low, though results showed that they could be improved by increasing the cross flow velocity substantially, or perhaps using a different membrane module configuration (e.g. tubular ceramic). The 1.5 μm cut-off membrane offered the most acceptable fluxes, though haze removal and prevention efficiency after 4 weeks was not acceptable. A similar result was returned for the 0.9 μm membrane. For the 0.5 μm membrane, the lowest fluxes were recorded although haze remained below 10 NTU for up to 4 weeks after filtration under simulated in-bottle conditions.

IV. Contents

V. List of figures

VI. List of tables

VII. Nomenclature

General terms

A	area	m^2
c	concentration	$gL^{-1}, mgmL^{-1}$[1]
F	force	N
m	mass	kg
P	pressure	Pa, bar
R	ideal gas constant	$JK^{-1}mol^{-1}$
t	time	s
T	temperature	$°C$
u	velocity	ms^{-1}
V	volume	m^3
μ	dynamic viscosity	$Pa.\,s$
ρ	density	kgm^{-3}

Membrane processes

a, b	non-phenomenological fitting coefficients (diafiltration model)	$-$
d_p	pore diameter	m, nm
J	flux	$Lm^{-2}hr^{-1}$
k_b	complete pore blocking law flux decline constant	*depends on* n
k_c	cake filtration law flux decline constant	*depends on* n
k_i	intermediate blocking law flux decline constant	*depends on* n
k_s	standard blocking law flux decline constant	*depends on* n
M	mass of cake deposited per unit area of membrane	kgm^{-2}
n	pore blocking law index	$-$
$q(t)$	diafiltration permeate flow rate	m^3s^{-1}
Q	volumetric flow rate	m^3s^{-1}
R	species rejection coefficient	$-$
R_a	adsorptive fouling resistance	m^{-1}
R_c	cake resistance	m^{-1}
R_{cp}	concentration polarisation resistance	m^{-1}
R_f	fouling resistance	m^{-1}
R_g	gel layer resistance	m^{-1}
R_i	irreversible fouling resistance	m^{-1}
R_m	intrinsic membrane resistance	m^{-1}
R_p	pore blocking resistance	m^{-1}
R_r	reversible fouling resistance	m^{-1}
$T\%$	percentage species transmission	$\%$
$u(t)$	diafiltration diluent flow rate	m^3s^{-1}
VRF	volumetric reduction factor	$-$
x	distance from membrane surface	m
y, x	mass fraction of species in permeate/retentate	$-$
α	separation factor	$-$
α_s	specific cake resistance	mkg^{-1}
δ	thickness of concentration polarisation boundary layer	m
τ	pore tortuosity	$-$
ϕ	porosity	$-$

Fluid flow and mass transfer

a, b	dimensions of rectangular duct	m
d_h	hydraulic diameter	m
D	diffusion coefficient	$m^2 s^{-1}$
k	intrinsic permeability constant (Hagen-Poiseuille equation)	m^2
k	mass transfer coefficient	ms^{-1}
L^*	channel length	m
L_c	concentration profile length	m
L_u	velocity profile length	m
Re	Reynolds number	–
Sc	Schmidt number	–
Sh	Sherwood number	–
$\alpha, \beta, \omega, a, b$	mass transfer relationship constants and indices	–
$\Delta x, L$	thickness of porous medium	m
ε	surface porosity	–
τ	wall shear stress	Nm^{-2}
γ_w	wall shear rate	s^{-1}

Instrumentation and measurement

L^*, a^*, b^*	CIE Lab 1976 colourspace coordinates	m
R_a	surface roughness	m
R_c	radius of curvature	m
E	streaming potential (zeta potential measurement)	mV
E	modulus of elasticity (AFM)	MPa
k	conductivity (zeta potential measurement)	μScm^{-1}
k	spring constant (AFM)	Nm^{-1}
x, Z_n	cantilever deflection (AFM)	m
X, Y, Z	CIE XYZ 1931 colourspace coordinates	–
ζ	zeta potential	mV
θ	contact angle	$^\circ$
ν	Poisson ratio	–
σ	charge density	Cm^{-1}
Ψ_d	diffuse layer surface potential	mV
Ψ_i	inner Helmholtz layer surface potential	mV

Thermodynamics and other

r_a	relative difference in Hansen space	m
E	energy	J
RED	relative energy difference	$-$
V_m	fluid molar volume	$m^3 mol^{-1}$
γ	interfacial tension	N
γ_{lv}	liquid-vapour interfacial tension	N
γ_{sl}	solid-liquid interfacial tension	N
γ_{sv}	solid-vapour interfacial tension	N
δ	Hildebrand or Hansen solubility parameter	$MPa^{1/2}$
δ_d	square root of dispersion force contribution to cohesive energy density	$MPa^{1/2}$
δ_h	square root of H-bonding force contribution to cohesive energy density	$MPa^{1/2}$
δ_p	square root of polar force contribution to cohesive energy density	$MPa^{1/2}$
ΔH_v	latent heat of vapourisation	Jkg^{-1}
ε_0	permittivity of free space	Fm^{-1}
ε_r	dielectric constant of water	Fm^{-1}

Statistics

n	Sample/test number	$-$
p, t, U, W	statistical test values; probability, Student's t test, Mann Whitney U test and Shapiro-Wilk test respectively	$-$
r^2	determination coefficient	$-$

VIII. Abbreviations

(n)MWCO	(nominal) Molecular weight cut-off
ACN	Acetonitrile
AFM	Atomic force microscopy
βLG	Beta lactoglobulin
BSA	Bovine serum albumin
CA	Contact angle
CA	Citric acid
CA	Cellulose acetate
CEB	Chemically-enhanced backwash
CFV	Cross flow velocity
CIE	Commission Internationale d'Eclairage
CIP	Clean-in-place
COP	Clean-out-of-place
CP	Concentration polarisation
CTC	Cut, tear, curl
CV	Control value
CWS	Cold water soluble
DSS	Danish Separation Systems
DTA	Doctorial training account
EC	European Commission
EDL	Electrical double layer
EDTA	Ethylenediaminetetraacetic acid
EPDM	Ethylene propylene diene monomer
EPSRC	Engineering and Physical Sciences Research Council
EtOH	Ethanol
FO	Forward osmosis
FP	Fluoropolymer
FSA	Food standards agency
FSMS	Food security monitoring system
FTIR	Fourier transform infra-red spectroscopy
FV	Flow valve
GA	Gallic acid
GMBH	Gesellschaft mit beschränkter Haftung
GMP	Good manufacturing practice
HACCP	Hazard analysis and critical control points
HPLC	High performance liquid chromatography
IChemE	Institution of Chemical Engineers
IEP	Isoelectric point
IHP	Inner Helmholtz plane
IPA	Isopropyl alcohol
IRE	Internal reflection element
IUPAC	International Union of Pure and Applied Chemistry
LUT	Lappeenranta University of Technology
MeOH	Methanol
MF	Microfiltration
MPI	Milk protein isolate
MTC	Mass transfer coefficient
NF	Nanofiltration
nPrOH	nPropanol
NS	No significance
NTU	Nephelometric turbidity units
O.D.	Outer diameter
ODE	Ordinary differential equation
OHP	Outer Helmholtz plane
PAN	Polyacrylonitrile
PC	Polycarbonate
PEEK	Polyether ether ketone
PEG	Polyethylene glycol
PEK	Polyetherketone
PES	Polyethersulfone
PP	Polypropylene
PS	Polysulfone
PTFE	Polytetrafluoroethylene
PVDF	Polyvinylidene fluoride
PVP	Polyvinylpyrrolidone
PVPP	Polyvinyl polypyrrolidone
PWF	Pure water flux
RC	Regenerated cellulose
RIS	Resistance-in-series
RO	Reverse osmosis
RTD	Read-to-drink
SAXS	Small angle X-ray scattering
SDS	Sodium dodecyl sulfate
SEM	Scanning electron microscopy
TEM	Transmission electron microscopy
TF	Theaflavin
TMP	Transmembrane pressure
TR	Thearubigin
UF	Ultrafiltration
USA	United States of America
USB	Universal serial bus
UV	Ultraviolet
VRF	Volumetric reduction factor
WPC	Whey protein concentrate
ZP	Zeta potential

1. Introduction

1.1 Tea: no longer a commodity

Infusions of tea are the most consumed flavoured beverages in the world [1]. The tea plant (*Camellia Sinensis* var. *Sinensis* or *Assamica*) is generally cultivated at high altitude (>1200 m) in tropical or sub-tropical regions of central and eastern Asia, and Africa [2]. In 2010, China accounted for 33% of world tea production, with India second, producing 1.4 and 0.97 million tonnes respectively [3]. The average market price in the period 2008-12 was 2.72 $/kg [4] and, despite being classified as a commodity crop, products made from tea infusions hold a significant share of the global soft drinks market [5]. Products such as powdered and iced teas, commonly referred to as ready-to-drink (RTD) teas, occupied 8.7% of the $522 billion market in 2012-13 [6].

In the Chinese and other Asian markets, green tea infusions reign supreme – accounting for 70% of domestic consumption. Globally speaking, 70% of production and 80% of exports are accounted for by black tea [7]. Whilst many infusions are consumed in the traditional way, the surge in growth of RTD tea products is ongoing, and the market place ever-diversifying [5]. RTD products have huge inter-country variation in terms of taste, flavour and functionality, which is achieved by the addition of citric acid, sugar and sweeteners, vitamins and fruit flavourings [8].

It is clear from these figures that the popularity of tea will continue to be a lucrative market for commodity traders. At the same time, the conversion of commodity crops to consumer products is likely attributed, in part, to innovations in the food manufacturing sector. The addressing of consumer needs to manufacture improved products, in terms of health giving properties, without compromising taste and other sensory appeals, has created a market drive with strong competition. For companies in the business of food production, the solution for most is making foods with ever-increasing functionality through technological advancements.

1.2 Functional foods, black tea, and the consumer

The role of food products today is somewhat different than it was in the past. Food is expected to offer something more than just nutrition and satiety. It should offer some protection from disease and enhance physical and mental well-being [9-11]. Outlining functional foods under these terms provides a sound definition, though other authors insist on a more specific one. That is; it is a food by which ingredients with an added nutritional value have been added, and this is announced to the consumer [9, 12]. Another definition is that it can be any food product where fortification using 'special constituents' leads to beneficial physiological effects, as well as decreasing risk of diseases, improving the body's condition, or even curing ailments [11].

Siro *et al.* (2008) [11] suggested (using Japan as a case study) that production of functional foods benefits commerce within the food sector, as well as aiding in lowering the healthcare budget. The realisation Japan had of an aging population lead to a technological shift. The nation became a forerunner in functional food production. In the UK, dietary awareness has been conveyed to the population by government bodies such as the Food Standards Agency, through schemes such as "Eat well, be well" and "5 a day". These initiatives aim to educate people about the benefits and drawbacks associated with certain foods. It would be naïve not to assume the food industry would use this as a powerful marketing tool. Further, the consideration of so called 'fat taxes' and vegetable subsidies by governments are pushing the market ever forward into finding solutions to help resolve poor diets in the general population. These policies are already in effect in Denmark, for example [13].

With regard to specific products, Menrad *et al.* (2003) [9] focused on the European functional dairy foods market; in particular the largest domestic market, Germany. Dairy products were worth an estimated 21% of the $283 million total functional food market. Typical products in this sector would be pre- and probiotic bacteria-containing yoghurts and yogurt drinks e.g. Danone Activia® and Actimel®, and Yakult. However, the sector which contributed most to the market share was soft drinks. These can be functional to the consumer in terms of improving rehydration (e.g. Gatorade, Powerade), as energy and rejuvenation supplements and stimulants (Red Bull, protein supplements, herbal supplements), for aiding with weight loss (Slim Fast, green tea extract enriched products), or for promoting health and wellbeing (Vitamin Water, iced teas).

From a commercial perspective, foods with natural health properties which can be enhanced continue to rise in popularity. Secondly, the consumer has become more attuned to added ingredients such as colourants and preservatives, with synthetic additive not sitting favourably [14]. Lastly, producing foods which have extended shelf life is valuable to supply chain management as product stock levels can be controlled more effectively. Supply chain wastage has been shown to contribute to some 10% of sales in one case study [15]. Thus it is in the interest of the food industry to develop these functional products, which maximise the existing beneficial constituents, reduce harmful ones, and all the while, ensuring that sustainable production targets are met through the use of emerging technologies.

Whether or not RTD tea can be strictly classified as a functional food is a matter of debate. The health giving properties of the beverage are well documented, mostly relating to the effects of its polyphenolic constituents [16-18]. It would seem logical that if RTD tea was bettered and enhanced beyond what would be considered a natural foodstuff (e.g. a standard tea infusion) through some technological intervention, then by previous definitions, it would be classified as a functional food.

1.3 Food process engineering and membranes

The planet faces serious challenges in maintaining food security in the new millennium. Global population is set to increase to 9 billion in the next few decades meaning an increased demand for food [19]. Decreasing population growth correlates with increased wealth, and with increased wealth comes increased consumption [20]. Factors such as trade policy, urbanisation, changing consumer attitudes and market liberalisation have been key drivers in an increased per capita food consumption and market diversification [21]. The provision of energy, fresh water and food, in a sustainable and affordable manner, are the outstanding issues facing society. Food process engineering plays a part in each one of these areas [22].

The food supply chain ranges from the arable environment right through to product delivery to the consumer. As with most industries it requires continual update and refinement. With this comes the need for process innovation. In terms of crop production, biotechnology and advanced farming techniques play essential roles in crop intensification and yield improvement. It employs expertise in fields such as genetic engineering, developmental biology, crop science and agronomy among others. Advancing treatment processes, extractions, transformations, combining of ingredients, hygienic production and product safety are generally the tasks of food scientists and engineers. On the other hand it is particularly the fundamental mechanical and chemical engineering principals which are of great relevance for making precise and controlled physicochemical or biochemical changes to foodstuffs. Yanniotis *et al.* (2013) [22] identified four cornerstones which could help to promote technical innovation and make improvements to the food process engineering sector, through intensified research:

1. *Development of adjusted processes and food products.* This will lead to a better understanding and application of specific micro-structure and chemical interactions by application of knowledge in the chemical engineering science domain.
2. *Process efficiency improvement.* Saving water and energy, and minimising pollution and waste, enables production of food at lower cost and environmental burden, without compromising quality.
3. *Food safety insurance.* This would encompass improved hygienic design of equipment and packaging, as well as better food safety models, both through improved microbiological techniques and computational modelling.
4. *Product quality improvement by intelligent design.* This area would advance process control and process automation, provide better integration and communication between unit operations, and allow improved management of production lines to offer flexibility or personalisation of products.

Chemical engineering research and design often considers the study of single unit operations on a production line. These unit operations generally have a specific function to achieve before material is passed forward to the next unit.

Dairy processing can be used as an example to demonstrate processing advancements. Upon receipt, raw milk must be cooled, stored and tested. After this, pasteurisation, homogenisation and standardisation are carried out. Only when these operations have been completed can the finished milk product can be bottled and sent to market, or sent for further processing to make cheese, yoghurt etc. Each operation here uses specialised pieces of equipment which require continual design improvement and refinement, expenditure through energy, maintenance costs, and water and chemicals for cleaning. An innovation in this industry came through the invention of the *simultaneous emulsification and mixing nozzle*. The nozzle was similar in action to a standard high pressure homogenising nozzle, though a lateral injection of skimmed milk was introduced after the standard nozzle which further disrupted flow patterns and enhanced droplet break-up whilst simultaneously allowing for standardised mixing. The introduction of this system meant that the standard homogeniser and compositional standardising apparatus (and connecting manifolds) were combined. This offered dairies reduced capital expenditure and up to 90% lower energy consumption [23].

The dairy industry also provides a sound case study for the development of membrane processes in food process engineering. Many technological innovations in membrane related processes within the wider process engineering field, particularly ultrafiltration and microfiltration, arose from dairy focused applications [24]. The ability to reduce water content of feed stocks for cheese making, remove bacterial spores for cold pasteurisation, or fractionate proteins to give added value streams, reflects the versatility membrane processes can offer. This versatility, the attraction of being operated at ambient temperatures and moderate pressures, and the relative ease of scale-up, are reasons for their rise from the forefront of technology in the 1960s, to their maturation and ubiquitous use today. Section 2.1.6 depicts the widespread application of membranes across the food sector.

In view of membrane filtration of black tea, a number of references exist in the research domain [25-33], all published no earlier than 2002. It demonstrates the novelty and relevance surrounding the application of membrane processes in ready-to-drink (RTD) or powdered (instant) black tea production. Specifically the removal of the haze characteristic in pre-prepared tea infusions is what membrane processes offer to remediate more effectively than other more well-established haze treatments, without the requirement for additives. This is the predominant focus of the body of research surrounding tea processing with membranes thus far. Section 2.7 reviews current knowledge and state-of-the-art relating to tea chemistry and haze, as well as detailed summaries of membrane-related work to date.

The performance of membranes in food processing is limited by a number of factors, though none more so than fouling. The deposition of material on or inside process equipment, specifically the module and porous network of a membrane, acts to restrict flow rates and transfer of solutes. It is a complex subject spanning many scientific disciplines and shows numerous interplaying phenomena. The characterisation, scientific basis, as well as the engineering interpretation and solutions to fouling are detailed in section 2.4 and are employed extensively in this work. Understanding why fouling limits performance allows the chemical engineer to make rational changes to improve processes. Some novel solutions relating to food processing are reviewed by Mérian and Goddard (2012) [34]. Membrane process performance can be altered in four ways in order to reduce the effect of fouling:

1. *Manipulation of process variables to minimise or obstruct fouling.* This spans a wide range of practical considerations (both physical and chemical) such as module design/configuration and related fluid mechanics, mass transfer and transport phenomena, temperate and pressure, membrane material and membrane synthesis.
2. *Feed-stock pre-treatment to modify filtration behaviour.* This area can involve addition of particulates or chemical adjustment (e.g. conductivity/pH) to disrupt fouling layer build-up, modify solubility, or reduce attachment to membranes.
3. *Optimisation of cleaning regimes to efficiently remove fouling.* Clean-in-place (CIP) acting to remove foulants from membranes as efficiently as possible enables shorter process down-time, and lower chemicals and energy consumption. Cleaning agents can also modify subsequent fouling phenomena.
4. *Pre-treatment of membranes to modify performance prior to operation.* Membranes can take years to develop as commercial products, and companies are ongoing in efforts to enhance their product to gain a market edge. Ensuring membranes are treated correctly prior to use by rinsing and cleaning has been shown to effect subsequent operation, not just in the short term. Additionally, chemical coupling by surface grafting, or by other techniques, can influence membrane performance.

This thesis focuses on aspects of membrane fouling and its remediation by membrane pre-treatment with respect to black tea ultrafiltration and microfiltration processing.

1.4 Research scope

1.4.1 Pre-treatment in place

As has been discussed, improving process performance by development of modified processes, improving efficiency and product quality are three of the four cornerstones of enhanced food processes. This work focuses on improving membrane performance by alcohol pre-treatment, which has been selected as an adsorbent to modify membrane surfaces and matrix characteristics. Solvent permeation of membranes has been reported by some authors [35-41] though most relate to nanofiltration applications, and use of the solvent not as the pre-treatment agent but as the feedstock solvent itself. Kochan *et al.* (2008) [35] showed that alcohols could be used as wetting agents to affect permeability of ultrafiltration membranes though these authors conducted limited characterisation to ascertain the reasons why the changes occurred. They cited these reasons as being a 'pore unlocking' mechanism due to the lower surface tension of alcohols compared to water. To date there exists no suitable explanation of how pre-treatment with alcohols (followed by subsequent removal) affects the membrane's physical or surface chemical properties, and how this then affects the subsequent filtration of an industrially relevant feedstock.

1.4.2 Modifying performance: the trade-off

It is a common acceptance within the membrane technology community that there exists a trade-off between permeability and selectivity (or in a more general sense, reduced operating cost and improved quality). If efficiency is gained for one, it is typically lost for another. This trade-off has been mentioned in a number of works [42-44]. For a given separation there are cause and effect relationships which have opposing outcomes, brought about by changes in process variables. For example, if one increases the permeability of a membrane by increasing pore size, the sieving effect of the membrane is diminished. Similarly if one increases the feed temperature to give a lower viscosity feed, the solubility of the components changes, and previously high resolution separations can be lost. These relationships bring about the need to optimise processes with high precision. For improvement of a membrane process, these two aspects can be regarded as separate efficiencies, and combined, reflect the overall process efficiency. The effect can be appreciated graphically, as shown in Figure 1-1. In relative terms, a process would be placed somewhere along the 'typical membrane' channel. For a process to overcome the trade-off, a movement towards the top right or bottom left would be observed. Naturally, reducing the efficiency in terms of both permeability and selectivity would be concluded as a negative result. If the process shows an increase in either efficiency attribute, whilst the other remains constant or increases also, it can be deemed a positive result.

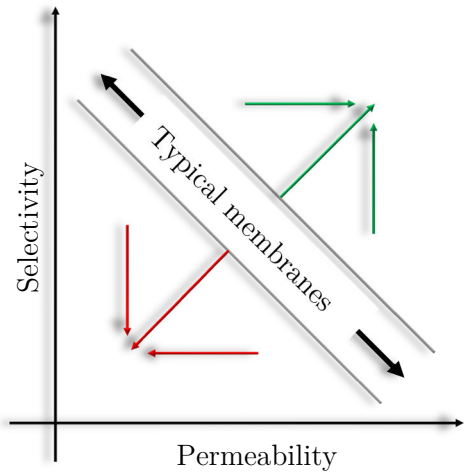

Figure 1-1 - The permeability-selectivity trade-off

With relevance to filtration of tea using alcohol pre-treated membranes; it was hypothesised that an increase in permeability for pure water would be seen after treatment, as was shown in previous literature [35] and further, for tea filtration. The motivation for filtering tea is to remove haze. However, this results in polyphenols loss from the tea filtrate. Rejection of haze and polyphenols relate to the 'selectivity efficiency' of the membrane. Now, two variables have been introduced as system outputs on the selectivity axis, the combined result of which becomes somewhat harder to qualify. In this instance, the relative importance of each parameter must be assessed on a case by case basis regarding the individual processing target.

The trade-off consideration provides a basis for assessing how alcohol treatment affects the process as a whole. It is considered that the haze removal characteristic of tea, along with measurements pertaining to tea quality refer specifically to being present on the selectivity axis. Changes in through-put (which is allied to energy consumption) and membrane cleanability (reflecting down-time and cleaning efficiency) relate to the permeability axis, or more generally, the cost reduction.

1.5 Thesis outline

The thesis has been divided into nine chapters with five experimental work packages delivering the research objectives. The work packages are segments of work contributing towards the general thesis scope. The overall scope was to develop an improved black tea membrane separation process by application of an alcohol pre-treatment strategy to modify membranes prior to filtration and to investigate process alternatives for haze removal.

Chapter 2 presents a review of the relevant literature and surrounding scientific theory in order to contextualise research carried out and outline gaps in current understanding.

Chapter 3: in light of the literature review, the research objectives are stated defining the scope of the overall body of work.

Chapter 4 details the materials and methods used for experimental and theoretical work completed.

Chapter 5 reports and analyses results concerning the alcohol pre-treatment method developed relating to membrane performance, as well as changes to the specific surface measurements relating to fouling propensity. Filtration of model foulants aims to reinforce the findings.

Chapter 6 utilises the treated membranes for ultrafiltration of black tea, allowing comparison of treated and untreated membranes simultaneously with regard to permeability and selectivity.

Chapter 7 shows how the membrane process, this time operated in a diafiltration regime, highlights the shortfalls that untreated membranes have regarding polyphenols transmission, though this is then viewed positively in terms of stream enrichment on the retained side of the process.

Chapter 8 demonstrates the longevity of the treatment method over multiple foul-clean cycles and offers perspectives relating to the fouling and cleaning synergy of both tea fouling *per se*, and with incorporation of pre-treated membranes.

Chapter 9 investigates microfiltration as a different process regime for haze removal in black tea as an alternative to ultrafiltration, and shows that high concentration streams can be effectively clarified.

Chapter 10: conclusions are made surrounding the scientific work in a general context relevant to the entire thesis. Also presented are experimental results which show potential future developments relating to the results in Chapters 5 – 9.

The results sections contain a brief introduction to the motivations and contain specific literature examples relating to why given experiments were carried out. They also show information about the structuring of the experiments and specific analyses performed.

1.6 Outputs and awards

Substantial elements of the results presented in this thesis have been accepted for publication in peer reviewed journals.

Peer reviewed journal papers

Argyle, I.S. and M.R. Bird, *Microfiltration of high concentration black tea streams for haze removal using polymeric membranes.* Desalination and Water Treatment, 2015, 53(6) p. 1516-1531, DOI: 10.1080/19443994.2014.953401

Argyle, I.S., A. Pihlajamäki and M.R. Bird, *Ultrafiltration of black tea using diafiltration to recover valuable components,* Desalination and Water Treatment, 2015, 53(6) p. 1532-1546, DOI: 10.1080/19443994.2014.953400

Argyle, I.S., A. Pihlajamäki and M.R. Bird, *Black tea liquor ultrafiltration: effect of ethanol pretreatment upon fouling and cleaning characteristics*, Food and Bioproducts Processing (IChemE Transactions C), 2015, 93 p. 289-297, DOI: 10.1016/j.fbp.2014.10.010

Oral presentations at international meetings

'Ultrafiltration of black tea liquor in diafiltration regime and recovery of valuable components' presented at Engineering with Membranes, St. Pierre d'Oléron, France, 3 - 7th September, 2013

'Fouling and cleaning phenomena for ethanol pre-treated membranes used to ultrafilter black tea liquor' presented at Fouling and Cleaning in Food Processing, Cambridge, UK, 31st March - 2nd April, 2014

Poster presentations at international meetings

'Structural and Surface Modification of Polymeric Ultrafiltration Membranes by Alcohol Pre-treatment and Subsequent Fouling Implications' presented at Euromembrane, London, UK, 23 - 27th September, 2012

'Removal of haze from high solids content black tea streams using microfiltration' presented at Engineering with Membranes, St. Pierre d'Oléron, France, 3 - 7th September, 2013

Other presentations

'Integrated membrane processes for health promoting beverages' presented at the Postgraduate Research Showcase (University of Bath Faculty of Engineering and Design), Bath, UK, 31st March, 2012

'Modification of polymeric ultrafiltration membranes by alcohol pre-treatment and subsequent fouling implications' presented to visiting researchers from University of Twente (Netherlands), Bath, UK, 24th August, 2012

Awards

Wolf Hamm travel bursary awarded as match-funding for attendance at Engineering with Membranes 2013, St. Pierre d'Oléron, France, by the IChemE Food and Drink Special Interest Group

2. Literature review

The following chapter gives an overview of definitions and classical theory surrounding aspects of membrane technology, food science and engineering, surface chemistry and related fields. A review is provided of the current scientific literature discussing food-related filtration processes, membrane fouling and membrane modification, with emphasis on black tea processing and the requirement for membrane processing.

2.1 Membrane processes for separations

A membrane is a permselective phase barrier which is commonly associated with the barriers surrounding the cells making up living organisms, among other forms. In the context of this thesis, they are indicative of synthetic porous sheets of polymer or porous ceramic tubular elements. They act to selectively exclude some material whilst being permeable to others. The penetrating solution or suspension is referred to as the feed, and the filtrate is termed the permeate. Mass transfer is achieved by application of a driving force between feed and permeate e.g. electrical or chemical potential [45]. This thesis however focuses solely on pressure-driven membrane separation processes.

2.1.1 Process classification

Membranes are able to discriminate between material sized over several orders of magnitude, ranging from large bacteria, bacterial spores and fat globules down to ionic components and small organics.

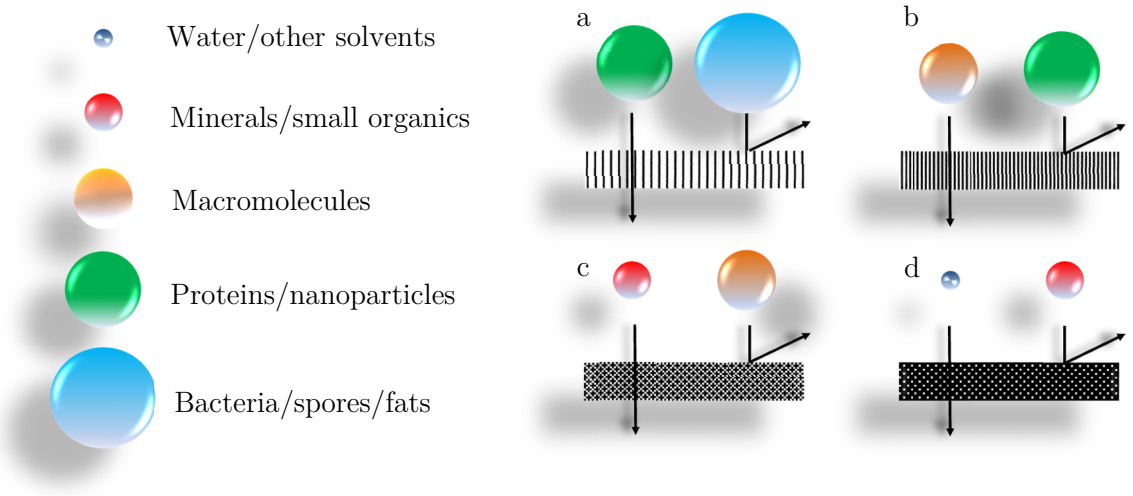

Figure 2-1 - Membrane process classification, a) microfiltration, b) ultrafiltration, c) nanofiltration, and d) forward and reverse osmosis

Figure 2-1 shows a schematic representation of the various process categories. Approximately speaking, microfiltration (MF) will reject particles in the 0.1 – 1 µm range, ultrafiltration (UF) will exclude particles from 0.01 – 0.1 µm, nanofiltration (NF) operates

effectively for separation in the 0.001 – 0.01 μm, and sub-nanometre separation occurs via forward and reverse osmosis (FO and RO respectively). For MF, the pore size is normally quoted in terms of the nominal pore diameter e.g. 0.22 μm. For UF and NF, nominal molecular weight cut-off (nMWCO) is generally expressed in terms of molecular weight, as the forerunning applications of UF were for biological solutions such as proteins, where particle size is defined by molecular weight [46]. Manufacturers however, given advancing production and characterisation methods, are starting to quote UF membranes in terms of pore dimensions too. For FO and RO, membranes are normally quoted in terms of their desalination capability i.e. the nominal salt rejection for various mineral salts (or other more application specific measures).

The pore diameter at which 90% of pores are less than is deemed the nominal pore rating, and the nMWCO is the lowest molecular weight in which 90% of particles with the molecular weight are rejected. Further discussion about membrane characterisation is provided in section 2.2.4.

Membranes are also classified as being symmetric or asymmetric in structure. This characteristic is measured across the membrane thickness. Symmetric membranes consist of a single material across their cross-section, this being the case no matter if the pores are homo- or heterogeneously distributed [47]. Asymmetric membranes are made up of differing materials in stratified layers, normally an active layer (which achieves the separation) and support layer (which improves mechanical integrity).

2.1.2 Mode of operation

There are two modes of operation for membrane processes, dead-end and cross-flow filtration (see figure 2-2). In dead-end filtration, pressure is applied on the feed side forcing material towards the membrane surface. All material transferred from the bulk solution and through the membrane flows in a perpendicular fashion. Build-up of material creates a filter cake layer on the surface which can also aid the membrane in achieving separation, and this continues to grow with volume filtered [48]. Dead-end filters find use in small-scale applications such as sterile syringe filters or filter funnels as well as inline cartridge type filters for removing large or insoluble particulates prior to various unit operations. Membrane bioreactors can also use this operating regime, and more recently the configuration has been applied in forward-osmosis processes.

Cross flow filtration differs in that whilst pressure is also applied on the feed side of the membrane, a tangential flow of liquid is applied across the membrane surface brought about by recycling the feed from a separated tank. The stream which has been passed over the membrane surface and returns to the tank is named the retentate. The action of cross flow, which is applied at a specified flow rate equating to a cross-flow velocity (CFV) aids in the removal of material deposited on the surface. This in turn results in comparatively higher flow rates (more commonly termed membrane fluxes) compared to dead-end filtration. The mode of operation also enables higher feed concentrations to be filtered given that pore blockage/fouling build-up is mediated by the shear forces exerted at the

membrane-bulk interface. In practice, membrane permeability is reduced over time and arises from factors such as concentration polarisation and fouling [45]. Cross-flow filtration is ubiquitous in large scale membrane systems and finds application across numerous chemical and bioprocessing sectors.

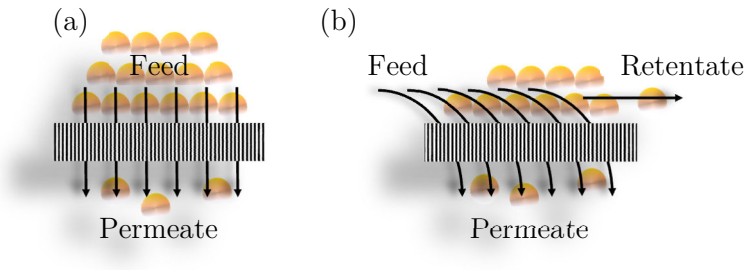

Figure 2-2 - Modes of operation for membrane filtration, (a) dead-end, and (b) cross flow operations

2.1.3 Processing regimes for cross flow systems

The processing regime for cross flow membrane systems can vary depending on application. This is defined by the nature of the desired separation.

Single pass operations can be required in applications where feeds contain shear sensitive material which can be degraded by continuous circulation in pumping circuits and pipe geometries e.g. proteins or for shear thickening and thinning fluids. Single pass operations are advantageous as the retentate and permeate streams can be passed to the next unit operation in a continuous manner. They run at higher fluxes and have greater throughputs than recycled retentate streams. A disadvantage of these systems is they require relatively high membrane areas to perform (and thus more or larger modules), which adds a greater capital cost. Multi-stage single pass operations, sometimes referred to as membrane cascades, allow continuous flow of the retentate through process operations. These systems can be designed with various filtration grades e.g. an MF unit feeds a UF unit which in turn feeds an NF unit. Single and multiple pass flow diagrams are shown in Figure 2-3a and 2-3b.

When a recycle loop is introduced, the membrane process can be classified as a semi-batch, fed-batch (e.g. diafiltration) or feed-and-bleed operation (see Figure 2-3c and 2-3d). Whilst in theory they should run at steady state, often the system dynamics are more complex, which in turn requires more advanced process control. When designing these membrane systems, the regimes must be assessed and selected relative to the requirements of the filtration being performed e.g. defining which is the target stream, what degree of recovery is required (and at what purity), is the operation to be run at constant flux, what filtration time scale is estimated before clean-in-place etc. These questions can be answered, to a degree, by pilot studies and theoretical design. Carrying out mass balances for the process is often a process engineer's first consideration upon generation of initial filtration data. Since most membrane systems contain no generation or consumption of components (no

chemical reaction), the general mass balance for the system or given component simplifies to:

$$\text{Input} = \text{Output} + \text{Accumulation}$$

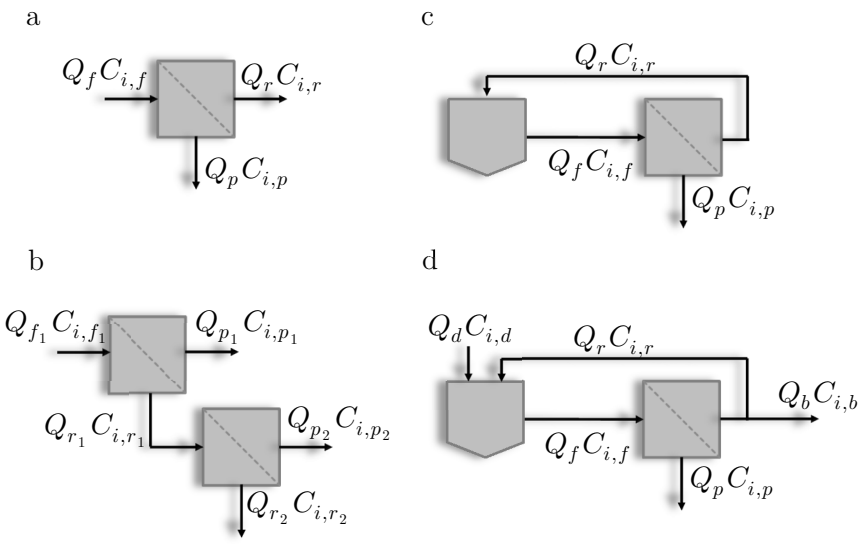

Figure 2-3 - Membrane processing regimes, (a) single pass, (b) two stage single pass, (c) semi-batch with total recycle, and (d) fed-batch ($Q_b C_{i,b} = 0$) or 'feed-and-bleed'. Q refers to volumetric flow rate, C_i is concentration of component i, and f, p, r, d, b refer to feed, permeate, retentate, diluent and bleed streams respectively

2.1.4 Membrane and module configuration

As with many process engineering unit operations, differing designs are made for various applications. Module design is crucial to enhancing the membrane process in terms of throughput, flow dynamics and fouling control, as well as allowance of considerations such as spatial confinements, process variable stipulations and cost.

Membrane modules fall into one of four categories; flat sheet, hollow fibre, tubular or spiral wound. Diagrams for these modules are detailed in Figure 2-4. The module configurations offer advantages and disadvantages with respect to one another, these are highlighted in Table 2-1.

Flat-sheet modules (or plate and frame modules) are the simplest design concept. The membrane is normally mounted over a spacer which leads into a permeate duct. Material is flowed across the membrane under pressure forcing a fraction through. Materials of construction for the housing can range depending on application though stainless steel is common, particularly for food applications. Advantages include low volume hold-up in the module which is useful for high value recovery e.g. biologics/therapeutic proteins. Membrane replacement is relatively straightforward also [49].

Tubular membranes work on the same principle though in cylindrical form. A solution is fed into channels under pressure and is subsequently forced through the membrane pores into a void space between the membrane outer and module inner wall. Given their natural pipe-like geometry and customisable channel diameter, tubular membranes are useful for high flow rate applications, particularly when high solids load feed are being filtered. Combining these attributes with the materials used for tubular membranes (ceramics such as aluminium or titanium oxides), tolerance to high pH and temperature make these systems suited to dairy applications where stringent hygiene measures (and thus often harsh cleaning agent usage) must be upheld.

Spiral wound modules are of interest where high volume throughput is required given their compact nature and high area to module volume ratio. Membranes are layered with mesh spacer materials (which also promote turbulence) often in enveloped arrangements. Permeate is fed around the inner envelope radially towards weep holes following transmission. It is then ejected from the module in a central permeate duct. These modules find application in the biotechnology and desalination sectors particularly.

Finally, hollow fibre membranes consist of fibre bundles with a range of diameters. After sealing on the outer fibre edge, feed is permeated into the lumen (central cavity) under pressure, and material is collected on the outer (ablumenal) side (or vice versa). These membranes are highly versatile and find application in a diverse range of applications from tissue engineering to gas separations [50-52].

Table 2-1 - Comparison of membrane module configurations (adapted from Mulder (1999) [45])

	Module configuration			
Attribute	*Flat sheet*	*Tubular*	*Hollow fibre*	*Spiral wound*
Flow requirement	low	low	high	high
Area: volume	average	low	average	high
Capital cost	average	average	high	low
Fouling tendency	average	low	high	average
Cleanability	high	high	low	average
Maintenance	average	low	average	low
Selectivity	average	average	high	average

2.1.5 Application to membrane modification and filtration of tea

The requirements for this project were that the module for experimentation would be utilised both for treatment of membranes and filtration of black tea of varying concentration. Given the presented information and the need to carry out surface analysis of membrane in differently fouled and cleaned states, a flat-sheet system was selected as the most suitable. With low liquid hold-up, solvent usage would be minimised and the relative disposability of membranes inside a plate-and-frame unit meant post-experimental sectioning was possible to a greater degree.

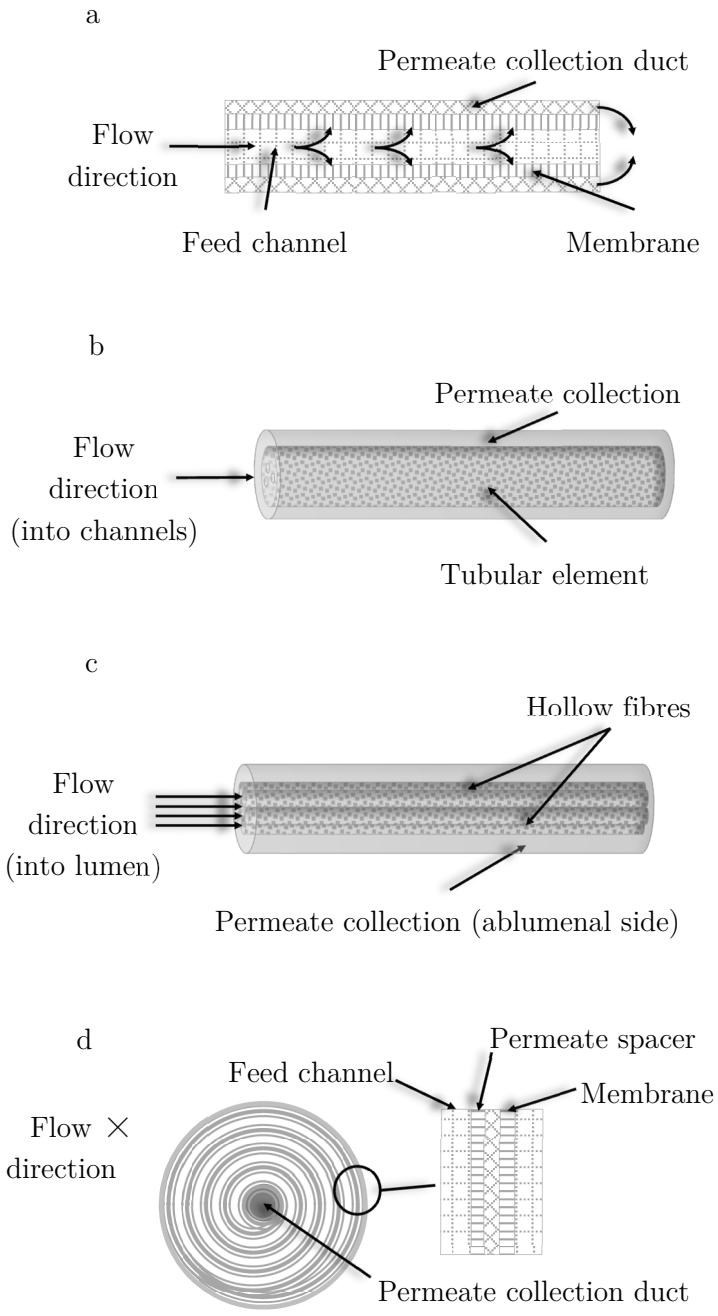

Figure 2-4 - Module configurations, (a) flat-sheet, (b) tubular, (c) hollow fibre, (d) spiral wound

2.1.6 Membrane processes in the food industry

Membrane processes cover a diverse range of applications within industrial sectors such as pharmaceutical, biotechnology, waste treatment and desalination of sea and brackish water, gas separations in the petrochemical and biogas industries [45, 46, 53-55]. Perhaps one industrial sector in particular that has welcomed advances in membrane technology over the past 40 years is the food industry. The complex nature of food stuffs and the ever-growing need for efficiency without compromise of standards has led many manufacturers to consider membrane processes as alternatives to other unit operations. This section shows

applications of MF and UF in terms physicochemical transformation of feed stocks and highlights the way in which membranes have affected the *status quo* in food processing.

2.1.6.1. Microfiltration applications

RO and UF were already established as commercial technologies in the 1980s though until the early 1990s, the leap from the research domain to industrial state-of-the-art had only been made with regard to wine and vinegar clarification [56]. At the time of writing, the aforementioned authors commented that commercial MF implementation for beer, gelatine and fruit juice streams was about to take place; whey, brine and egg MF processing was in development. Fast-forward two decades and the changes are long since passed.

MF of feeds now commonly functions as a sieving process for removal of spores, bacteria, somatic cells, fat globules and haze agglomerates; examples of which are shown in Table 2-2.

The process can be operated at ambient temperature and relatively low TMP (typically 0.1 – 2.0 bar) [24] meaning a lower energy consumption over alternatives such as centrifugation or high-temperature pasteurisation. This type of processing also allows for lower chemical interference, such as replacements for haze solubilisation. The high fluxes are sufficient to decrease the processing durations over more time constrained methods such as fining. Absence of high pressures as well as thermal and chemical treatment in these processes ensures the degradation or transformation of food products is limited to; another reasoning for their suitability to food engineering application.

Table 2-2 - Current state-of-the-art applications of MF in various food sectors

Industry	*Feed*	*Retentate*	*Permeate*	*Aim*	*References*
Dairy	- milk - whey - MPIs*	- skimming casein - bacteria - fat - high M_w protein	- milk - whey - MPI	- concentration - clarification - fat removal - pasteurisation	[57-59]
Sugar	- sugar beet molasses	- insolubles	- solubles	- suspension-free solution	[60]
Wine and Vinegar	- red/white wine - red/white vinegar	- yeast - bacteria - colloids - mold	- wine - vinegar	- secondary fermentation cessation - clarification - stabilisation	[61-64]
Beer and cider	- lager - ale - cider	- yeast - bacteria - colloids - proteins	- lager - ale - cider	- bright beer - clarification (fining) - yeast recovery	[65-68]
Fruit juice	- orange - apple - passion-fruit - kiwi - pineapple	- fibres - colloids	- clear juice	- clarification	[69-73]
Other Beverage	- green tea	- plant-matter - colloids	- clear tea	- clarification	[74]
Bio-polymers	- gums: xanthum guar Arabic	- bacteria - spores	- bio-polymer	- pasteurisation	[75-77]

*MPIs – milk protein isolates

2.1.6.2. Ultrafiltration applications

UF has been widely applied in a range of processes in the food industry given its gentle product treatment, low energy consumptions and high degree of selectivity [78]. UF is predominantly used as a separation tool and for concentration (de-watering) of products; the separation is typically carried out at between 1 and 10 bar, and mechanistically, as both a sieving and charge based separation. Its growth in food processing has been driven in the most part by developments in the dairy industry. Pouliot (2008) [24] noted that following the establishment of consistent membrane manufacturing processes in the 1960s, the 1970s was the decade which saw the arrival of the first UF-based cheese manufacturing processes and, by the 1980s, separation of more specific dairy components (e.g. α-lactalbumin and β-lactoglobulin) was achievable. Nowadays, UF has become such an integral part of processes, the operation of which is known with such precision, that the process is being implemented for novel separations in a seemingly limitless range of cases as demonstrated in Table 2-3.

Table 2-3 - Current state-of-the-art and novel applications of UF in various food sectors

Industry	*Feed*	*Retentate*	*Permeate*	*Aim*	*References*
Dairy	- milk - whey - MPI	- concentrate - fats - coagulants - whey proteins - other protein fractions	- process water - salts - lactose - protein fraction	- skimming - solids recovery - protein isolation - lactose reduction	[79-81]
Sugar/ sweeteners	- sugar beet juice - stevia extract	- proteins - colloids - plant matter	- sugar beet juice - stevia extract	- purification - clarification	[82, 83]
Wine	- white wine	- high M_w protein-poly-saccharides	- low M_w haze active proteins	- clarification - chill haze prevention	[84, 85]
Fruit juice	- kiwi - blood orange - passion-fruit	- proteins - colloids - plant matter - concentrate	- clear juice -process water	- dewatering - clarification	[86-89]
Other Beverage	- black tea (tea extract) - green tea	- colloids - haze agglomerates	- clear tea	- clarification - chill haze prevention	[27, 31, 90]

The ability of commercial UF membranes to effectively discriminate between products with close molecular weights, without the requirement for solvent-based extractive processes or temperature swings, complements current trends in the wider processing industry. Developing specialised methodologies and material specifications for an ever-widening range of food stuffs to which UF is applied provides a fruitful workload for process engineers. Of fundamental importance to this development is knowledge of the system

operability, material properties and membrane characteristics, as these can influence process variables. Equally as important is fouling. Understanding and consideration of these areas allows the evolution of process improvement strategies. The following sections will focus on the process fundamentals surrounding membrane science with relevance to both the experimental work completed within this thesis and in the broader context of food processing using membranes.

2.2 Membrane materials, fabrication and characterisation

This section will focus predominantly on polymeric membranes used for MF and UF applications. An introduction to the types of materials used and current trends in synthetic membrane science is given, followed by a review of membrane preparation methods. Following this, a review of the methods used for membrane characterisation is given.

2.2.1 Membrane materials

For the separations detailed in sections 2.1.6.1 and 2.1.6.2 to be achieved, research in the field often focuses on use of industrially available membranes or membrane systems. This has the benefit of being a relatively fast path to commercial exploitation. System technologies have now advanced to an extent that manufacturers can offer specific or even bespoke systems for given applications.

Table 2-4 - Polymers used for MF and UF membranes, common format and general properties

Material	*Module/format*	*Typical property/structure*
polysulfone/polyethersulfone (PS/PES)	fibre, flat sheet, spiral	hydrophilic asymmetric
poly(vinylidene fluoride) (PVDF)	flat-sheet, fibre	hydrophobic asymmetric/symmetric
polyacrylonitrile (PAN)	flat-sheet, fibre	hydrophilic symmetric
polyetherketone (PEK/PEEK)	flat-sheet, fibre	hydrophilic/hydrophobic asymmetric/symmetric
polypropylene (PP)	flat-sheet, fibre	hydrophobic/hydrophilic symmetric
polycarbonate (PC)	flat-sheet	hydrophobic/hydrophilic symmetric
polytetrafluoroethylene (PTFE)	flat-sheet, fibre	hydrophobic symmetric
cellulosic (cellulose acetate/ regenerated cellulose) (CA/RC)	flat-sheet	hydrophilic symmetric/asymmetric

The array of polymers used for different applications reflects the need for differing structure-property relationships in various applications [91]. Aside from surface chemistry

aspects such as charge and hydrophobicity, cost and stability (chemical, thermal etc.), selection of a polymer with respect to the solvent/non-solvent preparation system dictates how the membrane will perform [92, 93]. This being due to differing pore structures obtainable from varying solution chemistry and other such preparation conditions [94]. Membrane material is central to the desired application. Table 2-4 shows common polymeric materials used for commercial MF/UF membranes.

2.2.2 Fabrication

A range of fabrication techniques for polymeric membranes are reviewed in Table 2-5. Of applicability to this work are the phase inversion methods; the predominant techniques employed to make MF/ UF membranes.

Table 2-5 - Membrane fabrication techniques

General principal/technique		*Description*
phase inversion	immersion precipitation	polymer solution is immersed in a non-solvent causing demixing of solvent and precipitation
	evaporative phase separation (solution casting)	solvent or solvent/non-solvent blend is evaporated to precipitate the polymer
	thermally-induced phase separation	solvency is reduced by a decrease in temperature which precipitates the polymer
	vapour-induced phase separation	non-solvent vapour (e.g. humid air) causes demixing of the solvent/polymer blend
interfacial polymerisation		a polymer support membrane (e.g. polysulfone) is immersed in aqueous phase (e.g. ethylene diamine). The impregnated support is then immersed in an organic phase (e.g. trimethyl chloride in toluene) which cross-links to form a thin-film composite membrane [95]
track-etching/chemical etching		polymer films are irradiated, damaging the film in linear (latent) tracks forming pores, which can be further opened by chemical treatment
stretching		polymer sheets are heated to a liquid state and extruded before stretching [91]
electrospinning		A potential is applied between a droplet of polymer solution and a collector, a doped syringe extrudes a tailored-property fibre which is bundled at the collector to form an amorphous membrane

As already mentioned, solution chemistry is an important factor for these methods, and the use of additives as pore forming agents or pore modifiers is well-established to modify morphology and properties [91]. Organics such as poly(ethylene glycol) (PEG) or polyvinyl pyrrolidine (PVP) are added to polymer dope solutions to improve membrane performance [96-98]. One particular study by Ochoa *et al.* (2001) [99] discovered that adding low

concentrations of PVP (up to 2 wt.% relative to total polymer) as doping agents into PES casting solutions improved membrane permeability and modified pore size distribution; the M_w of the PVP having influence over pore size also. These authors speculate that PVP permeability is increased due to greater hydrophilicity as a result of the presence of the carbonyl group on PVP. Lafreniere *et al.* (1987) [98] attributed the pore size increase in the same polymer system to PVP's role as a non-solvent swelling agent, which creates macrovoids upon its entrapment in the polymer matrix. This is supported by the findings of Marchese *et al.* (2003) [100] who suggest that an effective membrane thickness decrease is apparent, given the increased macrovoid presence in the membrane sub-layer.

2.2.3 Polymer-solvent interactions

Of fundamental importance to membrane fabrication for immersion/precipitation techniques is the dispersion of polymers in solution. Knowledge of system formulation for preparation of casting solutions is paramount for successful membrane preparation. The same theories can also be related to the prediction of how prepared membranes may react to certain solvents, which has relevance to this work and to broader organic solvent membrane separations.

Hildebrand (1916) [101] theorised a solubility parameter derived from a fluids internal pressure, which could be used to benchmark relative solvency or miscibility when combined. Later work showed that this internal pressure was proportional to a term called the cohesive energy density – the energy required to disperse a volume of molecules to an ideal gas – and the theory was expanded accordingly [102]. Hildebrand (1936) [103] later defined the solubility parameter δ as the square root of this cohesive energy density term (see eq. 2-1). It was the first time a single number could be assigned to a component of a system in order to measure its miscibility with another component, also having a δ term. The closer these terms are to each other, the better the solubility of one in the other.

$$\delta^2 = n\left(\frac{\partial E}{\partial V}\right)_T = \frac{\Delta H_v - RT}{V_m} \qquad (2\text{-}1)$$

Where n is a proportionality constant connecting the system internal pressure, $(\partial E/\partial V)_T$, with the cohesive energy density (right hand side) where ΔH_v is the latent heat of vapourisation, R is the ideal gas constant, and V_m is the fluid molar volume. The constant n is close to unity for nonpolar molecules making internal pressure and cohesive energy density equivalent for these fluids, though this relationship breaks down when polar forces are present. This fact, where only dispersion forces are considered, makes the prediction of solvency for two fluids particularly unsuitable in systems where hydrogen bonding or other polar interactions occur, for example, alcohols, water, and polymers. These arguably represent the majority of situations.

A tool more applicable to the real-world was developed by Charles M. Hansen and published in 1967 [104]. The method involves treating the Hildebrand parameter as a lumped parameter comprising the summation of the relative contributions from dispersion forces (δ_d), polar forces (δ_p) and hydrogen bonds (δ_h); each term having a respective

cohesive energy density (see eq. 2-2). These relative contributions can be represented in a three-dimensional map termed the Hansen solubility space.

$$\delta^2 = {\delta_d}^2 + {\delta_p}^2 + {\delta_h}^2 \tag{2-2}$$

In practical usage, it is more fitting to relate these terms for two solvents (for miscibility assessment) or for a solvent-polymer system (solvency or swelling indication). Numerous experiments have been performed with a range of polymers and solvents since the use of these parameters began, and now an expanse of data are available in the literature [105]. These experiments involve the controlled mixing of the component parts of the system and analysis to measure the degree of dissolution. As a general example, the solubility of a polymer can be assessed based on the performance of solvents to dissolve it. Following experimentation, a point in the three-dimensional Hansen solubility space can be plotted with a circle with a radius r_o which envelops the solvent position. This analysis is represented in Figure 2-5.

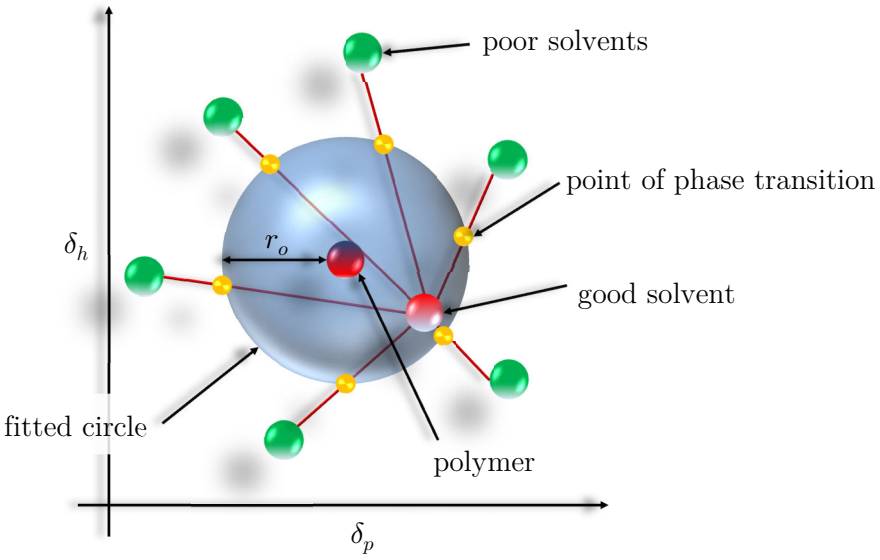

Figure 2-5 – A two-dimensional simplification of the three-dimensional Hansen solubility space for determination of parameters and interaction radius of a substance e.g. a polymer. r_o is the experimentally determined sphere representing the interaction radius i.e. the boundary between good solvents (inside of sphere) and poor solvents (outside of sphere) After Milliman *et al.* (2012) [106].

Assuming prior knowledge of the solubility parameters (δ_{x_p}) and interaction radius (r_o) for a given polymer, and the solubility parameters for the proposed solvent ($\delta_{x\,sol}$), equation 2-3 can be applied to assess the relative distance (r_a) between the two in the Hansen space. Following this, calculation of the relative energy difference (RED) by division of the relative difference by the interaction radius as shown by equation 2-4 is made.

$${r_a}^2 = 4(\delta_{d_p} - \delta_{d\,sol})^2 + (\delta_{p_p} - \delta_{p\,sol})^2 + (\delta_{h_p} - \delta_{h\,sol})^2 \tag{2-3}$$

$$RED = \frac{r_a}{r_o} \tag{2-4}$$

If the *RED* is less than one it would be concluded that the solvent is question would dissolve the polymer. If this value is around unity it would be concluded that the system would show partial solubility e.g. swelling. If the value is much greater than one the polymer would be stable and no dissolution would occur.

The parameterised system for measuring solubility of polymers offers a powerful tool for application in a range of fields. Notable from Figure 2-5 is the idea of varying the proportion of good solvent added into a poor solvent up to a point where dissolution could occur (though perhaps not as efficiently as with a pure, good solvent). With regard to mixing solvents; the parameters change linearly with volume proportion. Not only does this allow for facile parameter calculation of a solvent blend, but also provides a means to optimise the system in terms of solvency capacity, cost, safety and minimisation of solvent loss through evaporation.

2.2.4 Membrane Characterisation

Membrane characterisation of properties such as species rejection presents a means of rating a membrane. When working with UF membranes, both membrane charge and the ionic environment in which the molecules reside can play key roles in species rejection [107], though cut-offs for some proteins or other macrosolutes may differ. For specific applications, testing must be carried out to ascertain the performance on a case by case basis. Nevertheless, formalisation of membrane properties in terms of solute rejection is a useful starting point and necessary in an industrial context. Techniques for measuring this, and the measurement of pore size, are discussed in this section.

2.2.4.1. Solute rejection and nMWCO

The rejection of components is measured in terms of a ratio between the concentration change in the feed stream and the permeate stream as shown in eq. 2-5.

$$R = 1 - \frac{C_p}{C_f} \tag{2-5}$$

where R is the rejection coefficient, C_p is permeate concentration, and C_f is the feed concentration.

In order to calculate nMWCO, the membrane is challenged with a variety of molecules with known molecular weight. This type of test is normally performed with low concentrations of inert and cheap molecules such as PEGs or dextrans. They are inert in terms of chemical stability and charge, so as to avoid degradation and fouling. The concentration can be measured with relative ease in mixtures of varied molecular weight e.g. with size exclusion chromatography.

Upon calculation of rejection coefficients for each molecular size, a graph similar to that of Figure 2-6 can be produced. This shows MWCO plots for three UF membranes. The plot of solute size (either absolute size or M_w) versus rejection yields a sigmoidal curve (fitted in this instance arbitrarily to a 3 parameter sigmoidal model). The M_w for which 90% of species are rejected represents the nMWCO (as denoted by the dotted line across the PM10 curve). For a perfect membrane (dot-dash line) there is a sharp cut-off at a single given M_w, any solute larger than this having 100% rejection. An absolute rating would be the lowest M_w where 100% of the given component is rejected.

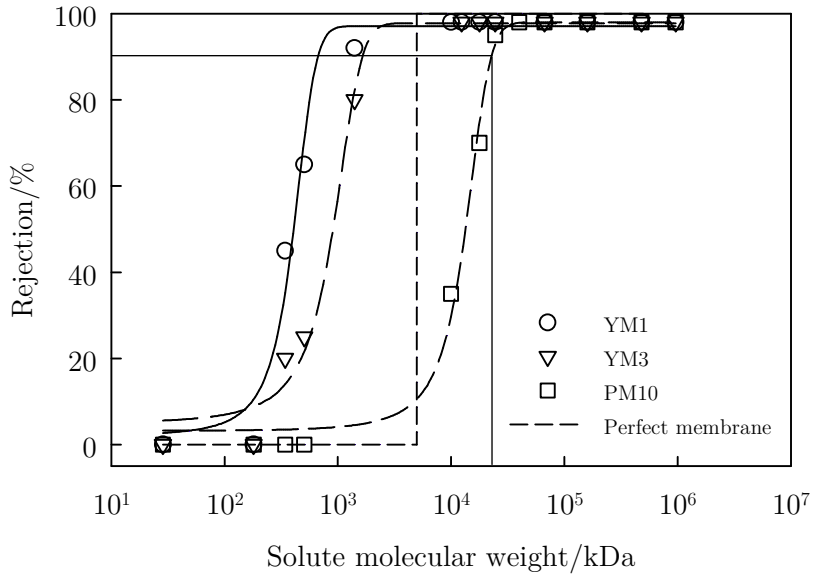

Figure 2-6 - Solute size and rejection for various Amicon membranes (data reproduced from Cheryan (1998) [46]; dotted line denotes nMWCO)

2.2.4.2. Pore size distribution measurement

The IUPAC recommendations for physisorption in gas-solid systems; micropores are those with $d_p < 2\ nm$, mesopores are $2\ nm < d_p < 50\ nm$, and macropores are $d_p > 50\ nm$ [108]. Whether these should extend to liquid-solid separations with porous membranes is a matter of speculation though they can provide a useful guideline. For MF membranes, pores would fall only into the macroporous range. For UF, pores could span all three of these categories, though the majority of the distribution would lie in the mesoporous band. Pore size distributions for membrane pores at the mesopore scale can generally be modelled on log-normal distributions in terms of pore number or equivalents, such as liquid displacement in the case of porosimetric techniques, or amount of gas for monolayer physisorption.

Knowledge of the pore sizes and distribution thereof is perhaps one of the most useful measurements a membrane manufacturer or user can possess. Being able to relate pore sizes to relative size of molecules allows for a better understanding of feasible separations for respective membranes, as well as providing a means to test other theories e.g. separations where charge is the dominating rejection-affecting mechanism over size. There

are a number of techniques used for assessing pore size distribution, some with greater resolution than others across the micro- and nanoscopic ranges and smaller.

These techniques can be loosely divided into visual and physical techniques, fluid permeation tests, or solute permeation tests (as discussed in 2.2.4.1). A non-exhaustive list for techniques to measure pore size distribution is shown in Table 2-6.

For solute permeation tests, extraction of the pore distribution can be made by assuming pores to be equivalent in diameter to the solute Stokes' radius with knowledge of particle diffusivity, a methodology for which is displayed clearly by Singh *et al.* (1998) [109].

Table 2-6 - Techniques for measuring pore size distribution or cut-off

Characterisation principle		
Visual/physical analysis	*fluid (gas/liquid) permeation*	*solute permeation*
scanning electron microscopy (SEM)	gas sorption	PEG filtration
transmission electron microscopy (TEM)	bubble-point method	dextran filtration
atomic force/scanning tunnelling microscopy (AFM)	gas permeation	protein filtration
Small angle x-ray scattering (SAXS)	mercury intrusion porosimetry	
	liquid-liquid porosimetry	
	liquid-solid porosimetry	

Visual techniques involve taking a picture of the membrane surface and post-processing the image to give pore sizes. Nakao (1994) [110] gave a review of imaging and post-processing methodologies of SEM micrographs, amongst other fluid permeation techniques. One drawback of the top-down surface imaging is the lack of insight into the underlying pore structure and distribution. Yan *et al.* (2006) [111] showed this effect clearly (see Figure 2-7). The authors do not specify exactly how the inner pore structure image was produced, though it shows clear differentiation from the left-hand image. Also clear is that the pore size and morphology changes drastically through the membrane cross-section. Quantifying the pore diameters in a formalised probability distribution function thus proves challenging if sub-surface features are accounted for.

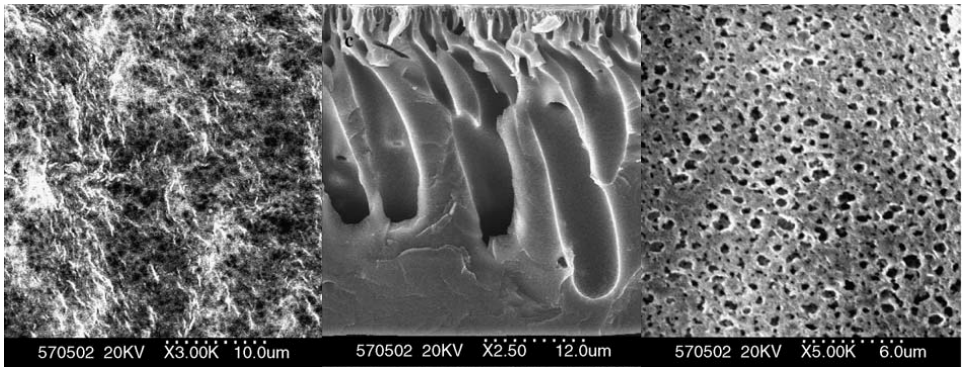

Figure 2-7 - SEM micrographs of a PVDF UF membrane; membrane surface (left), cross-section (middle), inner pore structure (right). Reprinted from Yan et al., (2006) [111]. Copyright 2006 with permission Elsevier.

Ochoa *et al.* (2001) and Singh *et al.* (1998) [99, 109] used AFM and solute permeation to elucidate their pore size distributions (an example of which is seen in Figure 2-8). A pore size distribution was extracted from image data for three membrane types, all within the z-axis (peak/trough) range of 20 nm. The process used to extract the distribution was based on pore area resulting in estimation of the Feret pore diameter. Whilst being a mathematically sound methodology, obtaining a representative measurement from small sample areas of membranes (area ~600 nm^2 in the case of Ochoa *et al.* (2001) [99]) poses large time constraints, as AFM gives relatively low information yield to bulk sample representation (in terms of area analysed).

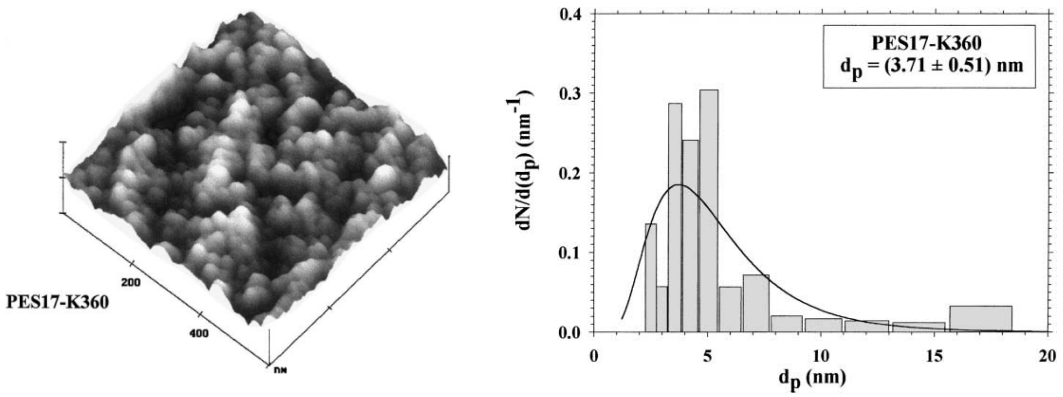

Figure 2-8 - AFM micrographs (left) and corresponding pore size distribution with log-normal probability function fitted (right). Reprinted from Ochoa et al., (2001) [99]. Copyright 2001 with permission from Elsevier.

Fluid permeation methods receive much focus in the literature given the direct method of obtaining data [112-114]. Porosimetric techniques involve the forcing of a non-wetting fluid into porous networks, this being extended to immiscible liquids for liquid-liquid displacement, or melting point changes for liquid-solid displacement porosimetry. In the context of mercury intrusion porosimetry, mercury is forced under pressure into pores; a given pressure corresponds to a pore diameter. The volume of mercury is recorded for the pressure increment allowing for the incremental volume/mass of mercury to be ascertained. Pressure is related to a pore diameter by a force balance (the Washburn equation) – the

force required to overcome the surface tension and achieve breakthrough into the pore (eq. 2-6).

$$P = -\frac{4\gamma cos\theta}{d_p} \tag{2-6}$$

where θ is the contact angle of mercury with the material (normally 140°), γ is the surface tension of mercury, d_p is the porous diameter and P is the pressure. The total volume of mercury which fills the sample is the total membrane porosity. A benefit of this method is the relatively large sample size that can be measured ensuring representative data over SEM/AFM techniques. It is however destructive and reclamation of all mercury is not-possible, there are also concerns that there may be contortion of samples for less dense/stiff materials [115]. The technique does however give resolution and discrimination of pore diameters down to < 2 nm and as low as $\pm$ 1 nm precision.

2.3 Membrane performance and engineering aspects

2.3.1 Membrane flux

Membrane flux is of great interest to the process engineer. Flux, as has been mentioned briefly, is the flow rate of material (be this on a mass or volume basis) through the porous membrane per unit area. The flux is proportional to the driving force (pressure) between feed and retentate and is related by the permeability of the membrane (or indeed any porous medium) and the distance through which permeation occurs. The original works by Henry Darcy in 1856 [116] helped him formulate the defining law (eq. 2-7); it forms the basis of experimental flux and resistance measurements.

$$Q = \frac{-kA}{\mu}\frac{(P_p - P_f)}{L} \tag{2-7}$$

where Q is the volumetric flow rate, k is the intrinsic permeability constant of the medium, A is the permeation area, μ is the permeating fluids dynamic viscosity, $P_p - P_f$ is the differential pressure between the feed and permeate, and L is the distance travelled (or thickness of the medium). The differential pressure for a membrane system is normally defined as the transmembrane pressure (TMP) and referred to as ΔP.

For membrane performance, standardising the flow rate by the area permeated gives the membrane flux (J), and combining the permeability constant of the medium with the thickness to give the specific membrane resistance R allows the generalised membrane formula (eq. 2-8) to be defined as follows:

$$J = \frac{\Delta P}{\mu R} \tag{2-8}$$

where:

$$R = -\frac{L}{k} \tag{2-9}$$

2.3.2 Theoretical flux

The Hagen-Poiseuille model relates the flux to the pressure drop across the membrane, the pore diameter and applied TMP considering the fluid viscosity, the membrane thickness (or channel length) and surface porosity as in eq. 2-10 where ε is the fractional surface porosity, d is the pore diameter, ΔP is the TMP, μ is the fluid viscosity, Δx is the thickness, and τ is the pore tortuosity. The model is diagrammatically represented in Figure 2-9.

$$J = \frac{\varepsilon d_p^2 \Delta P}{32 \Delta x \tau \mu} \tag{2-10}$$

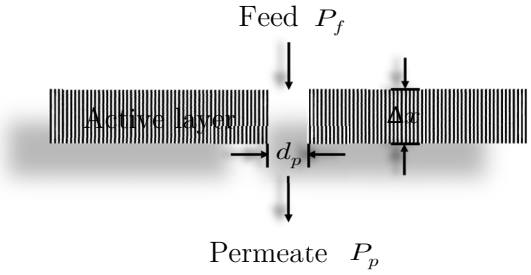

Figure 2-9 - Diagrammatic representation of the Hagen-Poiseuille model (where $\Delta P = P_f - P_p$)

Application of the model assumes no fouling and negligible concentration polarisation to be present. Whereas Darcy's law assumed a constant permeability for the medium, the Hagen-Poiseuille equation accounts for system geometry. For an ideal membrane system, pore diameters are assumed to be perfectly uniform in terms of circularity and width. For a practical application of this model however, pore distribution can be highly heterogeneous and thus inclusion of the distribution profile may be necessary in predictions of fluxes. Pores can be tapered from one end to another, as well as being tortuous.

2.3.3 The pressure-flux relationship

The influence of TMP on flux has been studied by numerous authors e.g. [25, 117, 118]. Evans and Bird (2006) [25] showed a strong dependency of flux on pressure during repeated 30 minute filtrations of black tea. A moderate difference was seen in terminal flux for 1.0 to 4.0 bar TMPs though initial fluxes showed stronger variation resulting in flux averages of *ca.* 30 $Lm^{-2}hr^{-1}$ at 1.0 bar and *ca.* 50 $Lm^{-2}hr^{-1}$ at 4.0 bar. De Barros *et al.* (2003) [119] did not record significant terminal flux increases differences when filtering pineapple juice at 0.2, 0.8 and 2.0 bar. These researchers found that during the early stages of filtration, flux decline was observing a pore blocking model though it reduced to cake filtration towards the latter stages of flux; this likely limited the flux at a standard value regardless of TMP (pore blocking phenomena is discussed in 2.4.2.2).

Both equations 2-7 and 2-10 show a proportional relationship between TMP and flux. The other variable in these equations which also affects flux is viscosity, itself a function of temperature, solution concentration and for non-Newtonian fluids, shear rate. Increasing temperature and decreasing concentration (both reducing viscosity) would give increased

flux for a given membrane and TMP (as shown by De Barros *et al.* (2003) [119]). There is however a deviation from this relationship at high TMP and high concentration. In this region the Hagen-Poiseuille model breaks down.

Figure 2-10 shows this effect. In the pressure dependant region, back diffusion from the membrane into the bulk is minimal, if not negligible, and the membrane flux remains linear with TMP. When pressure is increased, the dominance of the back diffusive effect from the membrane to the bulk is greater as polarisation layers are consolidated (discussed further in section 2.3.4). This is the mass transfer dependant (or limiting flux) region. Increasing pressure in this region can have little or no effect on flux and has even been shown to impact negatively on flux [30]. In order to affect flux in this region, a strategy is to disrupt the boundary layer by enhanced mixing at the membrane surface, achieved by increasing the CFV. Mass transfer - flow regime relationships are discussed in more detail in section 2.3.5.

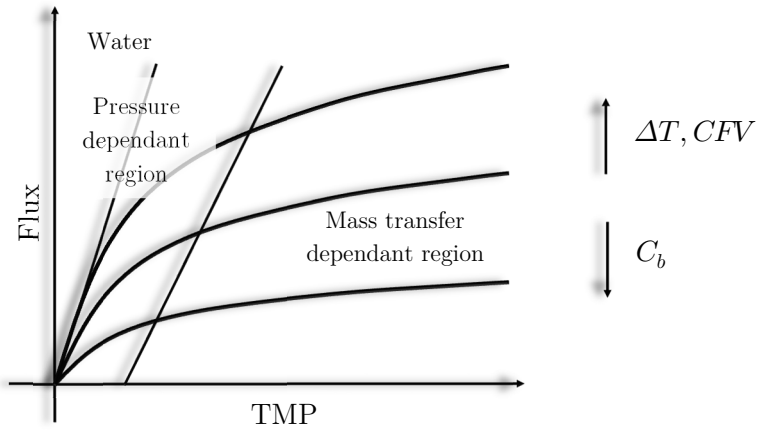

Figure 2-10 - Pressure-flux relationship and influence of operating parameters

2.3.3.1. Critical flux hypothesis

Operating in the sub-limiting flux regime is famously associated with the hypothesis of Field *et al.* (1995) [117] and the concept of critical flux. This is that, '*On start up there exists a flux below which a decline of flux with time does not occur; above it fouling is observed*'. This means that if the TMP at which the critical flux occurs is exceeded, then the membrane becomes fouled irreversibly and that if the TMP is subsequently reduced, the prior TMP-flux operation cannot be recovered i.e. a TMP higher than before is required to give the previous flux. This work is somewhat seminal in the area of MF and has subsequently been applied to UF processes in numerous studies (e.g. [120, 121]). The argument for the existence of critical flux has informed process design of constant flux operations whereby the TMP does not require continual adjustments (increases) to maintain a constant flux situation.

Some processes have 'strong critical flux' in which there is a long and well-defined linear flux-TMP relationship (closely allied to PWF), whereas a 'weak critical-flux'

displays a more short-lived linear relationship and the critical flux is lower (yet still stable with time). Later, the idea of sustainable flux arose, whereby a low fouling rate is accepted as inevitable, and the operational TMP accounts for this [122].

2.3.4 The concentration boundary layer

For a membrane which completely or partially rejects a solute ($0 < R \leq 1$) the rate of solute transport through the membrane is less than the rate of convective transport from the bulk to the membrane surface. Thus there exists a boundary layer over which a concentration gradient is apparent and there is an accumulation of solutes at the membrane surface. This concentration gradient thus provides a driving force for material to diffuse away from the membrane surface back into the bulk (by consideration of Fick's first law of diffusion). This is shown graphically by Figure 2-11.

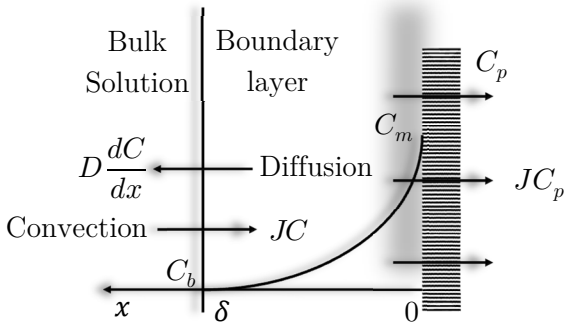

Figure 2-11 - Concentration polarisation boundary layer at the membrane surface gives rise to resistance (δ is the boundary layer thickness between 0 (at the membrane surface) and tends in the x direction to the bulk solution concentration)

2.3.4.1. Concentration polarisation

Completing the mass balance across the boundary layer gives equation 2-11. The ODE can be solved by considering: $\lim_{x\to 0}(C) = C_m$ and $\lim_{x\to \delta}(C) = C_b$, which yields eq. 2-12.

$$JC = D\frac{dC}{dx} + JC_p \tag{2-11}$$

$$J = \frac{D}{\delta} ln\left(\frac{C_m - C_p}{C_b - C_p}\right) = kln\left(\frac{C_m - C_p}{C_b - C_p}\right) \tag{2-12}$$

where k is the mass transfer coefficient. The following analyses are of great practical importance as they link the theoretical concentration maximum at the membrane surface to the bulk value. They give rise to two rejection coefficients, apparent and maximum (R_{app} and R_{max} respectively). Substituting rearrangements of eq. 2-5 into eq. 2-12 and linearising gives eq. 2-13, the final form, from which k, R_{max}, and C_m can be determined.

$$ln\left(\frac{R_{app}}{1-R_{app}}\right) = ln\left(\frac{R_{max}}{1-R_{max}}\right) + \frac{J}{k} \tag{2-13}$$

Noteworthy about equation 2-11 is the absence of a pressure term and thus no relationship between pressure and flux can be ascertained from this model. This implies that the model is only valid in the mass transfer dependant.

2.3.4.2. Gel layer model

For instances such as dewatering of feeds where 100% rejection of solute is present, the gel layer model can be employed. The model is based on a thin film assumption with a homogenous gel layer i.e. gel layer concentration (C_g) is constant at any distance from the membrane i.e. a highly polarised system. Eq. 2-12 thus becomes:

$$J_{lim} = k_g ln\left(\frac{C_g}{C_b}\right) \tag{2-14}$$

where k_g is the mass transfer coefficient for the gel layer and J_{lim} is the limiting flux where any increase in TMP will have no effect [123, 124]. Pressure independent flux is discussed further in 2.3.3.

2.3.5 Mass transfer – classical correlations and current trends

2.3.5.1. Dimensional analysis

An appreciation of the mass transfer with respect to operating parameters, system geometry and fluid properties can be taken from dimensional analysis by use of the π theorem. The product of the dimensionless groups (Reynolds number (eq. 2-17) and Schmidt number (eq. 2-18) gives a general correlation for the ratio of convective to diffusive mass transfer in a channel of hydraulic diameter (d_h) (eq. 2-19). This is termed the Sherwood number (eqs. 2-15 and 2-16).

$$Sh = A(Re)^{\alpha}(Sc)^{\beta} \tag{2-15}$$

where:

Sherwood number	$Sh = \frac{kd_h}{D}$	$\frac{convective\ mass\ transfer}{diffusive\ mass\ transfer}$	(2-16)
Reynolds number	$Re = \frac{\rho u d_h}{\mu}$	$\frac{inertial\ forces}{viscous\ forces}$	(2-17)
Schmidt number	$Sc = \frac{\mu}{\rho D}$	$\frac{viscous\ forces}{diffusive\ mass\ transfer}$	(2-18)
hydraulic diameter*	$d_h = 4\frac{ab}{2(a+b)}$	(for rectangular ducts)	(2-19)

*$d_h = d$ for circular channels. For slits, since $a \gg b$, $d_h \to 2b$; where a is channel width and b is channel depth.

For these correlations, k is the mass transfer coefficient as previously defined, u is the cross flow velocity in the channel, μ is fluid viscosity, ρ is solution density and D is the diffusivity. The constants α and β are dependent on the development of both velocity and concentration profile development in the channel. A is related to physical property variations in the system and is typically not determined from first principles [46] though a solution can be made using corrections for density, viscosity and diffusivity (see Kozinski and Lightfoot (1972) [125]). There are a number of solutions for these correlations as shown in Table 2-7.

For laminar flow situations where velocity profile is fully developed and concentration profile is developing i.e. $L_u < L^*$, $L_c > L^*$ where L^* is channel length, L_u is velocity profile length and L_c is concentration profile length, eq. 2-15 is rewritten as:

$$Sh = A(Re)^{\alpha}(Sc)^{\beta}(d_h/L)^{\omega} \qquad (2\text{-}20)$$

Table 2-7 - Mass transfer correlation models and constraints [46, 126, 127])

Flow regime	*Correlation name*	*Constants*	*Condition*
Laminar ($Re \leq 2000$)	Graetz-Leveque	$A = 1.86$, $\alpha = 0.33$, $\beta = 0.33$, $\omega = 0.5$	$L_{u,C} < L^*$
	Grober	$A = 0.664$, $\alpha = 0.5$, $\beta = 0.33$, $\omega = 0.5$	$L_u < L^*$, $L_C > L^*$
Turbulent ($Re \geq 2000$)	Chilton-Colburn/Dittus-Boelter	$A = 0.023$, $\alpha = 0.8$, $\beta = 0.33$	$Sc < 1$
	Deissler	$A = 0.023$, $\alpha = 0.875$, $\beta = 0.25$	$1 \leq Sc \leq 1000$
	Harriot-Hamilton	$A = 0.0096$, $\alpha = 0.91$, $\beta = 0.35$	$Sc > 1000$

An appreciation of the relative entry lengths of the channel to the development of longitudinal velocity and concentration profiles can be found using eqs. 2-21 and 2-22.

$$L_u = BRe^x d_h \qquad (2\text{-}21) \qquad\qquad L_c = \frac{0.1\gamma_w {d_h}^3}{D} \qquad (2\text{-}22)$$

where B and x are 0.06 and 1 for laminar flow, 4.4 and $\frac{1}{6}$ for turbulent flow, and γ_w is the wall shear rate.

2.3.5.2. Influence of cross flow velocity

Now that the Sherwood number has been defined, a theoretical appreciation of how to improve solute mass transfer i.e. mass flux through the membrane is clear. Increasing the Sherwood number is a result of either an increase in convective mass transfer or decrease in diffusive mass transfer. An increase in the cross flow velocity would have the result of increasing the Reynolds number and since $Sh = f(Re, Sc)$, Sherwood number and thus

mass transfer would increase (given that the diffusivity coefficient and channel diameter remain constant). This effect occurs due to the increased shear stress induced by an increase in cross flow velocity, and in real terms, it affects the system by sweeping material from the membrane surface - the overriding principal of cross flow filtration. Belfort *et al.* (1988) [48] attribute the thinning of the polarisation layer to this phenomenon. Bartlett (1998) [128] stated that increasing mass transfer is achieved by reduction of this polarisation effect.

2.3.6 Generalising the pressure-flux relationship

2.3.6.1. Resistance-in-series

The resistance-in-series model provides a practical means of attributing the flux of the membrane to different causes of resistance. It is widely applicable given its non-phenomenological and generalised approach to membrane filtration. Resistance to flux can be caused by the intrinsic permeability of the membrane (2.3.1), concentration polarisation (discussed in section 2.3.4), and fouling (section 2.4).

By expansion of the resistance term in eq. 2-8, the generalised membrane equation becomes:

$$J = \frac{\Delta P}{\mu(R_m + R_{cp} + R_f)} \tag{2-23}$$

Where R_{cp} is the resistance due to polarisation effects and R_f is the fouling resistance. The equation is analogous to electrical resistors in series and has found application in a number of membrane filtration studies [26, 129, 130] as it gives good indications of the relative contributions to flux loss. A detailed description of the methodology to determine the relative resistances is shown in section 4.5.1.

Leberknight *et al.* (2011) [131] show application of this model for concentration of proteins with different membrane materials in corn ethanol processing. The authors break down the resistance components into four categories: membrane, gel, irreversible and in-pore fouling resistances as proportions of the total resistance. They found that the irreversible fouling for 5 kDa PES membranes was 4-fold that of other membranes (5 and 100 kDa cellulose, 100 kDa PES). Cassano *et al.* (2007) [132] used a similar methodology though they attributed their resistances to the membrane itself, the cake layer, a reversible fouling resistance (defined as the PWF upon acid cleaning) and an irreversible layer which could not be removed after acid cleaning. It was found that the membrane resistance when clean was the most substantial (68% of total), and the reversible fouling accounted for 27% of the total. Around 3% was 'non-reclaimable' following their post-foul cleaning protocol.

These demonstrations show the versatility of this model to allow the experimenter to relate a membrane flux at any point during a foul-clean cycle to a resistance, and moreover, the effect of a given event on membrane performance. It must be stated that only fluids with the same properties can be used to define resistance values. In the most case, deionised water is this fluid, with flux being measured between foul or cleaning events.

2.4 Membrane fouling

Fouling is by definition the process of making something fouled or dirty [133]. Indeed fouling relating to membrane processes is the deposition of material onto the surface or into the porous network. Fane and Fell *et al.* (1987) [134] state that if flux decline is not reversible by a change in operating conditions, the effect is termed as 'fouling'.

In an ideal membrane separation process there should be a constant flux of solute equal to the pure water membrane flux, with 100% of the desired transmitted solute permeating the membrane, and 100% of the desired retained solute remaining in the retentate. In reality this does not occur and as a result, a decline in flux is observed due to accumulation and deposition of solutes. Consequently there is a partial blocking of the membrane. This partial blocking and subsequent solute attachment (if any) is the effect of fouling, and is related to both physicochemical properties of the feed solution as well as properties of the membrane, such as porosity [134].

The characterisation of fouling for model solutions and real feed stocks in membrane systems is a complex area of study, reflected by the wealth of literature in the scientific domain. In order to review and analyse this literature, an introduction to the definitions for types of fouling is made alongside practical examples. This foundation then allows for a theoretical understanding and mechanistic insight of more specific scenarios relating to the reasoning of how and why fouling occurs; the summation of this being a broader picture of membrane fouling as a field of research.

The section characterises the nature of foulants, the reasons why deposition of foulants reduces membrane performance, and the inter-play between membrane properties and foulant types.

2.4.1 Building a mechanistic picture

Liu *et al.* (2001) [135] proposed four types of membrane foulant classifications:

Inorganic fouling (or scaling): Fouling layers are formed on or within membranes due to an accumulation of inorganic precipitates. This can occur when the concentration of inorganics in solution reaches its saturation point. Chemical bonding (ionic interactions) between inorganic ions and membranes/other foulants can also occur as a combinatory mechanism [136], this being noted specifically by Sahachaiyunta *et al.* (2002) [137], who showed that the addition of trace amounts of Fe^{3+} ions exacerbated silica fouling on RO membranes.

Particulate fouling: In the context of biologically or chemically inert species; these particles accumulate on membrane surfaces and inside pores acting to reduce flux, though are not associated with adsorptive mechanisms. They are considered small enough relative to pore diameters to cause plugging effects. Hydraulic cleaning is deemed sufficient to remove these foulants [138].

Biological/microbial fouling: Biofilms are formed by the deposition and attachment of bacteria or other microorganisms to the membrane surface; proliferation then occurs. The excretion and accumulation of material in the form of a hydrated gel matrix termed extracellular polymeric substance (EPS) (into which the organisms become embedded) is the result [139]. The EPS structure forms a barrier, shielding the organisms from hydrodynamic forces and chemical cleaning agents [45]. It has been shown that biofilm development can have an extremely rapid formation [140]. In another study it was shown that polyether urea membranes have a reduced biological fouling tendency over polyamide and PS membranes [141].

Organic fouling: Organic molecules are highly varied given their diverse chemical functionality and molecular weight. As a result of this, membrane-foulant and foulant-foulant interactions are wide ranging, the effects becoming more complex when considering foulant mixtures and solution chemistry e.g. solvent type, pH, ionic strength. Much focus has been given to the deposition and attachment effects of this foulant type in relation to membrane fouling [142-145]. The aforementioned studies show generally that for a range of feeds, a significant proportion of the total hydraulic resistance during filtration was not due to polarisation or cake layer resistance, but due to the deposition (and sometimes adhesion) of organic molecules in the pores or on the membrane surface.

2.4.2 Effect on membrane process performance

2.4.2.1. Resistance due to fouling

Having defined fouling as a deposit build-up on or in the membrane and considering the resistance in series model discussed earlier in 2.3.6.1, refinements to the model can be made regarding the resistance due to fouling resistance term (R_f). With knowledge of the various types of foulants, characterising the mechanisms of deposition or attachment is now a logical step.

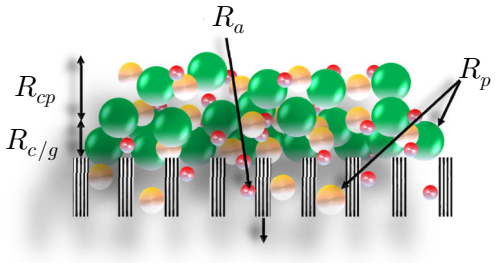

Figure 2-12 - Schematic representation for the differences sources of fouling resistance

The fouling resistance term R_f can be expanded to give a re-work of eq. 2-23 as follows:

$$J = \frac{\Delta P}{\mu(R_m + R_{cp} + R_p + R_a + R_{c/g})} \tag{2-24}$$

Where R_p is resistance due to pore blocking, R_a is resistance due to adsorptive fouling, R_c and R_g are cake and gel layer resistances respectively. This is represented in Figure 2-12.

2.4.2.2. Flux decline analysis

Flux decline in membrane filtration is a result of fouling and polarisation effects [146]. It has been related to a number of phenomena relating to hydraulic blockage of the membrane by various mechanisms. Its correlation with filtration time is generally accepted to abide by constant pressure blocking laws as originally developed by Hermans and Bredée (1936) [147] and adapted to their accepted form during application to non-Newtonian fluid filtration by Shirato *et al.* (1979) [148]. In terms of application to Newtonian fluids in membrane systems, Hermia (1982) [149] is widely credited with the common power law forms used for analysis of dead-end membrane filtration flux declines.

Tracey and Davis (1994) [150] conveniently divided the blocking mechanisms into two categories - internal and external fouling - as depicted in Figure 2-13. They apply two models, termed the standard blocking models and the pore blocking model (also called the complete blocking model), to resistance data for internally fouled polycarbonate track-etched membranes. In a similar vein to the earlier work of Hermia (1982) [149], the standard blocking model (giving rise to R_a) assumes that foulant deposits along the pore walls causing pore constriction (decrease in pore diameter) i.e. the pore number to membrane area ratio remains constant. The degree of constriction is dependent on the total volume filtered. The pore blocking model (giving rise to R_p) assumes that pores are completely plugged, therefore reducing the number of pores available for permeation, though pore diameter remains constant, and the same proportionality to volume filtered applies. Both of these models attribute the mechanism of decline to be a resistance change to the membrane, which contrasts the external fouling models where resistance of the membrane remains constant throughout, though remains a factor of the changing total filtration resistance.

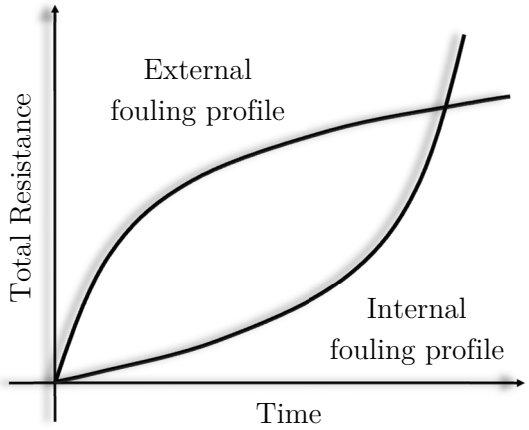

Figure 2-13 - Resistance profiles for internal and external fouling, after Tracey and Davis, 1994 [150]

The external flux decline model is termed the cake filtration model, which assumes a defined mass of solute is deposited on the membrane surface and is again proportional to filtrate volume. For this model a cake specific resistance can be defined independently of membrane resistance i.e. R_c. Prior to this study, Hermia (1982) [149] defined a fourth law of blocking named the intermediate blocking law which assumes a partial cake build-up on the membrane surface, though this model also accounts for unblocked or partially blocked pores. The basis of the models is shown in Figure 2-14.

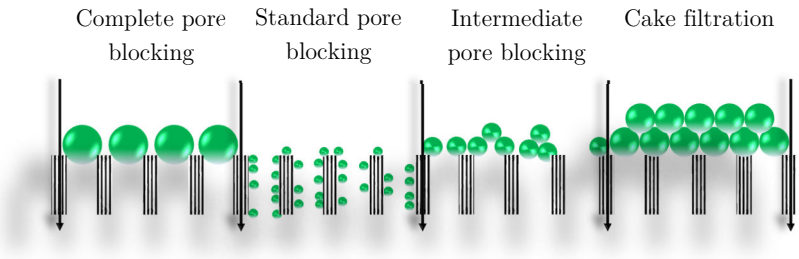

Figure 2-14 - Schematic description of blocking laws for membrane flux decline

Field *et al.* (1995) [117] developed these models further for cross flow filtration by accounting for solute removal. In the case of the complete pore blocking model, particles are removed from the mouths of pores to counter the effective decrease in available surface area. For intermediate blocking, a 'back flux' factor functions on the same basis. For standard blocking, since pore constriction inside pores is shielded from cross flow shearing, the model remains unchanged from the dead-end model. Finally for cake filtration, a cake erosion term is added; this is a time dependant term expressed as mass of cake removed per unit membrane area. If the rate of cake removal is assumed to be constant, the removal term reduces to a constant value.

For a mathematical description of the parameterised models, and methodology for solutions in the cross flow regime, refer to section 4.5.2.1.

2.4.3 Studying the nature of membrane surfaces

Flux and rejection are accepted as the universal performance parameters for assessing membrane performance during filtration. For membrane scientists to improve process performance, a deeper understanding of the membrane surface characteristics can lead to a mechanistic insight into how solutes and fluids can interact with the surface and pores. Surface science principles: the study of physicochemical interactions at phase interfaces, provide the foundation for this understanding. Specifically, looking at the adsorption potential (physisorption or chemisorption) at interfaces by consideration of wetting and chemical functionality can provide an appreciation of solute behaviour at membrane surfaces. Looking at the electrical double layer distribution of charges and dipoles can provide insight into solute-solute and solute-surface interactions. The remaining part of this section will review methods for studying virgin, fouled, and cleaned surfaces.

2.4.3.1. Wetting

Wetting or wettability is a measure of how readily a liquid contacts a solid substrate. The degree of wetting for liquids (predominantly aqueous solutions or water for UF) has long been recognised as a gauge for fouling potential, the general opinion being that more hydrophobic surfaces will adsorb material more readily, and this correlates positively with greater fouling tendency [151-153].

The reasoning for this increased sorption potential is hydrophobic interactions. Although not fully understood, one theory is that these interactions exist due to the exclusion of water and the formation of a solvation shell at the hydrophobe-water interface [154]. The solvation shell is formed due to energy minimisation at the interface through hydrogen bond rearrangement and is thus thought of as an entropic (thermodynamic) effect over the commonly assumed van der Waals force interactions between hydrophobic molecules [154]. The hydrophobic effect plays a pivotal role in protein folding, and the resulting structure and functionality through association of hydrophobic amino acid residues.

For measuring the wettability of a surface a number of techniques exist surrounding the behaviour of water on the surface. A force balance between the three phases (solid-liquid, solid-vapour, and liquid-vapour) at the 'triple point' of a droplet of water placed on the surface can be made (see Figure 2-15) using a goniometer (other apparatus used could be a Wilhelmy plate or tilting plate).

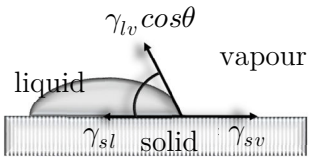

Figure 2-15 - Force balance for a sessile drop on a surface in surrounding vapour phase

The contact angle (θ) between the water and the surface is the unifying parameter which enables the completion of the force balance (eq. 2-25) and thus a measure of the surface wetting potential.

$$\gamma_{lv} cos\theta = \gamma_{sv} - \gamma_{sl} \tag{2-25}$$

where γ is the interfacial energy (or surface) between the phases, and subscripts s, v and l stand for solid, vapour and liquid respectively.

For contact angles below 90°, the surface is deemed hydrophilic, and for those above 90° where a bead of water forms, the surface is hydrophobic. For membranes used for aqueous phase based separations, the use of hydrophilic membranes is normal. A spontaneously wetting (hydrophilic) membrane allows for complete wetting of the porous network without the need for wetting agents to 'fill' the pores. The wetted membrane surface enables exclusion of hydrophobic foulants on or in the membrane structure by the presence of a thin water film. Figure 2-16 shows broad contact angle classifications.

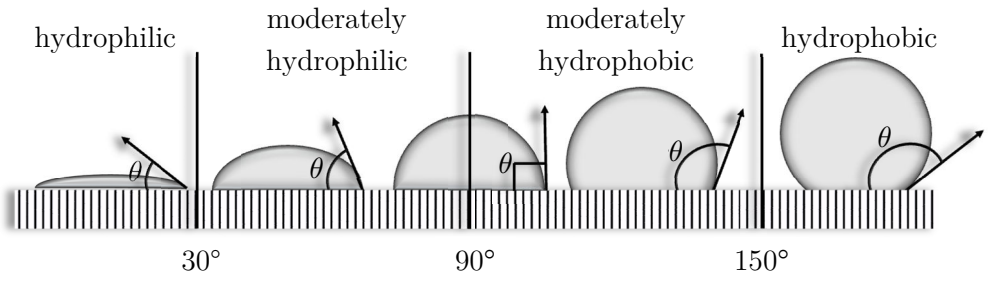

Figure 2-16 – Wetting classification

There is a depth of literature for membrane wetting characterisation using contact angles, for example [129, 155, 156]. These authors used the sessile drop method (water placed on upright surface). Using the same principal though inverted 180°, the captive bubble technique involves resting a buoyant bubble on the surface surrounded by the liquid phase. This method has been used by Susanto *et al.* (2009) [157] and Zhang *et al.* (1989) [158] among others; the latter asserting that by keeping the membrane wet, prevention of changes in surface properties is eliminated, which could arise as a result of drying or humidity variations. The complete immersion of the sample is also more reminiscent of the membrane *in situ*.

2.4.3.2. Wetting - deviations from ideal surfaces

Since membrane surfaces are heterogeneous (rough and porous), an appreciation of how this might affect the wetting properties must be considered.

If a surface is rough and pores are present, a droplet of water can bridge over air pockets which affect the contact angle. In this instance there are two models to describe the contact angle behaviour on the textured surface - the Cassie-Baxter and Wenzel models – both of

which describe the deviation from the intrinsic contact angle in equilibrium conditions, though for slightly differing circumstances (see Figure 2-17).

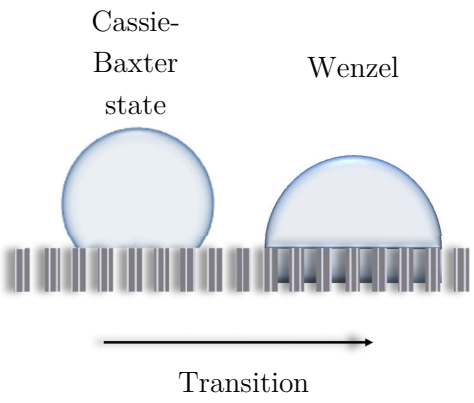

Figure 2-17 - Schematic representation of Cassie-Baxter and Wenzel wetting models

For the Cassie-Baxter model [159], a droplet sits over the surface voids of a heterogeneous surface and the water surface tension of the water at the water-air interface within the trapped air-pockets prevents full wetting of the surface. The contact angle measured is related to the fractional coverage of the surface by the droplet and the roughness ratio (ratio of true area to apparent area). Wenzel (1936) [160] described the case where there is a homogenous, rough surface on which the water droplet covers all of the surface area i.e. the free energy in the system has equilibrated to a minimum. When transitioning between the states, a 'mushroom state' can be formed where a small portion of rough troughs become wetted, though a full Wenzel state has not been achieved. For membranes which have been dried, with effectively bottomless pores (assuming the situation at the nano-scale), a droplet could form at any point within this transition. Wenzel (1936) [160] explains that roughness is an inherent property of wetting meaning that when considering membrane contact angles, an appreciation of the roughness change to the virgin surface contact angle is necessary for comparisons to be made.

2.4.3.3. Zeta potential

Electrostatic interactions between molecules are critical to explaining mechanisms behind batteries and electrode operation, ion exchange processes, crystal structures, drug aggregation and milk stability, among many others. The origin of charge at a membrane surface interface is due to dissociation of acidic or basic groups giving rise to charges [161]. Equally the dissociation of species from solutes gives rise to charged particles, the degree of dissociation being quantifiable by assessment of the dissociation constant (pK_a or pK_b). Determination of the zeta potential (ζ potential) inside membrane pores and on membrane surfaces is key to understanding electrostatic interactions which could arise from a surface chemistry perspective, this in turn can allow inference of interactions that could occur between organics, such as proteins and other food components [162].

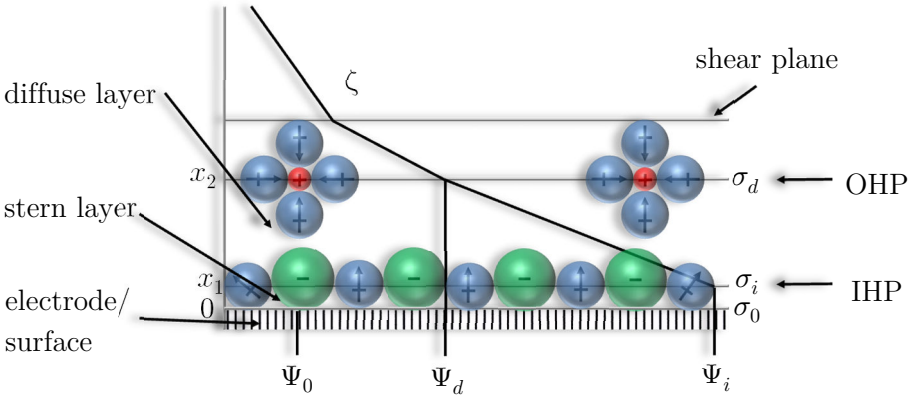

Figure 2-18 - Electrical double layer model for an aqueous ionic solution (after Hunter (1981) [163]). IHP – inner Helmholtz plane, OHP – outer Helmholtz plane. Ψ_0 is the surface potential, Ψ_d is the diffuse layer surface potential, Ψ_i is the IHP potential, σ_0, σ_i, and σ_d are the charge densities at the surface, IHP and OHP respectively, x represents distance from the surface. Blue molecules represent solvent molecules, green represents negatively charged ions and red represents counter-ions (in this case, cations). For streaming potential measurements, flow across the surface is induced i.e. left to right.

ζ potential is not directly measurable for membrane systems though it can be derived from streaming potential measurements. A streaming current is induced through a membrane by permeation with an ionic solution. A variation in ion density occurs at the solid-fluid interface due to the membrane's surface charge, with oppositely charged ions to the membrane surface's charge being attracted close to the interface. This creates an immobilised 'Stern layer' of ions along the wall. The direct effects of this are counter-ions (those oppositely charged to the Stern layer charge - the same as the wall) being attracted near to the surface to balance the excess charge. These counter-ions are not immobile and can flow however; this is termed the diffuse layer. The net result is a double layer system termed the electrical double layer (EDL), the thickness of which is called the Debye length and is a direct function of salt concentration. The convective flow of the permeating solution under hydrostatic pressure creates a stream of counter-ions giving rise to a potential through the pore [164]. Detection of this potential gives rise to a measurement of streaming potential. A model of the EDL is shown in Figure 2-18.

Practically, the measurement of streaming current and inference of ζ potential is relatively simple and has been made by a number of researchers. Perhaps the forerunners in the streaming current methodology in relation to membranes are the past and current workers from Lappeenranta University of Technology, Finland, who have contributed a large body of work over some 25 or so years. Some of the key publications in the area [107, 164, 165] demonstrate the versatility of the technique for membranes, and the relationship to subsequent fouling effects on membrane surfaces and inside pores. Arguably the seminal work for application of this methodology, by Nyström *et al.* (1989) [164], gives a review of data acquisition and subsequent interpretation. The analytical solution to the Helmholtz-Smoluchowski equation provides the necessary underpinning theory to relate the streaming current to the surface ζ potential (see eq. 2-26). Chan and Chen (2004) [162] state that most systems measure the sign (+/-) and change in a system rather than the absolute

value. Thus any derived quantity should be used for comparative purposes rather than focus on absolute numerical values.

$$\zeta = \frac{\Delta E}{\Delta P}\frac{\mu k}{\varepsilon_0 \varepsilon_r} \tag{2-26}$$

$\Delta E/\Delta P$ is the finite change in streaming potential with respect to TMP, μ is viscosity or the electrolyte solution, k is the solution conductivity and ε_0 and ε_r are the permittivity of free space and dielectric constant of water respectively.

Other groups have also used this or similar methodologies for interesting applications. Molina *et al.* (1999) [166] used streaming current measurements to confirm numerical solutions relating to charge density and surface potential theory for well-defined micro-porous membranes of varying pore size. Kim *et al.* (1996) [167] compared results for electro-osmotic and streaming current methods for ζ potential calculation and found that those values elucidated from the former method were greater than those from streaming current tests. This result was attributed to a greater directional charge produced from applying a potential to the system.

In terms of membrane fouling, measurement of pristine surfaces and those when fouled and cleaned gives an idea of how likely species are to attract to the surface. Cleaning efficiency can be ascertained when considering charge regeneration also. Nabe *et al.* (1997) [153] showed that membranes, differing only by charge for a given pH, showed differing protein sorption properties. The positively charged membrane showed greater sorption capacity of a protein (bovine serum albumin) since it is negatively charged at pH 6.8. Contrastingly the authors showed that while the sorption capacity was greater, the more polar nature of the positively charged (i.e. more hydrophilic) membrane meant removal of protein was easier during rinsing and thus the membrane was deemed to have fouled less. The conclusion was that surface energy was a more important factor than electrostatic interactions for the given system. Weis *et al.* (2005) [168] showed that when fouling a membrane with spent sulphite liquor, subsequent foul-clean cycles were insufficient in returning the membrane to their original charge when cleaning with a surfactant based cleaning agent. They concluded that the surfactant molecule was attaching to the membrane/foulant layer after each foul-clean event. It was also found that the use of NaOH was more effective than the surfactant based cleaner in terms of regeneration of original surface charge. This type of information is invaluable when it comes to food processing application where not only hygiene standards need to be upheld, but consistent performance is a necessity also. This study also demonstrates membrane fouling and cleaning synergy, which is discussed further in section 2.5.4.

2.4.3.4. Electro-viscosity

The electro-viscous effect (or electro-viscous retardation effect) is a phenomenon arising as a result of applying hydrostatic pressure to an ionic solution through a capillary on the surface of which there exists a charge. Upon establishment of a streaming current there exists an electrical potential in the opposite direction due to the imbalance of counter-ions

in the positive axial direction. Given this potential in the opposing direction to the flow, movement of mobile counter-ions occurs against the convective flow (in the negative axial direction). Since in an aqueous solution, counter-ions are hydrated (as was shown in Figure 2-18), the movement of the counter ions induces flow of solvent molecules in the negative axial direction creating a resistance to the convective flow. This manifests itself as a greater apparent viscosity [169]. The effect is shown in Figure 2-19.

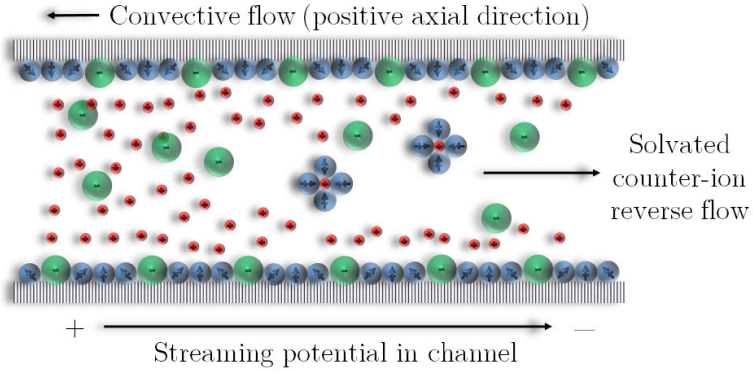

Figure 2-19 - Representation of the electro-viscous effect

Huisman *et al.* (1998) [170] provided a methodology for predicting membrane zeta potential through pores based on this phenomenon. They show flux variation for different ionic strength solutions and pHs, relating this to an apparent viscosity change, as specified earlier by Levine *et al.* (1975) [171]. In their earlier work, Huisman *et al.* (1997) [172] provided a plot of apparent viscosity against changing Debye length to pore radius ratio (salt concentration to pore diameter ratio in relative terms) and showed a viscosity maximum at the point where the pore radius is 2.5 times the Debye length. For a 1.0 mM KCl solution, the authors state that a measurable viscous range would be present for pores between 6 and 600 nm, which fits the approximate range for MF and UF membranes. The phenomenon has implications for membrane fluxes when considering that if a reduced surface charge was observed inside the pore, there would be a direct mechanism for flow enhancement through the pore, given the reduced counter-ion reverse flux. It implies this phenomenon may also extend to solute behaviour if the transmitting solute has significant acid or base dissociation.

2.4.3.5. Topographical analysis

Atomic force microscopy (AFM) is used for analysis of membrane morphology with regards to pore and surface characteristic. Discussed briefly in 2.2.4.2 was the use and merits of using AFM in determining pore size distribution. This section discusses how AFM is used to gauge the roughness of surfaces.

An AFM (sometimes referred to as Scanning Tunnelling Microscope) uses a probe - a sharp nanoscopic tip - attached to a cantilever which can detect sub-micron sized features. The resolution is provided by a laser focused on the back of a cantilever which is reflected and detected by a photodiode detector. Information relating to the precise position in the x-y plane (provided by a piezo-electric motor) and the z-axis change from cantilever deflections,

upon engagement of the tip with the sample, is collected. Cantilever deflections are brought about by probe-sample contact (contact mode or tapping mode with a set-point relating to the force applied by the probe) or solely intermolecular interaction between sample and probe (non-contact mode) (see Figure 2-20). The information enables construction of a 3D image over the desired scan area by way of a raster scan at a pre-set frequency. Tapping mode is the standard mode of operation today as it gives high lateral resolution and lower contact forces (less indentation of soft samples) [173]. The average roughness (R_a) is calculated by taking the average in the z-axis to give the x-y reference plane, then calculating the average deviation in the z-direction from the reference plane (see 4.4.1.4).

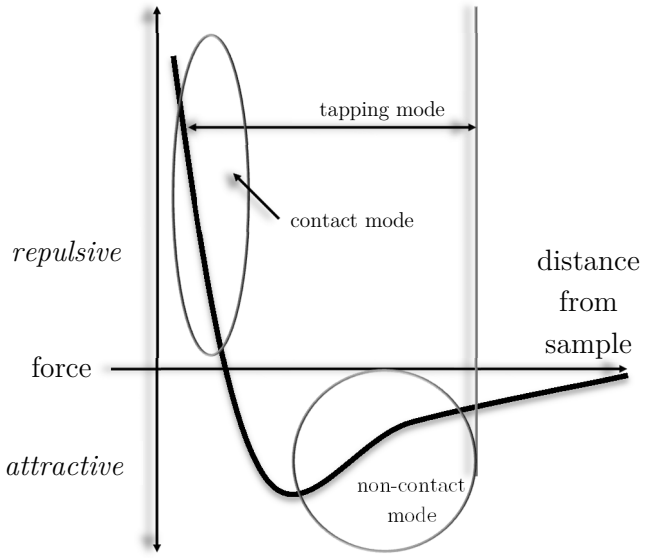

Figure 2-20 - van der Waals curve showing distance-force regions where AFM modes are operated

The use of AFM for studies of membrane surfaces is common, particularly with regard to membrane fouling [109, 174, 175]. The hypothesis that roughness plays an important role in fouling tendency has been confirmed by Weis *et al.* (2005) [168] among others. They show that despite being more hydrophilic, a rougher regenerated cellulose (RC) membrane had a greater fouling tendency for spent sulphite liquor over a more hydrophobic but smoother PES membrane. Evans (2008) [176] observed that a rougher fluoropolymer membrane (FP) with a 30 kDa cut-off fouled more substantially than a 10 kDa membrane of the same material (and manufacturer), and in turn, the smoothest 100 kDa membrane fouled the least. This trend was reinforced by ζ potential measurements showing that the 100 kDa membrane had the strongest negative charge, and the charge reduced in the same order as the roughness increased.

2.4.3.6. Specific membrane-foulant interactions

As well as being a topographical mapping tool, AFM can be used as a force gauge to measure intermolecular interactions. This can be done by bringing the probe (typically silicon nitride) near to a control surface, then retracting again to give a 'snap-in, snap-out'

of the tip resembling the adhesive and retraction forces acting at the molecular level, with resolutions possible in the piconewton range [162].

The technique was developed by Ducker *et al.* (1991) [177] who measured the forces between a silica sphere and a flat silica (mica) surface and concluded that the force curves were consistent with double layer theory, though at close distances, results were skewed somewhat by what they thought to be hydration forces. A similar methodology was applied later by Bowen *et al.* (1997) [178] at the University of Wales, Swansea for measurement of double layer interactions on MF and UF poly-carbonate membranes during probe to sample approaches. These authors showed that for a silicon oxide colloidal sphere approaching the surface (both negatively charged in the ionic conditions used) there was increasing electrostatic repulsion with decreasing NaCl concentration (see Figure 2-21). At close separations, there was again deviation from double layer theory, though the authors this time attributed this to steric effects.

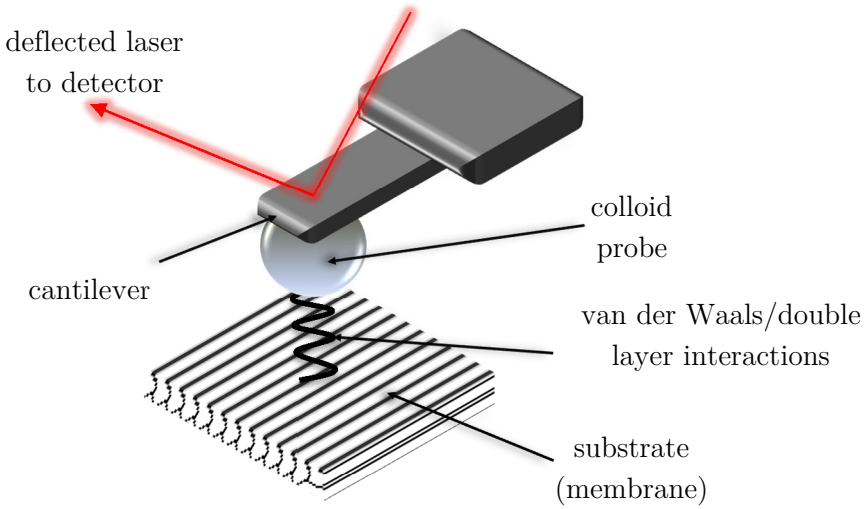

Figure 2-21 - Principal of colloidal probe AFM

Following these novel developments, attention then focused on looking at other molecule-specific interactions for more relevant components, such as proteins. Bowen *et al.* (1998) [179] reported differences in approach curves for clean silica-silica (probe-surface) interaction and BSA-doped silica onto a BSA doped surface, the interaction of BSA-BSA being weaker than for the all silica situation. Results showed good agreement across a pH range compared to theoretical prediction. This result has also been shown by Chan and Chen (2004) [162] where a BSA fouled PES membrane showed weaker and shorter range forces with a BSA-doped probe compared to the BSA-doped probe in the proximity of clean membrane surface.

The technique of colloidal probe AFM has wide applicability in membrane fouling given the specificity it has. The ability to quantify the strength and range of electrostatic attractions gives an exciting dimension to the study of membrane fouling.

2.4.3.7. Surface component detection

Attenuated total reflectance - Fourier transform infrared (ATR-FTIR) spectroscopy is used predominantly in membrane science as a tool for confirming the presence of certain chemical species which have deposited on membranes through detection of functional groups and chemical bonds. IR radiation typically covering a frequency range of between 4000 and 400 cm^{-1} is focused onto an internal reflection element generally made from zinc selenide or germanium crystal [45, 162]. A sample is placed under pressure on the crystal; the beam undergoes total internal reflection and penetrates the sample by a short distance at each reflection interval. The beam is deflected a number of times producing an evanescent wave at the sample-crystal interface, with various wavelengths being absorbed based on the sample chemical composition. Absorbed wavelengths can be assigned to vibrating (stretching or bending) of various functional groups in specific electronic spaces. Information is detected at a detector in the length domain and converted to wavenumber via Fourier transform. Depth profiling is possible through adjustment of the incidence angle.

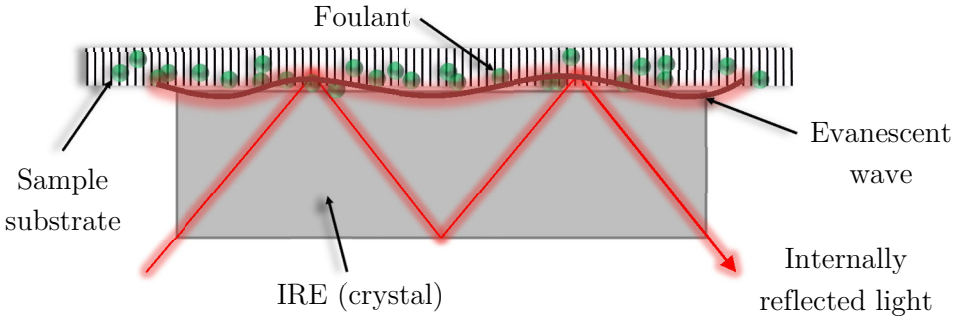

Figure 2-22 - Principal of ATR-FTIR

The use of FTIR for clean and fouled membranes is well-reported e.g. [180, 181]. Pihlajamäki *et al.* (1998) [182] probed polysulfone membranes which had been fouled with proteins at their isoelectric pH. Using variable angle FTIR and a calculation by Harrick (1979) [183] for estimation of penetration depth, they showed that BSA was adsorbed below the membrane surface as opposed to on the surface. FTIR was used by Väisänen *et al.* (2002) [184] to show compositional changes in the foulants upon cleaning when studying cellulose and PES membranes used for treatment of paper mill circulation water. They showed that different membranes responded contrastingly to non-ionic surfactant based cleaning, with surfactant desorption (and consequent flux decline during rinsing) correlating with membrane hydrophobicity. The presence of key foulants and surfactants was confirmed on membranes at various points during fouling and cleaning cycles.

The complex and varied nature of foulants can make FTIR interpretation somewhat inconclusive. Nyström *et al.* [185] showed that detangling spectra proved difficult when studying lactoferrin and BSA fouling given that the membrane possessed OH groups at similar wavenumbers to the proteins. This can be rectified by using a methodology shown by Chaufer *et al.* (2000)[186]. Difference (dry membrane) and double-difference (membrane

and water) experiments can be performed before spectral subtraction. The spectrum in question can then be used to give an indication of the foulant chemical profile without interference from substrates or masking/amplification from water. This method was used by Evans *et al.* (2009) [28] when assessing the black tea deposition on cellulose and FP membranes. They observed that 30 kDa FP membranes showed a greater adsorption potential of black tea components over 10 kDa and 100 kDa membranes of the same material; the degree of fouling correlating with the surface roughness. Also shown was greater deposition on FP membranes over cellulosic membranes, reflecting the hydrophilic nature of regenerated cellulose. The method was demonstrated by Rabiller-Baudry *et al.* (2002) [181] in the context of skimmed milk fouling of PES UF membranes also.

2.5 Cleaning of membranes in food processing

Cleaning of food processing equipment is required under governmental legislation to maintain food hygiene standards. This is enforced in the UK by the Food Standards Agency (FSA); the framework is consistent across the EU and enforced by national food agencies. Food safety, in practice, requires the need for certain measures to be upheld. For example, Good Manufacturing Practice (GMP), the implementation of Hazard Analysis and Critical Control Point (HACCP) audits in plants, and a structured Food Safety Management System (FSMS) are the minimum requirements. Whilst being the safeguards of the industry as a whole, a case by case approach is made given the variety of food stuffs, and thus risks, in the supply chain.

Trägårdh (1989) [187] defined cleaning as:

> *"a process where material is relieved of a substance which is not an integral part of that material"*

This is a sound definition as it implies that pieces of equipment are not intrinsically clean until all dirt or residue, regardless of size, is removed. Also described is the distinction between cleaning and disinfection. With this comes the ability to structure cleaning and disinfection processes as shown, in Figure 2-23

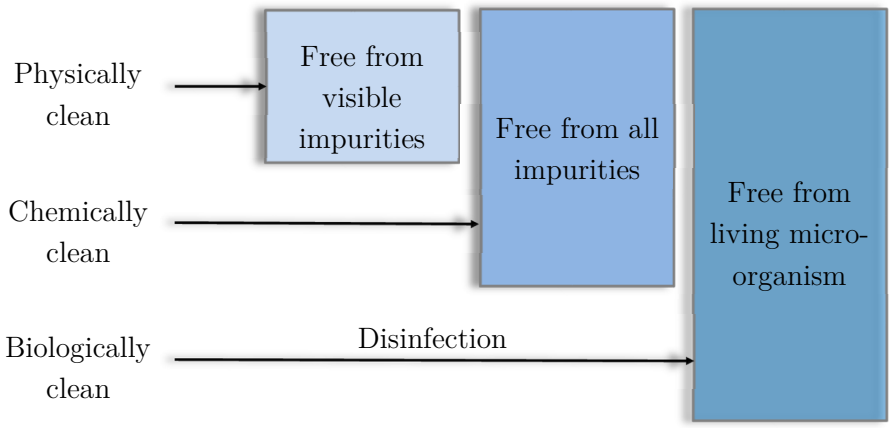

Figure 2-23 - Cleaning and disinfection definitions

The complex nature of food stuffs, the need to remove fouling and prevent micro-organism growth, and the necessity to meet the legislative framework's requirement mean membranes in food processing need regular cleaning compared to those used for wastewater or water treatment. There are a number of strategies to achieve cleanliness. These are discussed in the following section.

2.5.1 Cleaning methods

The goal of cleaning is to restore pieces of equipment to their original state of operation and leave them in a hygienic manner. This can be achieved by a variety of techniques although few are completely satisfactory when implemented on their own. A combination of treatments can achieve the desired results. Cleaning methods are shown in Table 2-8 together with membrane-related examples.

Table 2-8 - Cleaning methods and their modes of action

Cleaning type	*Mode of action*	*Literature example*
Hydraulic	Fluid hydrodynamics are used to remove foulant deposits e.g. using turbulent flow or flow reversal (back flush/pulse)	Yeast cell MF and intermittent air bubble and back flushing (and both) showed a flux increase (Qaisrani and Samhaber (2011) [188]) Nitrogen gas back flow and RO water back wash (both constant and pulsed) was used to enhance flux during MPI* filtration. Back flush showed best improvements when combined with high cross flow, though solids transmission decreased (Head and Bird (2013) [189])
Mechanical	Scouring action on apparatus or suspended scourers lift away surface foulants/cakes layers (generally limited to tubular systems given spatial confinements in other modules)	Sponge balls were used as scourers to remove pulp mill foulant from RO membranes prior to surfactant/chemical cleaning. For non-pre-treated membranes the sponge balls in combination with a surfactant formulation (Triton-X 100) offered a flux recovery of over 100% compared to 79% without the use of sponge balls (Maartens et al. (2002) [190])
Chemical/biological	A heterogeneous chemical or enzymatic reactions occurs between the cleaning agents, surface, and foulant, which degrades/transforms foulants or foulant-membrane linkages	A semi-empirical model was developed linking foulant swelling ratio, deposit thickness, Kozeny porosity and rates of removal to the recovery of flux for a stainless steel MF membrane fouled by WPC* and cleaned using NaOH at varied concentrations (Bird and Bartlett (2002) [58])
Electrical	Electrical gradients can be used to draw charged particles away from membrane surfaces into bulk feeds where they can be washed away. Micro-cavitation can also occur which could have mechanical scouring effects	Electrical current pulsations into stainless steel membranes (as cathode) showed that filter cake resistance when filtering TiO_2 particles was reduced as a function of applied current, indicating that electrical charge could assist in cleaning during filtration i.e. simultaneous fouling and cleaning (Bowen and Sabuni (1991) [191])

*MPI – milk protein isolate, WPC – whey protein concentrate

2.5.2 Chemical cleaning

Chemical cleaning is a complex area of study. Individual foulants are inherently variable in terms of their chemical composition and when combined, present their own, often unique challenges. The action of chemical cleaning is a three phase interaction between membrane surfaces, cleaning agents (or detergents), and foulants. The chemical energy of the detergents performs work on the system through chemical transformations of foulants to reduce the adhesive bond strength to the membrane surface, or the cohesive bond strength of foulants to other foulants. Trägårdh (1989) [187] and later Lin *et al.* (2010) [192] proposed a six stage mechanism for the action of chemical cleaning incorporating mass transport and reaction considerations. This has been visually represented in Figure 2-24.

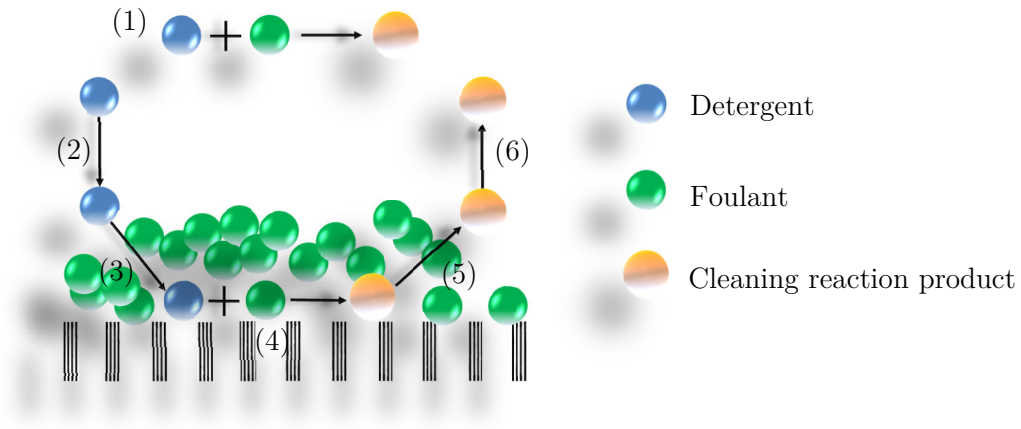

Figure 2-24 - Generic representation of a hydrolytic or oxidative cleaning mechanism during membrane chemical cleaning. (1) bulk reactions, (2) detergent transport to the bulk-fouling layer interface, (3) detergent transport through the fouling layer, (4) foulant-detergent reaction at the membrane surface or in fouling layer (breaking of adhesive and cohesive bonds), (5) transport of reaction products to the bulk-fouling layer interface, and (6) transport of products from the interface to the bulk

When selecting chemical cleaning agents, Shorrock and Bird (1998) [193] stated three considerations:

1. Membrane chemical resistance to the detergent
2. Nature of the foulant
3. Severity of foulant deposition

Generally for commercial membranes, extensive compatibility testing is available for various common detergents and detergent cocktails. The second two points however mainly rely on, firstly, knowledge of the system in terms of feed composition and the possible membrane-foulant and foulant-foulant interactions. Secondly, the optimisation of the cleaning regime for the given detergent. Optimisation relies on factors such as the chemical concentration and thermal effects, and, specifically for membrane systems, hydraulic considerations [194]. Generally, cleaning at moderate to high temperatures, with low TMP and high cross flow velocity gives the best performance [195, 196]. The interplay of cleaning protocol parameters have been highlighted by a number of authors. Bird and Bartlett (2002) [58] showed that concentration and temperature were the predominant factors affecting cleaning efficiency when rejuvenating MF membranes fouled by whey proteins. These studies were reinforced by the findings of Liu *et al.* (2001) [135] who showed that NaOH concentration and inclusion of sodium hypochlorite into the alkali cleaning solution were effective strategies in enhancing flux recovery, along with cleaning duration and temperature.

In terms of detergent selection, cleaning agents can have general or specific function. Table 2-9 shows common cleaning agents and their functions.

Table 2-9 – Common membrane cleaning agents and their specific functions [193, 196, 197]

Detergent class	*Function*	*Example agents*	*Example foulant removed/destroyed*	*Removal mechanism*
Acids	Inorganics and oxides dissolution	Hydrochloric acid Nitric acid Citric acid	Ca/Mg salts	Solubilisation
Alkalis	Fat saponification and organics solubilisation	Sodium hydroxide Potassium hydroxide	Fats Proteins	Saponification Swelling/gelation (hydrolysis)
Disinfectants	Micro-organism destruction and organics oxidisation	Sodium hypochlorite Hydrogen peroxide Peracetic acid	*S. aureus* *Salmonella* *C. botulinum* *B. cereus*	Disabling of enzymes, chlorination of amino acids, protein synthesis inhibition
Sequestrants	Mineral removal and deposition prevention	EDTA Citric acid	Calcium scale	Chelation
Surfactants (anionic, non-ionic, cationic)	Wetting promotion, foulant binding, cell disruption	Linear alkyl benzene sulphonate Alkyl sulphates SDS	Fats, oils Proteins Bacterial biofilm	Binding and solubilisation Cell attachment inhibition
Enzymes	Digestion of specific components (fats, proteins, sugars)	Amylases Proteases Lipases	Polysaccharides Proteins Fats	Hydrolysis

2.5.3 Chemical cleaning in practice

Lin *et al.* (2010) [192] described four operating strategies for chemical cleaning of membranes. These were:

1. Immersion of fouled membranes directly into detergent – clean-in-place (CIP)
2. Soaking membranes in a separate holding tank containing detergent – clean-out-of-place (COP)
3. Detergent addition to the feed stream – chemical wash (CW)
4. Detergent combined with a hydraulic mode of action – chemically enhanced backwash (CEB)

Although being useful for classifying operations, it is typical for most cleaning strategies which are defined under the CIP banner to incorporate some form of hydraulic action to compliment the chemical cleaning effect.

A standard cleaning regime would usually incorporate a thorough membrane rinsing stage to remove all loosely bound or residual bulk fouling material from near to or on the fouling

layer. This is achieved by applying a shear stress on the fouling layer by cross flow of water, often in a turbulent flow regime. Following this, applying the cleaning solution, also in a cross flow manner, now gives a double effect. The chemical reaction mechanism acts to chemically degrade or modify the foulants as has already been discussed, and a removal mechanism through the applied hydraulic effects. If the six stages of chemical cleaning are then reconsidered, applying shear and turbulent mixing will enhance transport of detergents to the interface and act to increase the rate of removal of the outermost foulants, thus enhancing transport through the fouling layer. The removal of reaction products will also be enhanced due to the tangential flow of material across the surface.

The numerous factors which are combining during cleaning leaves researchers with a somewhat complex problem and one which is difficult to summate in theoretical terms. Most models which have been postulated are generally developed through empirical observations, and would thus not be universally applicable given the variability in physico-chemical interactions between differing membrane materials and modules, foulants and cleaning agents. It is through experimentation that optimisation of cleaning strategies occurs. A rigorous example of cleaning strategy optimisation was carried out by Chen and co-workers [194]. They used a factorial design approach to refine input variables for the optimisation of a cleaning protocol for UF and RO processes used for the treatment of sewage effluent. They defined chemical and physical cleaning parameters before comparing the optimised regimes with a membrane company's recommendations. For the RO membrane the water usage was more than halved. For the UF membrane the cleaning procedure was sufficient in up-modifying the permeate flux of the process 4-fold during 12 hours of subsequent filtration.

2.5.3.1. Efficiency

Though multiple factors contribute to the efficiency of cleaning (concentration of detergents, duration, pumping expense, subsequent membrane performance etc.), membrane cleaning efficiency is generally simplified, at the first instance, to flux recovery ratios. This is the percentage of the original pure water flux which can be recovered following cleaning (see 4.3.1.6).

A number of authors have used various arrangement of fluxes and resistances for fouled, cleaned and virgin membranes using pure water and feed stocks interchangeably in order to enumerate their respective cleaning efficiencies. A summary of which was given by Lin *et al.* (2010) [192]. In terms of finding a unified parameter, most authors opt for the most simplistic case, the flux recovery ratio using solely online operational data. Chen *et al.* (2003) [194] incorporated water usage and permeate quality into their assessment. Though not applicable to many applications and only compared qualitatively, inclusion of these factors offers a more holistic view of real cleaning efficiency and gives stronger commercial relevance given the parameters used.

2.5.4 Membrane cleaning and its synergy with fouling

Surface reactions occurring on membrane surfaces between foulants and detergents can result in the formation of secondary products or selective removal of certain components. This can lead to differential performance of the membrane upon re-fouling due to surface modifications occurring over multiple foul-clean cycles. This was shown by Weis *et al.* (2001) [198]. These authors showed that even though fluxes were returned to acceptable levels, study of residual foulant and ζ potential proved these membranes were not returned to an intrinsically clean state. Zhu and Nyström (1998) [199] had earlier realised the importance of studying charge and the presence of species when evaluating chemical pre-cleaning and cleaning of membranes fouled with proteins. They showed that removal of BSA and lysozyme was incomplete after cleaning and that NaOH was possibly hydrolysing the para-positioned bond (relative to the ether group) of the PS polymer. Even though this was the case, NaOH gave the best flux recovery for fouled and cleaned membranes, and pre-cleaned, fouled and cleaned membranes. After pre-cleaning, NaOH also enhanced the resistance to re-fouling, manifested through improved filtration fluxes.

Study of membranes fouled with black tea has shown that progressive surface hydrophilisation occurs. Evans and Bird (2006) [25] showed that the contact angle of a water droplet on a fluoropolymer membrane's surface reduced from 62° to 43° after tea fouling and caustic cleaning. This showed the importance of using a moderately hydrophilic membrane (over a highly hydrophilic membrane such as cellulose) to aid adsorption of species, which could improve filtration performance. The predominance of fouling was easily removed to allow significant flux recovery ratios while leaving species which aided subsequent filtrations on the membrane surface.

2.6 Membrane modification

Membrane modification is the physical or chemical alteration of an existing membrane to give more refined properties over the standard membrane characteristics. Properties such as wettability, surface charge and roughness may be modified. The modification of these parameters has been shown to influence the fouling properties as discussed extensively by Rana and Matsuura (2010) [200].

The application of pre-treatments with respect to polymeric membranes can be divided into two areas:

1. Applying the modifying agent as a dope to the polymer blend prior to membrane synthesis
2. Applying the modifying agent to the pre-synthesised membrane surface or porous network

More correctly, (1) is deemed 'pre-treatment' and (2) is regarded as 'post-treatment', though in the context of this thesis both are regarded as pre-treatment strategies.

2.6.1 Common modification strategies

The strategies to achieve surface modification of membranes are loosely divided into a number of categories. Casting solution doping (and optimisation), adsorption and coating and surface chemical reactions and surface thin film addition are some of which will be discussed. Additionally the technique of micromachining to modify surface topology is present in the literature, though not in as great abundance as the others examples [201].

2.6.1.1. Casting solution doping

Prior to membrane casting, additives can be incorporated into the solvent/polymer blend to act as modifiers. Their roles can be as pore-forming agents in which their relative solubility can differ to the bulk membrane polymer and solvent/non-solvent system enabling the enhancement of cavities/voids of tailored size in the final membrane structure. The effect of PVP and PEG addition was discussed previously in section 2.2.2. The addition can be in the form of nanoparticles (or metal ions to form nanoparticles), copolymers with various functionality and, more recently, incorporation of metal organic frameworks into so called mixed matrix membranes. These have all shown promise in terms of property modification or separation enhancement [202]. Chou *et al.* (2005) [203] exploited the antimicrobial activity of silver nanoparticles by preparing doped cellulose acetate blends, which reduced activity of *S. aureus* and *E. coli*, even after leaching of silver following 180 days of immersion. Rajesh *et al.* (2011) [204] showed that addition of poly(amide-imide) into cellulose membranes improved porosity and that an 80:20 ratio of bulk polymer to additive was sufficient in enabling metal ion rejection of up to 99% over the un-doped membrane rejection of less than 90%.

2.6.1.2. Surface chemical reactions

Surface chemical reactions can be performed in a number of ways to change the top layer properties of membranes. Common methods include UV, low temperature plasma or gamma ray initiated grafting, and wet chemical grafting techniques [205-208]. These methods aim to initiate reactions between the surface and a specific molecule with desirable properties, such as stronger charge or greater hydrophilicity. Also connected to this but omitting the grafting step is plasma irradiation in gases such as CO_2, N_2, O_2, NH_3, and Ar [156, 209-211]. The creation of ionised surface groups increases surface energy and charge, with authors showing that protein and other macromolecular adsorption tendency onto the membrane surface is reduced for a range of common MF and UF membrane materials such as PES, PS, and polypropylene (PP) [212-214].

2.6.1.3. Adsorption/coating

Perhaps the simplest case to implement since any special reaction conditions are not normally required; adsorption involves the immersion or through fluxing of a modifying agent in solution, which acts to change the surface or pore properties.

Lohokare *et al.* (2006) [215] performed permeation/immersion studies on polyacrylonitrile (PAN) membranes using both aqueous organic bases (ethanolamine and triethylamine) and inorganic bases NaOH and KOH) as modifiers. For the organic bases they observed that

water permeation was enhanced for treatment durations up to 12 hours for triethylamine, and was improved for up to 6 hours treatment for ethanolamine before the treatment had a negative effect and permeability losses were recorded. These bases also has a consistently negative effect on BSA retention, the rejection coefficient dropping from >90% to between 80% and 90%, though only 63% rejection was recorded after 12 hours of ethanolamine treatment. They attributed the increases in permeability to hydrophilisation of the membrane due to hydroxyl and amide presence. The permeability losses were attributed to formation of cyclic intermediate components with a more hydrophobic nature. For the inorganic bases, treatment initially brought about flux increases of around 50% before a drop off to a value around half of the initial permeability after 25 hours treatment. This loss was mediated by the application of an HCl rinse following base treatment, which for both cases, provided no less than 50% permeability uplifts for up to 25 hours treatment. This base/acid treatment had little effect on BSA retention.

The hydrolysis of PAN has been investigated with relevance to NaOH treatment of membranes by Qiao *et al.* (2007) [216] who showed that flux uplifts correlated with hydrophilicity for different duration NaOH treatments. Reddy and Patel (2008) [217] showed that PES/PAN blended membranes were capable of being hydrophilised by alkali treatment, again attributing hydrolysis of –CN groups on the PAN.

Ma *et al.* (2007) [218] used hydrochloric acid as a pre-treatment for polyvinyl butyral membranes by immersion, following casting. Decreasing contact angle correlated with both increased treatment duration (at fixed acid concentration), and with increasing acid concentration. The mechanism was proposed to be an acid-catalysed hydrolysis of the polymer. Aside from the wetting property changes and some variation in pore morphology, performance was not significantly modified. Wei *et al.* (2011) [219] used pre-adsorption of selected species to treat their PS membranes prior to pharmaceutical waste water treatment. The protocol involved 240 minutes of fluxing with 1.0 wt.% citric acid or sodium bisulfite before rinsing. Species attachment was attributed to hydrogen bonding with the membrane, given the adsorbents high hydroxyl content. Upon confirming species presence using FTIR, they showed that both sorbents gave flux uplifts over 3 cycles, with sodium bisulfite showing the most prolonged uplifts, even after rinsing between filtration cycles. The flux changes were explained given the higher hydrophilicity of the modified membranes and a consequently lower fouling rate.

2.6.2 Permeation of membranes by alcohols

A particular area of interest with regard to this work is that of using alcohols to change the properties of ultrafiltration membrane surfaces and porous networks. To date there are gaps in surface science characterisation when these treatment agents are applied to pre-fabricated membranes. Also there is a significant lack of insight into how pre-treating can affect membrane performance. This aspect, as one of the overriding themes in this thesis, has been assessed with emphasis on surface science aspects.

Using alcohols as a pre-treatment is scarcely mentioned in the literature, though some indications into the effects it may cause can be taken from how the solvents behave as the permeating liquid. Lencki and Williams (1995) [37] carried out permeation studies with non-aqueous organic solvents (acetonitrile, methanol, ethanol) of varying dilution on 10 kDa and 30 kDa of both polysulfone and regenerated cellulose membranes (both on polypropylene supports). For the 10 kDa polysulfone membrane, increasing ethanol concentration increased the relative flux up to 5-fold for 100 wt.% alcohol concentration. Contrastingly for the 30 kDa membrane, the flux was halved at the same concentration of ethanol. The trend showed a steady decline in relative flux as ethanol concentration increased. For acetonitrile (ACN) permeation, both membranes showed flux declines. The effect on the 30 kDa membrane was a flux reduction of around 25% at 100 wt.% ACN. For the 10 kDa membrane the membrane became almost impermeable. The changes in flux were attributed to internal swelling of the membrane. Any reduction was attributed to an imbalance in swelling between the active layer and support which lead to a constriction of the porous structure. This constriction (as well as swelling behaviour which caused flux uplifts e.g. pore dilation) was analogised to a semi-empirical relationship where the resistance (R) of a porous medium under hydrostatic pressure (P) observed a relationship such that $R = aP^b$, where a and b are empirically derived constants. In other words, the swelling caused an effective internal hydrostatic pressure increase or decrease. The pressure term in this relationship was substituted for a difference between a '*total swelling parameter*' for the polymer and the solvent. For a more recognisable form not quoted in the aforementioned work; the independent variable used was the square of the relative distance between solvent and polymer in the Hansen solubility parameter space (as discussed in 2.2.3). Additionally it was the absence of a hydrogen bonding term of the solvent (ACN), and a good similarity in solvent total energy and polymer total energy, which most greatly affected membrane permeability.

Shukla and Cheryan (2002) [41] focused their attention on the performance of a wide range of UF membranes which were preconditioned by ethanol solutions. For a given membrane, 70 vol.% ethanol was applied as a conditioning solution using 4 different methods. The first was ramping the ethanol concentration from 0 vol.% to 70 vol.% in increments of 10 vol.%. The second was exposure to water, then directly to 70 vol.% ethanol. The third was direct exposure of a new membrane to 70 vol.% ethanol, and finally, method 4 was reducing the ethanol concentration from 100 vol.% ethanol down to 70 vol.% in increments. The value of 70 vol.% ethanol in water was selected as this was the optimum solvent blend for the filtration feed stock (corn zein). Each method showed variability for all membranes (a range of PS, PES, PAN, PVDF and cellulose) though method 1 proved the most successful in promoting flux and maintaining rejection. These authors showed that weight swelling was most significant in water, with 70 vol.% and 100 vol.% ethanol having less marked effects. The effect was attributed to the dielectric constant of water being greater than for ethanol, and contrasted the findings of Lencki and Williams (1995) [41].

Geens et al. (2005) [38] measured fluxes of binary alcohol mixtures (water, methanol and ethanol) when carrying out permeation tests on commercial hydrophilic NF membranes.

Their results showed that permeability was at a minimum for the alcohol-water which exhibited the greatest viscosity. The results lead to the conclusion that convective transport of the permeating fluid was the dominating transport mechanism. It was countered by the observation that the pure water flux for methanol and water was approximately the same when experimenting with their mid-pore size membrane (MPF-44), despite the viscosity difference being almost 2-fold. This effect was explained by the relative polarity of water compared to methanol and allowed better transmission of water over the methanol. It was justified by a comparison with pore size (implied through nMWCO rating) which showed that for smaller pore sizes, methanol transport was hindered more so than for larger pore sizes under the assumption that smaller cut-off membranes had a greater internal surface area. In summary, as pore size decreased, the effect of viscosity is lessened in replacement of surface-solvent interactions (where polymer hydration and solvation become key factors) for consideration of bulk transport of solvent through hydrophilic membranes. Another interesting observation was the significant effect that relatively low concentrations of alcohol in water had – this attributed to the relatively large changes in dielectric constant of the solution at low alcohol-in-water concentrations.

This work was followed by a semi-empirical model incorporating a lumped parameter accounting for viscosity, solvent-membrane interactions (a sorption parameter) and molecular size [39]. It was a progression from a number of previous modelling attempts [36, 220] and incorporation of classical theory, namely, the Hagen-Poiseuille model, as was shown described in section 2.3.2. In the aforementioned studies, Machado *et al.* (1999) [36] did not account for hydrophilic membranes and polar solvents, leading to a breakdown when considering alcohols or alcohol-water mixtures (where hydrogen bonding effects are significant). Bhanushali *et al.* (2001) [220] did account for the three effects mentioned in the study by Geens *et al.* (2005) [39] and arguably the only difference is the rearrangement of the model which combines the individual physical parameters into a lumped parameter as a numerator, as opposed to separating the adsorption term into a denominator coefficient.

Whilst some focus has been given to looking at the effects of solvents on UF membranes, aside from the study by Kochan *et al.* (2009) [35], no authors have specifically used alcohols as modifiers to enhance subsequent all-aqueous separations. The information reviewed in the last two pages represents useful considerations in terms of what effects solvents may have on transport of water post-treatment, and the related effects such as swelling and hydration of the porous network. For an insight into the results within this thesis specifically relating to this area of study, please refer to the results presented in Chapter 5.

2.7 Black tea

This section will cover aspects of black tea ranging from harvest to cup (or bottle).

2.7.1 Background, cultivation and preparation

The earliest reference to tea drinking is recorded in Chinese mythology dating back to 2737 BC. Shen Nung, a herbologist, noticed a pleasing aroma to some water his servant had been boiling after a tea leaf dropped into the kettle. He tasted the brew and began to spread the word about his new discovery. Despite this fabled story, tea related artefacts have been found in China dating back to the Han dynasty, (206 – 220 AD). Tea became the country's national drink during the Tang dynasty (618 – 907 AD) and remains as it today. Other historic references from Japan and India also indicate a belief in tea's medicinal qualities.

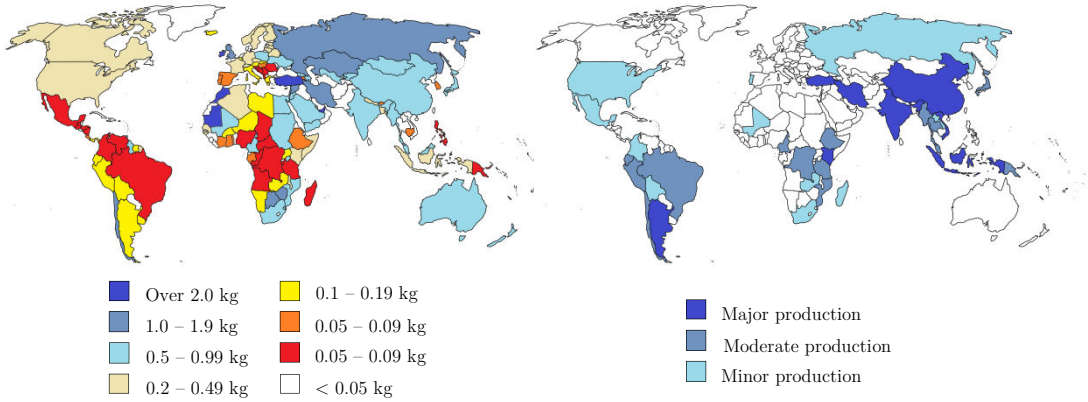

Figure 2-25 - Global annual *per capita* consumption (2009) (left) and global production (right) of black tea (data: [221, 222])

Today, tea drinking has spread to the entire globe (see Figure 2-25); Arabic countries, Western Europe, the Americas and Africa are all prolific consumers of various cultivars and preparations. This widespread liking for tea has resulted in a thriving global trade for industrial scale producers and traders, and development of trade networks and cooperatives for small-scale producers. Another result of this market is widespread research efforts in various aspects of technical and socio-economic tea-related science such as the pharmacological effects, agronomy and crop science, history, culture, economics, flavour and aroma science, plantation management and manufacturing [223].

Grown at altitude, tea leaves are picked from the top two buds of *Camellia Sinensis/Assamica* plants of three years old or more every one to two weeks [224]. Aside from variations in the growing conditions of tea plants, e.g. plant genetics and 'terroir', tea is categorised as being green, oolong, or black; this being defined by postharvest treatment. Green tea is produced by steaming the leaves upon harvest which halts the action of polyphenol oxidases; enzymes responsible for polymerisation of low molecular weight polyphenols to more complex molecules. For oolong and black teas, leaves are withered and rolled in order to break the plant material down, then partial or full fermentation

produces oolong and black teas respectively [225]. Fermentation is somewhat of a misnomer as the process is not fermentative, in the anaerobic or bacterial sense; it is actually an enzymatic oxidation [225]. Following fermentation, leaves are dried and subjected to 'grading' whereby they are broken down into small pieces through the orthodox or cut-tear-curl (CTC) processes. The orthodox process is said to produce a more aromatic product, whereas the CTC, which produces a finer 'primary' grade product suitable for tea bags, produces a stronger and darker liquor [226]. Tea in its prepared form is then ready for subsequent export, blending or processing for RTD preparation.

2.7.2 Ready-to-drink tea production

RTD teas are prepared first by extraction. This involves steeping leaves in hot water, as with any other tea infusion. Water should be freshly boiled for black tea and below boiling for green tea – this is due to the lower solubility of complex black tea polyphenols and the higher volatility of aromas characteristic of green tea. Mesh de-leafing (sieving) and centrifugal 'polishing' stages then remove solids (e.g. plant matter) before concentration, typically through falling film evaporation. De-creaming is carried out by alkali solubilisation or further centrifugation to remove insoluble matter, though at lower temperature to previous centrifugation stages. Further dewatering is carried out before treatment and bottling, or spray-drying for powdered tea products to be sold in hot water soluble form. The process is shown in Figure 2-26.

From a branding standpoint, products such as Lipton's iced tea (Unilever), Nestea (Nestlé) and Master Kong brand products are common in the market place. From label data, Lipton's iced tea contains 0.14 wt.% black tea solids in the final product. In comparison - for brewed strength tea- Astill *et al.* (2001) [227] showed much higher concentrations when comparing leaf to water ratios and extraction efficiencies from a typical teabag. They commented that numerous factors relating to agricultural and processing methods could affect tea strength. These values are displayed in Table 2-10.

Table 2-10 - Strength of standard tea bag infusions and extraction efficiency (bracketed) based on total extractable tea solids (data has been converted to wt.% from concentration based on 80 °C infusion using data from Astill *et al.* (2001) [227])

Infusion strength	*Brew time*		
wt.%	*30 s*	*60 s*	*180 s*
0.62	0.12 (20.0%)	0.20 (31.7%)	0.29 (46.7%)
0.93	0.17 (18.9%)	0.25 (26.7%)	0.36 (38.9%)
1.23	0.26 (20.8%)	0.36 (29.2%)	0.52 (42.5%)

RTD products can be further refined by centrifugation of tea infusions at given temperatures. Centrifuging cold tea infusions and removing the supernatant produces a fraction which is soluble at low temperatures, producing a cold water soluble (CWS) product. There are a number of patents relating to the preparation of CWS tea through various methods. A substantial amount of information is unavailable in the public domain given the product design element and thus commercially sensitive aspects of these preparations.

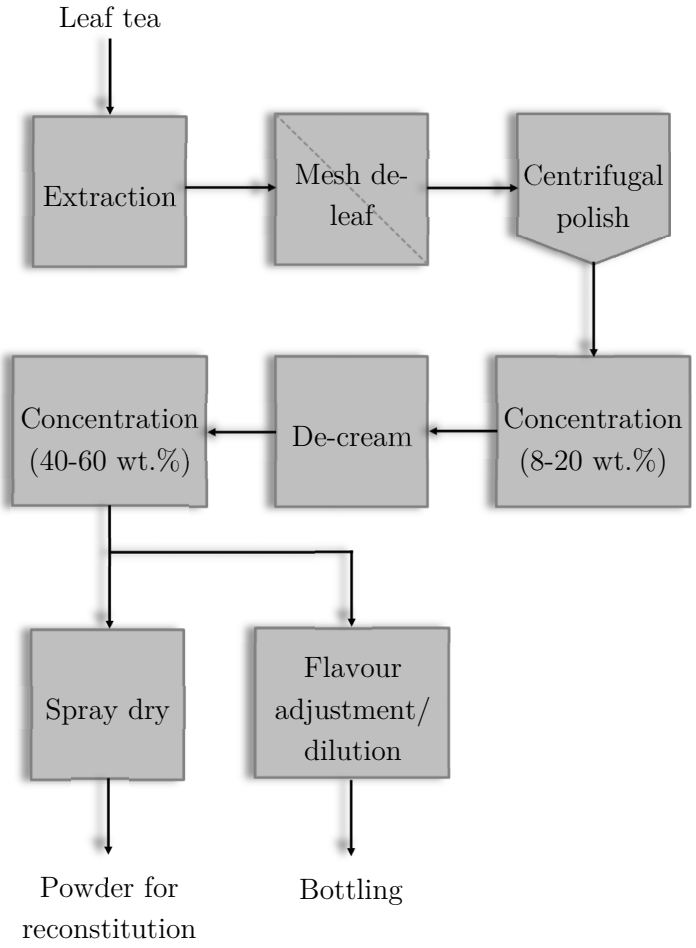

Figure 2-26 - Production of RTD tea (after Evans, 2008 [176] and c/o Unilever plc, Colworth)

2.7.3 Composition and chemistry of tea

Tea presents a plethora of constituents. In its raw form it is composed of polyphenols, alkaloids, amino acids, carbohydrates, proteins, pigments, minerals, fibre and cellulosic plant matter, organic acids and other trace or ill-defined elements [176, 228], see Table 2-11.

Table 2-11 - Composition of fresh tea leaves (wt.%)

Component	[229]	[230]	*Component*	[229]	[230]
Flavan-3-ols	25.0	22.0 – 26.0	Organic acids	0.5	0.5 – 0.6
Flavonols/flavonol glycosides	3.0	3.0 – 4.0	Monosaccharides	4.0	4.0 – 5.0
Phenolic acids	5.0	3.0 – 4.0	Polysaccharides	13.0	14.0 – 22.0
Other polyphenols	3.0	-	Cellulose/hemicellulose/fibre	7.0	4.0 – 7.0
Caffeine	3.0	3.0 – 4.0	Protein	15.0	14.0 – 17.0
Theobromine	0.2	0.2	Lignin	6.0	5.0 – 6.0
Amino acids	4.0	4.0 – 5.0	Lipids	5.0	3.0 – 5.0
Pigments	0.5	0.5 – 0.6	Ash/minerals	3.0	5.0 – 6.0

Perhaps the most interesting constituents with respect to health are the polyphenols, which are reported to have a range of physiological functions [16-18, 231, 232]. In black tea, polyphenols are highly complex molecules, which aside from their health giving properties, are associated with a higher quality tea infusion. The extent of which correlates with increased concentration [233, 234]. The diverse range of molecules are formed through enzymatic oxidation of green tea catechins (see Figure 2-27) by the activity of polyphenol oxidases and peroxidases [235]. A compositional breakdown of black tea constituents can be seen in Table 2-12.

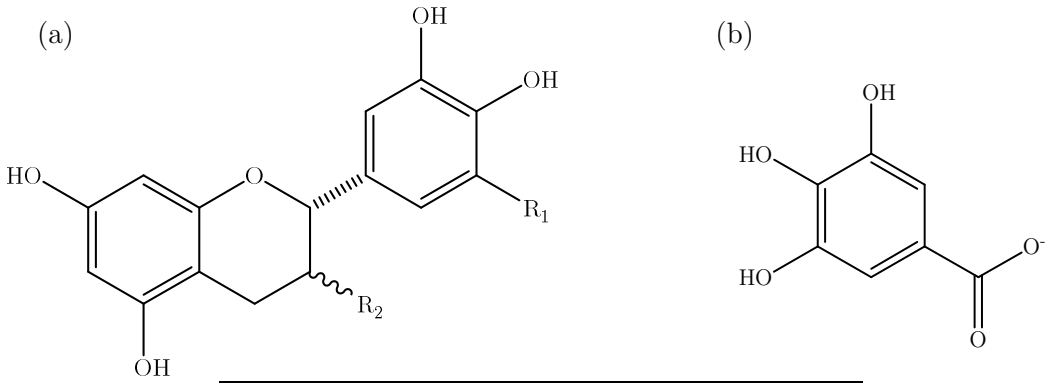

Compound	R_1	R_2	*chirality*
Catechin	H	OH	S
Gallocatechin	OH	OH	S
Epicatechin	H	OH	R
Epigallocatechin	OH	OH	R
Epicatechin-3-gallate	H	O-gallate	-
Epigallocatechin gallate	OH	O-gallate	-

Figure 2-27 - Green tea polyphenols - the building blocks of black tea polyphenols, (a) catechins, (b) gallate ion

Table 2-12 - Concentration of chemical constituents in black tea from various preparations (wt.%)

Compound		*Black tea (leaf) [236]*	*Black tea (extract) [237]*	*Black tea (beverage) [229]*
Polyphenols	Total	30.0 – 40.0	24.0 – 42.0	24.0 – 26.0
	Catechins	1.0 – 3.0	3.0	3.0 – 10.0
	Theaflavins	4.0 – 6.0	3.0 – 6.0	2.0 – 6.0
	Thearubigins	15.0 – 20.0	12.0 – 18.0	17.0
	Flavonols and flavonol glycosides	2.0 – 3.0	6.0	4.0
Proteins		15.0	10.7	6.0
Caffeine		4.0	8.0 – 11.0	3.0 – 6.0
Amino acids	(e.g. theanine, glutamic acid, aspartic acid)	4.0	13.0 – 15.0	3.0
Carbohydrates	(mono-/polysaccharide)	7.0	15.0	11.0
Cellulose	(hemicellulose, lignin, fibre)	30.0	-	-
Organic acids		-	10.0 – 12.0	2.0
Pigments		5.0	-	-
Ash	(minerals, mineral salts)	5.0	10.0	10.0

Theaflavins (TFs) are one group of flavan-3-ols which are well characterised and occur in non-, mono-, and di-gallated variations. They are defined by the presence of a benzotropolone ring formed through aromatic B-ring oxidative coupling of around 15% of the catechins to these and other oligomers [229, 238]. First through oxidation to gallocatechin quinones (enzymatic), and further by substitution and oxidation of these intermediaries into TFs (see Figure 2-28) [1].

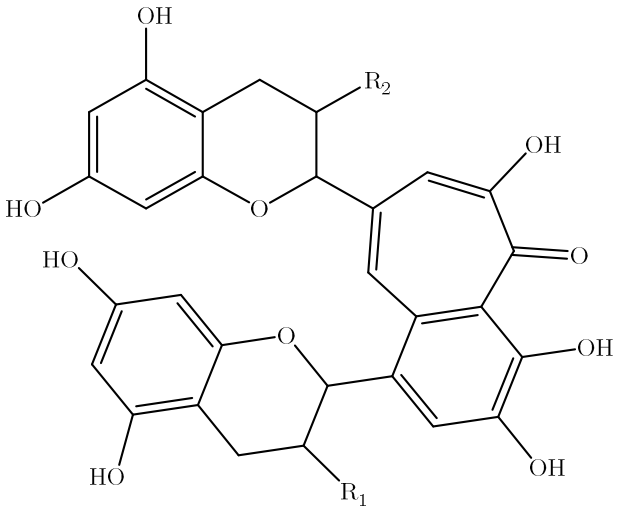

Compound	R_1	R_2	M_w
Theaflavin	H	H	561
Theaflavin-3-gallate	H	gallate	716
Theaflavin-3'-gallate	gallate	H	716
Thaflavin-3-3'-digallate	gallate	gallate	868

Figure 2-28 - Structure of theaflavin oligomers

TFs are water soluble, are said to contribute to the reddish-yellow appearance of tea infusions, and give tea its brightness [239]. The compounds are positively correlated with respect to a* and b* parameters (red and yellow respectively) in the CIE Lab colourspace (see Appendix A9). The aforementioned colour spectrum provides a useful measurement for gauging quality of tea with respect to pigmented polyphenolic structures. TFs can also homo-associate to form dimers via $\pi - \pi$ benzotropolone stacking and H-bonding [239]. Whilst green teas are described as being 'grassy', 'harsh' and 'bitter' with a 'slightly non-tangy astringency', black teas become 'flowery' with a 'pleasant tangy astringency' [240]. This is attributed to the conversion of catechins to TFs and other more complex molecules, collectively termed thearubigins (TRs).

The TRs are an ill-defined group of polyphenolic compounds and have been specifically classed as being polymeric proanthocyanidins [241]. Though speculated upon, a full understanding of the formation paths, resultant structure and individual component isolation is missing from the literature [1]. That said, they have been shown to comprise of di- and tribenzotropolone structures in theaflavic and non-theaflavic variants [242, 243]. The molecular weights can range from 700 Da to 40,000 kDa, and around 75% of the green tea catechins contribute to their formation via oxidative polymerisation [30]. The

appearance of TRs have been defined as being red by Liang and Xu (2001) [239] and red-brown by Scharbert *et al.* (2004) [244]. The former of these authors state that they give tea its flavour and body with ashy, acidic and astringent notes.

Caffeine is present in relatively high concentration. The alkaloid stimulant (194 Da) gives tea a bitter taste and its content ranges significantly. Some authors state that content is as high as 11.0 wt.% [230, 237]. Of the amino acids, theanine is the major component and is said to impart the relaxing effects of tea, as it inhibits caffeine stimulation and can reduce blood pressure [245, 246]. Pectin is the major carbohydrate in tea leaves and contributes to composition of haze, though not in haze formation itself [247, 248]. Proteins present in tea are normally fragments of ribulose biphosphate carboxylase or RuBisCo for short – the enzyme which catalyses the CO_2 fixation during photosynthesis [249]. Its limited solubility means only around 25% of it is extracted into solution [176]. Given the elevated infusion temperatures denaturisation is likely and thus fragments of the protein would contribute to the amino acid content of tea.

2.7.4 Tea cream

When tea cools it develops a haze. This is noticeable around the surface of a brewed cup which may appear mottled. RTD teas are normally consumed cold meaning the tea infusion shows increased turbidity as the temperature is lowered, with concentration, pH and time-temperature history all having affects [247]. The lowering of temperature occurs in the manufacturing process whilst making RTD teas and creaming occurs (a partitioning of phases), which eventually leads to precipitation. Tea cream, or the appearance of haze (muddying) in beverages, is generally not well-perceived by the consumer and limits shelf life. Creaming can also affect taste since molecules responsible for taste are present in the cream phase [250].

There have been numerous studies on tea creaming. It is generally agreed that the polyphenols are central to the hazing effect through association of their galloyl groups; limited solubility of these species is said to be a main driver of haze formation [250, 251]. Caffeine is neither an initiator nor essential to cream formation though it binds to galloyl groups and other team cream moieties with the effect of increasing their mass and density [238, 251, 252]. It can also lower the temperature of cream formation [250]. Calcium ion presence has also been shown to exacerbate cream formation through charge compensation during coupling with negatively charged TFs in solution at the natural pH of tea [239, 250]. Acidic conditions also favour formation of tea cream moieties by encouraging interaction between polyphenols and polysaccharides or proteins [239].

A number of parties have focused more on the polyphenol-protein interaction [233, 253, 254]. Siebert (1996) [248] took a generalised view of polyphenol-protein interactions for a variety of foods and drew similarities from wines, fruit juices and beers. It was found that apple juice haze was initiated by polyphenols, although in beer, the haze initiation was brought about by haze active proteins and polyphenols played a minor role in formation. This author later stated that a predominance of tea cream arose from polyphenol and

protein association, heightened by the presence of proline groups on the protein, and the mechanism was through H-bonds and hydrophobic interactions [255, 256]. The same mechanism is present inside the mouth where proline-rich salivary proteins bind to polyphenols resulting in perceived astringency [233]. The mechanism of interaction has been hypothesised to be that of a hydrophilic polyphenol association with a hydrophilic protein domain, the resulting hydrophobic residues turns to face outwards exposing the hydrophobic portion to water, thus causing precipitation [257].

2.7.5 Factors affecting tea cream formation

Tea cream dissolves at 40 °C though can remain partially formed up to 90 °C; this being due to the complex composition given contributions from polyphenol, protein, polysaccharides etc. [205]. Already discussed have been the effects or proline-rich proteins and calcium ion presence. The second reflects the need for tight control of water quality. Chao and Chiang (1999) [258] suggest up to 66% of calcium ions present in oolong teas were involved in cream formation, the association brought about by ionic bridging of polar groups in polyphenols [250]. The addition of chelating agents to tea has been shown to affect cream formation. EDTA was added to tea resulting in a halving of cream formation [250]. Two studies showed that calcium was a main driver in tea staining of porcelain cups through a bridging mechanism, and that EDTA was effective in breaking up this staining [259, 260].

Another factor which can affect tea cream formation is extraction temperature. Chao and Chiang (1999) [258] assert that extraction at below 35 °C would produce a haze resistant tea infusion, though efficiency of extraction would be low. The opposite was shown by Liang and Zu (2003) [261] who showed that tea cream particle mass, volume proportion and haze were increased upon cooling of infusions which has been extracted at increasing temperatures. The extraction temperature had marked effects on colour, where redness increased with increased temperature, though yellowness began to decrease between 40 °C and 50 °C [261]. This suggests that a small proportion of TFs are extracted at low temperature, and only when elevated temperatures are reached that TRs begin to be extracted with any great efficiency. It implies that tailoring of tea composition can be made based on extraction temperature as well as the degree of possible hazing that could occur.

pH has also been shown to effect tea cream particle size. Acidic conditions are associated with better extraction efficiency though at the expense of greater haze formation [239]. These authors showed from light scattering that cream moieties showed consistent sizes, with volume fraction maxima appearing for 0.5 μm particles at pH 1.2, 9.0 and greatest at pH 3.0 (that closest to tea infusions, ~ pH 5.0). At elevated pH (9.0), the intensity of particles was lowest suggesting some solubilisation was present. Studies have associated elevated pH with irreversible degradation of TFs and a formation of their anion salt leads to loss of their yellow-orange colour [239] and creation of a stewed flavour [262].

Storage and shelf life is perhaps one of the most critical factors for consumer products. Evans (2008) [176] states that an RTD product is generally 6 – 12 months. Liang and Xu

(2003) [261] studied formation of cream during storage at 4 °C noting that after 12 days there was a 45% increase in tea cream particles, confirming the relative speed of formation. The time course formation of haze has been studied by a number of authors. McMurrough *et al.* (1992) [263] showed that beer haze formation was fast and plateauing within 2 days. Grape, cranberry and apple juices were studied by Siebert (1999) [255] which showed much slower haze formation, taking 20 days for all juices to reach a steady state of turbidity.

2.7.6 Decreaming

Already discussed in 2.7.2 was the extraction and processing required to make RTD tea in soluble format. The inherent haze problem was also highlighted. Some common decreaming methods involve the alkali solubilisation of cream particulates or enzymatic treatment [31]. In terms of haze removal, Liang and Xu (2001) [239] showed good removal efficiency; the effects on flavour and appearance have previously been discussed. The need to readjust flavour is also apparent, and the chemical additives required to achieve these pH swings diminishes the naturalness of the product. Another method is fining of tea, which accelerates the precipitation of cream particulates. Fining sorbents such as chitosan, silica gels, PVPP and proteins have been used [90, 176], although fining is a time critical process and requires somewhat lengthier time scales to accomplish satisfactory results over pH modification. The risk of losing valuable component and diminishing quality is also present. Centrifuging is a highly effective separation tool, though the energy demands are considerable and the processing load is small. The complex geometries present in disc stack centrifuges and the strong fouling potential of tea means these apparatus require constant cleaning and maintenance to maintain function and hygiene. Therefore an alternative method is sought: one which can provide removal of the haze without chemical treatment i.e. a physical method.

2.7.7 Membrane processes and black tea

Membrane processes potentially offer the answer to solving the requirements for haze removal for RTD black tea producers. The physically based separation would ensure that no additives or major chemical reaction/degradation of components will occur and thus minimal effect on flavour and appearance. The high fluxes and simple geometric arrangement of membrane modules ensure fast processing on a continuous basis, and cleanability of equipment would be relatively facile, though not without further considerable research effort and process optimisation. The ability to tailor temperatures and size of operation mean the system is also adaptable for a range of tea characteristics and production facility sizes.

Table 2-13 is a full chronological review of the current state-of-the-art with regard to clarification of tea with membranes, produced with a view to gaining appreciation of where the short falls lie, the reasoning for the objectives presented in this thesis, and the future perspectives for this application.

Table 2-13 - Past findings in membrane clarification of black tea

Process specifics	*Author (year) [ref]*	*Scope and outcomes*
UF, ceramic, tubular (40 kDa)	Todisco *et al.* (2002) [30]	• Mass transfer and polyphenols transmission studied • Cross-flow velocity linked to increased mass transfer when working in the mass transfer limited region • Excessive TMP led to decrease in flux • Permeate tea quality remained stable for at least two months following filtration
UF, FP and cellulose (both 30 kDa), flat sheet, plate and frame	Evans and Bird (2006) [25]	• Assessment of processing conditions on resistances with varied TMP, effect on tea appearance and contact angle for fouled and cleaned • Cellulose membranes had ~50% better flux over FP • RC membrane suffered greater polarisation resistance • Rejection increase with TMP • RC limiting flux (mass transfer controlled) at 1.0 bar • FP limited at near to 4.0 bar • FP resistance decreased with increased cycle number due to hydrophilisation, no change in L*, a*, b* or solids rejection
UF, PS (30 kDa), Millipore stirred cell	Wu and Bird (2007) [33]	• Model solution of single and binary constituents filtered • TF linked to polarisation over other TF oligomers (e.g. TF-3-G) • Mass transfer of polyphenols linked to flux decline • TFs shown to aid in protein transmission and attributed to charge masking of protein • Caffeine shown to be ineffective at causing flux decline on its own, though reduced filtration flux was seen in caffeine-protein system • TR-protein system shown to lower flux and TRs shown to inhibit TFs transmission • Presence of TF-3-G and TF-3'-G aided in flux recovery over other oligomers
UF, FP and cellulose (10, 30, 100 kDa of both), flat sheet, plate and frame	Evans *et al.* (2008) [176]	• Relationships between surface properties and tea quality/membrane performance • FP generally showed lower fluxes over cellulose membranes • FP 30 kDa showed better transmission than 10 and 100 kDa • All cellulose and FP 30 kDa membrane showed >90% polyphenols transmission and 100% TFs transmission • Cut-off deemed unsuitable criteria for membrane selection • Fouling produced stronger negative charge • Rougher membranes correlated with increased fouling propensity • Interaction/repulsion of species suggested as mechanism for greater TFs rejection from more strongly charged membranes • Net charge of membrane linked to restoration of original permeability
UF, cellulose (100 kDa), flat sheet, plate and frame	Evans *et al.* (2009) [29]	• AFM used in colloidal probe format to probe attachment phenomena of TF-3-G • Stronger adhesion forces noted for virgin and fouled/cleaned membrane • Cleaning prior to fouling reduced adhesion strength • Fouled membrane shown to have lower adhesion, meaning fouling prevents further fouling

(Table 2-13 continued)

Process specifics	*Author (year) [ref]*	*Scope and outcomes*
UF, FP and cellulose (both 30 kDa), flat sheet, plate and frame	Evans and Bird (2010) [27]	• Investigation into fouling mechanism and cleaning efficiency • RC membrane again shown to be mass transfer limited due to polarisation • 52% of resistance for FP and 72% for cellulose attributed to polarisation • Reversible fouling correlated with feed concentration for FP membrane • 36 °C feed temperate exacerbated fouling over 50 °C though rinsable fouling proportion of total increased suggesting that tea cream formation reduced foulant-membrane interaction • Ionic strength increase (NaCl) raised total resistance by 33% though deposition onto membrane reduced due to greater polarisation • 2.5-fold increase in irreversible fouling resistance following calcium addition (44% of total compared to 25% for $CaCl_2$ free feed) • Cleaning efficiency reduced with $CaCl_2$ addition)
MF nylon (200, 450 nm pore), UF PS flat-sheet (25, 50, 100, 500 kDa), all Millipore stirred cell	Chandini *et al.* (2013) [31]	• Operating regime and tea quality compared • MF favourable over UF process as haze removal met requirement with no quality loss • Processing at low concentration (< 2.0wt.%) offers best solids recovery • <5.2 NTU of extract achieved 30 days after filtration with MF membrane • Polyphenols retention shown to be high meaning waste in retentate stream (76.1% loss of solids)

2.7.8 Polyphenol-rich beverages: Application of membranes

Whilst membrane filtration of tea has a small yet growing presence in the literature, other polyphenol containing beverages can offer an insight into the behaviour of tea as a membrane feed. As already discussed, haze removal is generally the main driver for MF or UF processes for beverages such as fruit juices, beers and wines. Other processes such as dewatering (for concentrate production) or fractionation of components are also relevant in the context of this thesis. This section reviews relevant literature relating to this area of research and the thesis context.

Borneman *et al.* (1997) [264] studied the removal of polyphenols responsible for browning in apple juice and noted that around 30 – 40% of these species could be filtered out, with the optimum separation being achieved by incorporating PVP into the PES membrane casting solution. This compound was selected based on its pore forming capability (as indicated in 2.2.2) and that it efficiently adsorbs polyphenols. The function of PVPP (similar to that of PVP) has shown usage as a fining agent in other food applications [176].

Cassano and co-workers have had success in applying membranes to range of fruit juices (kiwi, blood orange, citrus, carrot) aimed at different outcomes [132, 265, 266]. For blood orange clarification, operating parameters were investigated during juice clarification with TMP and cross flow velocity found to most significantly affect permeate flux. Application

of flux decline pore blocking laws showed that flux decline indexes of $n = 1$ (intermediate pore blocking) or $n = 2$ (complete pore blocking). These values are rarely observed in filtration of real feeds though in this instance they were attributed to the presence of a high shear stress which prevented formation of a surface cake, despite the high solids load (> 12 °Brix).

Prodanov *et al.* (2008) [267] carried out fractionation of almond derived polyphenols using 10, 30 and 50 kDa centrifugal membrane cartridges, first by reduction to a fixed concentration factor, then further by diafiltration. Species detection and measurement through liquid chromatographic and mass spectrometric analyses showed that the membranes were capable of separating low M_w (< 1000 kDa) from high M_w species e.g. condensed tannins. This indicated that membranes were not separating through a size-based mechanism, as the predominance of species should pass through the 10 kDa membrane with limited size exclusion.

Ulbricht *et al.* (2009) [62] looked at the effect of polymer type on the adsorption of model wine components (tannic acid, dextran and arabinogalactan). They found that PES membranes (presumably hydrophilic) adsorbed at quantities equivalent to monolayer flavan-3-ol coverage compared to the very minimal adsorption onto PP equivalents. The sorption was attributed to hydrogen bonding of the hydrophilic species to the PES. The interaction was not present for the hydrophobic PP membrane. It was indicated that the greater loading of polyphenols onto the membrane surface could also be attributed to the inclusion of PVP in the PES membrane casting solution. Similar results were found by Susanto *et al.* (2009) [157] who, aside from showing that PVP influenced polyphenol fouling (of a model green tea species) onto PES membranes during adsorptive fouling studies. Results showed that net negative charge was increased due to fouling, and that hydrophilisation of PES membranes occurred as a result of this polyphenol deposition. They could not specify the exact mechanism of attachment though speculated that hydrogen bonds, hydrophobic interactions, $\pi - \pi$ stacking and water-membrane interfacial arrangements could contribute.

These studies are a select few of a range that interface food engineering and water science, with relevance to polyphenol behaviour and membranes. Additionally, there is limited knowledge surrounding MF of tea with only the reference presented in Table 2-13 providing insight into its haze removal performance. The interaction of tea with membranes in terms of both product quality and how the membrane surface properties influence tea filtration and fouling are significant and should be addressed.

The complex nature of these species and variability in membranes makes each specific system differ. It is clear that surface science plays a vital role in understanding the fouling and/or functionalisation phenomena which polyphenols can bring to the study of membrane processes.

3. Research objectives

The literature review focused on areas of theory and current research to date, which aids in drawing together the themes of this body of research. The key areas this thesis bridges are:

- The influence of membrane surface physical and chemical aspects and its relevance to black tea filtration performance.
- The modification of membranes with simple treatment methods and how they act to adapt the membrane for enhancement of black tea filtration and in a more general sense.

With this scope in mind, the specific research objectives were as follows:

- Investigate the modification of commercially available ultrafiltration membranes using primary alcohols in terms of performance advantages in terms of permeability.
- Characterise the changes made relating to the surface science and membrane structure.
- Elucidate how the modification to the membranes influences performance modifications of the treated membranes when carrying out ultrafiltration of both model foulants (protein) and black tea.
- Develop relationships and mechanistic insight between the performance of membranes, the fouling potential of ultrafiltration membranes fouled with tea, and how ethanol treatment influences this.
- Show that operating regimes for membrane filtration of black tea can be influential in creating streams of added value, and demonstrate membrane process versatility.
- Explore MF as an alternative filtration process to UF in order to achieve haze removal in black tea.

These objectives have been divided into work packages as detailed previously. Each experimental chapter was not specifically designed to be exclusive to a single point, though in some cases they are.

The methodology enabling the deliverance of these specific points is explained in the next chapter.

4. Methodology

This section will give an overview of the membrane filtration apparatus, as well as feeds and chemicals used in filtration experiments. Analytical methods are also detailed.

4.1 Apparatus

4.1.1 Cross flow filtration system

4.1.1.1. Membrane module

A DSS LabStack M-10 module (now Alfa Laval, Nakskov, Denmark) was used for microfiltration and ultrafiltration experiments. The module consists of 4 polysulfone plates which are stacked. They house one pre-cut membrane coupon in each. Plates are arranged in pairs and clamped together by a stainless steel frame comprising of 4 bolts. The total filtration area inside the module is 336 cm^2 (84 cm^2 per coupon). For each pair of membrane coupons, a single permeate collection duct leads to a permeate line, both of which are clamped in place above a balance for flux measurements. A schematic of the plates can be seen in Figure 4-1. Module dimensions can be seen in Appendix A3.

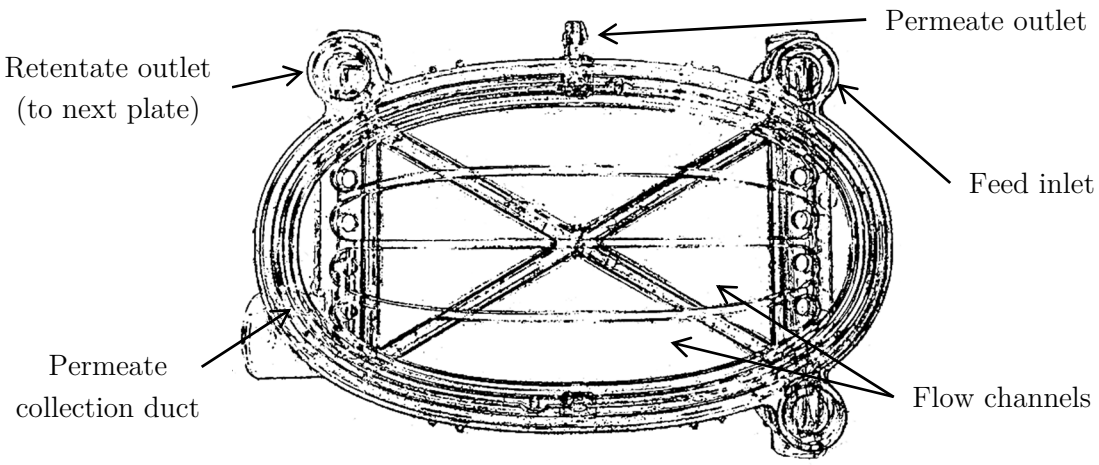

Figure 4-1 - Schematic of M-10 module plate

4.1.1.2. Cross flow filtration system

The M-10 module is mounted onto a purpose built DSS LabUnit M-10 filtration system (Figure 4-2). An additional purpose-built frame holds the feed tank. An inline gear pump feeds the module. Feed is passed through an inline heat exchanger prior to module entry. The retentate side of the module is passed through a diaphragm valve (FV-01), positioned for applying back-pressure to the module. Retentate can either then be pumped straight

to drain or returned to the glass feed tank. The total dead space of the filtration system was calculated to be 700 mL by dilution tests[1].

In typical lab-scale membrane systems, bypass circuits and secondary pumps are often deemed necessary to gain full operational range however the inclusion of a variable speed pump in this circuit eliminated this requirement.

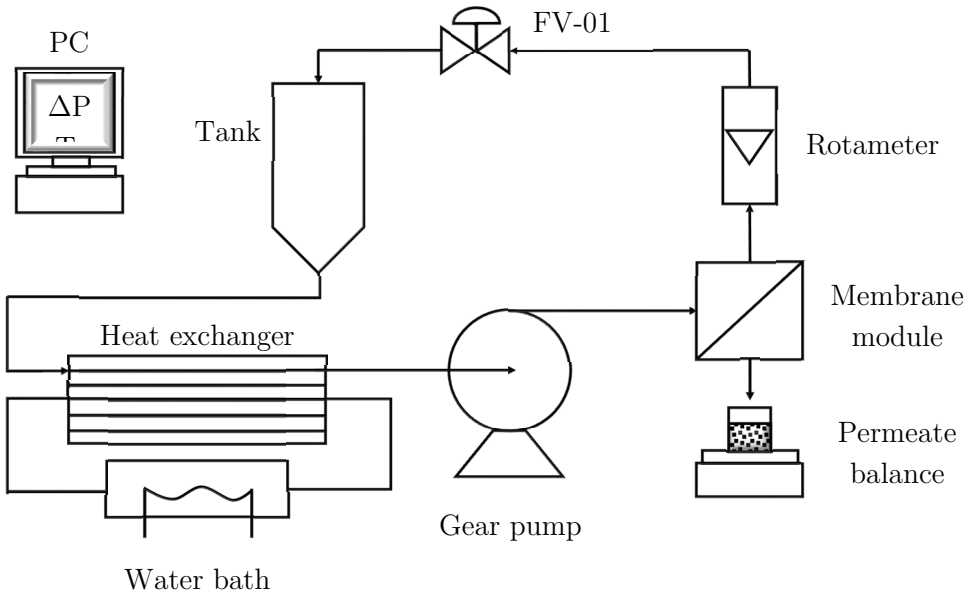

Figure 4-2 - Cross flow filtration system

4.1.1.3. Pump

The pump used on the M-10 filtration system was an ECO Gearchem variable speed positive displacement pump (Pulsafeeder, NY, USA) capable of delivering up to 7.0 bar differential pressure to the module.

4.1.1.4. Heat exchanger

The heat exchanger was of shell and tube design and made by Alfa Laval, Nakskov, Denmark. Hot water was supplied to the shell side of the heat exchanger via a water bath connected to an immersion circulator.

4.1.1.5. Rotameter

System flow rate was monitored by a rotameter mounted on the retentate side of the module. A flow rate range of 0.2 – 4.5 (± 0.015) $Lmin^{-1}$ was measurable. Full calibration information can be viewed in Appendix A2. Measurement of the flow rate enabled calculation of the cross flow velocity across the membrane surface; the range achievable was approximately 0.1 – 1.5 ms^{-1}.

[1] Dilution tests were carried out using tea solution. A known concentration was pumped around the circuit with permeate lines closed and dry weight tests performed after to enable quantification of the dilution.

4.1.1.6. Feed tank

A custom made 10 L conical borosilicate glass feed tank (Soham Scientific, Soham, UK) was used for holding water, feed solutions and cleaning agents. The tank was elevated to approximately 0.5 m^2 above the pump to ensure satisfactory pump priming. There was zero dead space between the tank floor and outlet fittings, enabling thorough rinsing.

4.1.1.7. Permeate flow rate

Permeate flow rate was monitored via mass readings from a balance (College B3001-S, Mettler Toledo AG, Greifensee, Switzerland) and had a systematic error of ± 0.05 g.

4.1.1.8. Pressure transducers

Pressure was monitored at the feed and retentate sides of the module allowing calculation of TMP. Transducers used were 0 – 7.0 bar and 0 – 4.0 bar for feed and retentate streams respectively (Druck, Leicester, UK).

4.1.1.9. Temperature monitoring

Temperature in the line prior to entry into the module was monitored by a thermocouple calibrated by a mercury thermometer over the range 10 – 90 °C.

4.1.1.10. Data acquisition

Data strings were collected from the balance, pressure transducers and thermocouple via a 4-channel remote data acquisition module (model ADAM-4012, Advantech, Milpitas, USA) and collated in LabView software v.10.0 (National Instruments, Austin, USA). Input data strings were processed to give output strings of TMP (bar), temperature (°C), density (kgm^{-3}), flux ($Lm^{-2}hr^{-1}$, $m^3m^{-2}s^{-1}$) and cumulative volume processed (m^3).

4.1.1.11. Pipes and fittings

Stainless steel 316 and high durability meshed flexible hosing were used for connection of system components. Regions of the circuitry in which elevated pressures were present comprised of steel, other regions used flexible hosing. ½" Dairy clamps were used for fitting of the M-10 module to the pipe manifold. Swagelok ½" fittings were used to attach pressure transducers and thermocouples to the system. Permeate line valves, drainage line valve and retentate-tank-drain valve were nylon clamps. The back-pressure valve was an EPDM diaphragm valve (GEMÜ Valves GMBH, Ingelfingen-Criesbach, Germany) and provided suitable flow control and/or system pressure in combination with the variable speed pump.

4.1.2 Pre-treatment system

A purpose built system was constructed in order to apply treatment agents to the surface and inner matrix of membranes.

The system was constructed in order to house the DSS LabStack M-10 module using the same 1/2" dairy clamp fittings as the cross flow filtration system. The system was designed to operate in dead-end mode in order to reduce solvent (treatment solution) usage by

sealing the retentate side of the M-10 module. A needle valve (CV-02) was fitted to the sealed end as a means to bleed any excess water/air from the module so as to ensure complete filling and complete immersion of the membrane with the treatment solution. The system was pressurised using nitrogen gas via a pressure vessel containing the treatment solution. Permeate was collected from the permeate collection lines as described previously. Measurement of treatment solution was not deemed necessary as static treatment of membranes under pressure was the chosen experimental method.

4.1.2.1. Pressure vessel and fittings

A stainless steel pressure vessel (Alloy Products Corp., Waukesha, USA) was used to house the treatments solutions (0 – 100 wt.% alcohol). The vessel was fitted with a check valve adjusted to 5.0 bar cracking pressure (CV-01), manual 1/4" needle valve for tank depressurisation (both Swagelok, Cleveland, USA), pressure gauge (Tempress, Risskov, Denmark), gas inlet pipe and outlet pipe. Treatment solution was forced out of the vessel via a 1/2" pipe connected to a 3/8" stainless steel dip-tube reaching to the tank floor. Treatment solution could be directed to drain or collection via a 3-way valve (Swagelok, Cleveland, USA) between the module feed line and tank. A system schematic can be seen in Figure 4-3.

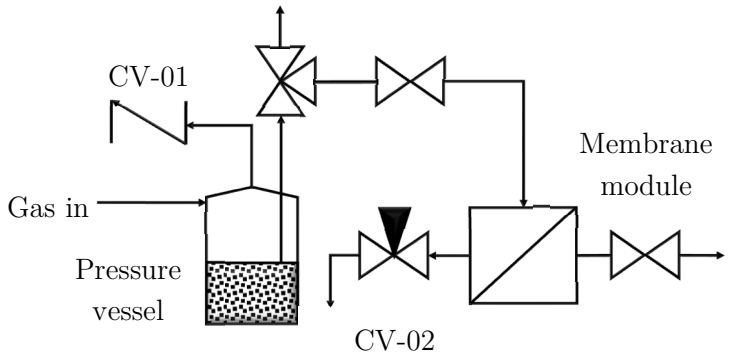

Figure 4-3 - Membrane pre-treatment system

4.1.3 Dead-end stirred cell system

Membrane characterisation and small scale filtration experiments were carried out using an Amicon dead-end stirred type cell model 8200 (Millipore, Billerica, USA). The diameter of the sealing gasket at the membrane surface was 63.5 mm giving an effective filtration area of 28.7 cm^2. The total feed volume allowable was 200 mL. The cell was constructed from polysulfone and nylon. Gaskets were made from silicone. All materials offered high resistance against corrosives and solvents meaning pre-treatment of membranes could be carried out *in situ* using this apparatus.

The cell was directly pressurised using nitrogen gas up to 4.0 bar via a suitable gas regulator. ¼" stainless steel pipes were used for pressurised lines, the line comprising of a gate valve (Swagelok) and pressure gauge (Tempress). The cell was placed in a water bath on top of a stirrer/hotplate allowing temperature control with an error of ± 0.5 °C and range from RT to 65 °C. The permeate line was 1/8" OD flexible hose which fed to a

beaker placed on a balance. The balance collected time and mass data strings directly. Data was processed using LabView software v.10.0 interfaced directly via USB2.0. Mass readings were typically recorded every 30 or 60 seconds, and converted to mass or volumetric flux. A diagram of the apparatus can be seen in Figure 4-4.

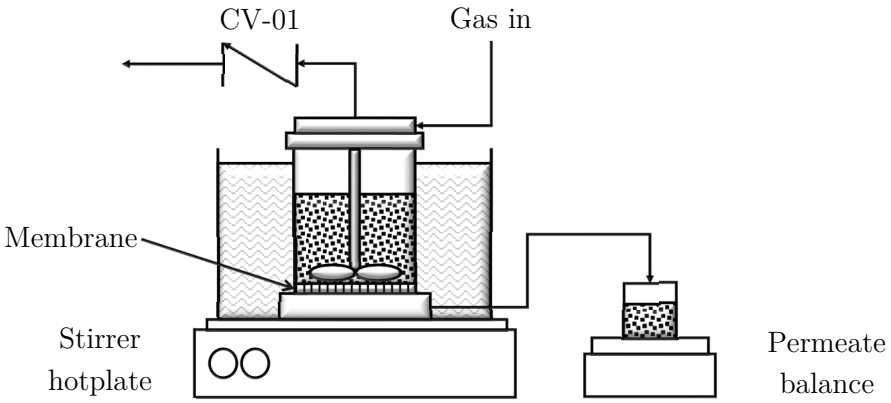

Figure 4-4 - Dead-end stirred cell system

4.2 Materials

4.2.1 Membranes

All membranes used were composite polymeric membranes consisting of an active layer cast onto a polypropylene support sheet (Figure 4-5). The active layers consisted of either fluoropolymer (FP) or polysulfone (PS). The membranes, supplied on 1000 × 8000 mm rolls, were all industrially available and are currently used in a range of application from paper pulp waste treatment to food processing. They were kindly donated by Alfa Laval (Nakskov, Denmark).

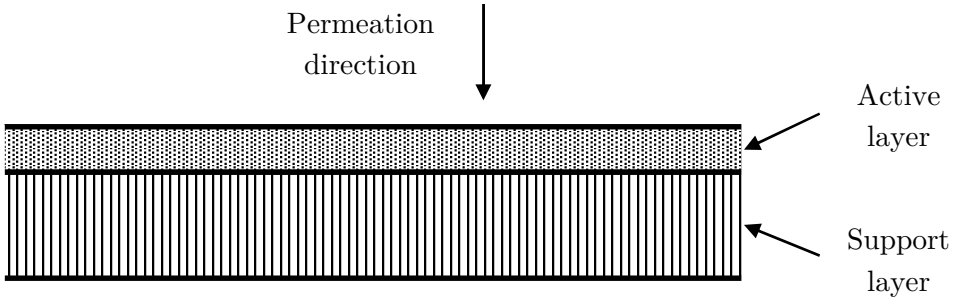

Figure 4-5 - Schematic of membrane structure

It is industry convention that MF membranes are classified in terms of nominal pore size and UF membranes in terms of nMWCO as described in 2.2.4.1.

4.2.1.1. Ultrafiltration membranes

For lower solids load experiments, pre-treatment experiments and small scale filtrations, UF membranes were used predominantly. Table 4-1 details these membrane.

Table 4-1 - UF membranes

Manufacturer product code	*Active layer material*	*nMWCO/kDa*
GR95PP	PS	2
GR60PP	PS	25
GR51PP	PS	50
GR40PP	PS	100
FS40PP	FP	100

Given the requirement for using aggressive cleaning agents and solvents, keeping within manufacturer's guidelines is paramount to avoid membrane degradation or accelerated ageing. Conditions for operational limits are outlined in Table 4-2.

Table 4-2 - Recommended operating ranges for UF membranes (source: Alfa Laval)

Material	*Process*	*pH*	*Pressure/bar*	*Temp./°C*
PS	Production	2 – 10	1 – 10	0 – 75
	Cleaning	1 – 13	1 – 4	0 – 70
FP	Production	2 – 10	1 – 10	0 – 60
	Cleaning	1 – 11.5	1 – 4	0 – 65

4.2.1.2. Microfiltration membranes

MF membranes were used for experimentation at high feed solids loading (typically > 5 wt.%). The only material used was PS. Details of the membranes are given in Table 4-3 and Table 4-4.

Table 4-3 - MF membranes

Manufacturer product code	*Active layer material*	*Nominal pore size/μm*
MFG1	PS	0.1
GRM RT5	PS	0.5
PSU RT1	PS	0.9
PSU RT8	PS	1.5

Table 4-4 - Recommended operating ranges for MF membranes (source: Alfa Laval)

Material	*Process*	*pH*	*Pressure/bar*	*Temp./°C*
PS	Production	2 – 10	1 – 5	0 – 75
	Cleaning	1 – 13	1 – 4	0 – 70

4.2.2 Reverse osmosis (RO) water

Water used for all experimentation and analysis was filtered using a Sirion midiRO system (Veolia Water, Paris, France). Water was tested regularly for quality and was rejected if the RO permeate conductivity was above 10 μScm^{-1}. Conductivity typically measured approximately 5.0 μScm^{-1}.

4.2.3 Filtration feeds

4.2.3.1. Lipton (Unilever) black tea liquor

Spray dried tea powder was supplied by Unilever R&D, Colworth, UK. The tea was stored in air-tight containers and reconstituted by dissolving in hot RO water (~90 °C) and agitated by a magnetic stirrer. Tea was adjusted to desired filtration temperature using ice baths and held at the filtration temperature in water baths. Tea was reconstituted within one hour prior to filtration and stirred for 20 – 30 minutes before cooling. Characterisation of the tea feed can be found in Appendix A. For most filtration experiments, a feed volume of 8 L was used meaning a reconstituted volume of 7.3 L was required per experiment, to account for system dead volume.

4.2.3.2. Finlays cold water soluble tea powder

CWS spray-dried tea powder was supplied by Finlays (James Finlay Ltd, London, UK). The tea was reconstituted at room temperature using RO water and agitated by a magnetic stirrer for 20 – 30 minutes. The tea was stored in separate bags of 1.0 kg quantities and reconstituted as required within 1 hour prior to filtration. Characterisation of tea can be

found in Appendix A. A feed volume of 8 L was used at 5 – 10 wt.% concentration and diluted as described in 4.2.3.1.

4.2.3.3. Bovine serum albumin (BSA)

Bovine serum albumin (Sigma Aldrich UK, Poole, UK) was used as an analogous protein for a number of filtration and AFM experiments at concentrations ranging from 0.05 – 1.0 $mgmL^{-1}$. A stock solution of 1.0 $mgmL^{-1}$ was made by dissolving 0.5 g of protein in 0.5 L of phosphate buffered saline (pH 7.4). The solution was degassed to remove any foam and stored at 5 °C prior to usage for up to 1 week. BSA has 583 amino acid residues in its mature form, a molecular mass of 66.5 kDa, and isoelectric point at pH 4.2.

4.2.3.4. β-lactobglobulin (βLg)

The same protocol was followed for βLg as for BSA. βLg was purchased from Sigma Aldrich UK. βLg has 162 amino acid residues, a molecular mass of 18.4 kDa and isoelectric point at *ca.* pH 5.0.

4.2.4 Membrane pre-treatment and cleaning agents

4.2.4.1. Alcohols

Analytical grade methanol, ethanol and n-propanol were purchased from Sigma Aldrich UK. Necessary concentrations were made in terms of wt.% using mass balances and RO water.

4.2.4.2. Phenolic treatment agents

Gallic acid and tannic acid were purchased as hydrated crystalline powder from Sigma Aldrich UK. The chemicals were reconstituted in RO water to desired concentrations and stored between 2 – 8 °C as advised by the manufacturer. As these chemicals have antioxidant properties, nitrogen was used to purge the head space in storage vessels prior to refrigeration if being stored for more than a couple of days.

4.2.4.3. Citric acid

Citric acid used for acidification of tea was purchased from Fisher Scientific, Loughborough, UK.

4.2.4.4. Sodium Hydroxide

Sodium hydroxide used for cleaning membranes was purchased from Fisher Scientific, Loughborough, UK. A standard concentration of 0.5 wt.%. was used for experiments as was carried out by Bartlett *et al.* (1995) [268] and was found suitable for cleaning of membranes fouled by tea [25].

4.2.4.5. Theaflavins

Four oligomers of theaflavins (TF, TF-3-G, TF-3'-G, TF-3-3'-DG were obtained from Unilever R&D, Colworth, UK. The species were obtained in a range of purities via HPLC. Purities are shown in Table 4-5.

Table 4-5 - Oligomers of theaflavins

Theaflavin oligomer	*Molecular weight/gmol^{-1}*	*Purity/wt.%*
TF	564	91
TF-3-G	716	82
TF-3'-G	716	95
TF-3-3'-DG	868	90

4.3 Experimental methods

4.3.1 Cross flow filtration

Standard protocols were adopted for pure water flux (PWF) measurements, rinsing, cleaning and final rinsing procedures. Specific conditions were used for filtrations and are specified in the necessary results section.

4.3.1.1. Membrane conditioning and compaction

An anti-humectant glycerol coating was applied to all membranes by the manufacturer to extend the shelf life when being stored. Before usage, all membranes were washed with 60 °C water for 90 minutes with 1.5 ms^{-1} CFV at 1.0 bar TMP prior to experimentation. This conditioning protocol was deemed sufficient for maximum glycerol removal as described by Weis *et al.* (2003) [269] and has thus been adopted for this thesis. Further information as to the effects of hot water conditioning can be found in section 4.6.2.

Another well-researched area regarding polymeric membranes is that of membrane compaction [270-272]. Work completed regarding this subject has been detailed in 4.6. To summarise, work carried out found that membranes were not subject to the same compaction effect as observed by the aforementioned authors but in fact by measuring water flux, increasing to a given elevated pressure, and then reducing to the original pressure value, water flux showed an increase overall. This would suggest that exposure to high pressure would enable water breakthrough into smaller pores and thus enhanced wetting and more complete filling of the porous network. For this reason, all membranes were exposed to 4.0 bar TMP prior to pure water flux (PWF) tests.

4.3.1.2. Pure water flux and hydraulic resistance

PWF (at single TMP – normally 1.0 bar) or permeability (over TMP range) of the membranes was tested after conditioning and compaction using RO water. This allowed calculation of the intrinsic membrane hydraulic resistance (R_m). For a given pressure, 10 minutes, with 20 seconds between mass readings was allowed for PWF measurement upon establishment of a consistent flux. Calculations for flux (J) ($m^3m^{-2}s^{-1}$) from permeate mass readings and resistance (R) are shown below (eqs. 3-1 and 3-2). A more detailed resistance break-down calculation is shown in 4.5.1.

$$J_t = \frac{m_{t+\Delta t} - m_t}{\rho A \Delta t} \tag{3-1}$$

where m is mass (kg) at time t (s), ρ is fluid density (kgm^{-3}), A is membrane area (m^2) and Δt is time between mass readings . The same calculation is also used for filtration fluxes.

Resistance is calculated using flux measurements by a rearrangement of the modified Darcy's Law as explained in 2.3.1.

$$J = \frac{\Delta P}{\mu R} \tag{3-2}$$

where ΔP is termed the transmembrane pressure (TMP)

4.3.1.3. Permeate recycle mode

For the majority of filtrations, returning the permeate to the feed tank after mass measurement was the standard procedure employed. This method ensures consistency of the feed throughout the filtration i.e. no concentration or dilution effects occurring in the feed. A discrepancy may arise given the build-up of material i.e. fouling although this is assumed to be insignificant in comparison to the feed volume (8.0 L).

4.3.1.4. Constant dilution diafiltration mode

Given variability in selectivity of components, operating in diafiltration mode was another method employed to investigate whether fractionation of components was possible whilst maintaining consistent fluxes. This mode is employed by adding a volume of diluent in to the feed tank at the same rate as the permeate flux. This has the effect of progressive dilution of the feed over time.

4.3.1.5. Rinsing

Rinsing of the membrane was carried out after fouling and prior to cleaning to flush the system of feed and to remove any unbound or loosely bound material mechanically before chemical cleaning. This enabled the measurement of a reversible fouling resistance, R_r. This was carried out for 15 minutes at 1.5 ms^{-1} CFV ($Re = 2024$) and 1.0 bar TMP at RT. PWF was measured for the duration of this process.

4.3.1.6. Cleaning

Chemical cleaning of the membrane was carried out using 60 °C NaOH solution at 0.5 wt.% for 10 minutes at 1.5 ms^{-1} CFV and 1.0 bar TMP with permeate lines open. In the case of UF membranes, cleaning was carried out with permeate lines open. For the case of MF, 8 minutes of cleaning was carried out with the permeate lines closed followed by 1 minute of open permeate line cleaning for each of the two permeate lines. Cleaning efficiency was quantified using equation 3-3.

$$J_r = \frac{J_{clean}}{J_{PWF}} \times 100\% \tag{3-3}$$

Where J_r is relative flux.

4.3.1.7. Pre-treatment with alcohols

Membranes were pre-conditioned and compacted, with the pure water flux being measured prior to pre-treatment.

After, the M-10 module was removed from the cross flow filtration system and on the pre-treatment system. Necessary fittings were clamped to the module. With the needle valve closed between the pressure vessel and module, the vessel was pressurised to 1.0 bar forcing the contents (treatment solution) of the vessel along the line. The needle valve was opened to allow the treatment solution into the module. Air was bled out from the retentate end via a second needle valve. When cleared of air, the permeate lines were opened to allow

treatment solution to permeate through the membrane leaving the membranes immersed in the treatment solution. The module was then isolated from the pressure vessel and left for 24 hours for static pre-treatment to take place. This was termed the *static* treatment method. Following treatment, the module was re-fitted to the cross flow system and all residual treatment solution was purged with water. The PWF was measured again allowing a new post-treatment resistance to be established for the membrane.

For treatment in the stirred cell, membranes were continuously fluxed with alcohol for 90 minutes with PWF measured before and after treatment and rinsing. This was the *dynamic* treatment protocol.

A summary of experimental procedures can be seen in Table 4-6.

Table 4-6 - Summary of cross flow experimental conditions

Operation	*Duration/min*	*TMP/bar*	*CFV/ms^{-1}*	*Temp/°C*	*Resistance measured*
Conditioning	90	1.0	1.5	60	-
PWF	10	0.5 – 4.0	1.0	22	R_m
Pre-treatment	24 hours (static) OR 90 minutes (dynamic)	1.0	-	22	-
PWF	10	0.5 – 4.0	1.0	22	$R_{m,2}$
Filtration	60 – 300	0.5 – 4.0	0.5 – 1.5	22 – 50	R_T
Rinse/PWF	15	1.0	1.5	22	R_r, R_{cp}
Cleaning	10	1.0	1.5	60	-
PWF	10	0.5 – 4.0	1.0	22	$R_{m,3}$

4.3.2 Dead-end filtration

Filtration and membrane characterisation was carried out in dead-end mode using the cell described in 4.1.3. Membranes were cut and mounted in the cell. This was followed by a conditioning and compaction stage using a stirrer bar. PWF was then recorded at 1.0 bar at RT. Filtration was then carried out in concentration mode with a fixed mass of feed (100 g). Experiments were run either to a pre-specified VRF or until all feed liquid has passed as permeate. VRF is calculated as follows:

$$VRF = \frac{V_p}{V_f} \tag{3-4}$$

where V_p and V_f are volume of permeate and feed respectively.

4.3.3 Adsorptive fouling measurements

The effect of adsorptive fouling was measured by following the same pre-conditioning and compaction protocol as previous. After measurement of PWF, the feed was added to the cell and left for the designated time to allow adsorption onto the membrane to take place. The cell was then rinsed and a new PWF was measured allowing a ratio ($J_{rel,ads}$) of pre-

and post-adsorptive fouling fluxes ($J_{initial}$ and J_{final}) to be calculated, thus giving a measure of the susceptibility of the membrane to adsorptive fouling (eq, 3-5).

$$J_{rel,ads} = \frac{J_{final}}{J_{initial}} \tag{3-5}$$

4.4 Analytical methods

Analysis is divided into two sections.

- Measurement of the membrane surface and porous network characteristics
- Analysis of feed, retentate and permeate streams

4.4.1 Membrane characterisation

Surface chemistry aspects of the membrane provide insight into the susceptibility of the surface or porous network to fouling. In order to characterise the membranes, a range of techniques were used as described in the following section.

4.4.1.1. Contact angle

Water and solvent contact angle were measured on a DataPhysics OCA 15 Pro goniometer. For sessile drop experiments in air, 1 µL of ultra-pure water was dosed onto the surface of membranes using a syringe and automatic dosing system. The membrane was fixed to a microscope slide with adhesive tape. The contact angle between droplet/air bubble and membrane surface was calculated on both sides (via the Young-Laplace model in-built into DataPhysics software), the procedure was repeated 15 times at various places over the membrane sample giving a total of 30 contact angle measurements. This was deemed sufficient to gain representative information about the hydrophobicity of the membrane sample.

4.4.1.2. Zeta potential measurement

Simultaneous flux and streaming potential measurements were made by measuring differences in electrical potential between feed/retentate and permeate sides whilst fluxing 1 mM KCl solution through 10.4 cm^2 membrane samples at 25 °C. Membrane samples were housed in a cross flow UF cell built in-house. The UF Membrane samples were thoroughly washed for 30 minutes with Milli-Q grade water at 1.0 bar prior to measurement. Electrical potential was measured using Ag/AgCl electrodes mounted ~2 mm from the active layer on the feed side of the membrane, and on the permeate side of the membrane, again ~2 mm from the support layer (see Figure 4-6). By recording this potential over a range of pressures (typically 0.5 – 1.0 bar), calculation of the membrane zeta potential can be made for a given pH using the Helmholtz-Smoluchowski equation (see eq. 3-6) and thus an indication of the charge density on the membrane pore walls.

$$\zeta = \frac{\Delta E}{\Delta P}\frac{\mu k}{\varepsilon_0 \varepsilon_r} \tag{3-6}$$

where ΔE is the streaming current (mV), ΔP is the applied TMP (Pa), k is the solution conductivity (μScm^{-1}), and ε_0 and ε_r are the permittivity of a vacuum and dielectric constant of water respectively. pH was modified using HCl or NaOH in the range of ~4.0 – 7.0, representative of the natural pH range of food stuffs. Care was taken to avoid mixing of the higher and lower pH streams so as to eliminate excess salt formation and thus fluctuations in solution conductivity. Electrodes were cleaned and regenerated after 10 sets of 5 – 6 pHs tested (i.e. 10 membrane samples).

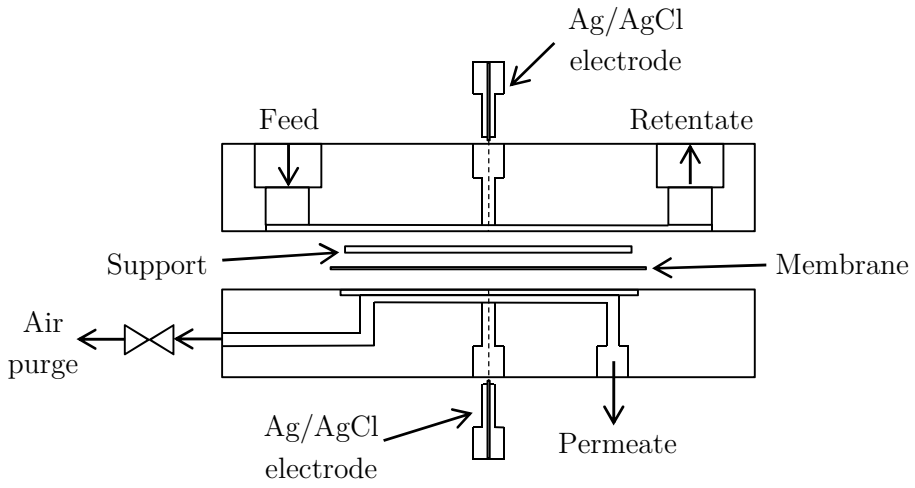

Figure 4-6 - Schematic of module used for streaming potential measurements

4.4.1.3. Fourier transform infra-red spectroscopy

An FTIR Spectrometer 100 Fourier transform infra-red spectroscopy (Perkin-Elmer, Waltham, USA) was used qualitatively to confirm the presence of fouling deposits and treatment agents. 64 interferograms were produced for each membrane sample or residue between 600 cm^{-1} and 4000 cm^{-1} wavenumber. The traces were interpreted by Perkin-Elmer Spectrum Express v.1.0 which detected characteristic peaks and matched them to molecular functional groups in its database.

4.4.1.4. Atomic force microscopy – imaging

Atomic force microscopy (AFM) was used to image surfaces of membranes in order to give an indication of surface roughness (eq. 3-9). The AFM used was a Dimension 3100 multimode scanning probe microscope (Veeco, NY, USA) with a Nanoscope IV controller (also Veeco). Tips were Olympus ORC8 tapping mode tips (Olympus Corporation, Tokyo, Japan), the tips have four cantilevers with a range of spring constants (0.05, 0.10, 0.39, 0.76 Nm^{-1}). Imaging was carried out over 2 × 2 μm scan areas. Surface roughness was calculated taking the arithmetic average of all cantilever deflections in the z-axis direction as shown below:

$$R_a = \frac{1}{N}\sum |Z_n| \qquad (3\text{-}9)$$

4.4.1.5. Atomic force microscopy – force and elasticity measurements

Colloidal interactions between foulants and membrane surfaces were measured using AFM (NanoWizard 3, JPK, Berlin, Germany). 10 µm silica spheres (Sigma Aldrich, Poole, UK) were attached to silicon nitride tipless cantilevers (UL-CT-NT, Veeco, NY, USA) using epoxy-based glue and cured using UV light for up to 8 hours. Exact colloidal diameter was characterised using a light microscope so as to enable force normalisation with contact area.

Blank colloid probes were calibrated against plain mica surfaces in 0.1 M NaCl buffer (adjusted to pH 4.5) so as to remove the effect of erroneous interactions between the colloid and surface and determine the probe's spring constant. Blank force measurements were carried out using the blank tip and the membrane sample (fixed into a well filled with NaCl buffer using adhesive tape) to quantify blank probe–membrane interactions. After calibration, tips were lowered into wells containing the model foulant solution (BSA) using the AFM piezo-electric motor. The colloid was submerged to a depth of approximately 2 mm and left to adsorb foulant molecules for 1 hour. After the allotted adsorption time, the tip was lowered into buffer solution to remove any unbound or excess foulant then brought into contact with membrane samples using an approach force of 30 nN. All measurements were made in the same buffer solution as for blank probe measurements. Measurements were collected from ten 90 × 90 µm areas with 9 ramps in each square (performed in a 3 × 3 grid).

4.4.1.6. Mercury intrusion porosimetry

Pore size distribution of membranes was measured on an Autopore IV mercury intrusion porosimeter (Micromeritics Instrument Corp, Norcross, USA). Wet membrane samples were freeze dried (by immersion in liquid nitrogen and dried under vacuum at RT). When prepared, membranes were divided into strips and packed into a 3 cm^3 penetrometer (Micromeritics ref: 16-0734, constant: 22.065 μLpF^{-1}). Total sample weight was between 0.5 and 0.6 g. Samples were evacuated down to 100 µmHg before Hg intrusion was carried out using customised pressure increments. First, a low pressure analysis was made from 0.54 psia (filling pressure) to 30 psia using 10 second equilibration times, Following this, high pressure analysis followed, from 30 psia to *ca.* 30,000 psia using 20 second equilibrations. The pressure range used represented pore sizes ranging from a maximum of 330 µm down to 6 nm (calculated using the Washburn equation, see 2.2.4.2). The range was used as it represents the pore sizes for UF membranes.

4.4.2 Stream analysis

4.4.2.1. Protein quantification

Protein concentration in samples was measured by way of the method explained by Bradford (1976) [273]. The method works on the binding of Brilliant Blue G-250 dye to proteins and peptides. In acidic conditions the dye exists in a red doubly protonated form absorbing at 465 nm, and upon contact with protein it binds basic and aromatic amino acid residues to form a stable blue un-protonated form detectable at a wavelength of 595 nm using UV-Vis spectrophotometry. The method used in this thesis is a modified method

developed by Bio-Rad Laboratories, Hercules, USA. The reagent is supplied by the same company.

The reaction of protein and dye gives two specific linear regions as detected by UV-Vis when calibrating with BSA standards. The first region, the 'standard assay', is between 0.05 – 0.5 $mgmL^{-1}$ protein concentrations when using 300 µL microtiter plates. Thus standard dilutions of 0.1, 0.15, 0.2, 0.25, 0.3, 0.4, 0.5 $mgmL^{-1}$ were prepared when feed/permeate streams were expected to be in this range. For this region, 10 µL of standards and samples were then injected into microtiter plates with 200 µL of 1:4 dilution Bio-Rad reagent. The second linear region lies between 8.0 μgmL^{-1} and 80 μgmL^{-1} and is termed the 'micro assay'. Suitable dilutions were made up in this range (10, 20, 30, 40, 50, 60, 80 μgmL^{-1}) and were then injected into plates together with 6 – 8 sample wells, reagent concentrate was added in the ratio of 160:40 µL (sample/standard: reagent).

Plates were incubated at room temperature for up to 1 hour before absorbance measurement at 595 nm using a Synergy HT multi-mode microtiter plate reader (BioTek, Winooski, USA). Blank subtraction was carried out on the standards to give a calibration chart for absorbance vs. protein concentration.

4.4.2.2. Total polyphenols quantification

Total polyphenols were assayed for using a modified method described by Singleton and Rossi (1965) [274]. The method was adapted for use in microtiter plates from standard macro-cuvettes used in UV-Vis analysis by the author. The method involved a scale down of the procedure into µL from mL quantities and saved 50 times the reagent over the macro-scale assay, but allowed for a considerable number more repeat measurements - typically 8 – 12 repeat absorbance readings were carried out.

The assay measures the reducing potential of samples by oxidation of phenolic hydroxyl groups by way of phophotungstate and phophomolybdate reduction. The reaction produces a blue colour upon precipitation of the oxidants yielding absorbance maxima at 765 nm. Sample absorbance was calibrated against gallic acid equivalents at suitable dilutions.

Gallic acid standards were made up from a stock solution of 1.0 $mgmL^{-1}$ made by dissolution of 1.0 g of gallic acid monohydrate (Sigma Aldrich, Poole, Dorset) in 1.0 L RO water. Serial dilutions of 10, 20, 25, 30, 40 and 50 μgmL^{-1} were made up before each sample set was analysed.

Tea samples were collected from experiments and upon cooling, were mixed with acetonitrile (ACN) (HPLC grade) purchased from Fisher Scientific, Loughborough, UK in the ratio 1.8:0.2 mL tea:ACN. A 100 µL aliquot of this was diluted with water in the ratio 0.1:4.9 tea/ACN: water to bring the blues intensity down to the calibration range. 50 µL of tea/ACN/water was added to microtiter plate wells containing 100 µL Folin and Ciocalteu reagent 2N obtained from Sigma Aldrich, Poole, UK (diluted 9:1 water: reagent). 50 µL of GA standards and reagent blanks (water) were added to other microtiter plate wells in quadruplet. After between 2 and 8 minutes, 80 µL of 7.5 wt.% sodium carbonate

was added to the wells to prevent any further reaction. The plates were incubated at room temperature for up to 8 hours prior to absorbance measurement. Absorbance was measured at 765 nm in a Synergy HT multi-mode microtiter plate reader (BioTek, Winooski, USA).

4.4.2.3. Dry weight analysis for total tea solids

Sample concentration was calculated by dehydration at 70 °C. Clean 10 mL glass test tubes were dried in an incubator set to 70 °C to ensure all water was removed. Tubes were then cooled to RT and weighed, samples were added and weighing was repeated giving 'tube mass' and 'tube + wet mass'. Sample tubes were returned to the incubator and left until dry. Sample weight was checked again after 5 days drying, and again after 6 days to ensure complete dehydration; 'tube + dry mass' was recorded. Sample concentration was then calculated by subtraction of 'tube mass' to give 'wet mass' and 'dry mass' and thus a total solids fraction of tea could be inferred. Masses were measured to $\pm$ 5 $\times$ 10^{-5} g giving a systematic concentration error in the final measurement of $\pm$ 1.5 $\times$ 10^{-4} g.

4.4.2.4. Rejection of solutes

With compositional knowledge of feed, retentate and permeate streams, apparent rejection coefficients (R_{app}) could be calculated for protein, polyphenol and total solids. The rejection coefficient by definition is the fraction of a given solute i that does not transmit through the membrane, and is a dimensionless ratio between two concentrations defined mathematically as:

$$R_{app} = 1 - \frac{c_{p,i}}{c_{f,i}} \tag{3-10}$$

During small scale filtration experiments using protein and protein-polyphenol mixtures where a fixed volume of feed was allowed to permeate, a total percentage solute transmission (% yield) of solute i was given by division of permeate concentration at the end of the filtration $c_{p,i}(t_f)$ by feed concentration samples at the beginning of the filtration $c(t_0)$ as follows:

$$T\% = 100 \times \frac{c_{p,i}(t_f)}{c_{f,i}(t_0)} \tag{3-11}$$

4.4.2.5. Colour determination

C.I.E. L*, a* and b* tristimulus values were measured by measurement of the transmittance of tea samples across the visible spectrum (values of between 380 nm and 770 nm used here). Tea samples were transferred into 10 mm path disposable macro cuvettes (Fisher Scientific, Loughborough, UK) and loaded into a UV-Vis spectrophotometer (UV-1601, Shimadzu Corporation, Kyoto, Japan). Transmittance was measured and converted by UVPC Color Analysis v.3.0 (also Shimadzu) to L*, a* and b* colour coordinates. Tea samples were measured in triplicate with mean and standard deviation of values providing the measure and error accordingly. Further information is provided in Appendix A9.

4.4.2.6. Refractive index

Refractive index was quantified in terms of °Brix using a digital handheld refractometer (r^2 Mini, Reichert, NY, USA). Although the °Brix measured lacks the precision of dry-weight measurements (± 0.05 °Brix), they were an invaluable 'on line' measure of tea concentration. The measurements were of particular importance for the high solids load experimentation where the resolution of concentration measurement required is lower. For these experiments, turbidity measurements were to be carried out within 2 hours of filtration and at constant concentration to avoid haze reformation. Practically, measurement of the refractive index gives an estimate of concentration almost instantaneously upon filtration and thus necessary sample dilutions for haze measurements could be made.

4.4.2.7. Haze measurement

Haze of tea samples was quantified by measurement of tea sample turbidity at room temperature. Tea samples were loaded into a glass cuvette and mounted in the turbidimeter (model HI 93703, Hanna Instruments, Woonsocket, USA). The instrument was 3-point calibrated using turbidity standards of 0, 10 and 100 NTU.

For stability measurements over long times (up to 8 weeks), samples were stored at 5 °C. Prior to measurement, samples were equilibrated to room temperature and turbidity was measured. Samples were then re-refrigerated.

4.4.2.8. Simulated iced tea beverages – tea dilution

In order to quantify haze in terms of realistic products, tea was diluted with water and citric acid to simulate the addition of sweeteners in a finished iced tea beverage. More acidic conditions typically induce stronger protein-polyphenol interactions, the primary source of haze in many beverages. By addition of citric acid, a more realistic scenario is created for the tea to simulate 'in bottle' conditions.

Tea sample °Brix values were used to dilute tea samples from their bulk retentate/permeate concentration. The necessary volume of tea concentration was added to a beaker with an adjustable pipette. To this, 1 mL of 3 wt.% citric acid was added and the volume made up to 100 mL using RO water in a burette. Final concentration of both tea and citric acid was 0.3 wt.%. The solution was mixed thoroughly and colour and haze measurements were made as previously described. The protocol described here was developed through personal correspondence with Dr. Huafu Wang and Wycliff Odoyo of James Finlay Ltd, London, UK.

4.4.2.9. pH and pH adjustment

pH was monitored for feeds, samples and analytical solution using a bench-top pH meter (Jenway 3305, Bibby Scientific Ltd, Stone, UK). The meter was 3-point calibrated using buffer standards of pH 4, 7 and 10. The probe was stored in buffer and rinsed with RO water prior to immersion in samples. Feed and solution pHs were modified up using concentrated NaOH solution or down with concentrated HCl solution.

4.5 Modelling

4.5.1 Resistance-in-series model calculation

The resistance-in-series (RIS) model provides a useful insight into the relative contribution of varying types of resistance related to membrane filtration and fouling as described in 2.3.6.1. The overall governing equation is an expansion of the lumped resistance term R from the modified Darcy equation as explained earlier in 4.3.1.2. The expanded equation is as follows

$$J_f = \frac{\Delta P}{\mu(R_m + R_f + R_{cp})} \tag{3-12}$$

where $R_f = R_r - R_i$ and $R_T = R_m + R_f + R_{cp}$ (3-13) and (3-14)

In which J_f is the flux deemed to be the steady state flux during fouling, or indeed the flux during any part of the experimental cycle.

A typical diagram of how data may look and the resistances which are measured at different points over the filtration and cleaning cycle is displayed in Figure 4-7.

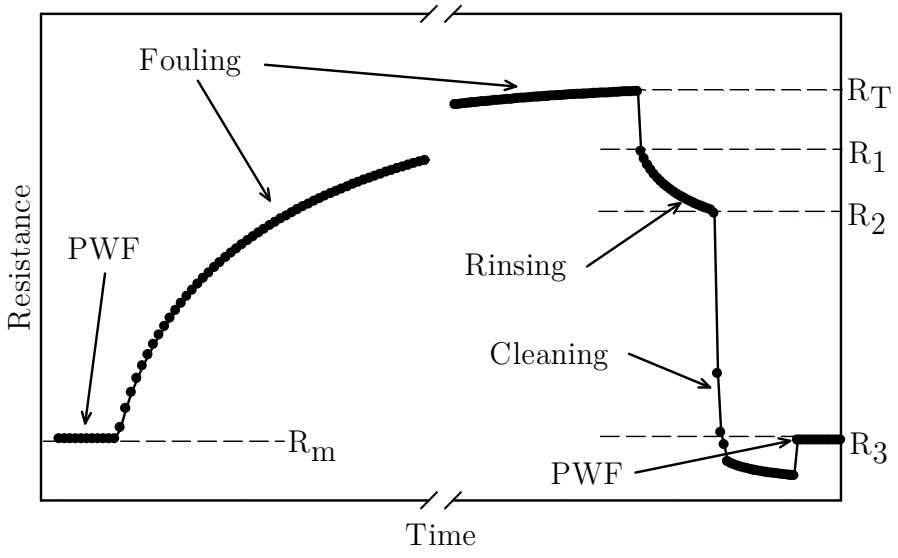

Figure 4-7 - A typical cycle for a single membrane experiment in terms of resistance

Given the resistances R_m, R_T, R_1, R_2, R_3, calculations for resistances due to fouling (R_f), which are broken down into reversible and irreversible fouling resistances (R_r *and* R_i), concentration polarisation (R_{cp}) and the membrane recovery after cleaning can be made as follows:

$$R_{cp} = R_T - R_1 \quad (3\text{-}15)$$

$$R_r = R_T - R_{cp} - R_2 \quad (3\text{-}16)$$

$$R_f = R_T - R_m - R_{cp} \quad (3\text{-}17)$$

$$R_i = R_f - R_r \quad (3\text{-}18)$$

Check: $$R_T = R_m + R_r + R_i + R_{cp} \quad (3\text{-}19)$$

4.5.2 Pore blocking mechanism determination

As described in 2.4.2.2, the build-up of rejected particles at the membrane surface which causes severe limitations in flow rate typical of many filtration processes is characterised by a rapid flux decline. The methodology, as proposed by Hermia (1982) [149] and developed further by Field *et al.* (1995) [117], has been employed extensively by a number of authors (for example: [69, 119, 275]) as an analysis tool by use of experimental data, which gives insight into the blocking mechanism (complete, standard, intermediate blocking, or cake filtration) responsible for the process limitation. The governing power-law equation used is as follows:

$$\frac{d^2t}{dV^2} = k\left(\frac{dt}{dV}\right)^n \quad (3\text{-}20)$$

4.5.2.1. Cross flow filtration

The developments by Field *et al.* (1995) [117] incorporated the critical flux J^* into their equations to enable application for cross flow filtration. The governing equation for the cross-flow regime is defined as follows.

$$-\frac{dJ}{dt}J^{n-2} = k(J - J^*) \quad (3.26)$$

The equation was solved using MATLAB R2012b program by application of the inbuilt 'fminunc' minimisation function and 'ode45' differential equation solver. Experimental data was loaded into the program whereby the function found estimations for k and J^* to satisfy eq. 3-26 through a process of minimising the SSR. The program outputted the optimised k and J^* values for all values of n, with SSR and r^2 for deduction of the best fit. The MATLAB function file is shown in Appendix D.

4.5.3 Diafiltration

4.5.3.1. Basis for calculations

Diafiltration is characterised by diluent (typically water or buffer solution) being added to the feed tank at a pre-determined fixed rate ($u(t)$), or rate proportional to the permeate flow rate ($q(t)$), enabling the 'wash-through' of target micro-solutes in the permeate or progressive purification and/or concentration of macro-solutes in the retentate. The addition of a diluent acts to maintain or progressively dilute the feed so as to extend processing time. This would otherwise be limited by excessive concentrations in the retained stream resulting in lower flow rates due to higher CP or increased fouling. A batch diafiltration scheme is shown in Figure 4-8.

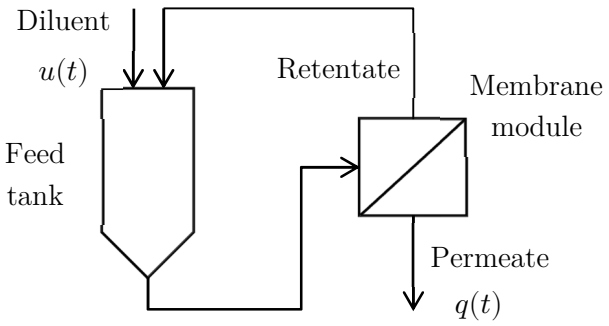

Figure 4-8 - Scheme for batch diafiltration operation

4.5.3.2. Mathematical derivation

Permeate volumetric flow rate can be equated to the change in volume of permeate over time as follows:

$$\frac{dV_p(t)}{dt} = q(t) \tag{3.27}$$

Change in feed volume at time t can be similarly expressed as the difference between permeate lost and diluent gained.

$$\frac{dV_f(t)}{dt} = u(t) - q(t) \tag{3.28}$$

If solutes are now considered, a mass balance can be expressed for the concentration of n number of solutes i at a given time t if the diluent is solute free (i.e. water).

$$\frac{d}{dt}V_f(t)c_{f,i}(t) = -q(t)c_{p,i}(t) \qquad \text{for} \qquad i = n \tag{3.29}$$

By use of the product rule, eq. 3.29 can be rewritten as

$$c_{f,i}(t)\frac{dV_f(t)}{dt} + V_f(t)\frac{dc_{f,i}(t)}{dt} = -q(t)c_{p,i}(t) \qquad \text{for} \qquad i = n \tag{3.30}$$

Substituting eq. 3-10 and using a rearrangement of the rejection expression as defined in 4.4.2.4 for solute i, $c_{p,i}(t) = c_{f,i}(t)[1 - R_{app,i}(t)]$, gives;

$$V_f(t)\frac{dc_{f,i}(t)}{dt} = c_{f,i}(t)[q(t)R_{app,i}(t) - u(t)] \tag{3.31}$$

This sets the initial value problems for describing both total volume of feed and concentration of solutes i in the system.

$$\begin{aligned} \frac{dV_f(t)}{dt} &= u(t) - q(t) \\ V_f(0) &= V_f^0 \end{aligned} \tag{3.32}$$

$$V_f(t)\frac{dc_{f,i}(t)}{dt} = c_{f,i}(t)[q(t)R_{app,i}(t) - u(t)]$$
$$c_{f,i}(0) = c^0_{f,i} \tag{3.33}$$

The derived equations form the basis of stream composition analysis in chapter 7.

4.6 Membrane characterisation

4.6.1 Water permeability – virgin untreated membranes

RO water fluxes for membranes were measured at a range of TMPs after conditioning and compaction at room temperature with a 1.5 ms^{-1} CFV (for UF) and 0.5 ms^{-1} (for MF). Permeability is defined as the gradient of the pressure-flux relationship. As Darcy's law suggests, a linear relationship was found across all membrane types used, and is shown in Figure 4-9.

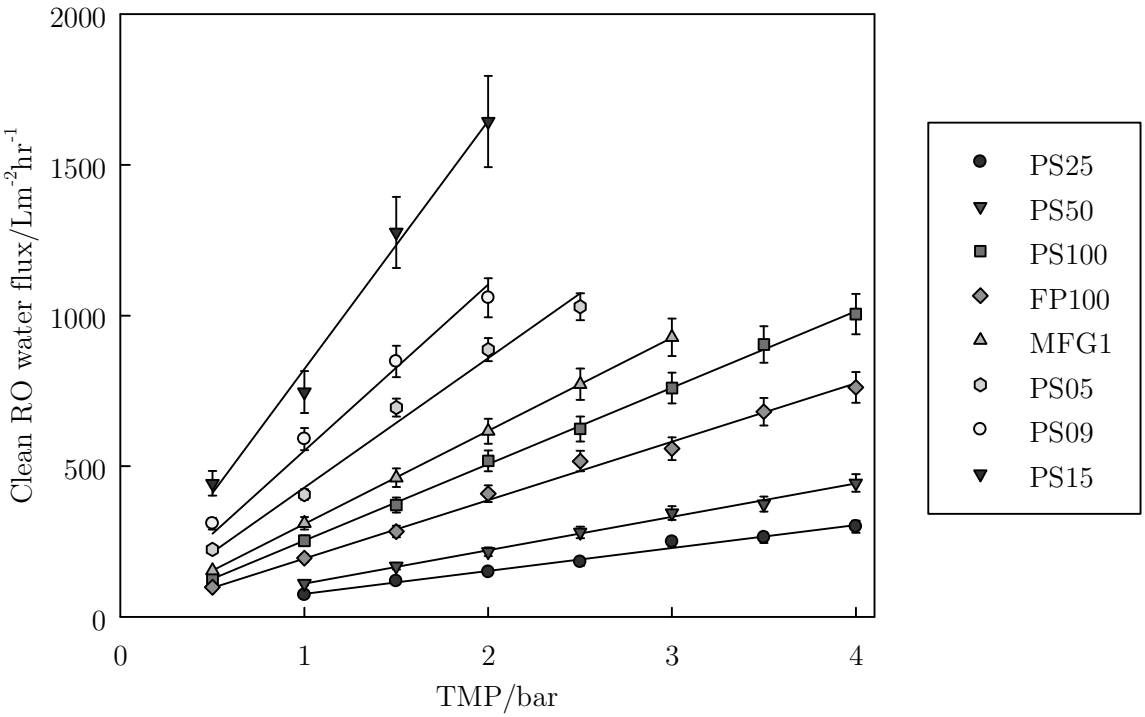

Figure 4-9 - Pure water flux measurements vs. TMP

Table 4-7 shows the permeability of all membrane used in the thesis. The largest proportional variability arose whilst using the tightest membrane, PS25, and the loosest membranes, PS09 and PS15, having errors of 8.7%, 6.1% and 9.2% respectively.

The significant variation in the flux for the PS25 membrane can be explained given the relatively small membrane areas whilst testing. Membranes were supplied on 1000mm × 8000mm rolls and inconsistencies in layer thickness are noticeable across the cross section with the naked eye. The membranes are typically used on spiral modules whereby

measurements in permeability would be less pronounced when dealing with the larger available filtration areas.

Table 4-7 - Water permeability of membranes at 22 °C

Membrane	*Classification*	*nMWCO or nominal pore size/ kDa or µm**	*Permeability/ $Lm^{-2}hr^{-1}bar^{-1}$*	*Resistance/ $\times 10^{12}$ m^{-1}*
PS25	UF	25	76.4 ± 6.7	4.950 ± 0.434
PS50	UF	50	110.1 ± 5.2	3.432 ± 0.162
PS100	UF	100	254.6 ± 7.2	1.486 ± 0.042
FP100	UF	100	190.8 ± 11.2	1.981 ± 0.116
MFG1	MF	0.1*	309.4 ± 1.5	1.222 ± 0.059
PS05	MF	0.5*	418.7 ± 18.1	0.903 ± 0.039
PS09	MF	0.8*	397.2 ± 30.8	0.754 ± 0.046
PS15	MF	1.5*	586.4 ± 76.3	0.457 ± 0.042

The permeability values presented here represent the global averages for all of the membranes over the experimental program and form the basis of normalisation calculations as detailed in Appendix A3.

4.6.2 Hot water conditioning

The purpose of hot water conditioning is to remove the glycerol anti-humectant from the membrane prior to filtration experiments. The method, as detailed by Weis *et al.* (2005) [269], involved washing the membrane thoroughly over a 90 minute period whilst changing water regularly to avoid reapplication of glycerol.

Figure 4-10a shows that during hot water conditioning, the PS25 membrane exhibited a flux decline over the 90 minute rinsing cycle, whereas the PS50 showed a moderate increase, this in part due to gradual temperature increase and thus lowered viscosity. Both PS100 and MFG1 in Figure 4-10b show gradual decreases with isothermal rinsing. In the case of the more open MF membranes shown in, significant reductions in flux are observed in Figure 4-10c. Evans (2008) [176] noticed similar trends when conditioning with a similar protocol whereby a 10 kDa nMWCO FP membrane displayed declining flux from over 1200 $Lm^{-2}hr^{-1}$ to 477 $Lm^{-2}hr^{-1}$. However, for the same material with nMWCO of 30 kDa and 100 kDa, the flux reduction was not so marked. Equivalent trends for the same range of regenerated cellulose membranes were not observed suggesting the phenomenon is highly material specific.

Weis *et al.* (2005) [269] found that the membrane contact angle increased, i.e. the surface became more hydrophobic after hot water conditioning, implying a lowered wettability of the membrane surface. This suggests that water is excluded more strongly from the membrane surface and would thus be prone to higher rejection; this effect is quantifiable as a lowered flux. Making the surface more hydrophobic prior to filtration sounds counterproductive, although as the data in Figure 4-10 suggests, a more consistent flux is attained, and with the removal of glycerol from the membrane, a reduction in process variability is achieved with the step.

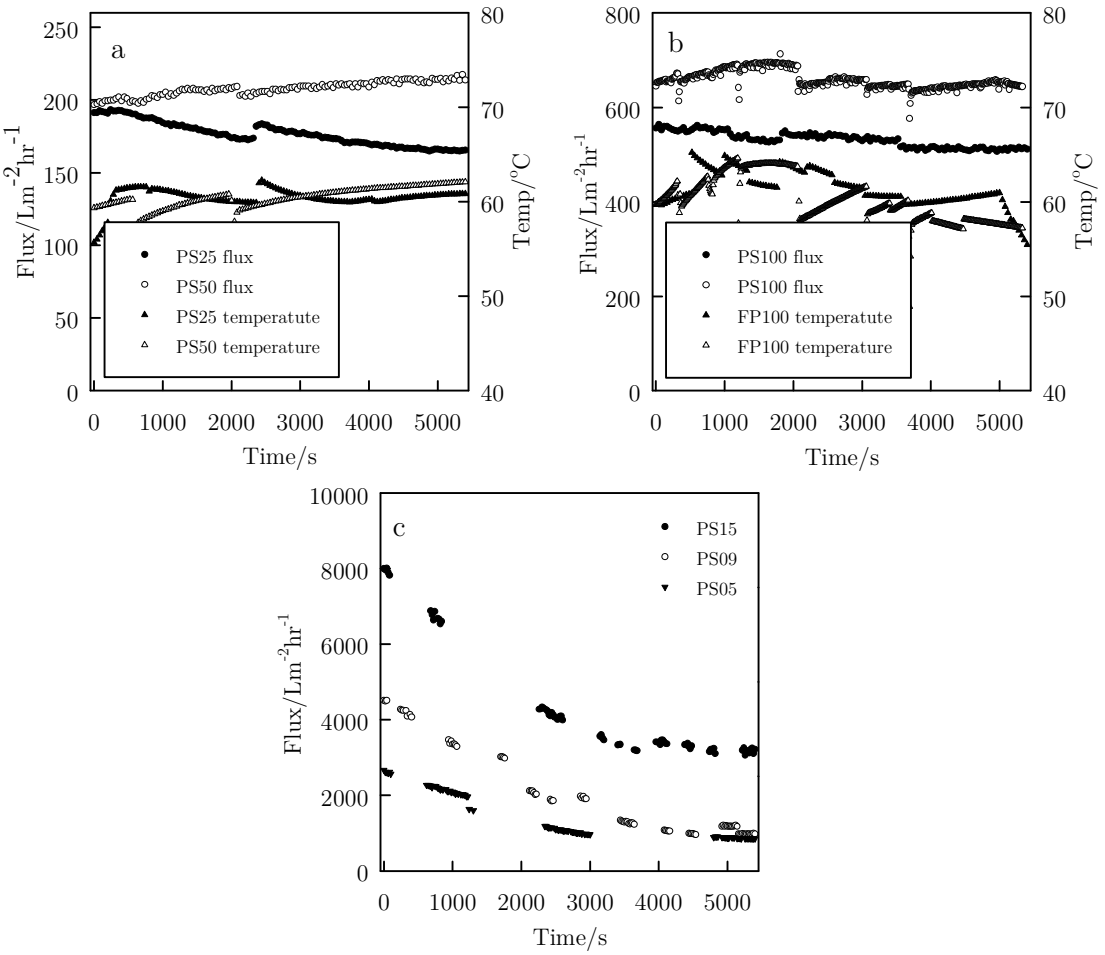

Figure 4-10 - Flux and temperature profiles for UF membranes; (a) PS25 and PS50 and (b) PS100 and MFG1. (c) Flux profiles for PS05, PS08 and PS15 MF membranes during hot water conditioning

4.6.3 Compaction and permeability

4.6.3.1. The importance of compaction

A number of authors have attempted to understand the phenomena associated with membrane compaction and have theorised their findings ([270-272]). All authors confirmed that after designated time and pressure exposure, permeability decreases were observed, with findings generally being attributed to polymer matrix compression as a result of the elasticity of the polymer. Pusch and Mossa (1977) [270] showed that cellulose acetate membrane permeability, when exposed to varying degrees of pressure, observed a non-linear trend with increasing pressure, and attempted to model the behaviour on a cubic relationship between permeability and pressure. Persson *et al.* (1995) [271] showed membrane thickness and relative membrane flux decreased with an applied 'pre-compaction' pressure through their polyaramide, polysulfone and cellulose acetate membranes; attributing some flux loss to compression of the support layer. Susanto and Ulbricht (2009) [272] showed for their doped PES membranes that over 50% of the permeability could be lost whilst measuring permeability gravimetrically over a 2 hour

compression cycle at 450 kPa. All of these findings highlight the importance of membrane 'run-ins' prior to experimentation.

4.6.3.2. Incremental TMP increases

It was a contrasting result to the above compaction examples which was found when experimenting with the membranes used in this thesis. The result was hinted after initial filtration experiments produced results with less than adequate repeatability and prompted some experimentation to gain consistency with similarly specified membranes.

Incremental TMP increases were made over a PS50 membrane on the cross flow apparatus with constant CFV of 1.5 ms^{-1} starting at 0.5 bar and in 0.5 bar increments. After two increases, a 0.5 bar decrease was made, followed by another two-step increase and so on up to a maximum of 3.0 bar TMP (data shown in Figure 4-11).

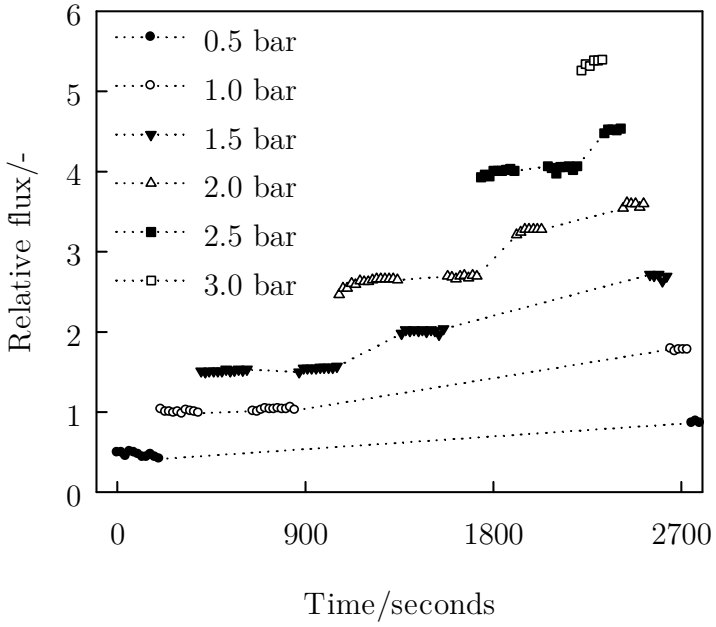

Figure 4-11 - Raw relative flux data for incremental pressure increases and decreases

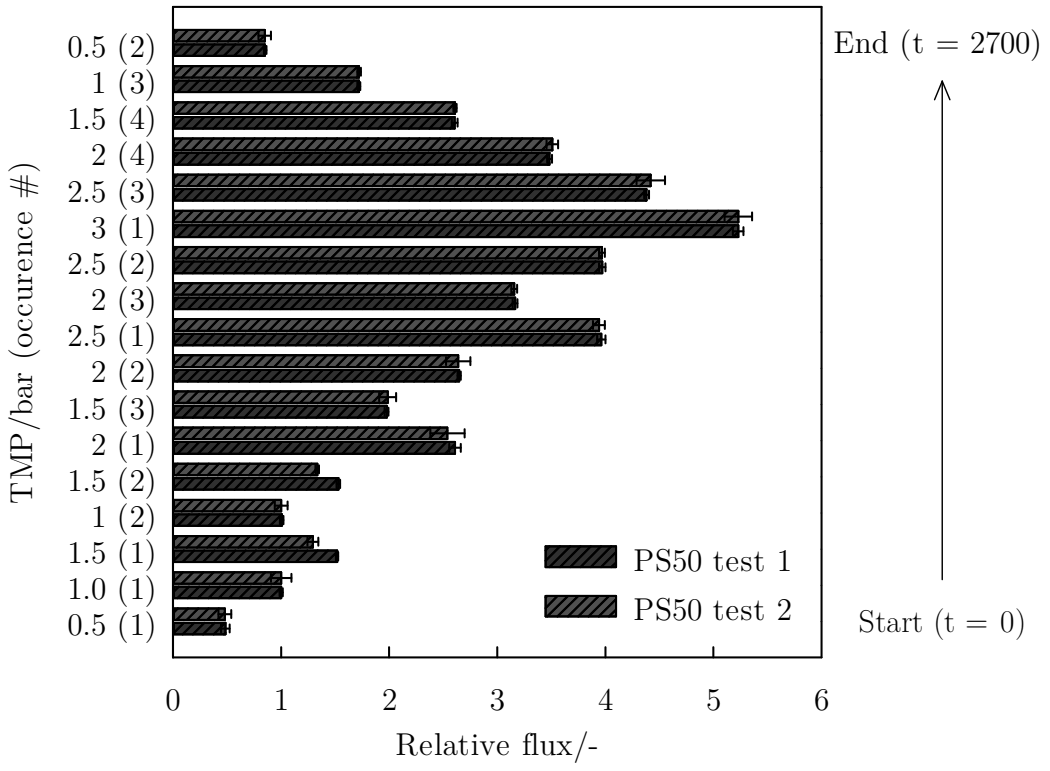

Figure 4-12 - Averaged flux data for incremental TMP increase experiments for PS50 membranes

Averaged flux results are displayed in Figure 4-12 (data are relative to the initial 1.0 bar averaged flux value for the given membrane). The raw data shows that even at 3.0 bar, no compaction behaviour or flux loss is seen and in fact when the TMP is decreased to a previous level, there is a relative increase in flux. When comparing the initial and final 0.5 bar TMP flux, there is a relative change from 0.484 ± 0.040 to 0.852 ± 0.013 for test 1 and 0.479 ± 0.059 to 0.848 ± 0.058 for test 2, the data representing an increase of 76 ± 6%. Table 4-8 shows the relative increase associated with different pressures. The largest percentage increase comes for the 1.5 bar pressure band where an 85 ± 4% flux uplift was noted.

Table 4-8 - Relative flux increases after incremental pressure increases after 3.0 bar maximum

TMP/bar	*Relative flux increase/%*
0.5	76 ± 6
1.0	72 ± 6
1.5	85 ± 4
2.0	36 ± 11
2.5	11 ± 9

A hypothesis for the observed flux increases could be in part due to overcoming the breakthrough pressure for fluid (water) entering the pores. Typically water would wet a hydrophilic polymer such as polysulfone. On the macro-scale, wetting of the apparent homogeneous (smooth) surface occurs, with large pores on the surface being spontaneously wetted by the fluid and thus allowing water transmission through the pores. In certain

regions, where small pores are present, a localised heterogeneous surface may exist where the wetting behaviour is resisted by localised surface roughness, enabling only partial wetting of the surface. The surface exhibits local hydrophobicity in these rough areas. For a given pressure, a wetting transition can occur whereby the thermodynamics of the system becomes favourable towards wetting of the surface over the non- or partially-wetted state in the rough areas (where the applied pressure overcomes interfacial tension between trapped air and wetting fluid) and the heterogeneous surface wets, and consequently, smaller pores are filled. This phenomenon is defined by the transition from a Cassie-Baxter wetting state to a Wenzel state (see 2.4.3.2). The theoretical breakthrough pressure P of a liquid with surface tension γ into a circular pore of throat radius r for a material with effective contact angle θ is given by the Young-Laplace equation - the same theoretical basis for that of mercury porosimetry (the Washburn equation) (see 2.2.4.2).

If the explanation follows, the largest flux uplift observed at 1.5 bar would suggest that the greatest proportion of inactivated pores lie in the corresponding pore throat radius for break-through at 1.5 bar. Such a simplistic conclusion may be too straightforward given the potential variability in apparent contact angle however. The theory could go some way to explaining the findings although internal swelling under pressure and incomplete relaxation upon depressurisation cannot be wholly discounted. An indication as to the magnitudes of the pores is shown in Figure 4-13. If there are areas of apparent hydrophobicity lying between arbitrary contact angles of 91° and 120°, pores activated by 1.5 bar pressure would range between approximately 15 nm and 480 nm. This assumes the apparent hydrophobic region spans the entire pore mouth or even greater area.

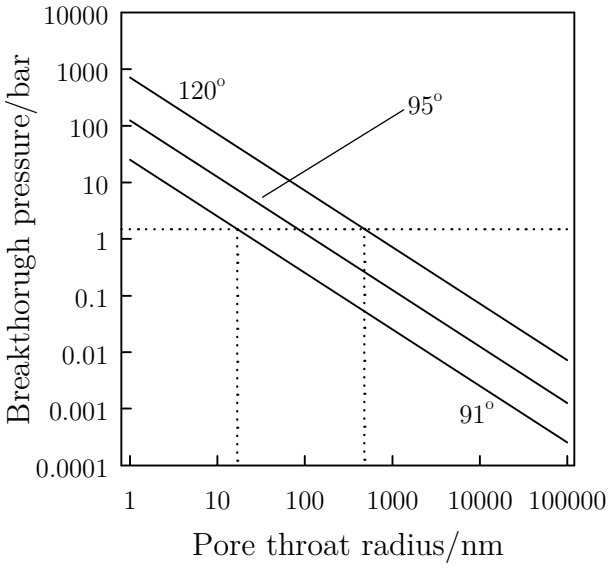

Figure 4-13 - Theoretical water breakthrough pressure for a range of pore throat radii at 3 water contact angles. Dotted lines indicate the range in which the pores would be filled under 1.5 bar pressure. Contact angles were chosen arbitrarily for illustrative purposes.

4.6.3.3. Conclusions for compaction and permeability tests

This section shows that exposing membranes to elevated pressures (elevated meaning exceeding typical experimental pressure) is required to give a consistent membrane performance not through compaction, but by ensuring complete, or at least consistent filling of pores. If this elevated pressure exposure is discounted, inconsistencies are likely to arise from membrane to membrane, especially if varying the operation temperature (differing surface tension and thus break-through) or during variable pressure (constant flux) operation. It is for this reason that all membranes used for experimentation were fluxed with 60 °C water at 4.0 bar and 1.5 ms^{-1}. This is to maximise both glycerol removal and activation of the highest proportion of pores possible. It can be deemed an extension of the hot water conditioning method described by Weis *et al.* (2005) [168].

4.6.4 Support layer

The membrane support layer was isolated by dissolution of the active layer in a suitable solvent (n-methyl-2-pyrollidine). This layer for all membranes was made from polypropylene and was not susceptible to dissolution in the solvent. After rinsing and drying, the layer was analysed for total porosity by dry-weight wet-weight analysis of 24 mm discs. The porosity of the layer was found to be 17.6% ± 0.8% and the layer thickness was 193 µm ± 11 µm (n = 45), determined using a digital micrometer. The porosity is somewhat lower than would be expected, however consistent values were obtained from 15 different wetted discs. The support is not expected to offer a high degree of hydraulic resistance despite its higher than expected density. Given that it is also situated on the downstream side of the active layer, susceptibility to cake fouling can be discounted. Blockage of pores is also unlikely given any material contacting this layer has previously permeated the much finer active layer first.

The layer was viewed under a light microscope to give an indication of the material structure. Figure 4-14 shows the individual polypropylene fibres which are tangled together creating a robust and inert support for the active layer. The fibres are estimated to be around 0.02 – 0.05 mm.

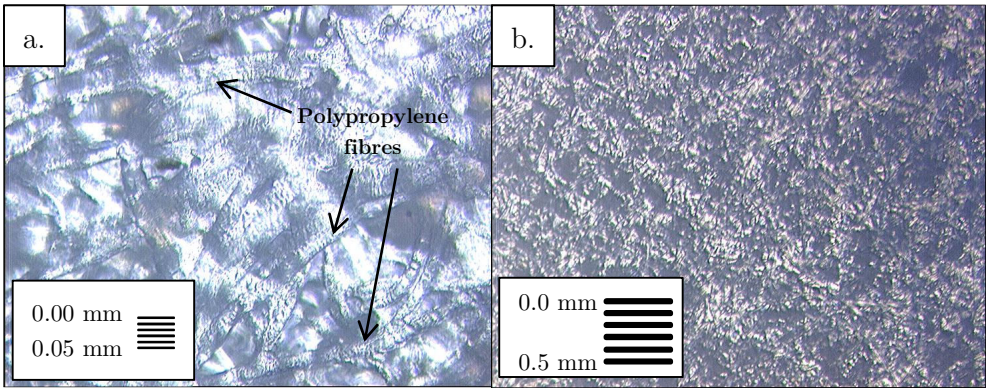

Figure 4-14 - Light microscope pictures of the polypropylene support layer

5. Polymeric membrane pre-treatment with primary alcohols

5.1 Introduction

The results in this chapter concern the application of alcohol pre-treatment to polymeric membranes and the modifications which arise. As was explained in chapter 1, defeating the efficiency setbacks incurred by fouling by modification of membrane properties is the strategy employed in this chapter.

Whilst studies characterising the effects of various organic solvents on ultra- and nanofiltration membranes have long since been established, less abundant in the literature are studies which observe the effects of the permeating solvent as the pre-treatment agent, or alternatively, the wetting agent. Kochan *et al.* (2009) [35] remain isolated in their attempts to specifically elucidate the mechanisms contributing to water flux uplifts for PS and PES resulting from prior isopropyl-alcohol (IPA), ethanol and acetone wetting. Characterisation techniques used in this study comprised of permeability measurements and contact angle (sessile drop) quantification, as well as more practical assessments such as BSA, dextran and sludge supernatant filtration. The treatment protocol was a 2 hour immersion of membranes into the wetting agent, with no attempts made to permeate solvent through the membrane matrix. The results showed that permeabilities for both flat sheet PS membrane (3-fold increase) and hollow fibre PES membrane (> 2-fold increase) were evident after immersion in 80% ethanol and 80% IPA treatment (unclear as to whether this is wt. % or vol. %). No change in hydrophobicity or filtration characteristic was observed, leading to the conclusion that no change in fouling propensity was evident. They considered pore 'opening' and wetting agent-membrane material compatibility (Hildebrand solubility parameters) as key influencing factors.

This chapter aims to document findings pertaining to alcohol pre-treatment of industrial polymeric membranes, with focus on PS membranes, given their ubiquity in a range of applications. Insight is provided by analysis of fundamental membrane properties such as hydrophilicity, surface chemistry and charge, as well as looking at morphological changes such as roughness, swelling and pore size distribution. Furthermore, model solution filtrations have been carried out in addition to fouling propensity analyses in an attempt to couple fundamental membrane properties to filtration performance. By application of a standard pre-treatment protocol, the aim is to show that (i) there are membrane permeability increases following alcohol treatment, (ii) membrane properties which relate to fouling propensity are changed, (iii) further changes related to membrane structure are incurred and (iv) the changes observed in (ii) and (iii) result in performance modification to the membranes studied.

5.2 Experimental design

A more detailed study of the effects of membrane wetting with alcohols was undertaken for flat-sheet PS membranes. Firstly, characterisation of increases in fluxes were assessed in an attempt to replicate the results shown by Kochan *et al.* (2009) [35]. For this, permeation of the membrane by the treatment agents [methanol (MeOH), ethanol (EtOH) and n-propanol (nPrOH)] was carried as opposed to immersion. This was deemed the most suitable approach so as to allow for complete wetting of the porous matrix and was implemented using two strategies, termed the *dynamic* and *static* protocols.

Dynamic: Unstirred fluxing of the treatment solution continuously for 90 minutes under 1.0 bar TMP. This was carried out in the stirred cell apparatus detailed in 4.1.3. This regime was used so as to minimise membrane usage, allow for more rapid repeatability and thus enable greater experiment repetition. It was hence used as the primary sample preparation method for the analyses presented in this chapter.

Static: Initial fluxing under 1.0 bar TMP for 10 minutes to fill membrane pores followed by permeate line closure and 24 hours resting under 1.0 bar hydrostatic pressure. Membranes were loaded into the plate and frame module as detailed in 4.1.1.1. This was attached to the pre-treatment apparatus (see 4.1.2). The predominance of experiments made using this regime were for filtrations carried out as detailed in subsequent chapters, though a comparison of methods is made here.

The treatment methods were carried out for selected samples using the three primary alcohols at a range of concentrations. Following this, insight into the changes brought about to the surface and internal properties were assessed by way of wettability (contact angle), charge (streaming potential/zeta potential through pores) and surface chemistry (FTIR). Morphological changes were assessed to measure swelling (by measurement of membrane thickness), qualitative measurements showed variation in membrane layer swelling (membrane roll/curvature), roughness (via AFM), tensile strength/elasticity (via AFM), and porosity/pore size distribution (via mercury intrusion porosimetry). Treated membranes were also challenged by model solutions (BSA and β-lactoglobulin), adsorptive fouling studies made using BSA as a sorbent, and AFM adhesion measurements made using protein-doped colloidal probes.

5.3 Effect of alcohol treatment on pure water flux

Membrane flux of polysulfone 50 kDa (PS50) membranes was measured before and after treatment using the dynamic method and three treatment agents.

5.3.1 Effect of Alcohol type and concentration

Alcohol-in-water mixtures confirmed that flux uplifts as a result of 90 minutes treatment were apparent, and that alcohol concentration influenced the modified flux to varying degrees. For MeOH treated membranes (Figure 5-1), 20 wt.% MeOH in water gave a relative flux uplift of 1.65 ± 0.10 compared to the untreated PWF of 110.5 ± 6.1 $Lm^{-2}hr^{-1}$ (based on the average of MeOH treated membrane samples only). There was no variability observed for 30 and 40 wt.% treatment (1.61 ± 0.03 and 1.63 ± 0.07) before 50 wt.% treatment induced a rise of 2.48 ± 0.03. Further increases in treatment solution to 100 wt.% induced a maximum relative rise of 2.98 ± 0.07. The plateau region and relative changes in flux were comparable when treating with EtOH (Figure 5-2), albeit with more variation in treated water fluxes, which is manifested in the error (standard deviation for n=3). For 20 wt.% EtOH, a rise of 1.66 ± 0.17. Using 30 and 50 wt.% alcohol concentration yielded rises of 1.76 ± 0.05 and 1.99 ± 0.04, and a maximum (again at 100 wt.% EtOH) of 2.87 ± 0.04. nPrOH treatment (Figure 5-3) also gave similar rises; 30 and 50 wt.% treatment showed relative uplifts of 1.69 ± 0.09 and 1.83 ± 0.12 respectively.

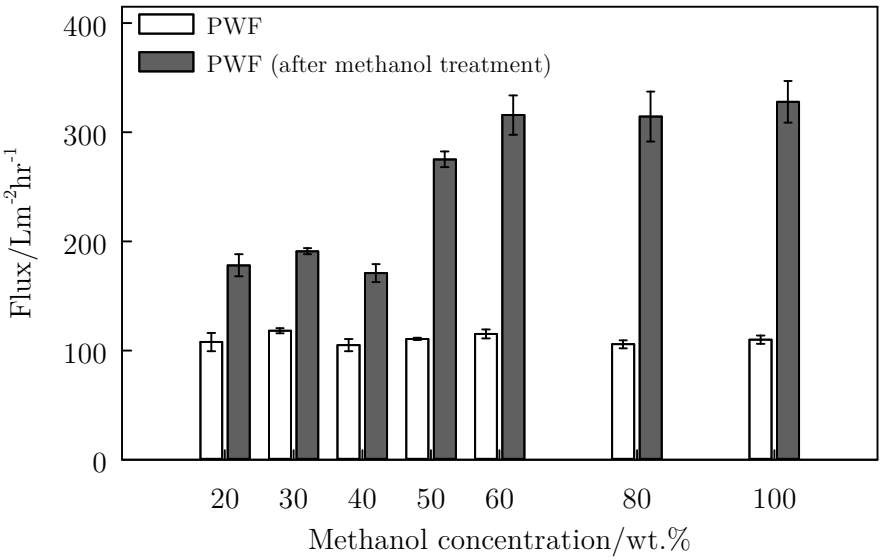

Figure 5-1 - Flux uplifts resulting from methanol treatment

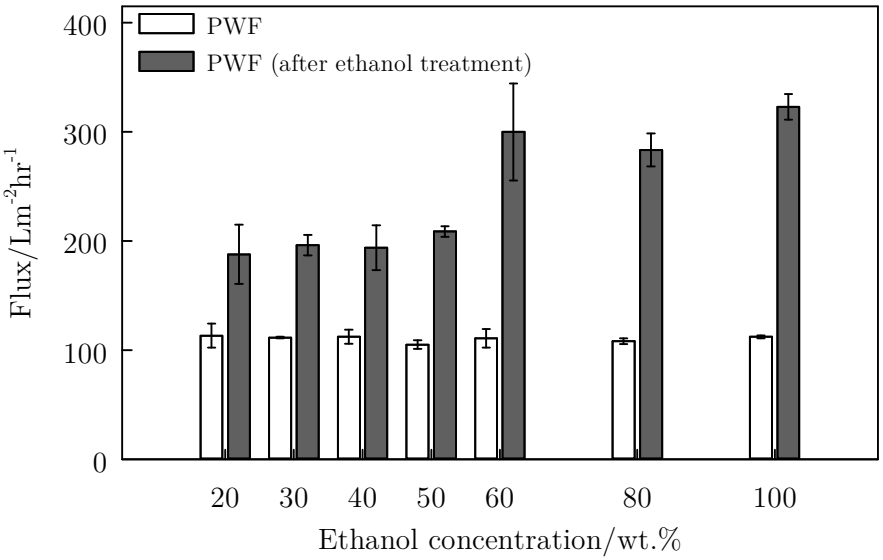

Figure 5-2 - Flux uplifts resulting from ethanol treatment

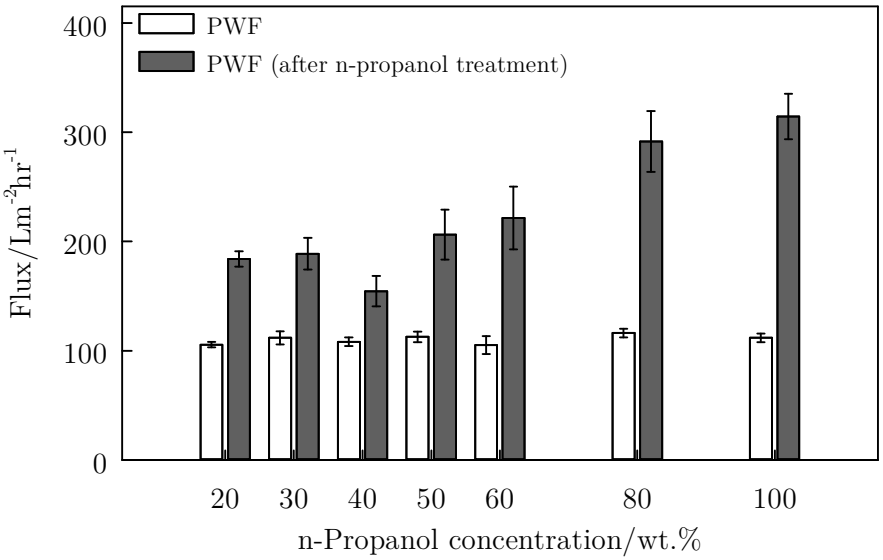

Figure 5-3 - Flux uplifts resulting from n-propanol treatment

The exact mechanism of flux enhancement at this stage was unclear, it was assumed that the plateau region is attributed to the associated maxima in viscosity for primary alcohol-in-water mixtures as shown by (Figure 5-4). This could occur given the occurrence of residual in pore alcohol which, given its higher viscosity, would be less easy to displace by water fluxing i.e. giving incomplete rinsing. The flux rises were apparent nevertheless, meaning whatever flux uplift mechanisms occurred overrode this effect. The flux uplift mechanism is also likely to be influenced by alkyl chain length of the alcohol. This could be due to increased polymer swelling (the alcohol having greater partial solvency over water) or due to sorption, and thus surface property modification, of the surface or internal structure. From these results it could be assumed that nPrOH is the least suitable swelling agent for polysulfone given it produces the lowest maximum flux uplift, though this is

shown later not to be the case (see 5.7.6). The interplay between solvent and water does appear to have a strong bearing on the flux increase, indicating the relative contributions that hydration and solvation can play in modifying PS membranes.

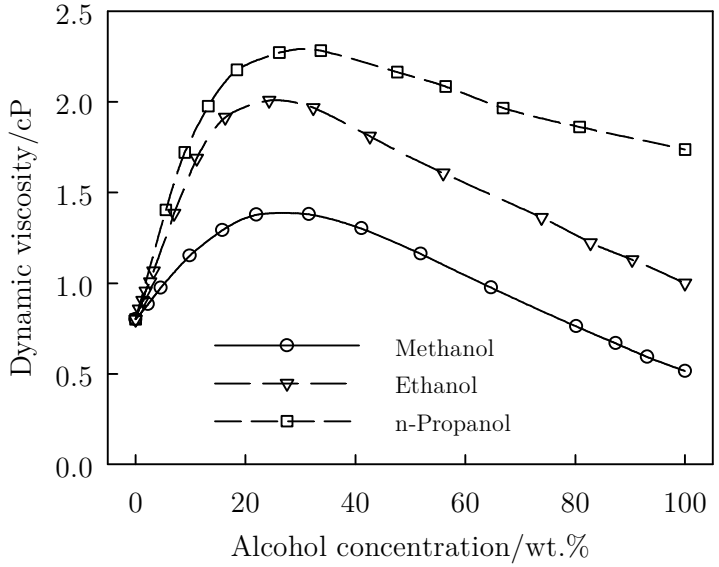

Figure 5-4 - Viscosity of binary alcohol-water mixtures (data obtained from [276])

5.3.2 Longevity of treatment and treatment protocol variation

Extended water fluxing (90 minutes) of PS50 and PS100 membranes was carried out before and after alcohol treatment for both static and dynamic methods to gain an appreciation of how enduring the flux modifications were. In theory, if swelling was the predominant mechanism for uplifts, de-swelling through water fluxing should also occur. Prior extended fluxing with water was carried out after hot water conditioning and 4.0 bar TMP exposure to ensure consistent baseline fluxes. The static or dynamic treatment method was then applied to samples before re-testing on their respective apparatus. For the PS50 membrane (sample data presented in Figure 5-5), both treatment methods showed some decline in flux after 90 minutes, indicating this de-swelling behaviour. The flux reduction was not significant however, and stabilised within 90 minutes. This was also the case for both treatment methods when considering the PS100 membranes.

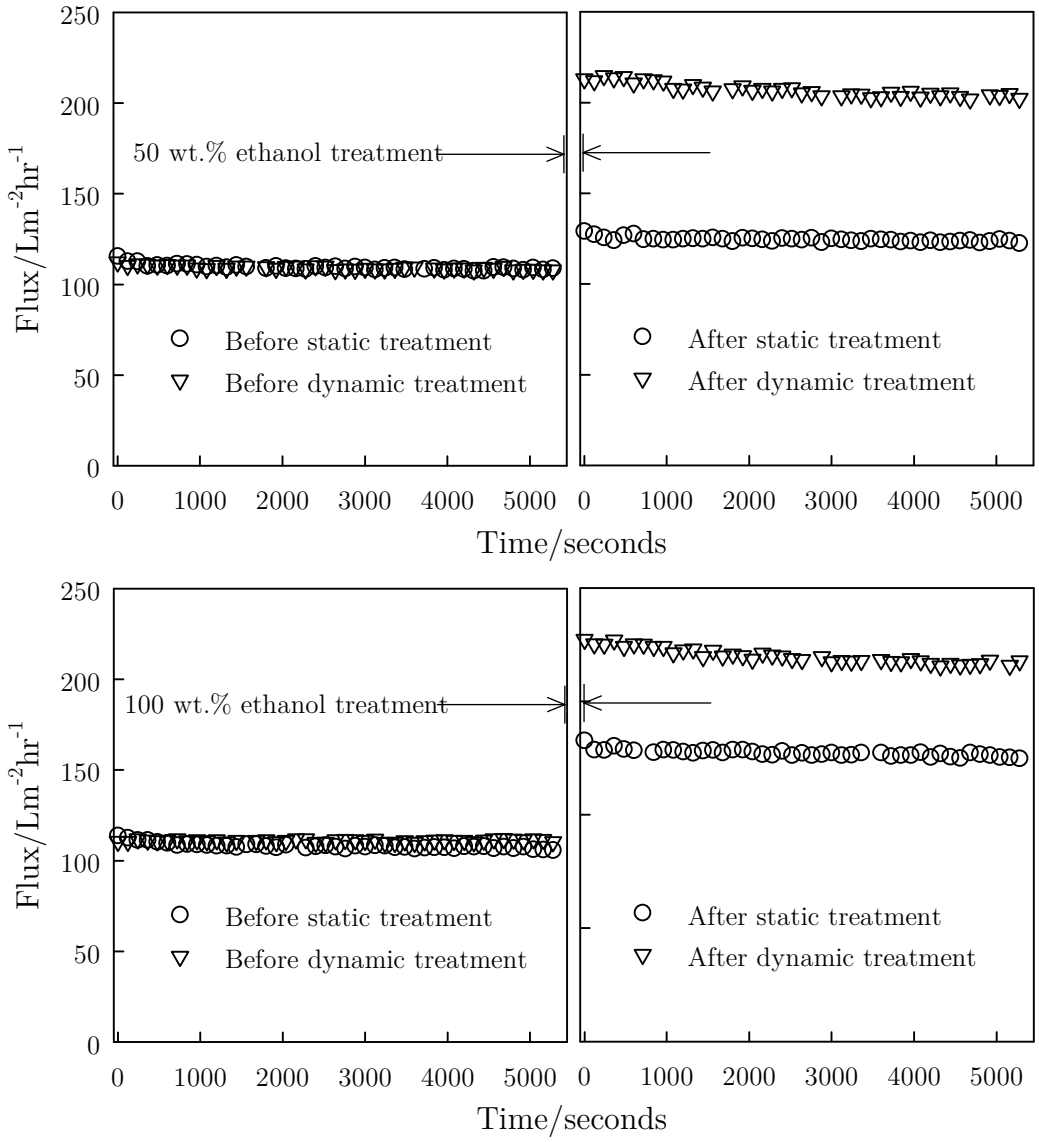

Figure 5-5 - Extended PS50 pure water fluxing before and after treatment with ethanol using two treatment methods

The disparity between static and dynamic methods for the PS50 membranes was significant, though less so for PS100 membranes. This is represented by the average relative flux changes obtained for both methods as indicated in (Figure 5-7). For the static method, the PS50 membrane showed uplifts of 1.43 ± 0.07 and 2.28 ± 0.04 for 50 and 100 wt.% ethanol treatment respectively, compared to 1.99 ± 0.04 and 2.87 ± 0.04 for comparable treatments in the dynamic regime. This effect was not substantially apparent for PS100 membranes (Figure 5-6), these showed for 50 and 100 wt.% EtOH an average increase of 3.75 ± 0.10 and 3.85 ± 0.06 in the static regime, and 4.01 ± 0.53 and 4.08 ± 0.43 in the dynamic regime. The dynamic treatment method showed significantly less consistency in this regard.

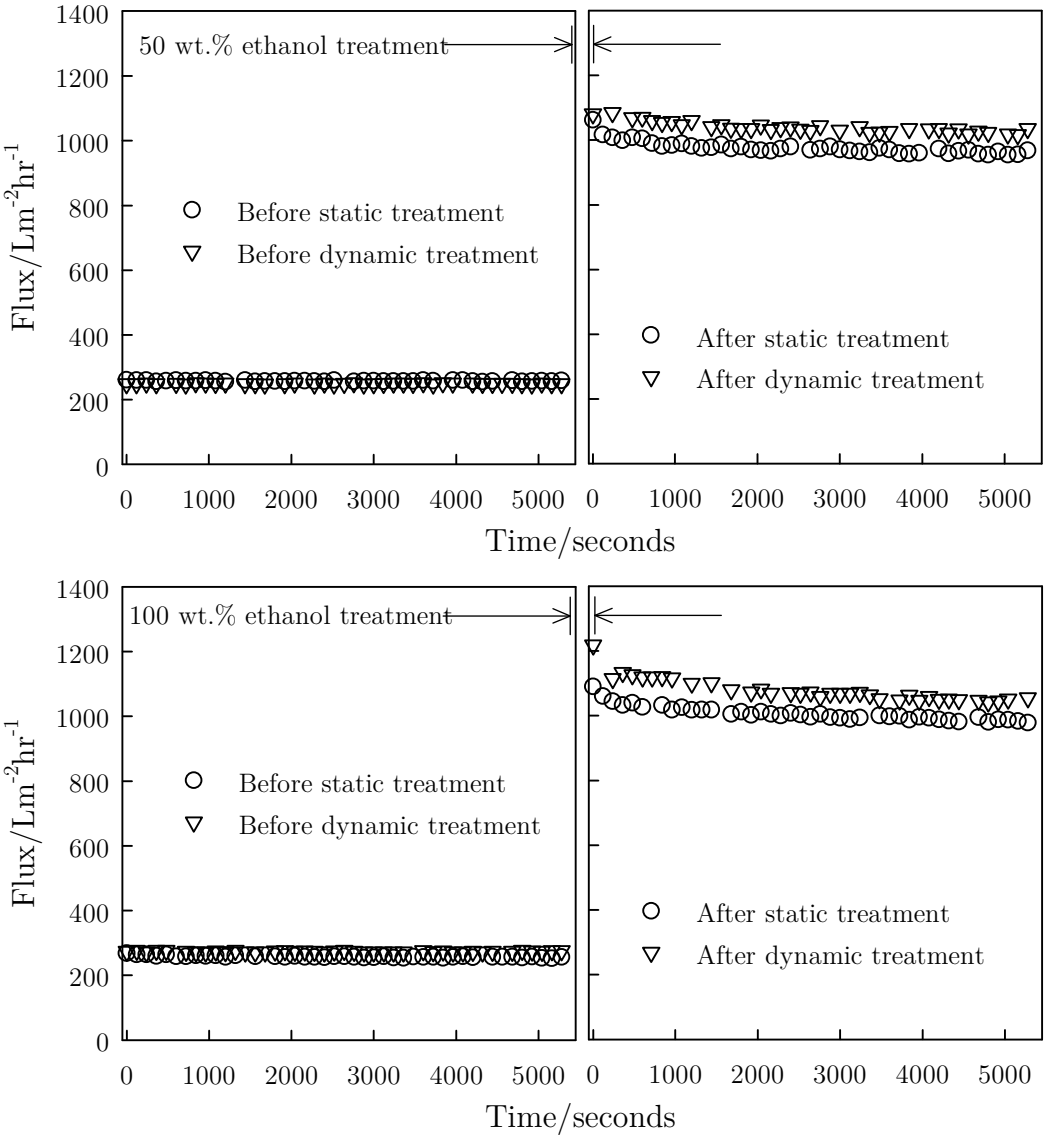

Figure 5-6 - Extended PS100 pure water fluxing before and after treatment with ethanol using two treatment methods

The findings provide some important information about the system and guidance on elucidating the modification mechanism. For the PS50 membrane, and potentially the PS100 membrane to a lesser extent; the degree of membrane swelling upon contact does not appear to be kinetically dependant on alcohol contacting duration for membranes studied here (since a 1 hour treatment gave more substantial uplifts over 24 hour treatment).

This is assuming that the action of moving fluid does not provide a shear induced effect which increases the rate of swelling. Also, the membrane structure or pore size plays an important role in flux uplifts, shown given the significantly greater increases for PS100 membranes over PS50 membranes. Additionally, the dynamic treatment method provided greater inconsistency in flux uplift measurements. The lower membrane area used for dynamically treatment membranes coupled with the greater susceptibility to membrane

disruption at the membrane edges caused by expansion (see 5.7.1 and 5.7.3) are a potential reasoning for this. Finally, the differing proportions of flux uplift when comparing untreated (relative flux equal to 1) and 50 wt.% treated membranes, and that when comparing 50 to 100 wt.% uplifts varies. In other words, there is an insignificant difference in treating a PS100 membrane with 50 or 100 wt.% EtOH, though these same treatment concentrations produce results with a significant difference for PS50 membranes.

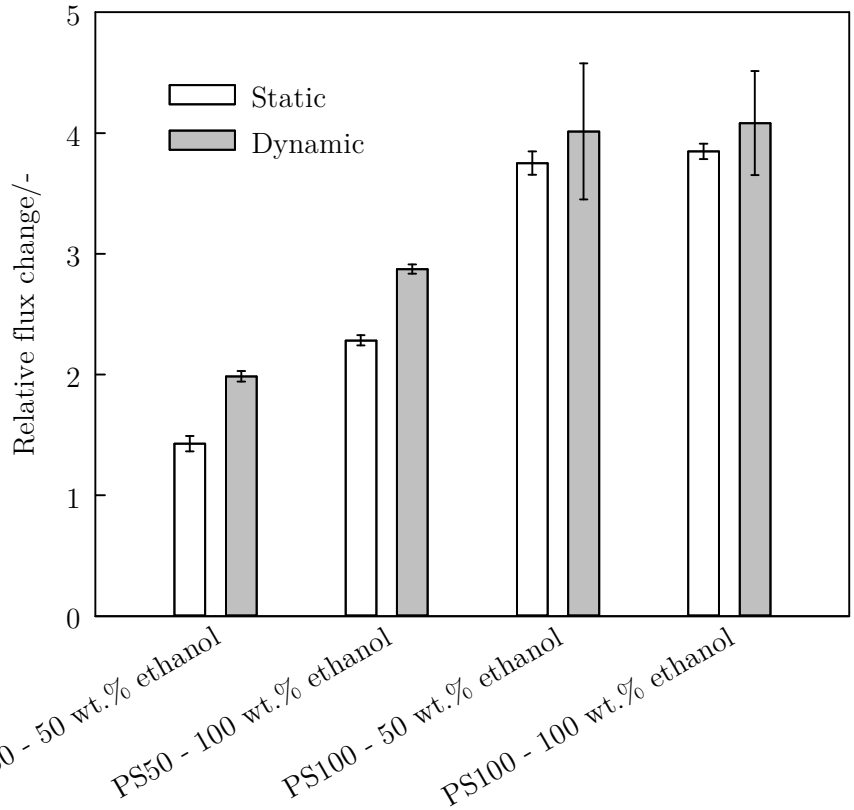

Figure 5-7 - Average flux uplifts using both static and dynamic treatment methods

5.3.3 Storage in water after treatment

Figure 5-8 shows fluxes for PS50 membranes stored in water following treatment and water purging after 24 hours and 14 days.

Apparent here are the comparable concentration vs. flux trends which were evident from post-treatment flux testing (Figure 5-1, 4-2, 4-3). After the second flux test (following either 24 hour or 14 day storage), these membranes were discarded (hence single measurements). The results do have some inconsistencies (e.g. post-24 hour storage of 20 wt.% EtOH treated membrane) though in the majority of cases, show that a drop off in treated flux is apparent. These indicate that the membrane does not return to its original state and the treatments induce some permanent alteration, at least within the timeframe studied. It is indicated that membranes may not fully equilibrate to their altered state by straightforward rinsing after treatment. Even though this is the case, characterisation experiments detailed in the following pages focused on the membrane state directly after

treatment and rinsing. This was to enable the 'maximum' effect of alcohol treatment to be apparent at the point of measurement.

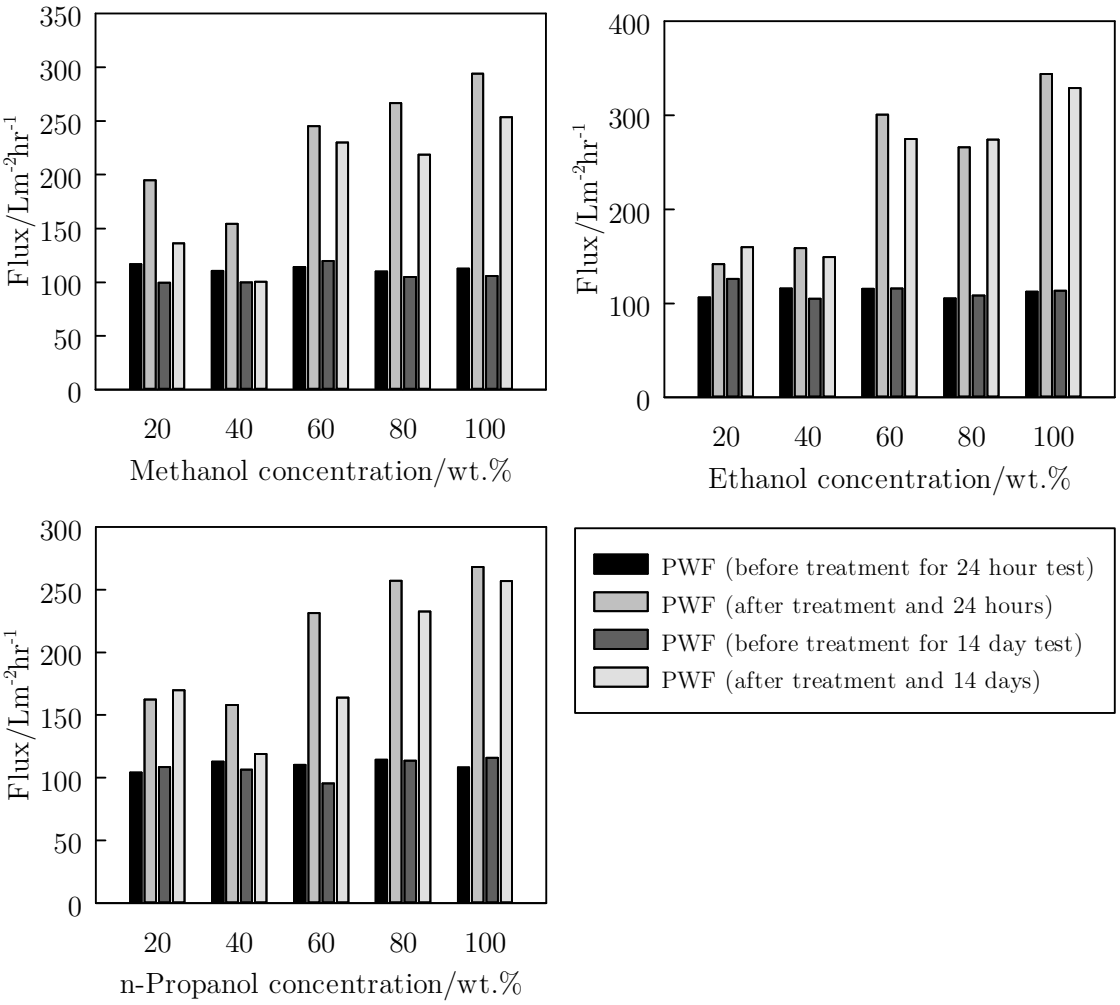

Figure 5-8 - Initial and post-treatment fluxes and following 24 hours or 14 days of storage in RO water

5.4 Surface contact angle measurements

Sessile drop contact angles were measured on air dried substrates (and after at least 12 hours after storage in a desiccator at RT). Five measurements across three membrane samples were used. Measurements in Figure 5-9, Figure 5-10 and Figure 5-11 have been compared against the control substrate (untreated membranes). The hypothesis was that pre-treatment using alcohols can affect the wetting properties of PS membranes. Thus the following null hypothesis was formulated as a basis for the statistical test (t-test), '*a change in contact angle is not a result of alcohol treatment*'. The two-tailed unpaired t-test significance is indicated for each averaged measurement where 'NS' denotes, no significance (< 95% probability of a change), '*' denotes a 95% or greater confidence, '**' denotes 99% or greater confidence, and '***' denotes a 99.9% confidence that the null hypothesis can be rejected.

5.4.1 Effect of alcohol type and concentration

Following MeOH treatment of PS50 membranes, all treatment methods produced a surface which was more hydrophobic over the untreated surface ($74.2^\circ \pm 1.9^\circ$) (see Figure 5-9a). The measurements show a gradual increase with increased MeOH concentration up to a maximum of $85.3^\circ \pm 0.9^\circ$ following 100 wt.% treatment. EtOH treatment (Figure 5-9b) also produced similar results. nPrOH (Figure 5-9c) again showed a similar trend, with 100 wt.% treatment producing the most hydrophobic surface out of all of the modified PS50 membranes ($86.8^\circ \pm 1.2^\circ$). Although the standard deviations of measurement show overlaps when comparing 100 wt.% treatment for the various alcohols, the nPrOH membrane showed a strong significance (***) against the null hypothesis when tested against the 100 wt.% MeOH and EtOH treated membranes. The lower alkyl chain length modifier (MeOH) showed no significant difference against EtOH treatment.

Rises in contact angle (hydrophobisation) were seen as a result which contrasted the initial hypotheses for why alcohols were being applied to membranes; to act as wetting agents and increase hydrophilicity. As discussed in 4.6.3.2, surface porosity can impart apparent hydrophobicity to otherwise hydrophilic surfaces and could have occurred due to swelling and thus expansion of pores. The degree to which surface porosity can influence apparent contact angle is appreciated by use of the Cassie-Baxter model (see Appendix D3). In order to indicate that the changes made in apparent contact angle may have been influenced by surface topological changes, the theoretical untreated membrane flux was used to approximate surface porosity using the Hagen-Poiseuille (see equation 2-10 and Appendix D3 for full analysis). This value was then used in the model to give the true contact angle from the apparent experimental values determined. For the example given in Appendix D-3, an arbitrary range of surface porosities was selected above this baseline untreated value to represent the trend that was seen for the experimentally determined results for the hypothetical situation that surface porosity increase was the only influencing factor. It was found that a surface porosity increase from 0.25 to 0.31 could influence the degree of change observed in apparent contact angle. This would seem to be a realistic range for a swelled membrane. Other factors could perhaps have been through rearrangement of the polymer

structure to produce a more undulated surface. This could also have implications with regard to fouling [28]. Another hypothesis considered was that there was some chemical modification to the surface. It was thought unlikely as only alcohol (or water) was present, and an absence of reagent in the treatment solution. This could not be fully discounted as impurities or other membrane constituents could be involved in some form of transformation. Both of these hypotheses were latterly investigated.

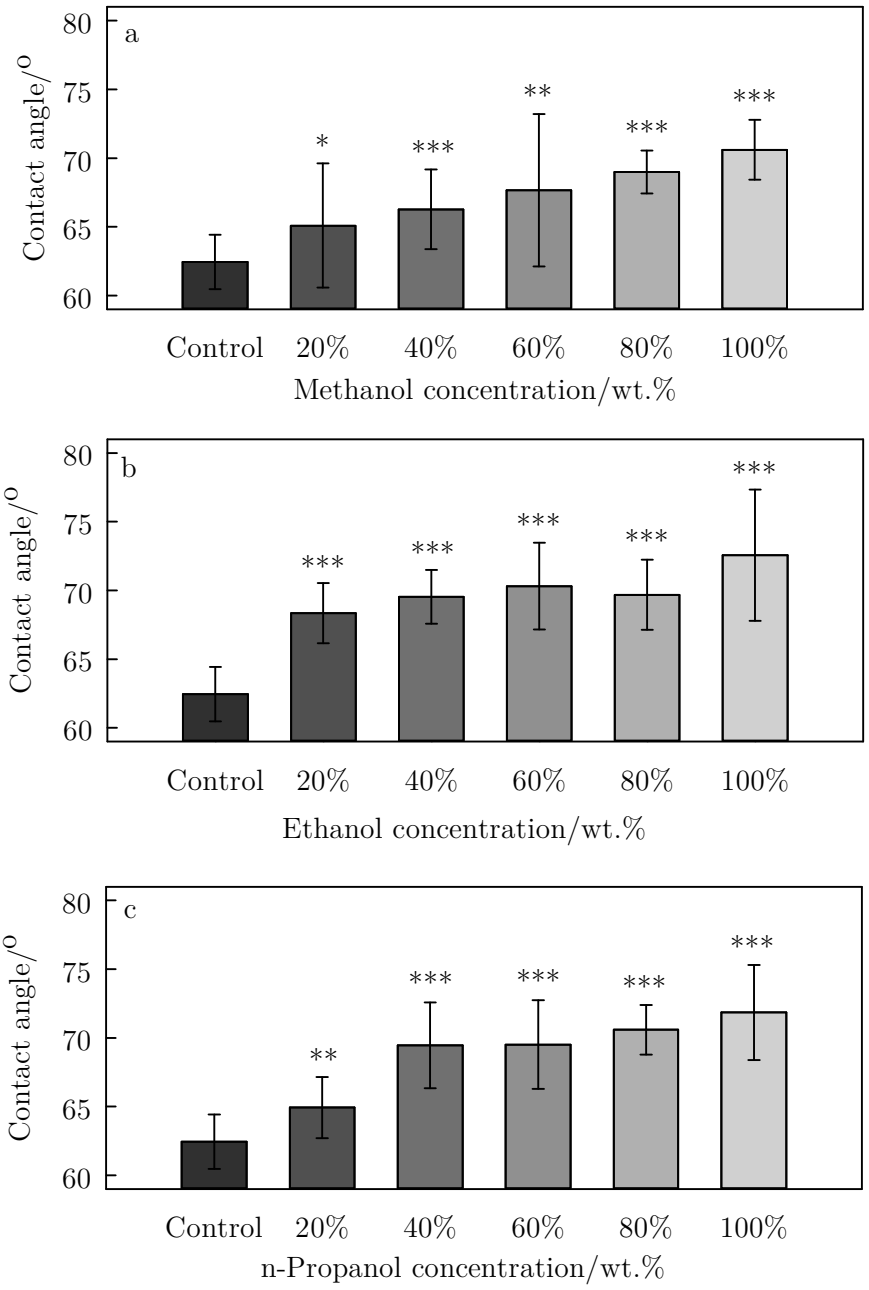

Figure 5-9 - Contact angles for PS50 membranes following treatment and rinsing

In order to first confirm that these changes were indeed a modification to the membrane as a result of the alcohol treatment methodology, measurements were repeated extensively for the 25 kDa and 100 kDa PS membranes.

5.4.2 Effect on various membranes

Figure 5-10 shows the same set of experiments repeated for the PS25 membrane. The untreated virgin surface displayed a contact angle of 62.4 ° ± 2.0 °, and with each alcohol type, displayed increases akin to what was observed for PS50 membranes. The overall degree of hydrophobisation was less pronounced. There was no significance in the degree of hydrophobisation between alcohol types leading to the conclusion that the alcohols acted in more or less a consistent manner, in terms of modification of wetting properties.

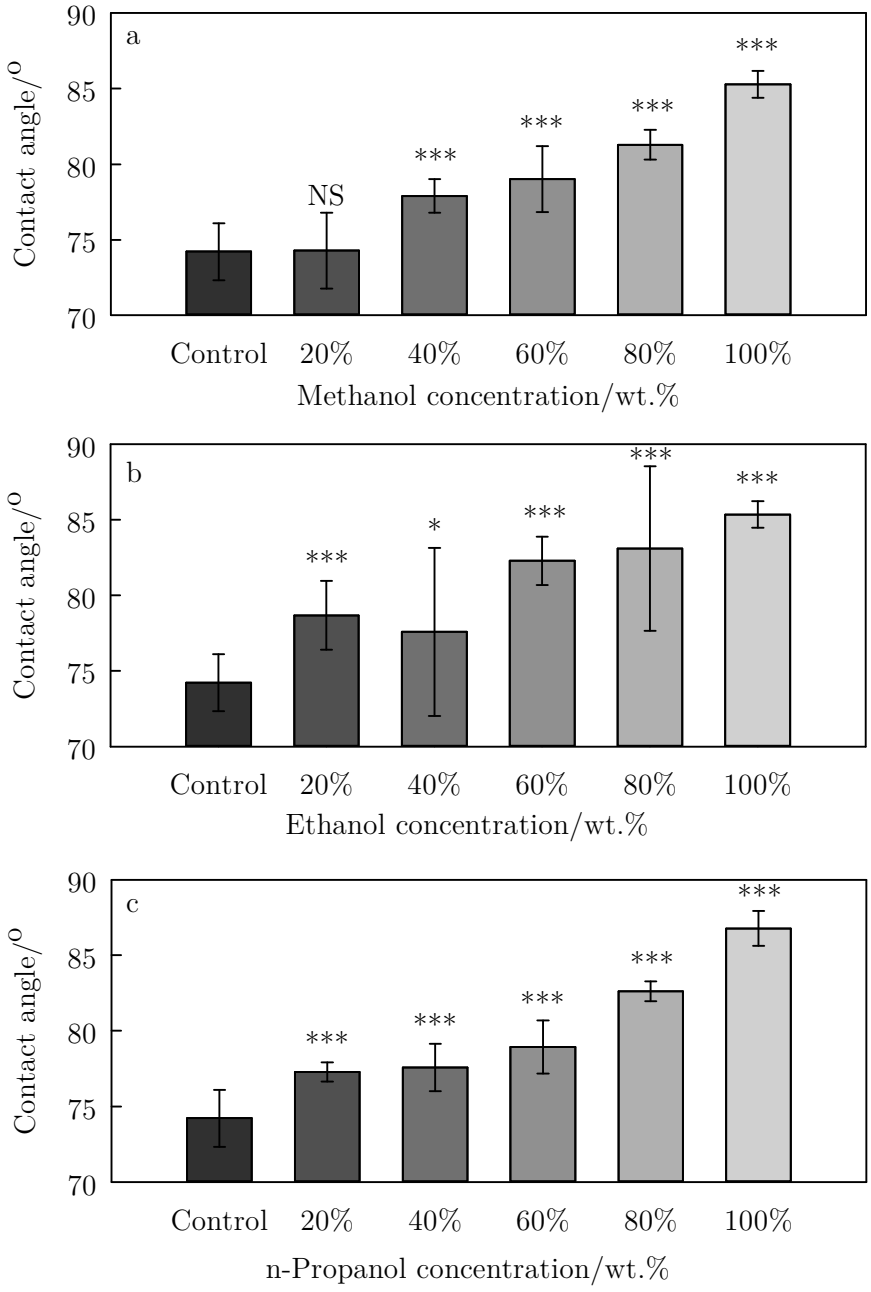

Figure 5-10 - Contact angles for PS25 membranes following treatment and rinsing

For PS100 membranes (100 kDa PS) (Figure 5-11), virgin untreated substrates showed contact angles between that of the PS25 and PS50 membranes (66.1 ° ± 1.7 °). 50 wt.%

EtOH and 100 wt.% EtOH treatment showed contact angles of 71.7° ± 3.0° and 73.8° ± 0.6° respectively and, although they show similar trends to previous data, the actual static contact angle may be different (since the image of the contact angle was taken so rapidly upon droplet application). The reading may therefore reflect more of an advancing contact angle. For hydrophilic surfaces these are typically higher than static or receding contact angles, as shown by Zhang *et al.* (1989) [158]. The inconsistencies in this measurement are reflected by the inconsistent rises for MeOH and nPrOH, though both still show a significant change against the control substrate.

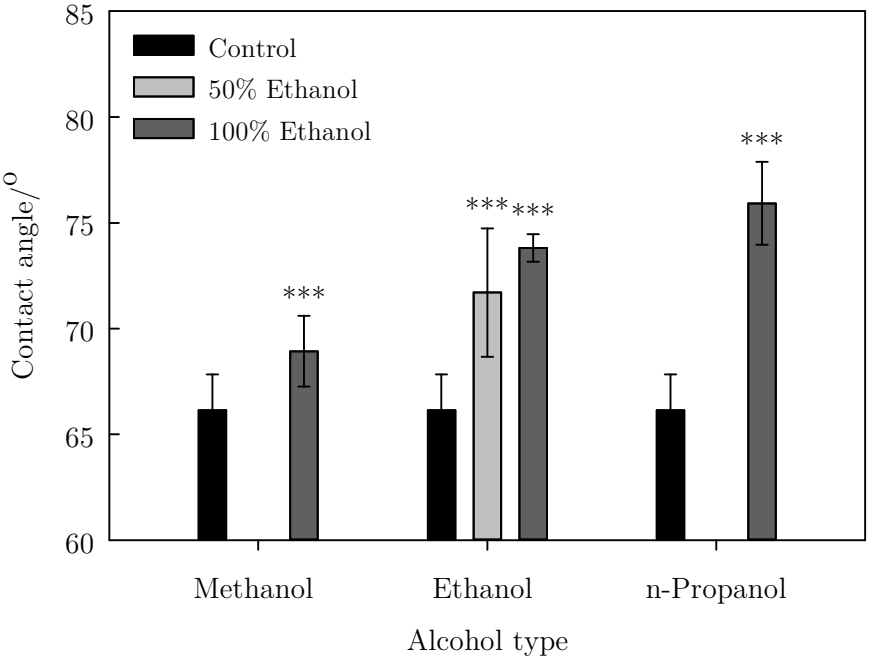

Figure 5-11 - Contact angles for PS100 membranes following treatment and rinsing

5.5 Through-pore zeta potential

Apparent zeta potential information of control and treated membranes was obtained using the method described in 4.4.1.2. Since contact angle gave an indication of surface energy, through-pore streaming potential measurement was opted for over surface charge measurements. Although not strictly comparable, it would be expected that surfaces displaying hydrophilicity (and thus greater surface energy) would exhibit a stronger absolute charge (either positive or negative). This combined with the contact angle measurement would thus give a more rounded picture of the membrane as a whole, from both surface and in-pore perspectives.

5.5.1 Effect of alcohol type and concentration

Figure 5-12 shows the control and treated apparent zeta potentials for PS50 membranes following RO water rinsing. Indeed the action of the alcohol is to reduce the net charge through the pore which links logically to the increased hydrophobicity. The degree of charge modification is somewhat inconsistent with respect to alcohol/water concentration (again

reflecting the partial overlap of error bars shown previously for contact angle measurements. For the 100 wt.% treatment, there is a clear distinction from the other data sets across the pH range tested. The charge reduction increments with alcohol concentration change are more visible for EtOH treatments (Figure 5-12b). The sequential reduction in charge with increased EtOH mass fraction firmly reflects the findings in contact angle modification. The result is also repeated with nPrOH treatment aside from the overlap for 20 and 40 wt.% treatments at *ca.* pH 6 (see Figure 5-12c).

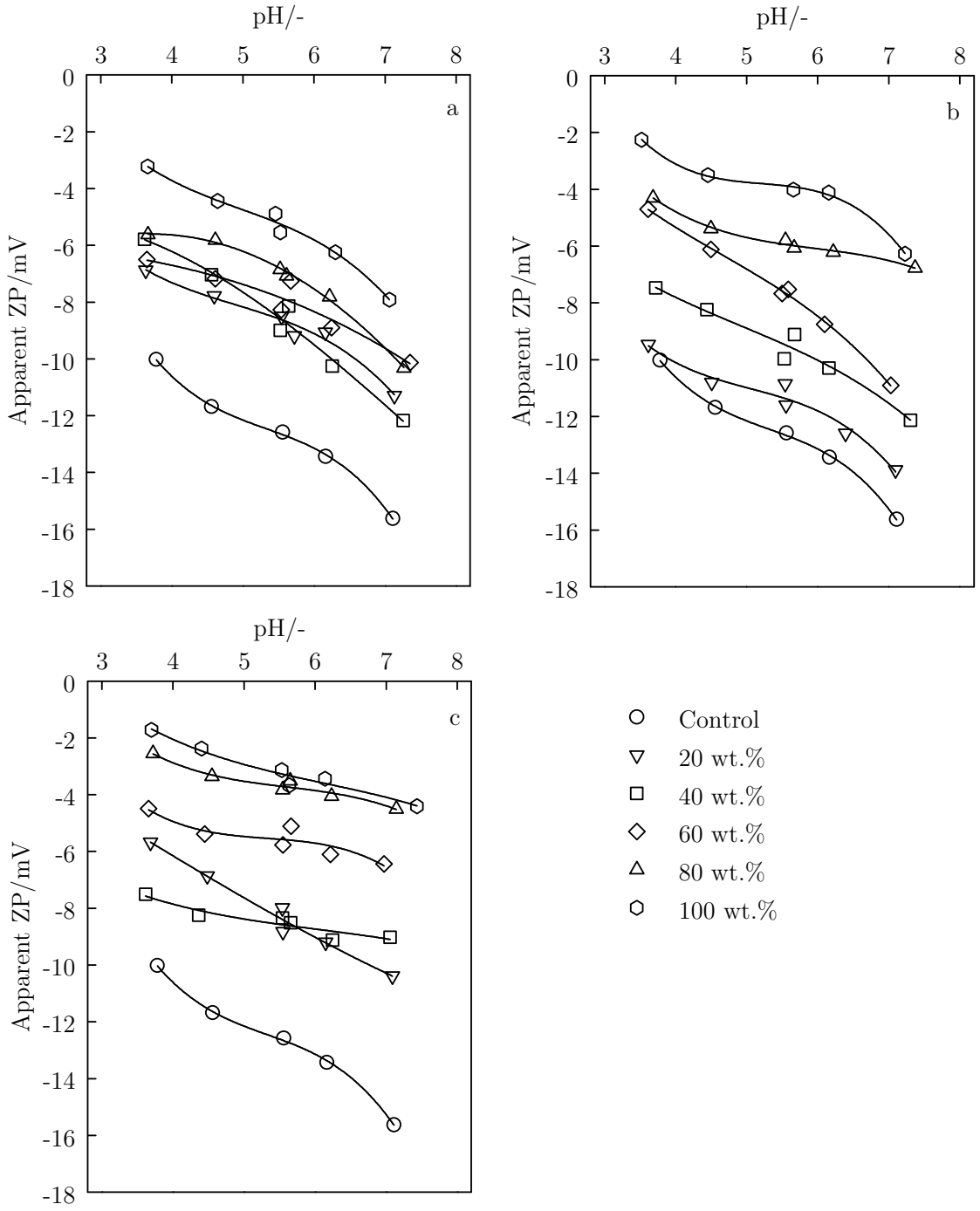

Figure 5-12 - Through-pore apparent ζ potential for PS50 membranes treated with various binary alcohol-water mixtures, a) methanol, b) ethanol, c) n-propanol

The results for these apparent ζ potential reductions may be explained as follows. A film of alcohol remained inside the pore; the alcohol molecule has a polar head (-OH group) and non-polar tail (alkyl chain) and thus a hydrophilic polymer would form H-bonds with this polar head, leaving the non-polar tail protruding into the pore space. This phenomenon could disrupt the EDL by partially shielding it from the ionic solution, given the lower conductivity of alcohol solutions compared to that of water. This would mean a reduced counter-ion (cation) presence in the slipping (shear) plane and thus a reduced streaming current detection. If this is indeed the case, a permanent charge modification to the polymer may not be occurring and the membrane could presumably return to its original state upon alcohol removal. Since longer alkyl chain length results in a lowering of polarity (lower dielectric constant for greater chain length), it would be expected that methanol would offer a stronger and more permanent modification to the membrane when in the proximity of a negatively charged surface. This was the case when comparing previously presented flux data but was not true when assessing the apparent ζ potential values obtained. In actual fact, nPrOH gave the lowest magnitude of charges out of all three ($<$ 2.0 mV at *ca.* pH 3.7), representing the greatest modification. This means that whilst adhesion of the alcohol to pore walls is likely to occur, there are other effects acting, probably relating to polymer dispersion/swelling.

If dispersion of the polymer is a factor then an expansion of pores is likely to occur due to swelling. It was hypothesised that this can occur through some modification in the charge density as a result of polymer dissolution, or more likely through pore size changes. The relationship between pore size and ζ potential has been shown for membrane applications both experimentally and theoretically [166]. A change in pore size can have strong implications for UF membranes especially, where pore diameters are of similar magnitude to the EDL thickness in electrolyte solutions (~ 4 nm for a 0.1 M NaCl solution). EDL overlaps which occur between opposing pore walls would be adjusted if pores expand, the streaming potential measurement would thus change accordingly i.e. shifting, in theoretical terms, towards a thin EDL assumption away from a thick (more overlapping) EDL assumption. In real terms, a greater co-ion presence in the shear plane and thus a lower value for a calculated apparent ζ potential.

With a through-pore ζ potential neutralisation would arise a reduction in the electro-viscous retardation effect as described in 2.4.3.4. Solvated counter-ion reverse flow through a pore with lowered net surface potential (modified EDL profile) would be reduced, since the balance of co-ion to counter-ion presence is the bulk pore space would be more uniform as a result of lower streaming potential. This effect could be a predominant means for how the flux of the membrane is modified as a result of apparent ζ potential changes when solutes are present, such as during filtrations. Since all flux measurements were conducted using RO water, these effects should have been predominantly eliminated during flux testing.

5.5.2 Effect of different alcohols on various membranes

Figure 5-13 shows the effect of 100 wt.% treatment with various alcohols compared to controls for PS25, PS50 and PS100 membranes. As was shown for the PS50 membrane (b), the PS25 (a) and PS100 (c) membranes showed significant apparent ζ potential reduction. The PS25 results do not indicate any obvious differences between the alcohol types though the trend of increased ζ potential reduction correlating with increased alkyl chain length is shown for both PS50 and PS100 membranes. The magnitude of charge for the largest pore size membrane (PS100) was also lowest for both untreated and 100 wt.% ethanol states which indicates that pore size and apparent ζ potential magnitude correlate reasonably. It was expected though that such a significant reduction in apparent ζ potential, especially for the PS100 which gains near charge neutrality, would foul more readily following ethanol treatment, since lower apparent ζ potential is well known to induce stronger fouling propensity.

The shape and sign of the apparent ζ potential profiles are indicative of the dissociation of surface groups [277]. The ζ potentials measured for the three untreated membranes are negative and the shape of the curve prior to treatment indicates that the membranes behave as a weak acid [278]. Ariza and Benavente (2001) [277] showed in their modelling attempts that adsorption of anions onto a PS membrane surface was insignificant compared to acid dissociation in ionic concentration similar to those used here (1 mM). The flattening and reduction of ζ potential profiles, as clearly shown for PS25 and PS100 membranes after treatment, is also suggestive of a lowering of ionic dissociation in response to the increasing OH^- ions presence in the bulk (increased pH). Möckel *et al.* (1998) [278] indicate that a reduction in the magnitude of charge is due to the material becoming less ionic. This further supports the idea that, if there was not significant change to the chemistry of material creating this change in its ionic character, then a film which shields the membrane surfaces from the bulk solutions influence occurred i.e. a thin-film sorption of alcohol molecules.

Confirmation as to whether any changes in the chemical nature of the surfaces occurred as a result of treatment was thus the next logical step, to allow insight into any reduction of surface ionisable groups. This is the focus of 5.6.

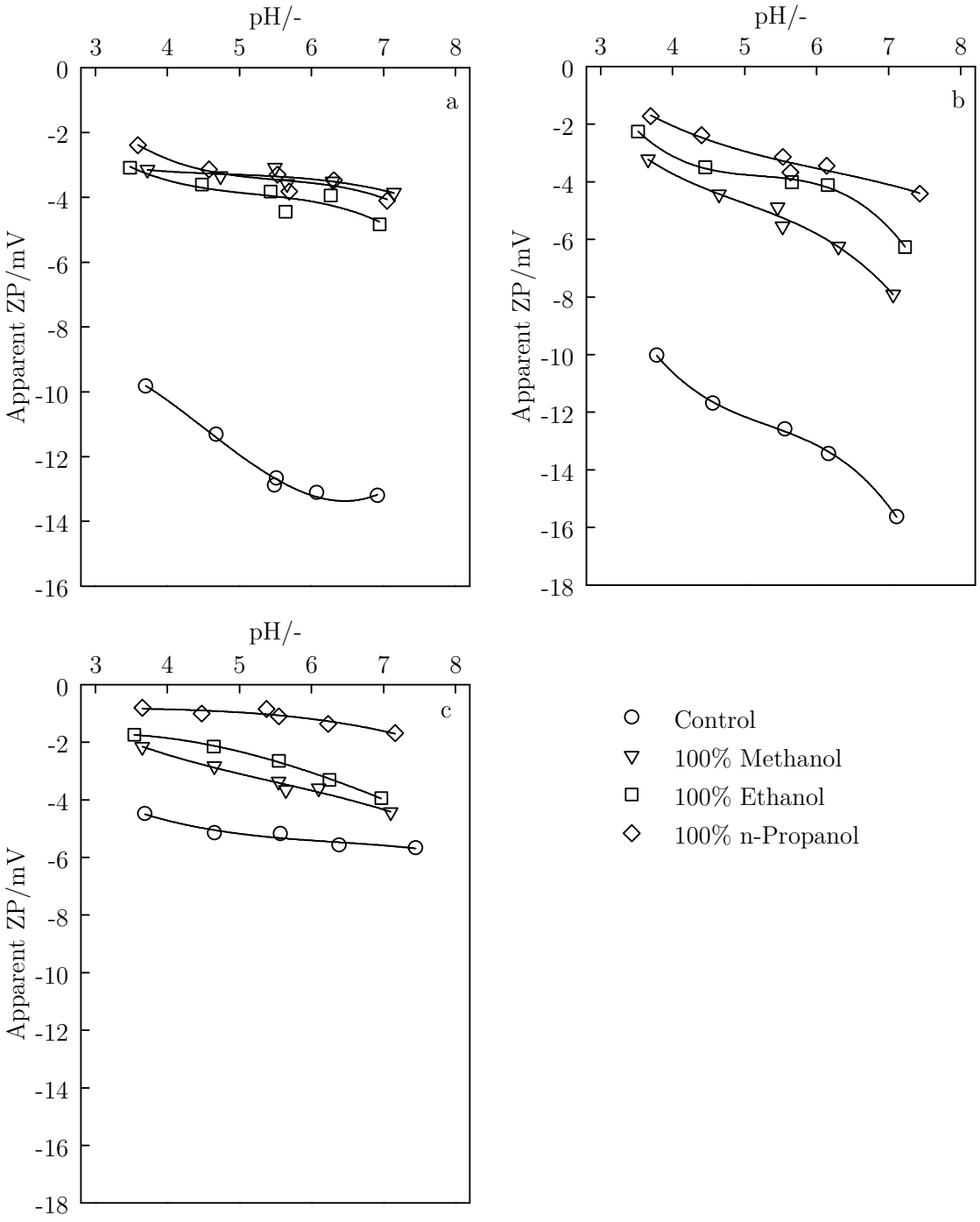

Figure 5-13 - Through-pore apparent ζ potential for a) PS25, b) PS50 and c) PS100 membranes treated with pure alcohols

5.6 Chemical characterisation

5.6.1 Membrane surface

FTIR analyses were undertaken to assess the chemical changes to the PS membrane surface as shown in Figure 5-14. Differences in FTIR spectra between PS and PES have been detected by analysis of bands in the 1590 – 1480 cm^{-1} region [279-281]. PS shows characteristic aromatic peaks at 1586 cm^{-1} and 1488 cm^{-1} whereas PES is characterised with bands at 1578 cm^{-1} and 1486 cm^{-1}. Additionally, weak bands at 1385 cm^{-1} and 1365 cm^{-1} are also characteristic of the methyl group presence in the structure of PS, these groups being absent in PES [279]. Thus it was confirmed that the membranes being used are PS. A confirmation of the exact polymer used was sought from the manufacturer though information was withheld (citing trade secrets as a reasoning).

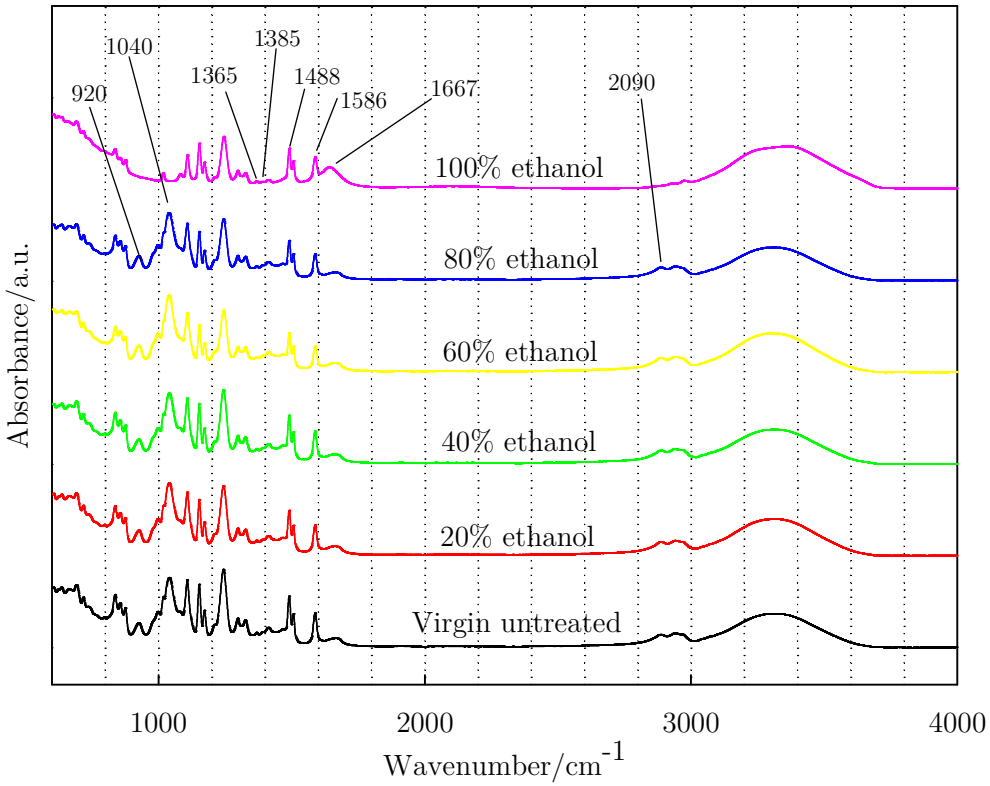

Figure 5-14 - Averaged FTIR spectra for PS50 membranes having received ethanol treatment at varying ethanol concentration

Peak identification and characterisation showed that there were disappearances in the spectral bands at 1040 cm^{-1} and 920 cm^{-1}, and near removal of the band at 2900 cm^{-1} for the 100 wt.% ethanol treated membrane, when compared to all other samples. Other bands were identical for all spectra. Though it was initially thought that this was some removal or transformation of surface groups, Belfer *et al.* (2000) [279], having conducted prior cleaning of their PES membranes with a water/ethanol exchange, found a disappearance of bands in these same spectral locations. They attributed this to enhanced removal of preservatives. They do not specify which preservatives were being eliminated however. Weis *et al.* (2003) [269] said that a peak at 1040 cm^{-1} on a virgin PS spectrum was due to

an aliphatic alcohol, probably glycerine. In a later study, Weis *et al.* (2005) [168] stated that use of a 60 °C hot water conditioning step acted to reduce the viscosity of glycerol preservatives from the membrane, and is thus sufficient for removal. Despite employing the same conditioning step to the membranes in this study (prior to treatment), it is clearly shown here that subsequent ethanol treatment of membranes reveals a more complete removal of this peak to yield a virgin PS membrane surface. In the same study it was indicated that a masking of the band at 1667 cm^{-1} was indicative of a fouled membrane. The spectra obtained here shows an increase for this peak after 100 wt.% EtOH treatment. This is an indication that this peak masking may have been due to preservatives not fouling, and the removal action of 100 wt.% ethanol treatment then further reveals this masked peak.

5.6.2 Leaching

Further to the surface study of the membranes, analysis of the alcohol permeating solution was carried out for PS25, PS50, and PS100 membranes. Briefly, 100 mL of EtOH was passed at 1.0 bar TMP through 5 hot-water conditioned virgin membranes, mounted in the stirred cell module in series, before recycling. This procedure was repeated 3 times. 50 mL of the triple filtered permeate was added to a Petri dish containing a clean glass microscope slide and evaporated at 40 °C. Background FTIR spectra of clean glass slides were generated before analysis of the residue left behind following drying (see spectra in Figure 5-15).

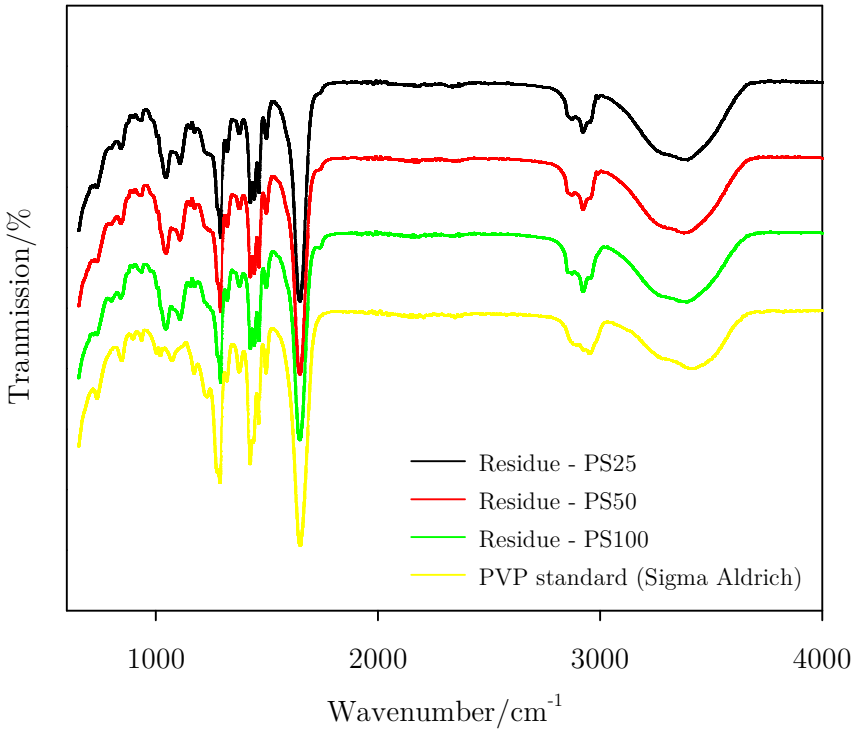

Figure 5-15 - FTIR spectra of residue obtained from three membranes compared to PVP reference standard

The residue formed a white gel-like layer over the slide, and had reduced to a white powder in some areas. A search score average of 0.702 (out of 1) was obtained for the IR spectra[2], indicating detection of polyvinylpolypyrrolidone (PVPP). This gave a strong indication as to the nature of the leachate following ethanol treatment. Literature searches revealed PVPP's use as a polyphenol complexing agent used for fining of wines and beers [282, 283] though no indication of it being used as a membrane additive was found. Polyvinylpyrrolidone (PVP) is a well-known pore forming agent used in PS/PES membranes [62, 264, 272, 284]. A sample of PVP was obtained (Sigma Aldrich, UK) and analysed using FTIR, Figure 5-15 shows the reference PVP to residue spectra, noting that the relative occurrence and intensity of bands is nearly identical.

To further confirm the occurrence of this leaching effect, the relative solubility of PVP in water and EtOH (and mixtures thereof) was checked using Hansen solubility parameters. Figure 5-16 shows the positions in the 3D space as compared to PVP. The relative distance of pure ethanol is a factor of 5 closer than that of water (28.7 $MPa^{0.5}$ compared to 5.6 $MPa^{0.5}$) which confirms the superior solvency of ethanol over water for this molecule. Comparing the positions of MeOH and nPrOH also shows that 100 wt.% nPrOH would give rise to an even greater wash-out of PVP whereas the effect of pure MeOH would result in less removal. Whether the leaching of PVP from the membranes is the removal of excess inner or outer PVP, resulting from inefficient encapsulation in the porous matrix, or whether it is removal of essential PVP from its 'correct' location, is difficult to speculate. Koga *et al.* (2010) [285] investigated the spatial dispersion of PVP in commercial PS dialysis membranes and found that whilst the dispersion was consistent using standard ATR-FTIR (for bulk area analysis), use of near-field IR revealed inhomogeneities in the PVP dispersion. The PVP ratio ranged from areas containing around 5% to areas containing over 40%. If this is consistent with the membranes in this study, the removal of PVP could cause micro- or nanoscopic pitting in the membrane sub-structure.

[2] Carried out using the in-built Spectrum Express software (Perkin Elmer, Waltham, USA)

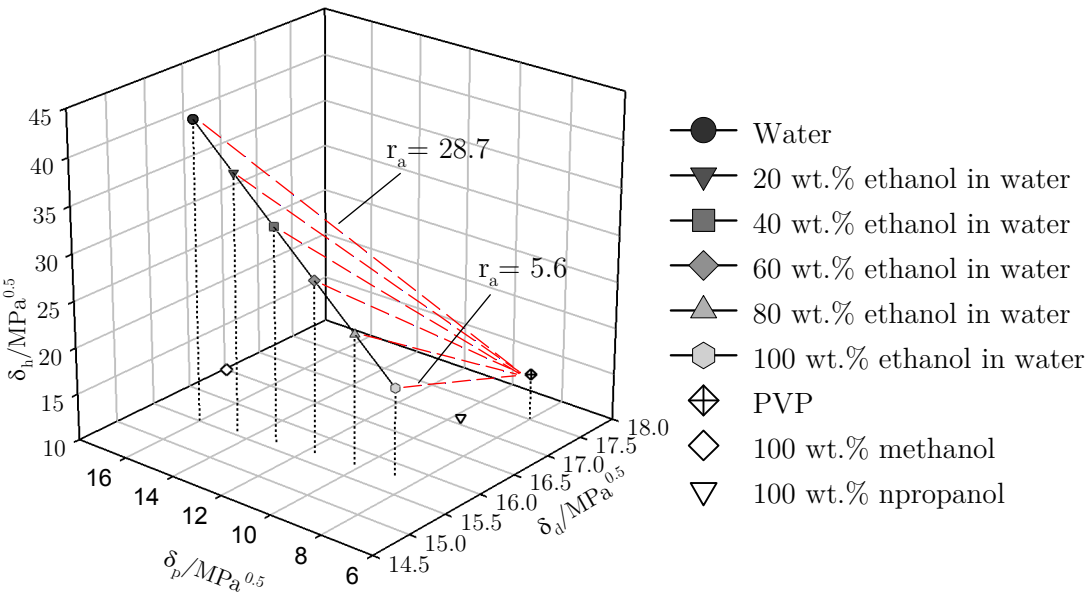

Figure 5-16 - Three-dimensional position of ethanol-water mixtures, as well as pure methanol and ethanol relative to PVP in the Hansen space

The washout of PVP has been indicated by some authors [286, 287]. Lindau *et al.* (1995) [287] found that using two of the same Alfa Laval membranes used in this study (50 kDa and 100 kDa), the action of repetitive fouling and cleaning of (up to) 0.08 wt.% octanoic acid and proprietary alkaline cleaning agent (P3 Ultrasil 11, Henkel Ecolab) gave rise to variability in PWFs during cycling. For the GR40 membrane (same as PS100 here), a relative PWF rise of up to 1.3 after 3 cycles was observed, though for the PS50 equivalent, a relative flux of 0.9 was recorded indicating a loss. It was speculated that these flux rises may have been due to PVP removal, though no conclusive evidence was presented. They do indicate that there was still a presence of PVP as gauged by FTIR within a GR10 (500 kDa PS membrane). Another speculation these authors had was the opening up of pores in their 'hydrophobic' membranes given the superior wetting effects of water mixed with octanoic acid.

5.6.3 Discussion

From the evidence gathered relating the flux changes to the surface chemical changes, a number of interplaying phenomena exist. The application of an apparently simple pre-treatment method has been shown to improve membrane performance in terms of PWF though arguably at the expense of desirable surface properties such as the hydrophilicity and high negative surface charge. What is clear about the treatment is that the alcohols are revealing the 'true' membrane with relatively un-intrusive treatment though this is at the expense of agents such as PVP, which can be integral in offering desirable surface characteristics. Marchese et al. (2003) [100] studied the fouling behaviour of PES/PVP membranes and stated that PVP, a highly hydrophilic polymeric substance, could influence the hydrophilicity itself. The results presented here affirm this suggestion given that the detection of PVP as a leachate during EtOH treatment has contributed to hydrophobisation of the membrane top layer. The flux increases are not as easily explained

simply by PVP removal. Its removal has been argued as being a driver in membrane flux increase [287], some authors others assert that its presence aids in flux increases [100, 288]. Marchese *et al.* (2003) [100] presented three reasons why incorporation of PVP acted to promote membrane PWFs:

1. It increases the pore density
2. It decreases the thickness of the dense (skin) layer due to the presence of macrovoids in the support layer
3. It promotes hydrophilicity on the membrane and inside the pores

The reasons here are valid though, aside from (3), they relate mainly to membrane pore formation. If the membranes are formed using PVP, and it is subsequently removed, an increase in porosity (pore space occupied as a fraction of total space) would rise. The consequence of this would be an effective increase in pore diameter. Also, the thickness of the dense skin layer would remain constant, and the macrovoids inside the support layer would be expanded. This would create a direct mechanism for flux enhancement as the effective pore diameter of the idealised membrane would increase. By consideration of the Hagen-Poiseuille equation, flux changes is response to the square of the area. Thus a slight incremental pore diameter increase would have dramatic effects on fluxes.

Apparent ζ potential of PES membranes, with and without PVP incorporation, have shown differences [272, 288]. Susanto and Ulbricht (2009) [272] showed slight increases in the negative tangential ζ potential of the order of around 2.0 mV between pH 5.0 and pH 9.0. Contrastingly, Malek *et al.* (2012) [288] showed a sizeable decrease in surface ζ potential between a 0.9:1 PVP/PES ratio and 1:1 ratio. The results did however come from separate samples with differing solvent/polymer/additive ratio. The magnitude of ζ potential changes shown in this thesis were significantly greater, and though the PVP content for the membranes was not known, no reviewed literature contains any indication of such dramatic ζ potential reductions. It would thus be fair to assume that the PVP removal is not the sole reasoning for flux uplifts, charge and wetting property modifications.

So far, discussion has centred around four theories which may partially contribute to the modifications shown:

1. There is a screening effect and the EDL's influence is shielded by adsorbed alcohol on pore walls
2. Pore expansion through swelling has changed the EDL profile overlap inside the pores
3. Swelling of the polymer has modified charge distribution through functionality or change of acid/base properties of the polymer
4. PVP removal by alcohol solubilisation reduced the membrane hydrophilicity and apparent ζ potential

Another point of discussion is the value to which the contact angle increases to. A phenomenon which has seen much speculation over recent years is that of flow

enhancement inside carbon nanotubes [289-294]. Water's adherence to surfaces, structural considerations inside nanotubes and the nanotube dimensions are all factors thought to influence mass transport enhancements of up to 5 orders of magnitude [290, 292]. The adherence of water to hydrophobic surfaces is lowest in the monolayer nearest the solid interface than for the following layers [295]. The result is interaction minimisation with the surface, which reduces drag compared to adjacent molecules in the bulk [292]. A review of contact angle data for water and graphite was given by Mattia and Gogotsi (2008) [293] in the form of a histogram and showed 45% to be in the range of 80 – 86°. These values are comparable to the treated membrane contact angles found in this instance. If assumptions are made about the wetting properties, such as the surface is sufficiently non-porous so as not to overestimate the measured sessile drop (i.e. Cassie-Baxter type wetting), then it would be fair to assume the wetting properties inside the pores are comparable. If the same adhesive properties of water apply in this instance, then the common assumption for enhanced flow though the nanotubes (or pores) is that of slip occurrence. This is normally quantified in terms of an extension of a parabolic velocity profile such that the value at the wall is non-zero (zero if a no-slip condition is applied), and the degree of extrapolation outside the wall is termed the slip length. Of course, factors such as pore wall roughness may give a reduced flow enhancement although the principle of increased slip is a likely factor given the system's similar wetting properties.

For a more complete picture of the modifications, so as to give a more rounded view of the effect of alcohol treatment, the next section highlights morphological and structural changes.

5.7 Structural and morphological changes

5.7.1 One-dimensional swelling

Membrane thickness measurements of PS25, PS50, PS100 and MFG1 membranes were made using a micrometer to gauge swelling for samples treated with EtOH. As a post experimental control, active layer polymer was dissolved from the polypropylene support layer to confirm that no support layer swelling had occurred. This enabled subtraction of the backing layer from the total membrane thickness to give active layer thickness changes (displayed in Figure 5-17). The support layer thickness was 193 ± 11 µm for n = 45. There was no significant difference between values for differing membrane types. The same statistical test conditions as for contact angle measurements were applied to the data sets here (where *NS* is $p > 0.05$, * is $p < 0.05$, ** is $p < 0.01$, and *** is $p < 0.001$).

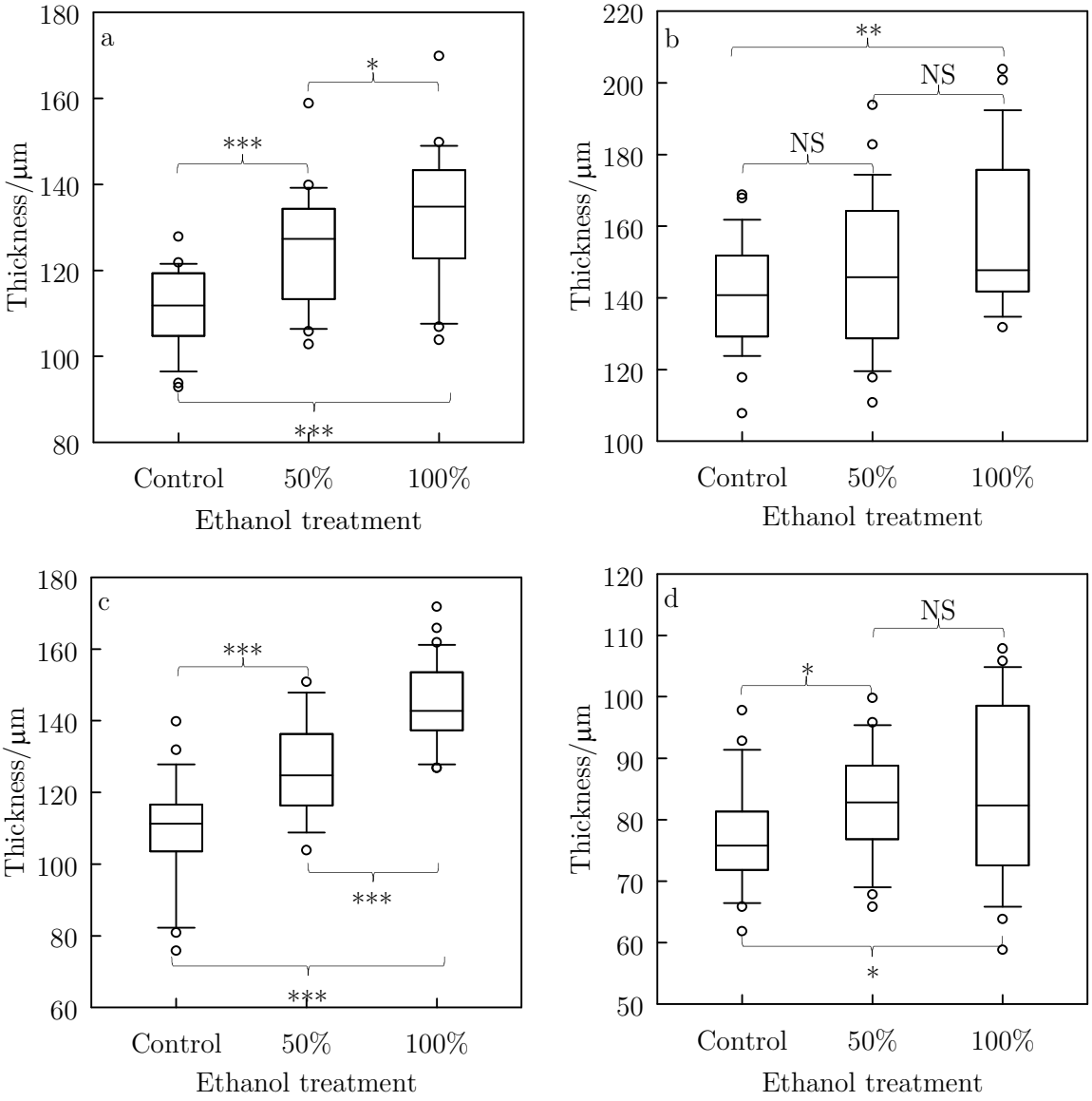

Figure 5-17 - Membrane thickness for a) PS25, b) PS50, c) PS100 and d) MFG1 for untreated (control), 50 wt.% and 100 wt.% ethanol treatment

Figure 5-17a shows the PS25 data. Between 0 and 50 wt,% and 0 and 100 wt.% EtOH there is a good probability that a significant change in thickness occurred, indicating top layer swelling ($p < 0.001$). The difference between 50 and 100 wt.% also shows moderate significance. This demonstrates the majority of change occurring to the membrane probably happened at low alcohol concentrations. For PS50 (Figure 5-17b) shows, on the whole, less swelling behaviour than both PS25 and PS100. There is a meaningful change when comparing 0 and 100 wt.% EtOH, though not when comparing the changes between 0 and 50 wt,% and 50 and 100 wt.% samples. The spread of data increases for EtOH treated membranes; the upper quartiles for both 50 and 100 wt.% (and medians) show increases over the control sample. More data would likely have revealed a more apparent correlation. The PS100 membrane (Figure 5-17c) shows perhaps the most consistency in terms of thickness (smallest upper and lower quartiles). Each data set displays a 99.9% certainty of thickness changes. The MFG1 shows lesser changes indicated by the 95% certainty of a change between 0 wt.% and 50 wt.% ethanol and 0 wt.% and 100 wt.% ethanol. The comparison between 50 wt.% and 100 wt.% shows no indication that a thickness change had occurred, again implying that the majority of thickness changes due to swelling occurs at lower alcohol concentrations.

Although quite a simplistic method of swelling detection and revealing quite some variation in data, the statistics applied for analysis reveal that changes to membrane thickness occurred. Gaining representative information for membrane-related studies relies on rigorous analysis, as the testing of large areas is sometimes not feasible. Since the membranes used here are segments from large rolls, samples were taken from the same location on the bulk sheet so as minimise variation. Macroscopic swelling is a strong indicator towards finding a reason why flux changes occur.

The expansion may or may not increase the pore size relative to the membrane as a whole. It is important to define the swelling of porous structures in terms of both micro- and macroscopic changes. For purely microscopic changes, the material which makes up the dense membrane layer would swell and expand, though no changes to the space the membrane occupies would be apparent; this would result in constriction of the porous network. For macroscopic swelling occurring solely, the total membrane space would expand, though no changes to the internal structure would occur and the pore space would expand. It is hard to envisage either of these processes occurring independently, although one may dominate. In the case of a membrane such as here, where expansion on the macro-scale has clearly been shown in tandem with flux changes, it would be assumed that the macroscopic swelling effect has the most influence.

5.7.2 Roughness

As was mentioned in 2.4.3.5, roughness of membrane surfaces can affect fouling propensity. AFM was used to gauge surface roughness of membranes in this instance. Control and 100 wt.% EtOH dynamically treated PS50 and PS100 membrane samples were scanned at a frequency of 256 Hz in tapping mode over an area of 1.6 µm × 1.6 µm. Two samples (approx. 1 cm^2) were prepared for each case, and scanned in four separate areas (giving 8 repeat measures in total). Average surface roughness was assessed using the mean deviation from the central plane in the z-direction as described in 4.4.1.4. AFM images obtained can be seen in Figure 5-18 and Figure 5-19.

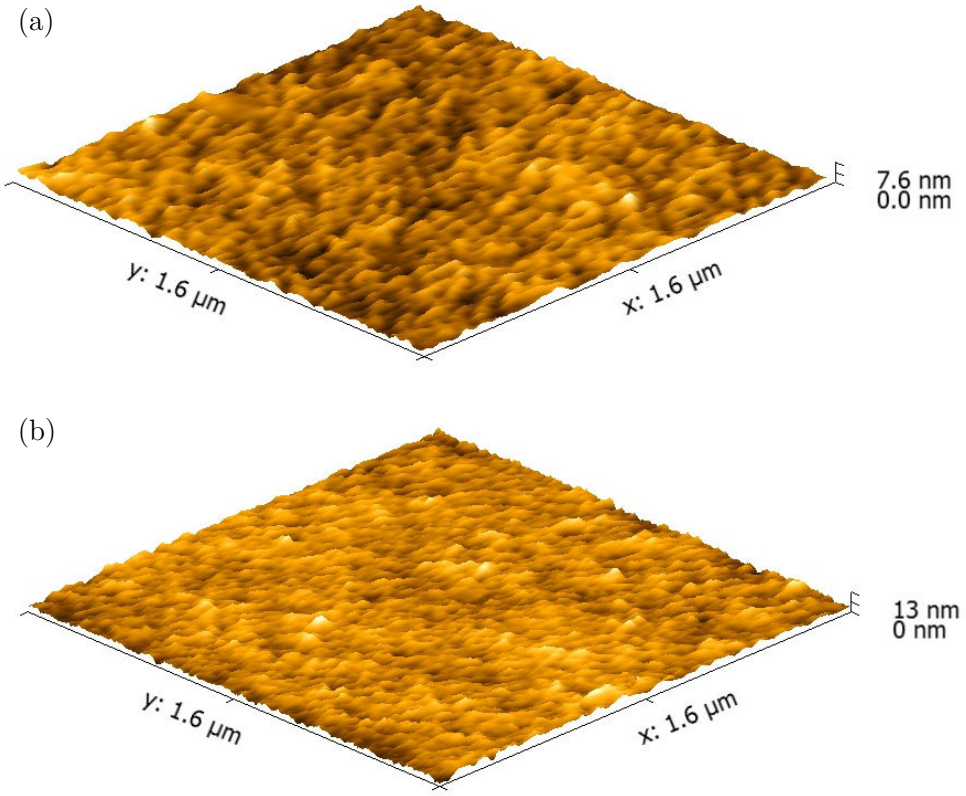

Figure 5-18 - AFM micrographs of (a) untreated and (b) treated PS50 membranes

It was indicated from thickness measurements that a morphological change occurred although it gave no indication of how the surface may change. Also apparent was the removal of PVP from the membrane as a result of treatment. Already mentioned was the possibility of pitting of the membrane surface as a result of large inhomogeneous regions of high PVP being removed and thus it was thought that a roughness increases may be apparent. Table 5-1 shows the data averages for both membranes. PS50 was the smoother membrane when untreated, its roughness increasing upon treatment though not to any degree of certainty when assessed by a t-test. The PS100 however showed a more significant increase in roughness and was assessed as showing a 95% significance against the t-test null hypothesis (that no change occurred).

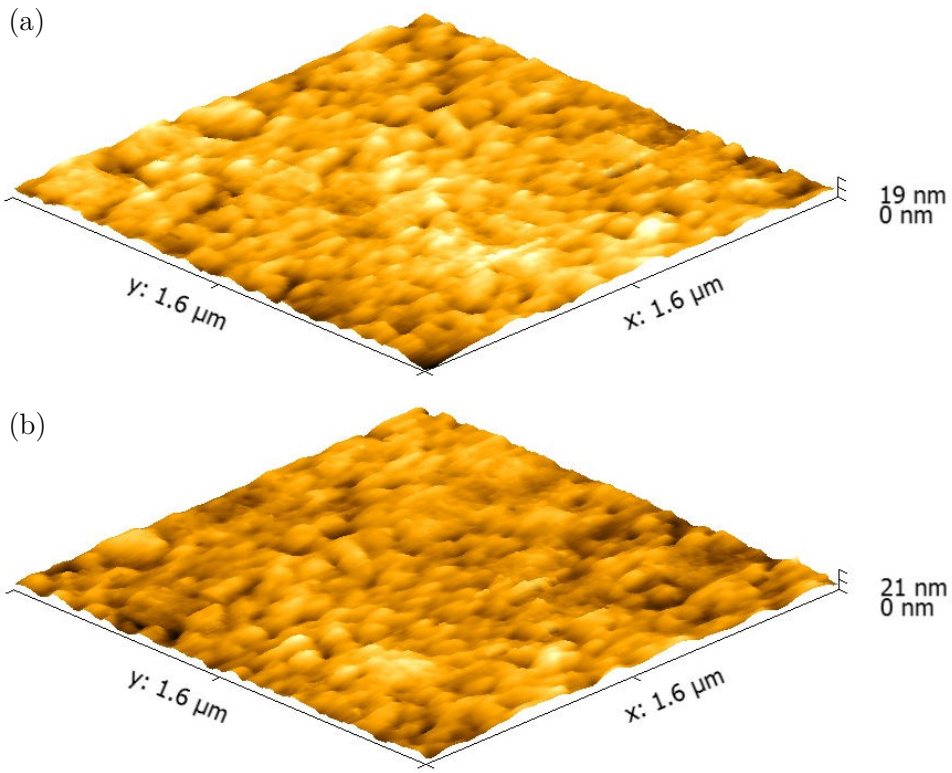

Figure 5-19 - AFM micrographs of (a) untreated and (b) treated PS100 membranes

Table 5-1 - Surface roughness measurements for untreated and treated membranes (n=8)

Membrane	*PS50*		*PS100*	
Treatment	None	100 wt.% ethanol	None	100 wt.% ethanol
Roughness (R_a)/nm	8.5 ± 0.9	10.8 ± 3.8	13.8 ± 3.3	17.3 ± 1.9
p-value (t-test)[3]	0.072		0.012	
Result of null hypothesis	NS – a modification cannot be proved significant enough to reject the null hypothesis		* - 95% confident that the null hypothesis can be rejected	

This data makes it difficult to conclude if any changes occurred. The use of tapping mode, although of paramount importance of imaging of soft samples, has been shown in be prone to drawbacks relating to the stiffness of samples [296]. For the membranes which have been treated, any change in mechanical properties of material as a result of EtOH treatment (such as elastic modulus changes as shown in 5.7.4) could result in increased tip indentation and thus higher amplitudinal variation between samples. In short, whilst the AFM data here may not be conclusive in indicating roughness changes, they can however help to reaffirm later suggestions that the tensile properties of the membrane surface are modified following EtOH treatment.

[3] t-test performed upon confirmation of data normality check (Shapiro-Wilk test)

5.7.3 Curvature

A qualitative assessment of the membranes was made by comparison of their shape prior to and after treatment. 9 PS50 and PS100 membrane sample discs were cut from the same radial point of the membrane roll so as to maintain consistent curvature (curvature originating from packaging in a roll). Following hot-water conditioning, three samples were held as controls, three were treated dynamically with 50 wt.% EtOH, and the remaining three with 100 wt.% EtOH. A picture of the samples is shown in Figure 5-20 and Figure 5-21.

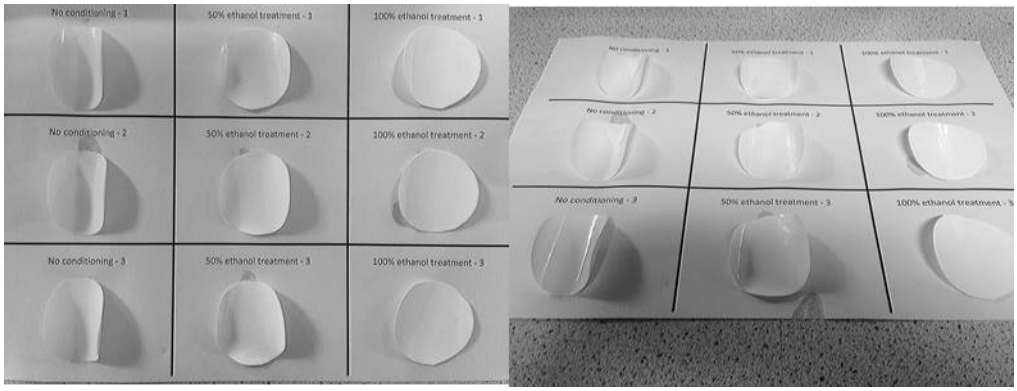

Figure 5-20 - Curvature of 50 kDa membranes for untreated, 50 wt.% and 100 wt.% ethanol treatment

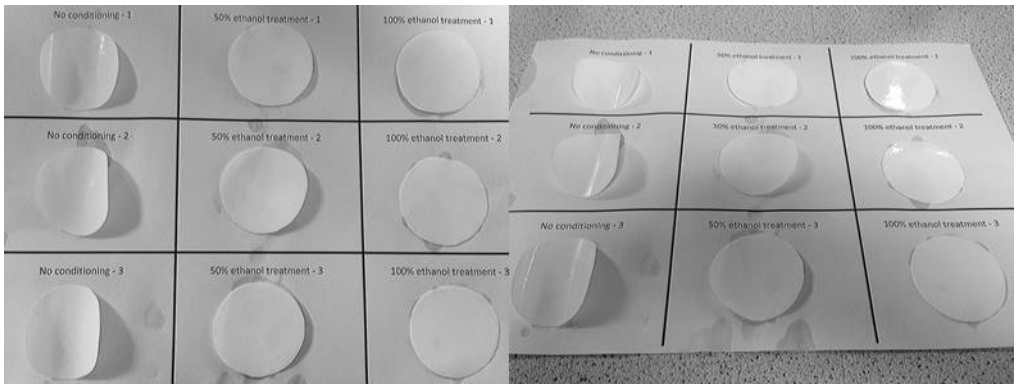

Figure 5-21 - Curvature of 100 kDa membranes for untreated, 50 wt.% and 100 wt.% ethanol treatment

Given the asymmetry of the membrane and thus the presence of essentially two surfaces, differential swelling of the layers can result in a deformation from the original state [297, 298]. In these tests, it was clear that both the PS50 and PS100 membrane top layers expanded to leave a more flattened membrane over the naturally curved control sample. It shows that the membrane expands in a three-dimensional fashion e.g. in the x-y as well as the z plane (as already confirmed). Heffernan et al. (2013) [297] showed that an NF membrane with polyamide as its active layer (cast on a PS sub-layer, supported by polyester) showed a relaxation in the natural curvature at moderate EtOH in water concentrations and a curve opposite to the natural curl of the membrane at high EtOH. It implied that the polyamide top layer swelled to a greater degree over PS, in this instance.

Tsui and Cheryan (2004) [299] indicated, using numerous sources, that swelling, dissolution or plasticisation can lead to loosening of the membrane structure resulting in loss of rejection and mechanical strength.

5.7.4 Elasticity

Measurement of the elastic modulus for untreated and 100 wt.% EtOH samples was made by taking analysis of the indentation of a spherical silica probe into the membrane surface. After calibration of the tip-sample contact point, the maximum indentation was calculated by subtraction of the maximum cantilever deflection from the total height change (the maximum distance the cantilever moves during ramping). The indentation is then used to calculate the elastic modulus of the sample [300] assuming a Poisson ratio of 0.5 and using the Hertz model (see Appendix C8). The assumptions of the model are that the sample displays absolute elasticity (returns to its original shape following deformation) and that the indentation is small compared to the sample thickness (meaning the underlying substrate or backing layer influence is negligible).

The AFM method was adopted due to the presence of the support layer. The data produced by Heffernan *et al.* (2013) [297] showed that use of a tensometer provided inconsistencies and/or lack of definition when attempting to separate mechanical properties of the active layer from support layers.

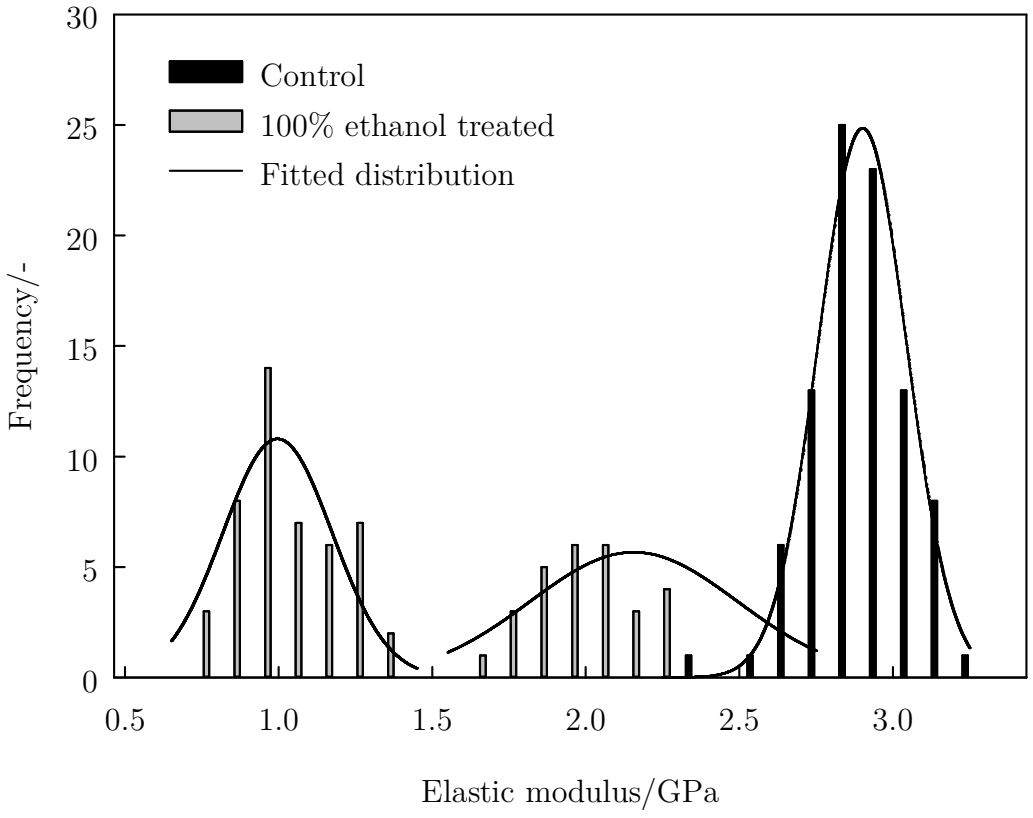

Figure 5-22 - Elastic moduli of PS50 membrane before and after ethanol treatment

Figure 5-22 presents a histogram of the data obtained from AFM experimentation. The figure shows clearly that the material elastic modulus is changed from a narrow normally distributed data set with a mean at 2.9 GPa to a bimodal distribution with peaks at 1.0 GPa and 2.2 GPa. This indicates a softening of the material, accountable due to a greater indentation into the surface brought about by a lower magnitude resistive force experienced by the cantilever. The reasoning for this bimodal distribution is unclear though some insight into why this occurs can be made by analysis of the raw elastic moduli data plots for each ramping experiment (see Figure 5-23). The plot shows that for the control membrane there is a relatively constant elasticity across the test region (2.9 ± 2.0 MPa). When treated, softer and harder zones form (though always softer than the control substrate) indicating localisation of material alteration (mean: 1.5 ± 0.6 MPa). This is particularly poignant given that these zones are grouped in batches of nine (remembering that measurements were made in 3 × 3 grids). It was not possible to ascertain the exact cause of this effect though it could be speculated that the heterogeneous distribution of PVP in the membrane is a cause, its subsequent removal could lead to surface pitting or sub-surface cavity expansion. This in turn could lead to apparent softening. Having said this, it is also expected that the swelling effect of ethanol would have a plasticisation effects on the polymer as was discussed in 5.7.3 which would influence the elastic modulus also.

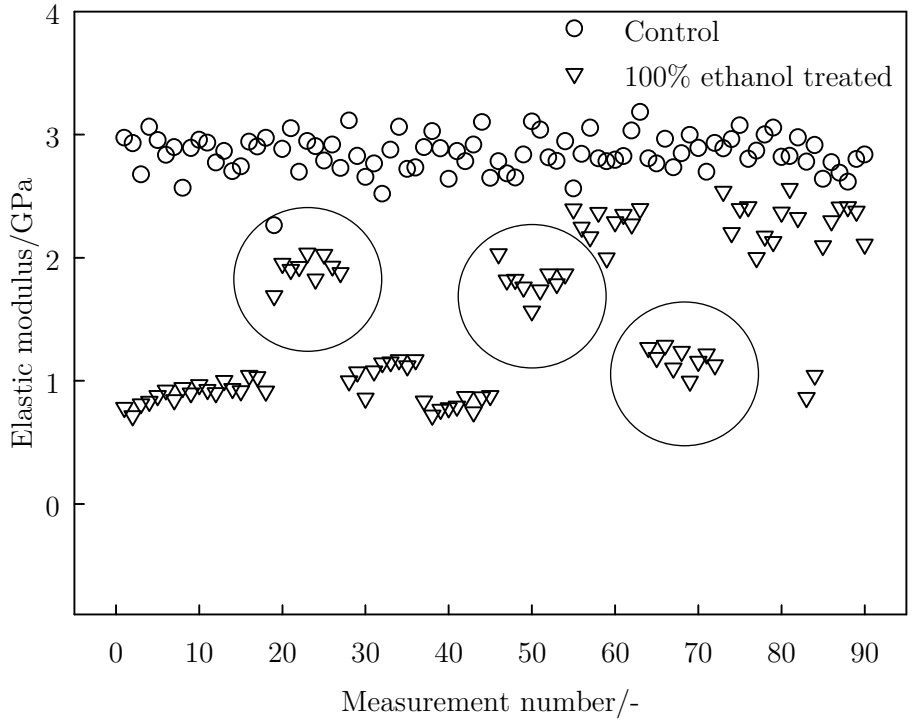

Figure 5-23 - Elastic moduli data of PS50 membrane before and after ethanol treatment highlighting region specific softening of membrane surface (circles)

5.7.5 Mercury intrusion porosimetry

Pore size distribution calculated from porosimetry data are presented in Figure 5-24 and Figure 5-25 for both control and 100% ethanol treated membranes. All pore size distribution profiles show a distinct separation between the active layer region (denoted as

region 1), through a transition region (denoted 2), and into the support layer region (denoted 3). Region 1 represents pores in the range; 6.7 – 5000 nm.

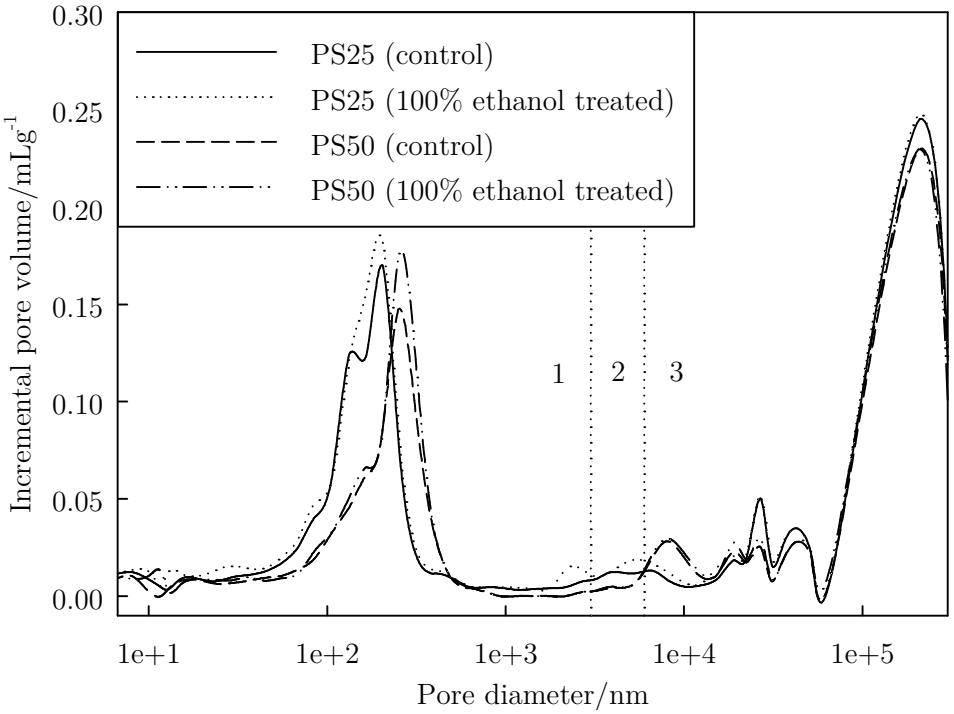

Figure 5-24 - Pore size distribution for PS25 and PS50 membranes measured before and after ethanol treatment

For PS25 (Figure 5-24a) there is a slight indication that more volume is being occupied by smaller pores in the 10 – 80 nm region. There is also a distinct increase in the volume of pores in the 100 to 300 nm pore size range for both PS25 and PS50 membranes. The same trend is identifiable for the PS100 and MFG1 membranes (Figure 5-25b) though an increase in macrovoid volume is noticeable in spaces from 300 to 900 nm. The total porosity of each sample is recorded in Table 5-2.

Table 5-2 - Bulk porosity (including support layer)

Membrane	*Untreated (control)*	*Treated (100% ethanol)*
PS25	52.3	51.8
PS50	53.1	55.4
PS100	59.7 ± 1.4	63.9
MFG1	60.5	63.8

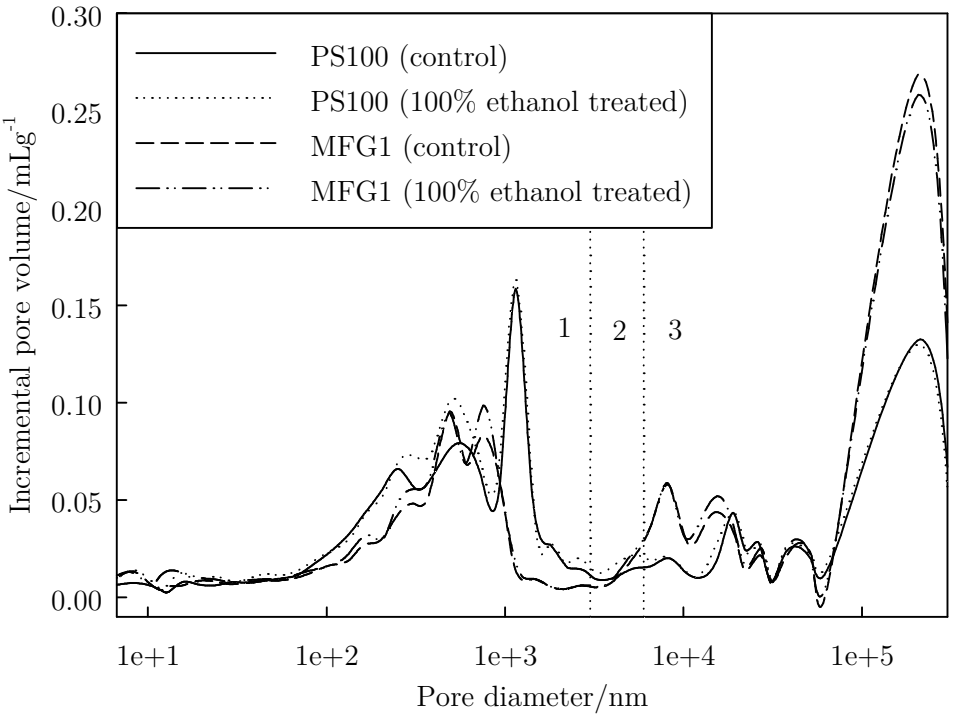

Figure 5-25 - Pore size distribution for PS100 and MFG1 membranes measured before and after ethanol treatment

It is difficult to interpret data at the sub-10 nm level since membranes are subject to elastic variability as previously shown. Deformation is likely to occur given the extreme pressures experienced during measurement. If expansion at the macro- or micro-porous level is occurring, or indeed if this is a result of the stripping away of PVP from inside the membrane sub-structure, then it would be expected that smaller pores would undergo similar changes. Another factor to consider is that some pores may not be measured using this technique. If pores are not open-ended, mercury may not have been able to penetrate into the sample, although this effect should be eradicated by vacuum de-gassing during sample preparation. Since the membranes are not rigid structures, the de-gassing protocols may however have resulted in collapsing of pores. Given that any one of these factors could have occurred, identifying which effect is occurring becomes somewhat speculative. What is certain from the findings are that if the greater porosity shown for all membranes (except PS25) in certain regions of the pore size distribution is not due to swelling of the membrane matrix, then the mechanical property changes (reduced elasticity) should be responsible for the observations.

5.7.6 Theoretical considerations

There is reasonable evidence to suggest that certain changes made to the membrane are a result of swelling, made by observation of dimensional and structural changes to membrane samples. An analysis of theoretical swelling can also act to reinforce this argument. Figure 5-26 shows a ternary plot of the relative positions of PS in the Hansen solubility space, as compared to water-solvent mixtures and a solvent known to dissolve PS. It is shown that the lower dispersive force parameter for nPrOH is relatively closer to PS than the other

water-solvent mixtures, and would thus induce the greatest swelling effect. The explanation however is not so straightforward given the relatively small molecular weight of MeOH (32 Da) compared to EtOH and nPrOH (46 Da and 60 Da respectively. The enhanced diffusivity of methanol between polymer chains could oppose the straightforward conclusions when based solely on Hansen solubility assumptions. This may be an explanation as to why there is indifference between MeOH, EtOH and nPrOH treatments in terms of relative flux changes and that nPrOH was deemed the least suitable swelling agent based solely on flux uplifts.

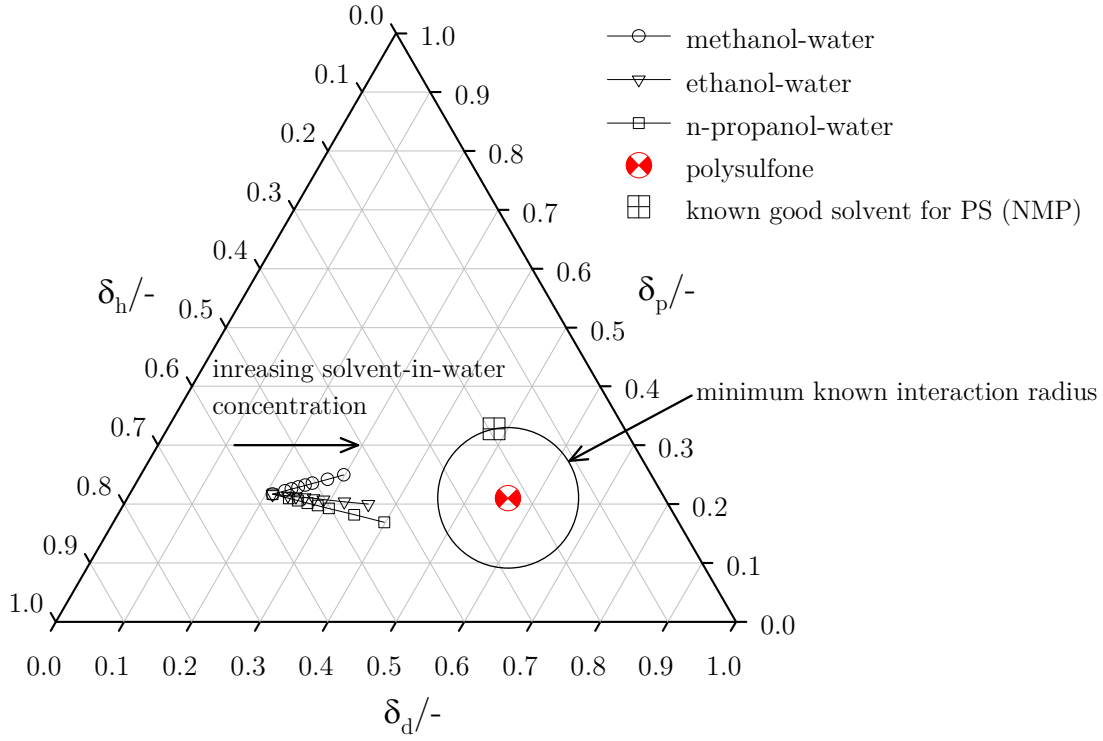

Figure 5-26 - Ternary Hansen space plot showing decreasing distance between treatment solutions and polysulfone as alcohol concentration increases

5.8 Protein filtration and fouling

Two model proteins were selected for filtration experiments on PS50 membranes which had undergone EtOH treatment. Experiments were run on membranes treated using the dynamic treatment method described in 5.2. 100 g of 50 μgmL^{-1} protein solution (protein dissolved in phosphate buffered saline at pH 7.4) was placed in the stirred cell module following PWF tests and filtered under unstirred dead-end conditions at 1.5 bar until 100 g of permeate had been collected. Protein concentration of the 100 g of permeate was quantified using the Bradford assay (see 4.4.2.1) to assess total solute transmission.

β-lactoglobulin (βLG) (18.4 kDa) was selected as a model solute as it should theoretically pass unhindered through the membrane. In real terms, this is reminiscent of a protein pre-filtration step aimed at removing any undissolved matter or large aggregates. Real applications of this process may be membrane fractionation of proteins (in dairy processing), chromatographic separation or as a bioreactor feed stock preparation step. Bovine serum albumin (BSA) (66.5 kDa) was selected as the second model solute as it should be rejected by the PS50 membrane. This step is reminiscent of a protein concentration step in which dewatering occurs prior to, for example, lyophilisation and/or crystallisation of a protein.

5.8.1 Flux of βLG and BSA

Figure 5-27 shows the flux curves from filtration of βLG. Datasets have been plotted vs. time for appreciation of total processing time and also normalised to fractional volume reduction for comparison of the progression of the process.

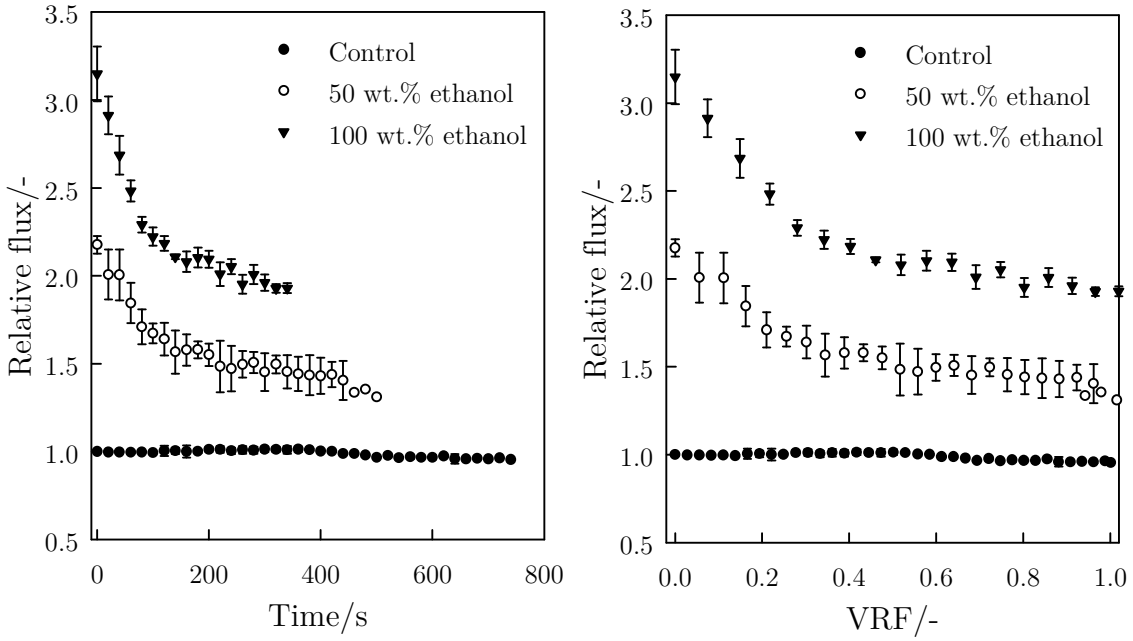

Figure 5-27 – 50 μgmL^{-1} *β*LG solution flux during unstirred 100% volume reduction experiments performed at 1.0 bar TMP. Time vs. relative flux (left), VRF vs. relative flux (right)

The figures show the pure water flux increase gained by treating with 50 wt.% and 100 wt.% ethanol is also apparent during dead-end filtration. For the untreated PS50 filtration there is no apparent flux decline suggesting that the filtration is operating at sub-critical flux. The duration of the volume (12 minutes) is likely not long enough for any adsorptive deposition to significantly affect the flux. During filtration using treated membranes, a flux decline is apparent. This may occur due to a stronger adsorption potential of the membrane; probably a factor of both increased binding kinetics and sorption capacity. This links consistently with reduced in-pore apparent ζ potential and hydrophobisation. The result is reinforced further since βLG is known to bind and aggregate through hydrophobic interactions [301, 302]. Another causation of the flux decline could be that if any additional small pores inside the membrane were 'unlocked' during treatment by the lower alcohol surface tension, they would be more inclined to be internally pore blocked resulting in a flux decline. The time for volume reduction is significantly reduced for treated membranes, with the 100 wt.% EtOH membrane performing the filtration operation in less than half of the time (5.5 minutes).

When filtering BSA (Figure 5-28) the result is contrasting. Whilst the initial flux is improved at the beginning of the process for treated membranes, the decline in flux reduces to a consistent flux irrespective of treatment type and so the improvements offered by the treatment are less apparent. In terms of total time needed to complete protein dewatering, the initial elevated fluxes ensure the operation is completed at a faster rate; 14 minutes in the case of 100 wt,% ethanol compared to 19.5 minutes for untreated membranes.

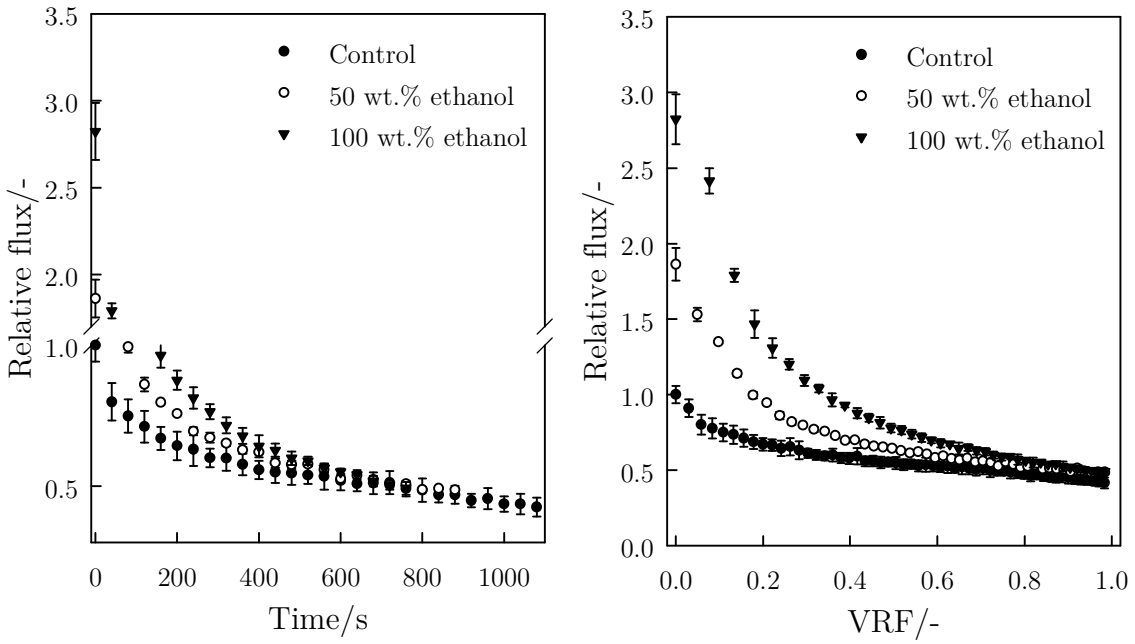

Figure 5-28 – 50 μgmL^{-1} BSA solution flux during unstirred 100% volume reduction experiments performed at 1.0 bar TMP. Time vs. relative flux (left), VRF vs. relative flux (right)

5.8.2 Rejection of βLG and BSA

The separation capabilities of the membranes for both proteins are shown in Figure 5-29 and Figure 5-30. βLG concentration in the collected permeate was lower than would be expected. The untreated membrane permeate contained 9.4 ± 3.9 μgmL^{-1} representing an 81% ± 8% rejection. Considering the protein molecular weight compared to the membrane nMWCO rating, this value is higher than would be anticipated. The high rejection may be due to accumulation of protein inside the membrane due to sorption through hydrophobic interactions. The results for the 50 wt.% and 100 wt.% EtOH treated membranes are not significantly difference ($p > 0.05$) and thus no information indicating modification of selectivity is observable. Total process rejection coefficients for 50 wt.% and 100 wt.% treated membranes were 75% ± 6% and 84% ± 7% respectively. These values also reflect the total protein recoverable in the retentate.

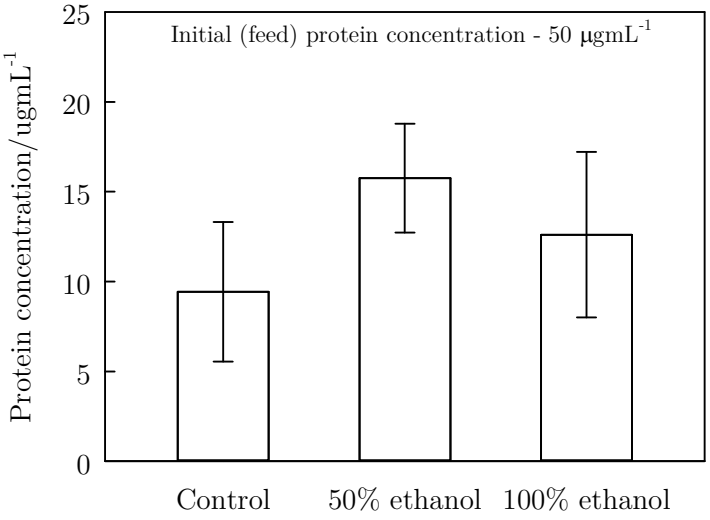

Figure 5-29 - 50 μgmL^{-1} βLG permeate concentration after unstirred 100% volume reduction experiments performed at 1.0 bar TMP

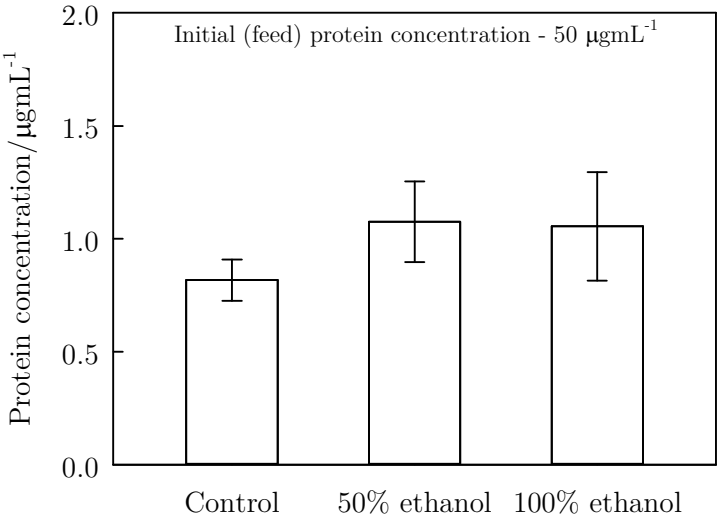

Figure 5-30 - 50 μgmL^{-1} BSA permeate concentration after unstirred 100% volume reduction experiments performed at 1.0 bar TMP

For BSA (Figure 5-30), the larger molecular weight of the species ensures a more robust rejection from the membrane. Again, no difference in permeate protein concentration can be concluded from the datasets. For all treatment types, 98% of protein was retained, though all with varying degrees of error.

The similarity in results relating to the membrane sieving capabilities are useful for aiding a description into the variability of fluxes, since conveniently, only a single process output variable has changed with any significance (relative flux). For small molecule filtration (small in comparison to membrane nMWCO), the mechanism of pore blocking is likely to differ compared to a large molecule. If the assumption that nMWCO is a proxy for pore size is made, it would be expected that only surface pore plugging effects would occur with a molecule that is the same size or larger than the pore mouth i.e. only for BSA in this case, not βLG. For dead-end filtration in the absence of surface shear, flux would eventually reduce to zero (for an infinite amount of feed) due to an increasing retentate concentration and exacerbated surface solute build-up. The BSA flux decline curves show that despite the initial flux values being closely proportional to the post-treatment PWF, pore blockage accelerates the rate of decline. Comparison by means of the VRF shows that the lowest flux value is consistent for all treatment types, meaning that the effect of ethanol pre-treatment is that of simply speeding up the process. The inevitable blockage happens at an earlier time, but not at an earlier equivalent stage of the process (in terms of volume filtered or feed concentration).

These data are instructive in providing firm evidence that the modifications to PS membranes made by ethanol treatment have an overall positive effect for these specific model scenarios. Since such noticeable changes have occurred to the membrane structure and chemical nature, it would be nonchalant to assume that no modification to membrane fouling propensity would occur.

5.8.3 Specific cake resistance analysis

If the mechanism of flux decline is accelerated by surface resistance factors only, an approximation of this would lie in classical dead-end cake filtration theory. It would be expected that a cake resistance (R_c) would be consistent for all three treatment types regardless of process time if this is the sole mechanism for resistance increase above the intrinsic membrane resistance R_m . Recasting the expression for flux as simply:

$$J = \frac{\Delta P}{\mu(R_m + R_c)} \tag{4-1}$$

and defining the cake resistance as the product of the specific cake resistance, α, and M as the mass of solids deposited per unit of membrane area gives:

$$R_c = \alpha M \tag{4-2}$$

where:

$$M = \frac{c_0 V_f}{A} \tag{4-3}$$

In which c_0 is the starting feed concentration, V_f is the total volume filtered and A is the membrane area. Flux is defined as:

$$J = \frac{1}{A}\frac{dV_f}{dt} \tag{4-4}$$

a combination of equations 4-1 to 4-4 gives the following ODE.

$$\frac{1}{A}\frac{dV_f}{dt} = \frac{\Delta P}{\mu(R_m + \frac{\alpha c_0 V_f}{A})} \tag{4-5}$$

This can be rearranged to give a linearised expression for the inverted volume differential with respect to time as a function of all but one known variables, and so providing an analytical solution for α as follows:

$$\frac{dt}{dV_f} = \frac{\mu R_m}{A\Delta P} + \frac{\alpha \mu c_0}{A^2 \Delta P} V_f \tag{4-6}$$

Finally, an assumption is that the differential is approximated by a discrete change in time with respect to volume filtered, as follows:

$$\frac{dt}{dV_f} \approx \frac{\Delta t}{\Delta V_f} \tag{4-7}$$

Now an analytical solution can be plotted with respect to V_f (Figure 5-31). By calculation of the slope of the fitted straight line and with knowledge of μ, c_0, A and ΔP, an approximation of the specific cake resistance, α, can be made. Calculated values for α, as well as the absolute slope values and determination coefficients, are presented in Table 5-3.

Table 5-3 - Fit parameters and specific cake resistance for 50 µgmL^{-1} BSA solution

Treatment	*Slope/smL^{-2}*	*r^2*	*α/mkg^{-1}*
None	0.071	0.9798	2.12×10^{15}
50 wt.% EtOH	0.086	0.9596	2.59×10^{15}
100 wt,% EtOH	0.103	0.9972	3.11×10^{15}

The differences in the slope are an objective description of the flux decline characteristics given that the membrane intrinsic resistance is only influential on the straight line's intercept. It is observed that the steeper slopes for the ethanol treated membranes are characteristic of an apparent increased specific cake resistance. Since the rejection and feed physical properties remain unchanged this cannot be possible and thus must be an artefact of differing fouling propensity. This could arise either from a physical deposition change, or a differing chemical interaction.

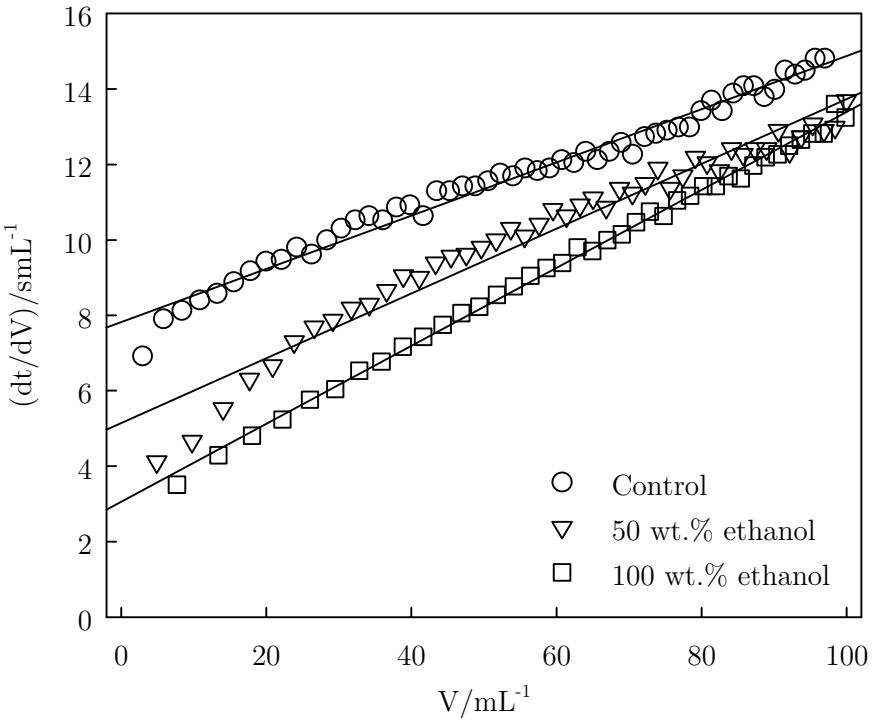

Figure 5-31 – Plot of volume filtered versus the inverse discrete volume differential

The plots show some deviation from the model fits, particularly at the early stages of filtration. This can be attributed to a break down in the model's description when the cake layer is very thin [303]. Another objective assessment from the plots is the curvature of the data. An upwards curving data set would be an indication that the cake specific resistance is increasing as filtration progresses. In this instance a conclusion would be that the cake would be compressible considering this observation, and would thus create an increased resistance as it grows. More apt for this example however is the observation of a decreasing slope over the duration. This would tend to signify the occurrence of fouling inside the membrane based on the fact that the effective membrane resistance would increase. As a graphical explanation - the y-intercept of the plot would be ever-increasing, thus limiting or reducing the apparent slope. This finding prompted a more detailed study of the specific BSA-membrane interactions. The idea was to elucidate the specific mechanism(s) of fouling with a view to understanding the limitations in applying the alcohol treatment methodology to bioseparations.

5.8.4 Adsorptive fouling of BSA

An assessment of adsorptive fouling is instructive in indicating the relative adherence of a foulant to a membrane surface. 20 g of a 1.0 $mgmL^{-1}$ BSA solution (same pH and ionic conditions as for filtrations) was placed onto a pre-conditioned, treated and PWF characterised membrane mounted in the stirred cell module. The sealed module was immersed in a water bath at 25 °C for 90 minutes to allow static sorption of protein to the surface. Gentle rinsing with water to remove excess and loosely bound material was carried out before PWF re-measurement using RO water.

The relative flux before and after adsorptive fouling of membrane is presented in Figure 5-32. Relative fluxes have been presented in two forms; relative to the untreated PWF, and relative to the treated PWF. When comparing 50 and 100 wt.% EtOH treated membranes to their treated PWFs, relative flux drops from 0.58 ± 0.10 to 0.32 ± 0.06 and 0.38 ± 0.08 for the respective treatments. The higher loss of PWF is an indicator of a higher general fouling propensity. If the untreated relative PWFs are compared the result is different. There is no difference for 50 wt.% EtOH, based on a t-test ($p = 0.473$) though there is an indication of an increase. For 100 wt.% treatment the result is 1.07 ± 0.23 and statistically significant ($p = 0.027$). This shows the flux after adsorptive fouling is greater than the original achievable BSA flux of the membrane i.e. the ethanol treatment has more than offset the untreated fouling effect of BSA.

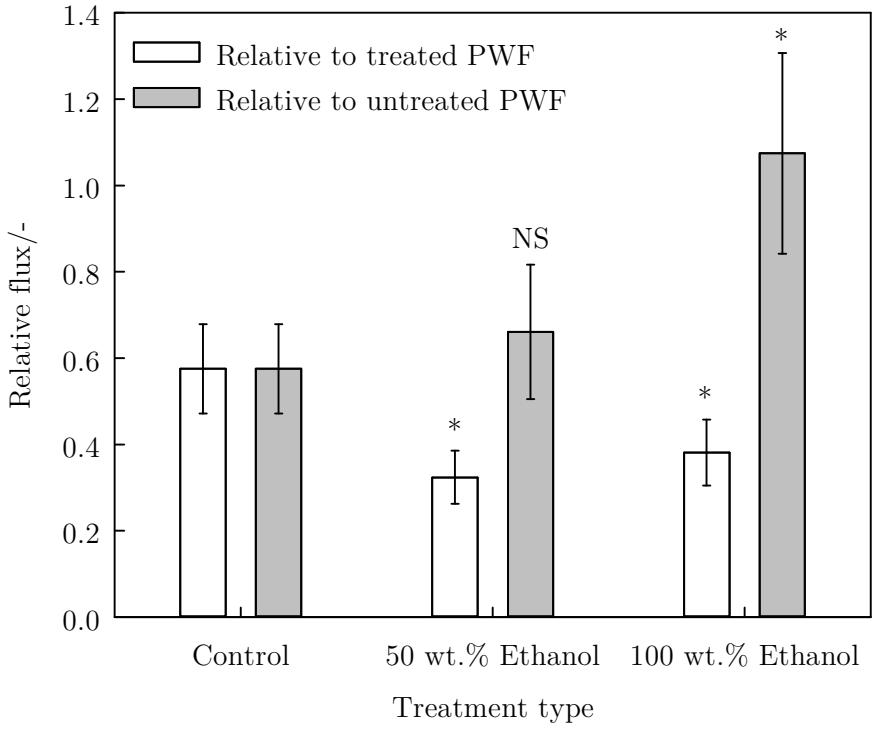

Figure 5-32 - Relative pure water flux following adsorptive fouling of BSA

5.8.5 AFM

In order to confirm the findings in section 5.8.4, a direct approach to measurement was used in the form of colloidal AFM probes, as described in 4.4.1.5. After functionalisation, probes were ramped downwards towards the surface with an approach force of 30 nN resulting in cantilever deflection. Some representative force curves are shown for the approach and retract (Figure 5-33). For both control and treated membranes, there was no negative (downward) deflection on approach, indicating there was no 'snap-in' occurring. This implies that BSA is not spontaneously fouling the surface through active formation of bonds, electrostatic or other interaction forces. A positive adherence was however measured (as shown by negative deflection or force) when retraction of the probe occurred. The total negative deflection is equal to the maximum adhesive force required to remove the probe from the surface. The work of adhesion (total work of removal) is the

integral of the region under the isometric force (zero) line. Both measures have been normalised against the probe radius (8.5 µm) in accordance with the method described by Bowen *et al.* (1998) [179].

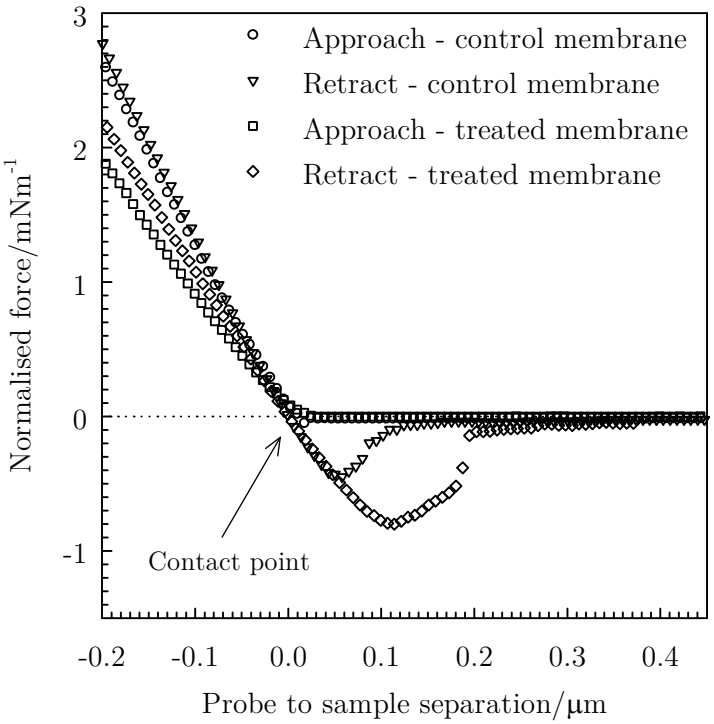

Figure 5-33 - Representative force-distance curves for PS50 membranes during approach and retract of BSA doped colloidal probe

5.8.5.1. Maximum adhesive force and work of removal

Figure 5-34 shows the data presented in box plot form for both maximum adhesive force and total work done to remove the probe from the surface. Using arithmetic means and standard deviations, overlap of both data sets exist. For maximum adhesion of untreated membranes, this value rose from 2.4 ± 1.6 mNm^{-1} to 3.9 ± 2.1 mNm^{-1}, and for work of removal, 4.0 ± 2.0 (× 10^{-7}) J to 5.7 ± 3.3 (× 10^{-7})J. It does appear, as adsorptive fouling studies suggested, that exacerbated fouling of treated membranes occurred as a result of treatment. This lead to the formulation of the null hypothesis for further data analysis; '*The membrane's propensity for BSA fouling remains unchanged following ethanol treatment*'. Data was tested for normality and failed (thus unable to perform t-test) prompting a non-parametric statistical test (Mann-Whitney rank sum test). The test is detailed in Appendix B. Both data sets show that for ethanol treatment, there is a greater than expected difference in the respective medians than would be expected by chance ($p < 0.001$), meaning the null hypothesis can be rejected. All test values are recorded in Table 5-4 and Table 5-5.

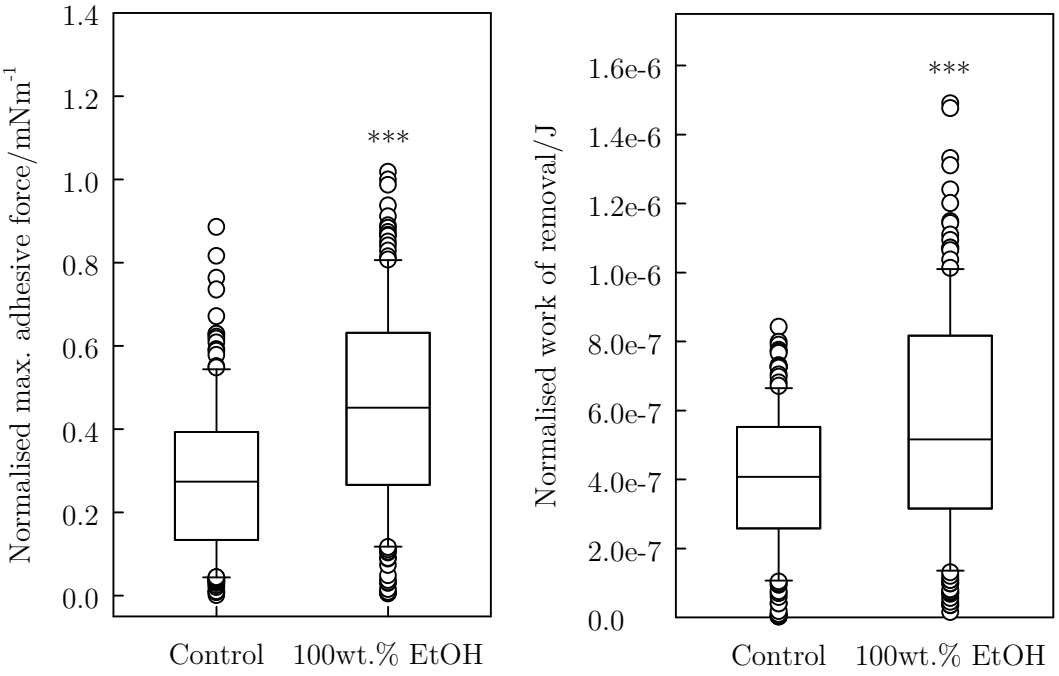

Figure 5-34 - Box plots presenting AFM data for the maximum adhesive force (left) and work of removal (right) between membranes and BSA-doped colloidal probe

Table 5-4 - Statistical test information for maximum adhesive force data

attribute	*value*
n	153
sum of ranks (T)	18657
Mann-Whitney U statistic	6876
$P < 0.001$	yes

Table 5-5 – Statistical test information for work of removal data

attribute	*value*
n	153
sum of ranks (T)	20181
Mann-Whitney U statistic	8400
$P < 0.001$	yes

5.8.6 Discussion of protein filtration and fouling

The results presented show that whilst ethanol treatment of membranes is giving a positive uplift in flux, the propensity for fouling is increased as a result of an increase in the adsorptive potential of the membrane following treatment. The adherence of BSA to the membrane is active in reducing the true capability that ethanol pre-treatment of PS membranes could have, had fouling propensity remained uniform. An increased BSA affinity for the membrane, shown by AFM and adsorptive measurements, gives two sets of

reinforcing evidence. The mechanism of attachment of the protein to the membrane is likely to be a factor of the membranes reduced charged and hydrophobicity. Since these measurements were performed at pH 4.5, very close to the isoelectric point (IEP) of BSA (pH 4.7 [304]), the protein molecule would carry a low net charge. This would enhance the deposition and aggregation. The increase in adherence at this pH would thus be attributed to hydrophobic interactions given the reduced hydration which previously shielded the membrane surface from molecular interactions. The interactions of BSA with membranes in this manner is well reported [305, 306]. The hydrophobicity of the membrane has been shown to increase the β-sheet content of adsorbed BSA and thus plays an important role in protein conformation within the fouling layer, and thus has an influence on subsequent fouling build-up i.e. protein-protein interactions [307].

For adsorptive fouling experiments (carried out at pH 7.4), the untreated membrane would carry a significant charge (*ca.* -16 mV) compared to the 50 wt.% and 100 wt.% ethanol treated membranes; *ca.* -12 mV (approximated from 40 wt.% and 60 wt.% treatments as shown in Figure 5-12) and *ca.* -6 mV respectively. The ζ potential of BSA at pH 7.4 (assuming a 0.1 M NaCl solution) is approximately -10 mV [308]. Palecek and Zydney (1994) [309] showed that flux was directly proportional to the square of ζ potential of protein molecules. This theory was later expanded to account for protein-membrane interactions, whereby the initial flux during filtration using PS membranes was fitted linearly to the product of protein and membrane ζ potential [305]. Results here do not show this as the other factors which have been identified as drivers in raising the flux (swelling, PVP removal, and slip) are more influential over the increase in protein deposition. Also possible is reduced electro-viscous retardation effect given the lower magnitude of charge.

5.9 Conclusions

The body of work presented here constitutes a significant deviation from the classical understanding of membrane modification and filtration capability given that selectivity essentially remains unaffected whilst performance is improved. The methodology employed shows that a profound and prolonged modification to membranes is made in terms of flux uplifts, hydrophobisation and reduced charged. The causation of these modifications has occurred through a number of structural and surface chemical changes. These are summarised below:

- There is an enhanced removal of preservative which reduces the membrane to a virgin state above which hot water conditioning could achieve.
- Leaching of a key pore forming agent (PVP), which potentially opens cavities inside the membrane sub-structure, is thought to be a driver in changes to wetting properties and surface charge.

- A net result of hydrophobisation and reduced surface charge is a reduction in the adherence of water in the membrane pores through hydrogen bonding.
- The reduced adherence of water molecules to pore walls causes increased slip in both pure water and filtration environment.
- Experimental and theoretical measurements relating to swelling of the membranes have been recorded which are thought to cause a macroscopic swelling effect.
- A degree of polymer dissolution (or plasticisation) occurs which relaxes the membrane top layer and producers a less elastic (softer).
- The partial dissolution of the polymer in alcohols relative to water has been confirmed by theoretical considerations as reinforced by mechanical indentation measurements.

Further to this, investigations into protein filtration lead to the following conclusions:

- Performance improvements are realised following ethanol treatment in terms of processing time for a given protein filtration operation.
- Modified membranes showed no distinguishable change in selectivity for the said operation.
- An analysis of cake resistance showed that changes to fouling characteristics had changed despite equivalent operations being performed; leading to a conclusion that adsorptive fouling propensity was modified.
- This was confirmed through consideration of ζ potential for both protein (BSA) and membrane, adsorptive fouling of a BSA, and through protein-functionalised AFM probing.

The results lead to the general conclusion below.

Filtration flux enhancements observed as a result of ethanol treatment are sufficient to outweigh the impact of increased protein fouling resulting from apparently detrimental modifications to the membranes; the result is an overall net improvement in performance.

The work presented in this chapter delivers a membrane science viewpoint of how the modification method can impact process performance. The subsequent experimental sections apply the method to an industrially relevant feedstock to assess its potential for implementation to a more complex feed in a food product based application.

6. Effect of alcohol pre-treatment on polymeric membranes during black tea liquor clarification

6.1 Introduction

This section applies the modified UF membranes in a processing situation, namely the filtration of black tea liquor for removal of tea cream.

UF for tea cream removal has been shown to be effective in reducing the haze characteristic of black tea using both ceramic membranes Todisco *et al.* (2002) [30] and polymeric membranes [25, 26, 28, 33]. Studies with polymeric membranes highlighted the potential for surface chemistry modification which has implications for influencing selectivity and fluxes through synergistic responses in fouling and cleaning phenomena. Attempting to mimic these responses by pre-treatment, with agents such as alcohols, opens up the potential for simple *in situ* pre-treatment methods.

Filtration of black tea has shown interesting characteristics in terms of filtration behaviour, especially due to the presence of polyphenolic species e.g. Wu and Bird (2007) [33]. It is a multi-component mixture, is relatively inexpensive to use for experimentation, and the filtration of which is industrially relevant.

6.2 Experimental design

Filtration was carried out over a range of pressures for treated and untreated membranes at 1.0 ms^{-1} CFV. The experiments were carried out on untreated membranes as control tests in order for benchmarking when testing treated membranes. Flux, total solids transmission and total polyphenols transmission was measured in order to understand membrane performance. Investigation into the effect of TMP on untreated and treated membranes was performed by TMP 'ramping' experiments. After water permeability measurement, TMP was incrementally increased every 30 minutes over the range 0.5 – 4.0 bar (or 0.5 – 3.5 bar) - the time deemed sufficient so as to gain quasi-steady state flux establishment following Evans and Bird (2008) [25]. Sampling of permeate was taken over the final 2 minutes of each pressure increment. These experiments were conducted for 4 membranes types (PS25, PS50, PS100 and FP100) with 3 treatment regimes (no treatment, 50% ethanol and 100% ethanol using the static pre-treatment regime. All experiments were performed with virgin membranes at 50 °C and 1.0 ms^{-1} CFV.

Table 6-1 - Experimental program for analysis of filtration performance of treated membranes

	Membrane type			
Treatment type	*PS25*	*PS50*	*PS100*	*FP100*
No treatment	0.5 – 3.5 bar	0.5 – 4.0 bar	0.5 – 4.0 bar	0.5 – 4.0 bar
50% ethanol treatment	0.5 – 3.5 bar	0.5 – 4.0 bar	0.5 – 4.0 bar	0.5 – 4.0 bar
100% ethanol treatment	0.5 – 3.5 bar	0.5 – 4.0 bar	0.5 – 4.0 bar	-

The aim of the experimental program was to show that alcohol pre-treatment of membrane has an effect on the filtration performance of black tea liquor in terms of membrane flux and mass transfer. This is to hypothesise that (i) the water permeability increases observed in chapter 5 can be converted to solute filtration environments, (ii) that modification of the surface chemistry would permit the transmission of more solutes through the membrane and potentially offer variable selectivity, (iii) the fouling characteristics of the membrane would be modified. It is the overall intention of this study to link the intrinsic membrane properties upon modification to the filtration behaviour.

In Chapter 5, methanol, ethanol and n-propanol were assessed for their ability to modify polysulfone membranes of varying cut-off. In order to minimise the experimental matrix, it was decided to reduce the number of treatment solvents to one - ethanol. Ethanol was selected given its merits in up-modifying water permeability of membranes, safer handling, and safer potential incorporation into processes involving foods.

6.3 Results and discussion

6.3.1 Filtration behaviour of modified membranes

6.3.1.1. Water permeability

Water permeability of membranes was measured before and after ethanol treatment and is displayed in Figure 6-1. The untreated PS25 membrane showed permeability increases of 55% and 62% for 50 wt.% and 100 wt.% ethanol respectively (71.0 ± 3.3 baseline, to 110.32 ± 10.2 and then to 115.3 ± 2.1 $Lm^{-2}hr^{-1}bar^{-1}$). For PS50, the permeability rose from an untreated average flux of 109.3 ± 4.3 to 167.6 ± 8.4 for 50 wt.% ethanol treatment and 245.7 ± 4.3 for 100 wt.% ethanol (rises of 52% and 124% respectively). PS100 changed from an average untreated permeability of 256.2 ± 17.0, to 961.9 ± 48.1 and 988.8 ± 11.3 for 50 wt.% ethanol and 100 wt.% ethanol respectively (representing 280% and 291% increases). The effect of ethanol concentration for PS100 membranes was most noticeable for the lower concentration of treatment solution. Contrastingly for the tighter pore sizes (PS25 and PS50) there was a more gradual flux increase shown for 50 wt.% EtOH. For FP100 membranes, the relative change in the PWF for FP100 membranes was less noticeable, perhaps due to the differing wetting properties of the material.

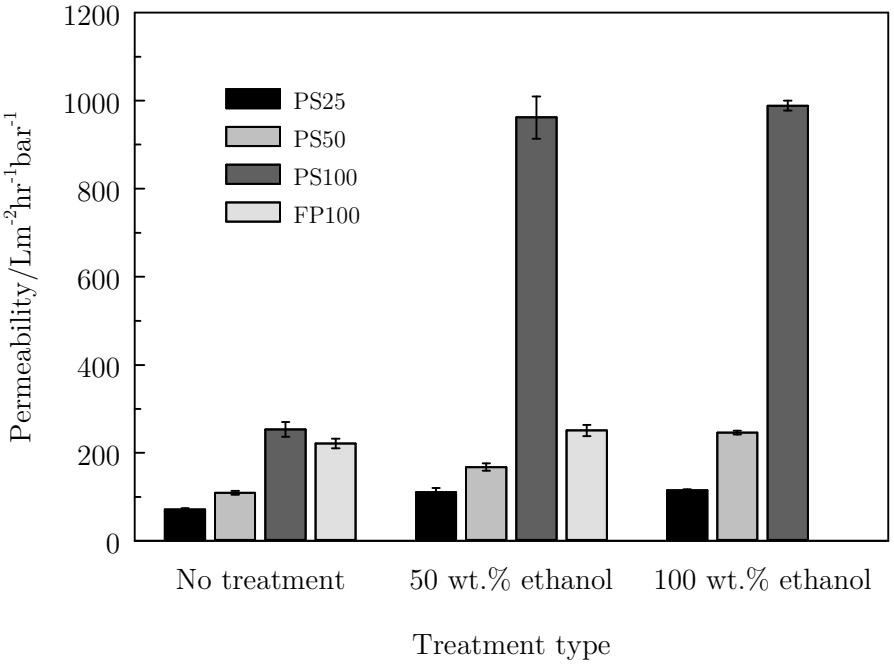

Figure 6-1 - Water permeability of membranes

A reason for this effect could be that the FP100 membrane, following hot water conditioning, has a resultant contact angle of 63.4° ± 1.6°, and PS100 exhibits a contact angle of 66.1° ± 1.7°. Given that FP100 is marginally more hydrophilic than PS100, ethanol has greater potential for enhanced wetting on the more hydrophobic surface i.e. PS100, given its superior wetting properties over water. Although this in theory would be apparent, it would be expected that the difference in contact angle (not statistically different) would

not be great enough to produce such a large variation in the resulting flux, and another explanation is sought. The finding that PS dissolution (and PVP leaching) occurs when in contact with the partial solvent ethanol, which brought about the most significant changes, the difference in swelling behaviour is likely to a major influencing factor. This is affirmed by the findings of Shukla and Cheryan (2002) [41] who report that PVDF membranes were substantially less inclined to swelling than PS and PES membranes of comparable pore size in solvents (water, 70 wt.% and 100 wt.% ethanol).

6.3.2 Permeability during filtration

Figure 6-2 shows the filtration permeability obtained during filtration of 1.0 wt.% tea solution at 50 °C. All trend lines are calculated using the RIS model, with experimental and model fluxes divided by TMP to give permeability.

For the PS25 membrane (Figure 6-2a) there is a moderate decrease in permeability across the pressure range for all treatment types. The membrane also exhibited lower fouling fluxes for ethanol treated membranes than for the untreated membranes at each TMP, meaning the effect of ethanol treatment, despite increasing the water permeability, also increases apparent fouling susceptibility. Also shown by (Figure 6-2a) is the arguably unchanged performance of the PS25 membrane with respect to ethanol treatment concentration. As displayed in Chapter 5, the PS25 membrane showed the lowest variability in post-ethanol treatment permeability change compared to PS50 and PS100, and it was shown that despite the surface chemistry aspects for all membranes displaying similar trends, steric aspects of these membranes i.e. those relating to the pore size and polymer matrix characteristics also correlated to the degree of performance change in terms of water permeability.

For the PS50 (Figure 6-2b and c) there is an incremental permeability increase at low TMPs for untreated, 50% ethanol treated and 100% ethanol treated membranes of respective cut-offs. For PS50, permeability is increased from 39.4 ± 5.6, through 53.4 ± 6.7, to 55.3 ± 5.9 $Lm^{-2}hr^{-1}bar^{-1}$ for no treatment, 50% and 100% ethanol respectively at 0.5 bar TMP. This corresponds to 36% and 41% increases for the respective ethanol treatments. Again as for PS25, there was no difference between 50% and 100% treatment (when errors are accounted for) when filtering at 0.5 bar. For PS100, the degree of change was comparable. A rise from 35.1 ± 5.4 to 53.0 ± 1.7, and then to 59.3 ± 4.4 (all $Lm^{-2}hr^{-1}bar^{-1}$) was shown for the same treatment protocols (51% and 69% respective rise for 50% and 100% ethanol). FP100 (Figure 6-2d) showed the largest rise in fouling permeability, from 23.0 ± 3.7 to 41.2 ± 5.6. This result is interesting given that this membrane gave the lowest water permeability response to the 24 hour ethanol treatment protocol over all PS membranes. As noted from the figures, the relative magnitude of errors for 0.5 bar filtration is greater. This was due to the less stable pressures at low pressures; the system stability was bettered when a greater back pressure was present.

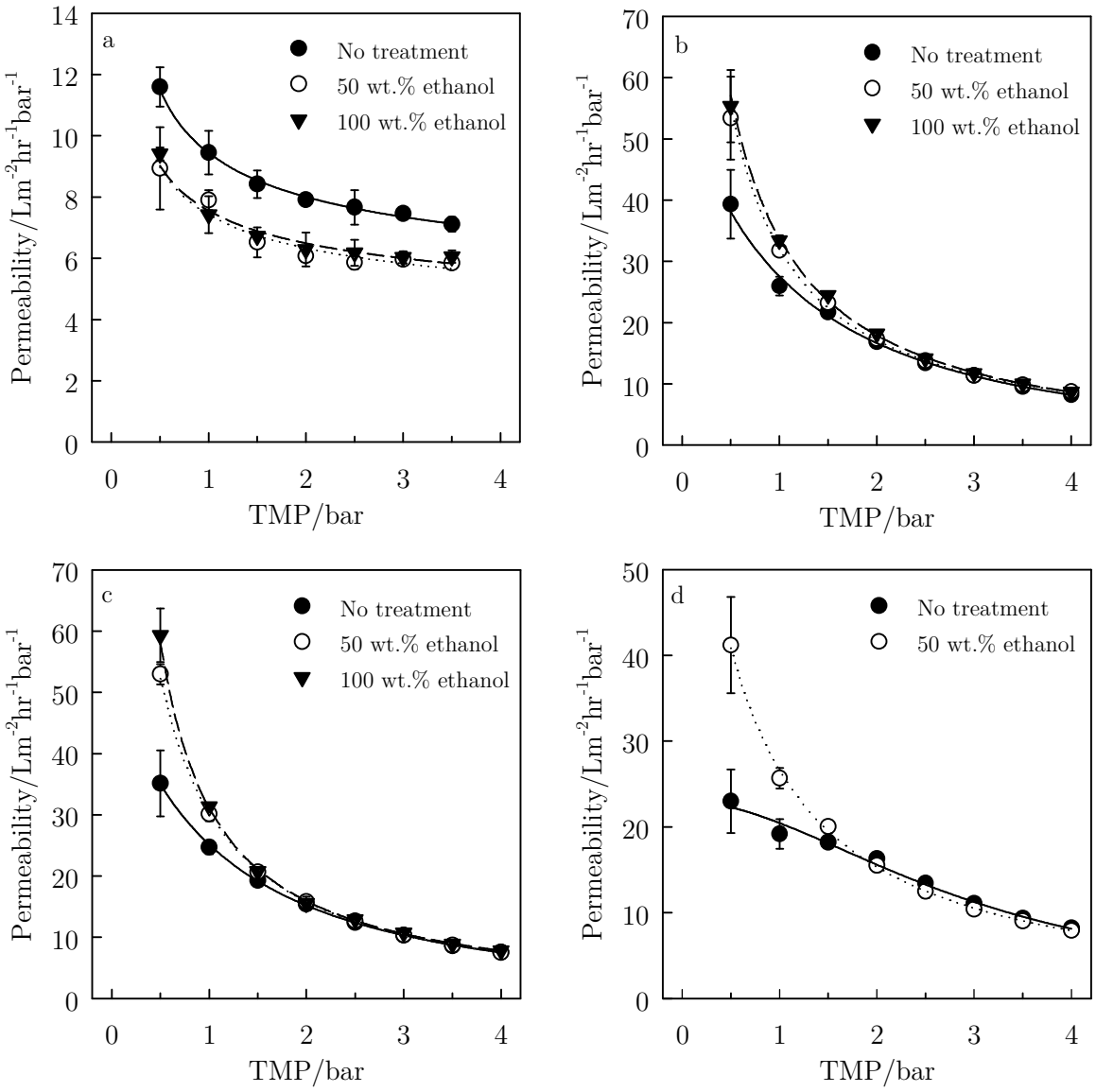

Figure 6-2 - Filtration permeability of 1.0 wt% tea at 50 °C for treated and untreated membranes at a range of TMPs. (a) PS25, (b) PS50, (c) PS100 and (d) FP100

For all membranes, the flux increase for filtration at 1.0 bar was less pronounced but still significant. The PS50 membranes showed an increase in permeability of 22% and 29% for 50 wt.% and 100 wt.% ethanol treatment respectively. The PS100 showed similar uplifts of 22% and 27% for the same treatment types respectively. FP100 showed 34% uplift in permeability after 50 wt.% ethanol treatment.

The data shows that at low pressures, the ethanol treatment effect on water permeability can be converted to the solute filtration environment with varying degrees of effect. The PS25 membrane appears to show more significant fouling despite an increased pure water permeability. In order to interpret these findings as a mechanistic picture, it is useful to present the finding as flux-TMP profiles so as to ascertain whether asymptotic (or limiting) fluxes play a significant role in the flux variability, not just between membranes of equal

specification and changing treatment type, but also how the membrane specification affects the performance.

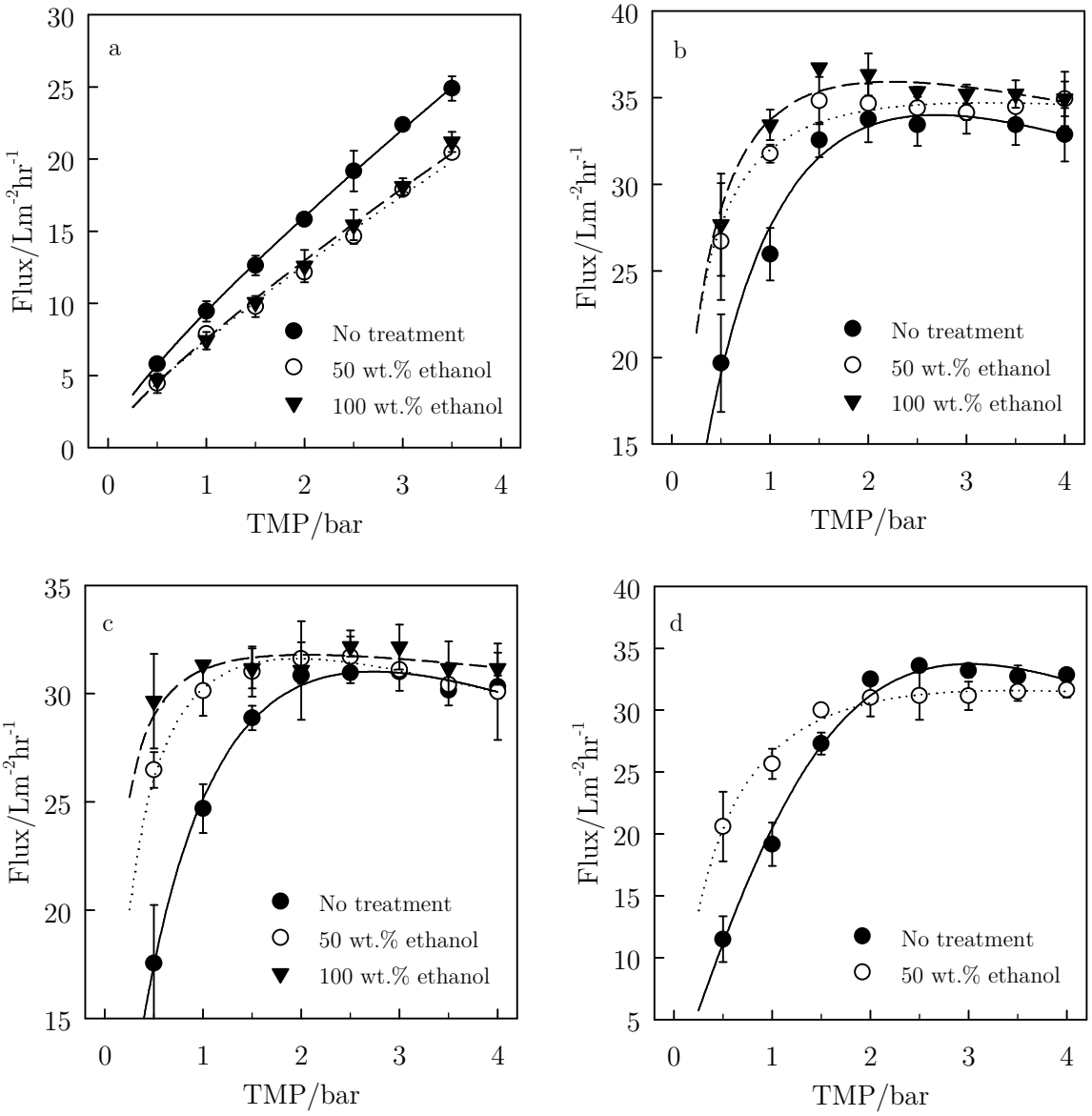

Figure 6-3 - Flux-TMP plots showing presence of limiting flux region for (a) PS25, (b) PS50, (c) PS100 and (d) FP100

Figure 6-3 shows flux-TMP plots for the pressure-flux experiments. These plots are useful for determining in what region the filtration is carried out, i.e. whether it is in the pressure controlled region, where flux has a near linear dependency on TMP, or in the mass transfer controlled region where fouling and CP aspects play a role in limiting or retarding flux increases, and pressure influences only the solute mass transfer (see 2.3.3). In Figure 6-3a (PS25 membrane), no limiting flux is achieved at the conditions chosen for the experimentation. These results mirror the findings of Fane *et al.* (1981) [310]. These authors show that membranes of similar specification can operate contrastingly with reference to the occurrence of an asymptotic flux at a given pressure, simply as a result of PWF

variation. Membranes of similar specification i.e. pore size can show more gradual increases in their flux-TMP relationships than higher permeability membranes. The authors show that membranes of similar specification can and cannot exhibit 'gel-polarised' behaviour and relate this to surface porosity and pore plugging. Pore plugging especially dominates filtrations where molecules are of similar size to the membrane pores. For the other membranes, limiting fluxes for untreated membranes are obtained at around 2.0 bar for PS50, 2.0 - 2.5 bar for PS100, and 2.0 bar for FP100. The limiting fluxes, although difficult to quantify given the drop off at high pressure, appear to occur earlier for treated membranes. This further supports the theory that for a given concentration of feed, limiting flux is influenced strongly by initial pure water permeability even if membranes exhibit small differences in morphology or pore size.

The results of these limiting flux experiments are significant regarding pre-treatment with alcohols. It has been shown that as long as the operating regime occurs in the pressure dependant region, any water permeability improvements gained as a result of the treatment method can be directly converted to filtration of solutes. The findings imply that as long as the filtration is not dominated by cake filtration, gel filtration and high CP (i.e. if it is in the pressure independent region), then improved fluxes can be realised. For applications where low concentrations are being used, such as diafiltration of macromolecules for 'wash-through' purification of a given solute, the treatment method could significantly enhance processing time/volume throughput.

6.3.3 Total solids rejection

As expected, PS25 (Figure 6-4a) offers the greatest rejection of solids across the TMP range, PS50 and PS100 (Figure 6-4b and c) offer very similar rejections. The FP100 (Figure 6-4d) shows that at low pressures, greater rejection is observed compared to the similarly specified PS100 membrane (c) although at elevated pressure ($>$ 3.0 bar) the performance is somewhat similar. An increase in rejection is shown for PS25 across the pressure range; for an untreated membrane, rejection ranges from 41.1 $\pm$ 0.7 to 61.7 $\pm$ 1.0 (all %) for 0.5 bar to 3.5 bar TMP. The rejection increases for 45.1 $\pm$ 0.6 to 63.8 $\pm$ 1.8 for 50 wt.% ethanol treatment and 46.8 $\pm$ 0.6 to 63.1 $\pm$ 1.8 for 100 wt.% ethanol treatment.

These rejections are in agreement with the lowered fluxes, as one would expect to see for a membrane with low permeability during fouling. The rejection increase is potentially due to tightening of pores as a result of membrane swelling which has been discussed in 5.7.1. As speculated in 6.3.2, complete pore blockage (pore plugging) is the likely dominating mechanism, however, increases in solids rejection (the production of lower concentration tea) suggest narrowing of pores due to foulant accumulation on the surface, as discussed by Jones *et al.* (2012) [311]. There is no distinguishable difference between treatment with 50 wt.% and 100 wt.% ethanol, this observation applying to all membranes. For PS50, a rejection decrease is observed for ethanol treatments at low pressure, although the difference in rejection at high pressure becomes statistically insignificant (at 4.0 bar, rejections for untreated, 50 wt.% and 100 wt.% ethanol treatment respectively are 57.2 $\pm$ 1.1, 57.2 $\pm$ 0.8 and 56.6 $\pm$ 0.9).

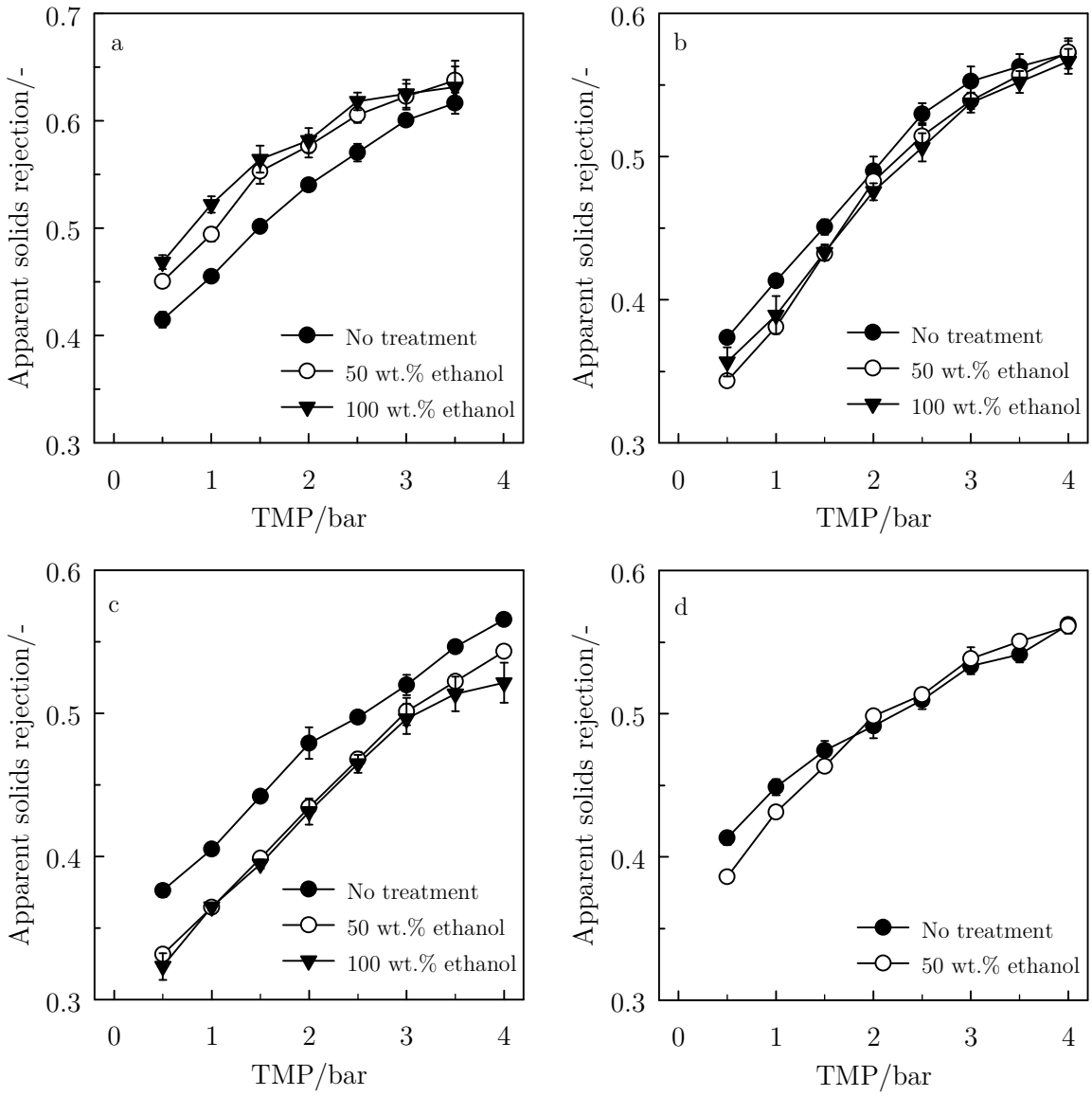

Figure 6-4 - Solids transmission for untreated and treated membranes. (a) PS25, (b) PS50, (c) PS100, (d) FP100

The most pronounced change in rejection occurs for treated PS100 membranes. Across the TMP range, a clear reduction in rejection occurs. At a TMP of 0.5 bar, percent rejections of 37.6 ± 0.5 for untreated, 33.1 ± 0.1 and 32.3 ± 0.9 for respective 50% and 100% ethanol treatments were recorded.

Ethanol treatment of membranes has shown to be effective in modifying the solids transmission characteristics of synthetic polymeric membranes. In their study, Jones *et al.* (2012) [311] attest that using a pre-wash (0.5 wt.% NaOH) had an effect on the solids transmission of the membrane for the initial and subsequent three filtration cycles. The modifications to the membrane surface chemistry after alcohol treatment (e.g. greater neutralisation of charge through the membrane pores) are allied with the observations of in the aforementioned study. In this study however, the chemical modifications are not the single factors changing and thus, aspects such as pore widening or constriction must be

considered as a result of swelling. The rejection findings further affirm the idea that for tighter membrane pores, swelling can lead to constriction (represented here by reduced solids transmission) and that when dealing with larger pore sizes, macroscopic expansion leads to increased solids transmission. In reality, both swelling mechanisms should occur simultaneously given the anisotropic nature of the membranes in study. It can be deduced from the measurements here that constriction indeed dominates for the tighter (PS25) membrane, whereas the opposite is true for the other membranes.

6.3.4 Total polyphenols transmission

The polyphenolic species are those which give the health giving properties, appearance and taste to tea, and thus ensuring loss of these solutes is kept to a minimum when conducting membrane filtration. Retentate and permeate samples were analysed to monitor this.

Figure 6-5 shows for all membranes there exists a greater rejection of polyphenolic species in comparison to the total solids. For PS25 (Figure 6-5a), over the pressure range there is a rejection rise from 57.9% ± 1.1% to 78.2% ± 1.6% (compared to the total solids change rejection noted earlier of 41.1%, rising to 61.7% over the same TMP range). This trend is apparent for all membranes analysed and is a detriment to the applicability of membrane filtration for tea treatment and perhaps the filtration of other polyphenol rich beverages. Results show that polyphenolic species are preferentially rejected from the membrane over non-polyphenolic species, at least for the system investigated here. Given the molecular weights of key species (TFs: 564 - 868 Da and TRs: ~700 – ~40,000 Da) it would be expected that if the separation was based on size exclusion alone, the majority would transmit the membrane, even if some intermolecular associations ($\pi - \pi$ stacking, H-bonding or ionic bridging) cause effective particulate size increases.

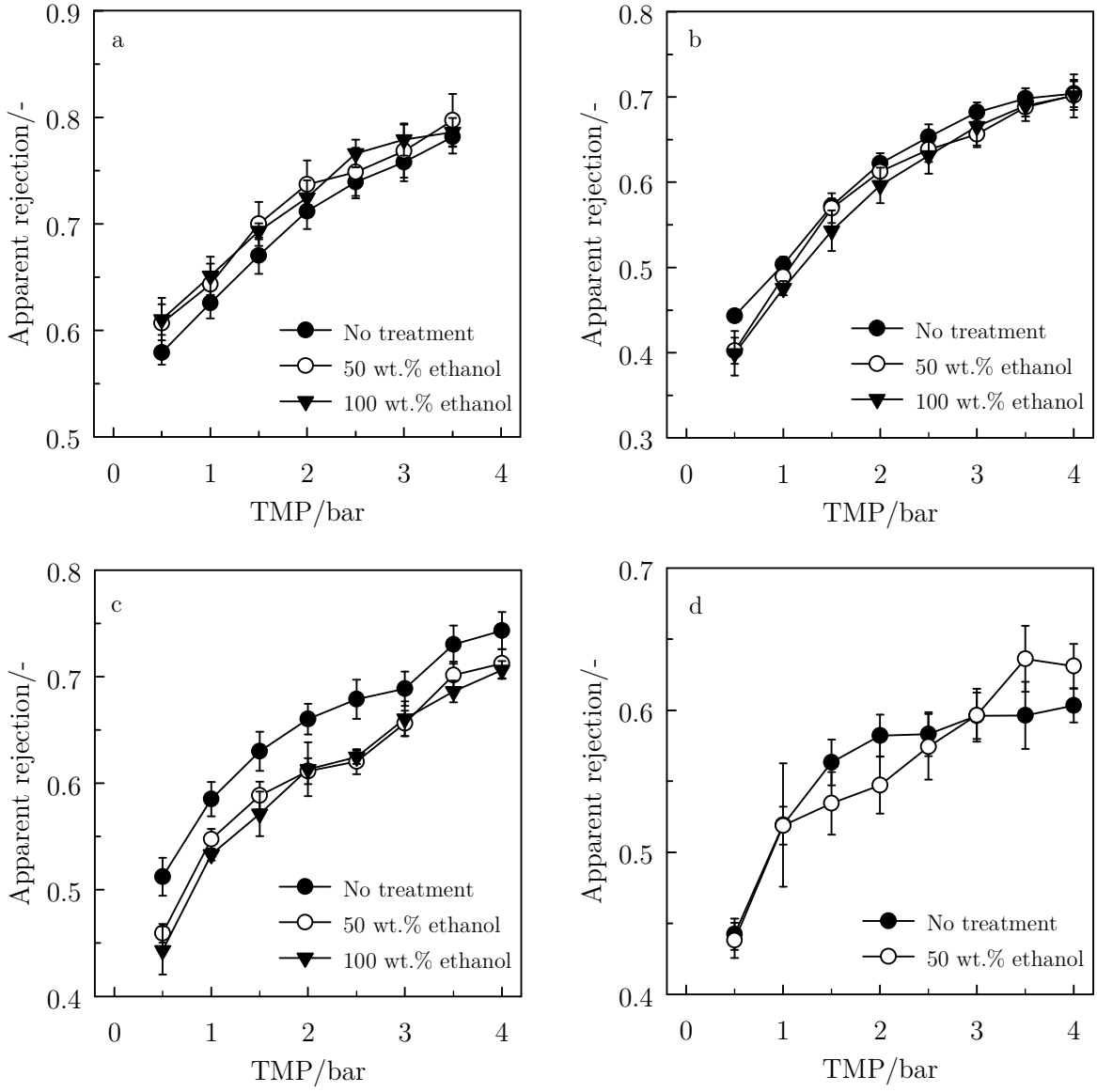

Figure 6-5 - Total polyphenolics rejection through membranes during filtration of 1.0 wt.% black tea at 50 °C. (a) PS25, (b) PS50, (c) PS100 and (d) FP100

It has already been shown that alcohol treatment reduces net surface (negative) charge to a more neutral value across the pH range and that hydrophobicity increases. If polyphenols are now considered in the system, a lowered affinity for H-bonding would be apparent for species interacting with the treated membrane over the untreated membrane. In addition, the high electronegativity of acid-dissociated phenolics would result in lower double layer repulsion from the more neutral membrane. This would thus allow more polyphenolics species (as well all other species, preferentially those which are hydrophilic) to transmit. The effect of this is shown in Figure 6-6c and partially in (b) and (d). The rejection coefficient is lower for ethanol treated membranes challenged with tea. In the case of PS100, a reduction in rejection is significant (51.2 ± 1.8 for untreated membranes, falling to 39.9 ± 2.6 at 0.5 bar for 100 wt.% ethanol). For FP100 (d), the explained effect is questionable with the magnitude of the error. For PS50 (Figure 6-6b) there is a marked change at the

lowest pressure, although there is still overlap of errors for the majority of TMP instances. The PS100 exhibited the lowest apparent absolute ζ potential at the filtration pH of between 4.5 and 5.0 following 100 wt.% ethanol treatment compared with PS25 and PS50. For PS25, the treatment reduced the negative charge to -3.6 mV, for PS50 the ζ potential was -3.1 mV and for PS100, this value was -2.1 mV.

6.3.5 Separation of polyphenols from solids

It has been shown that the membranes are rejecting a substantial proportion of the polyphenolic species over other constituents, meaning valuable product is lost. The ethanol treatment has improved this. Untreated membrane behaviour is in keeping with the findings of Evans and Bird (2006) [25] who found that total polyphenols were transmitted at *ca.* 75 - 90% levels through FP 10 kDa, FP 30 kDa and FP100 kDa membranes. The fractionation of the streams is best described as a single separation factor of polyphenolics from other constituents. This provides a useful measure of the filtration efficiency. The separation factor α is defined as the ratio of the proportion of target solute (polyphenols) in the permeate stream to the proportion of that species in the feed stream and is described mathematically as:

$$\alpha = 1 - \left(\frac{y_{TP} / y_{TRS}}{x_{TP} / x_{TRS}} \right) \tag{x}$$

where mass fraction of solutes in the feed/retentate and permeate streams are represented by x and y subscripts respectively, and solutes are specified by TP and TRS (total polyphenols and total residual solids respectively).

A separation factor of $\alpha = 0$ would mean a proportional separation, whereby the fraction of polyphenols in the feed stream is equal to those in the permeate stream. Given that there are higher rejection coefficients for polyphenolics than other species, the mass fraction of polyphenolics in the permeate stream is lower than in the feed stream, meaning $0 < \alpha < 1$. If $\alpha = 1$, there would be complete rejection of polyphenols and complete transmission of residual solids i.e. a perfect separation.

A comparison of separation factors for untreated membranes is shown in Figure 6-7. The results show that FP100 has the least influence on α. For high permeability operation (when the TMP is low, as was expressed in Figure 6-2), the FP100 exhibits almost proportional filtration behaviour ($\alpha = 0.12$). For the mid-range permeability there is an increase, which peaks when filtering at 2.0 bar, before further pressure increase results in the membrane transmitting both component groups with stronger proportionality once again. This would indicate that at higher TMP, any charge interactions which are preventing polyphenolics from transmitting the membrane are overcoming the double layer repulsive force. This has potential relevance for the use of low cut-off UF membranes (< 2000 Da) where size exclusion of molecules becomes a greater contributing factor in polyphenols separation.

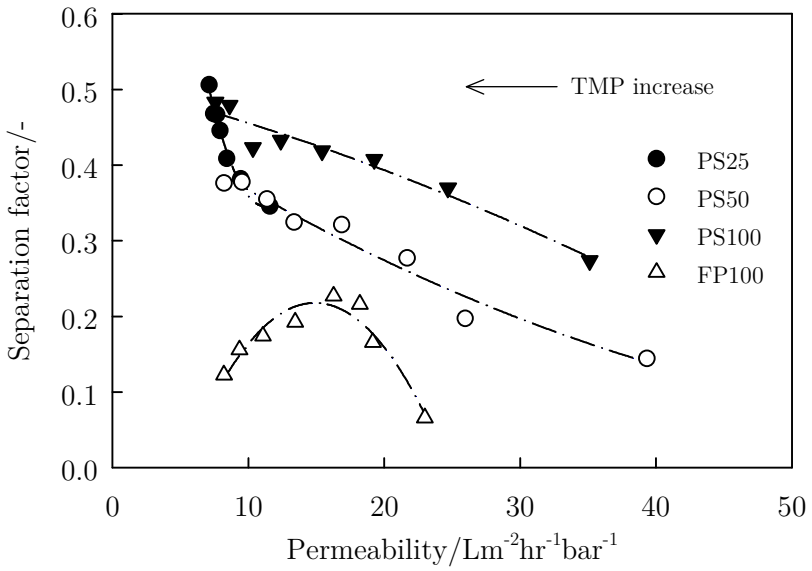

Figure 6-6 - Separation factor change with respect to permeability for untreated membranes

For PS membranes, Figure 6-6 shows that for a decrease in permeability, where increase in pressure takes flux values to or beyond the limiting flux, is detrimental to the filtration performance in terms of maintaining polyphenol levels. However this finding can be used advantageously. Application of the process in a diafiltration regime would mean that preferential wash-through of non-polyphenol species could be achieved. Such separation would be somewhat paradoxical, whereby the smaller molecules are left in the retained stream and the larger solutes and particulates are transmitted. This has been the subject of a further investigation (Chapter 7).

In order to analyse the separation factors for the treated membranes, the dependency of rejection coefficient for both total solids and total polyphenols was deduced as a continuous empirical function by fitting of the observed rejection coefficients to a power law function of the TMP in the form $R_{obs,TMP} = a(TMP)^b$, where a and b are empirically derived dimensionless non-physical parameters and are calculated purely for the purposes of curve fitting. The described fitting method gave determination coefficient values (r^2) of greater than 0.90 in all cases. By generating continuous functions for membranes of all treatments, deduction of the separation factor was possible, assuming an exact 1.0 wt.% feed concentration (this varied by ± 4 wt.% by comparison of experimental feed dry weight measurements perhaps due to evaporation of water), and a tea polyphenol mass fraction of 26 % of the unfiltered dry solids fraction (see Appendix A6).

For all PS membranes, there is a modification in α after ethanol treatment (Figure 6-7). This modification is not present for FP100, and is especially true for PS100 membranes modified by 100 wt.% ethanol treatment. It shows that treatment methods are allowing an improved transmission of polyphenols species through the membrane when compared to other constituents. The PS25 membrane shows the lowest separation factors, meaning relatively, more polyphenols are rejected by this membrane. Despite seeing lowered

rejections for solids and polyphenols, PS25 exhibits marginally improved preference for transmission of polyphenols following ethanol treatment.

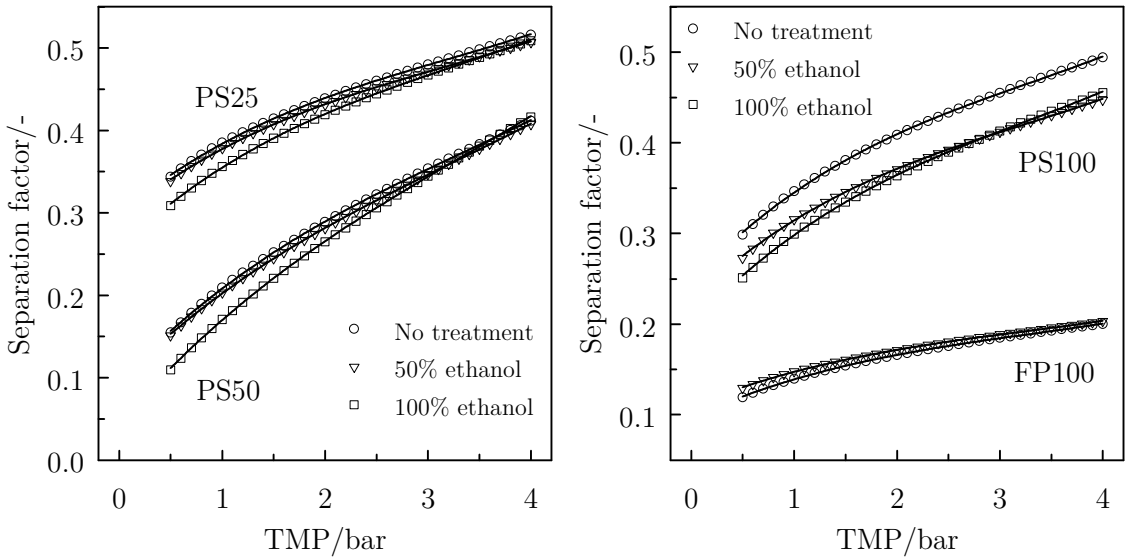

Figure 6-7 - Separation factor profiles for all membranes using 1.0 wt.% tea at 50 °C

The most striking observation about Figure 6-7 are the increases in α with TMP. The most prolific rise was for PS50 (0.15 to 0.41). In theory, better diffusivity due to the lower molecular weights of unbound polyphenol species over proteins, polysaccharides and tea cream aggregates would mean greater hindrance in terms of mass transfer, due to CP, in the membrane-bulk boundary layer. TMP increases the magnitude of CP also. For a given membrane, the mechanism of rejection due to membrane-solute interactions should not vary radically with TMP, thus the rise in separation factor and thus preferential rejection of polyphenols is *de facto* due to either CP or fouling. Mediating this effect by modification of the membrane charge is a viable strategy to minimise valuable species loss during filtration as a result of unfavourable fractionation. The effect is more noticeable at lower pressures where CP is likely to be less dominant. At the higher pressures, the convergence of the separation factor profiles indicates that the diffusive CP mechanism dictates over double layer/intermolecular interactions.

6.3.6 Colour measurements

Tea colour was measured by absorbance using a UV-Vis spectrophotometer. Absorbance was converted to the individual ordinates in the CIELAB colourspace as detailed in Appendix A9 for analysis of tea lightness, redness and yellowness. Lightness/colour has been plotted against permeate concentration and compared with unfiltered tea measurements to show any variability.

Figure 6-8 shows the lightness ordinate for all membranes. The distinct observation is that tea became considerably lighter after UF in all cases. Also prominent in these graphs are the much steeper negative correlation with respect to permeate solids concentration than for equivalent concentration of unfiltered tea. Tea filtered at 0.5 bar (where rejection was

lowest) gave the least shift from the darker unfiltered tea appearance. It can therefore be implied (given that a lower turbidity can be a contributing factor in lightness [176]) that more haze causing solutes are transmitted at lower TMPs. It could also be the case however that highly polymerised polyphenol species (TRs), which exhibit a positive darkness characteristic with increasing concentration, are also more preferentially transmitted at lower TMPs.

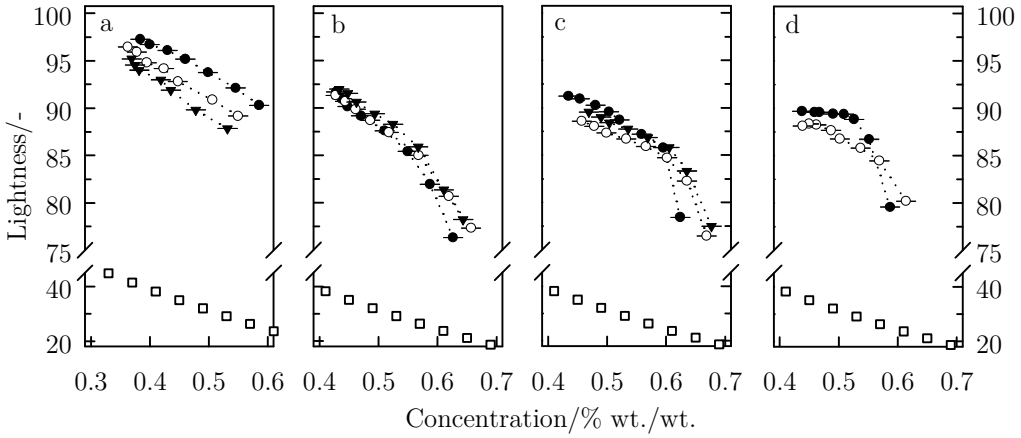

Figure 6-8 - Lightness measurements for tea permeates and unfiltered tea of comparable concentration. Data points: ● - no treatment, ○ – 50 wt.% ethanol, ▼ – 100 wt.% ethanol, □ - unfiltered tea. Charts: (a) PS25, (b) PS50, (c) PS100 and (d) FP100

There is a distinct trend with regard to permeate lightness for the PS25 membrane. The 50 wt.% and 100 wt.% ethanol treated membranes appeared to give a darker tea at comparative concentrations. This would mean that both haze causing solutes and more complex polyphenolic species are able to transmit the membrane more efficiently after ethanol treatment of PS25. This is also the case for PS100 and FP100, to an extent, although findings did show the resolution as clearly than as for PS25. For PS50, the discrepancy in lightness is too close to make a firm conclusion.

Redness, shown in Figure 6-9, generally shows a large decrease for all membranes, indicative of a loss of thearubigins (or other complex polyphenolic species). The loss is mediated for the PS25 membrane and the trend indicates that at higher pressure, there is some preferential transport of these solutes. It could be speculated that at lower pressures, the transmission of these species could be dominated by diffusion based transport (during lower flux operations). At mid-range TMP, the diffusive transport through the membrane could be balanced by back diffusion (CP) resulting in lower transmission. Lastly at higher pressures, there exists a stronger dominance of convective transport which overcomes the dominance of CP once again. This theory could only be true for PS25 as no limiting flux was observed (which was not the case for all other membranes in this study).

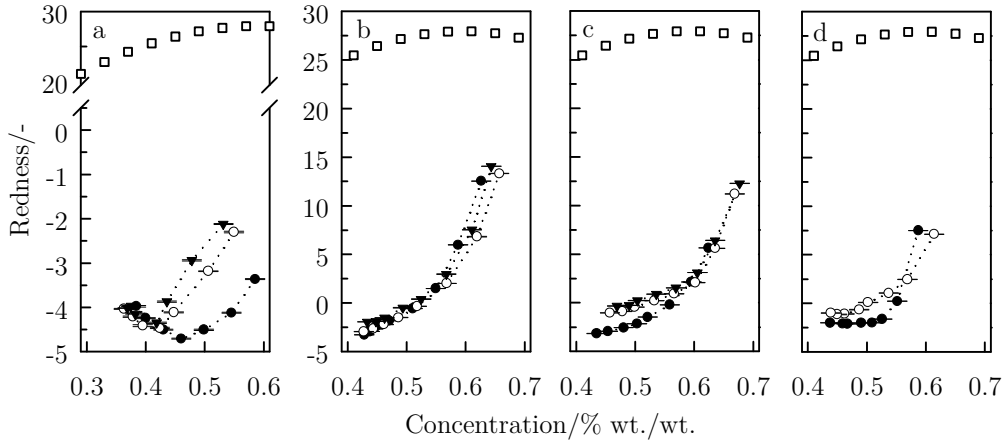

Figure 6-9 - Redness measurements for tea permeates and unfiltered tea of comparable concentration. Data points: ● - no treatment, ○ – 50 wt.% ethanol, ▼ – 100 wt.% ethanol, □ - unfiltered tea. Charts: (a) PS25, (b) PS50, (c) PS100 and (d) FP100

PS50 gives the best overall redness when filtering tea at 0.5 bar, 12.54 ± 0.02 with no treatment, 13.32 ± 0.02 with 50% ethanol, 14.08 ± 0.01 with 100% ethanol. This reaffirms the lightness information in that TRs concentration would negatively correlate to lightness and positively correlate to redness.

Yellowness measurements showed interesting trends (Figure 6-10). An increased yellowness over unfiltered tea was shown for all membranes, be it at only high permeate concentration (low TMP) for PS25. Ethanol treatment also gave a strong indication that yellow pigmented species (TFs) can be better transmitted, although a drop in yellowness is still apparent across the TMP range. For PS50, filtering to give a permeate concentration above 0.5 wt.% (below 2.0 bar TMP) resulted in a gain in yellowness for all treatment types The treatment type did not significantly affect the yellow species transmission in any case. For PS100, lower TMP operation (below 2.0 bar) allowed for an increased yellowness). After treatment, yellowness increases were observed up to 3.0 bar TMP for both 50 wt.% ethanol and 100 wt.% ethanol treatment. For FP100, treatment with 50 wt.% ethanol also allowed TFs to be better transmitted at increased TMPs. For higher concentration permeates (at low TMP) the yellowness was less intense when using a treated membrane over an untreated counterpart.

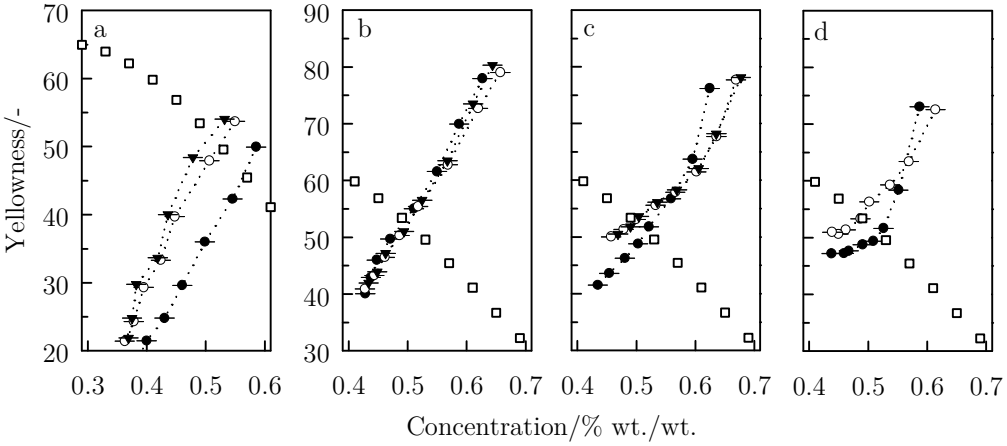

Figure 6-10 - Yellowness measurements for tea permeates and unfiltered tea of comparable concentration. Data points: ● - no treatment, ○ – 50 wt.% ethanol, ▼ – 100 wt.% ethanol, □ - unfiltered tea. Charts: (a) PS25, (b) PS50, (c) PS100 and (d) FP100

6.4 Conclusions

The results presented have produced some important findings. It is shown that the improved membrane fluxes noted as a result of ethanol treatment of PS membranes are observed in the filtration environment. This is not a general result however; it is dependent on the operating regime. Only when filtration is carried out with a TMP in the sub-limiting regime is the conversion of high water flux to high filtration flux made. This is confirmed conveniently by comparing the PS25 membrane to the PS50 and PS100 membranes. The PS25 did not reach a limiting value in the experimental TMP range and when filtering tea through a modified filter, the permeate flux was consistently greater over the operating range. The degree of uplift for the PS25 tea permeate fluxes directly mirrored the trends shown for the pure water permeability modifications with ethanol.

The FP100 membrane showed the least response to ethanol treatment, though the result in which the separation factor peeked at *ca.* 2.0 bar. This means that operating below and above this pressure impacts the polyphenols fractionation mechanism to a lesser extent, giving insightful operating information.

Also shown is that the rejection of polyphenols can be lowered following ethanol modification and is likely a direct consequence of changes to morphology and surface chemical aspects. Improved polyphenols transmission measured by assaying, and reaffirmed by colour measurements is a key finding and is further investigated in Chapters 6 and 7. Another important general point is the fractionation mechanism shown between polyphenols and all other species. In terms of the target stream (permeate) this is a set-back for developing membrane processes as removal of polyphenols would be deemed negative from a tea quality aspect. It does however present a mechanism which could be exploited to recover valuable components (e.g. from waste streams) or standardise tea composition in terms of polyphenol concentration. This fractionation mechanism, and

further its remediation by ethanol treatment of membranes, is the subject of the next section.

7. Ultrafiltration of black tea liquor in diafiltration regime

7.1 Introduction

Previously the observed rejection of polyphenol solutes were shown to be significantly greater than for all other solutes when conducting UF of black tea at 50 °C. For the purposes of producing reduced haze tea, UF works sufficiently. However, the non-preferential transmission of polyphenols and the limited total solids transmission means the process is somewhat detrimental to the production quality of tea and overall product yield.

Inherent variability in products, especially relating to polyphenols, can arise from factors such as agronomic conditions, leaf age, degree of fermentation and storage conditions [312], with geographical location of plant growth [227, 313] and seasonality [314] also causing variability. By exploitation of the fractionation mechanism reported in the previous chapter and operating in a constant volume diafiltration regime, it was hypothesised that enriching the retentate product, whilst maintaining a viable permeate product during UF, offers the potential for 'skimming' some polyphenol species from tea feeds. This would offer potential for creating a polyphenol rich stream as well as maximising tea solids yield in the permeate. Consequences of this action are that by having more control over the stream content upon UF, re-blending of streams could help to standardise batch to batch consistency. The process can offer advancements in processing when either:

1) A tea stream has a higher than required polyphenolic content. In which case processors would mediate additional bitterness and astringency in their product due to the increased presence of certain polyphenolic compounds (e.g. gallo-catechins) [244] (permeate target stream).
2) A lower quality tea feed is being processed or if a waste stream contains valuable solutes. In which case recovery of higher quality streams, in terms of polyphenolics, becomes feasible (retentate target stream).

Aside from results mentioned in Chapter 6, observations by Chandini *et al.* (2012) [315] and Subramanian *et al.* (2013) [32] mentioned aspects addressed in this study. The first article mentioned shows similar findings to results observed in this thesis; where there is a preferential rejection of polyphenolics over all other species leading to a lower quality tea permeate. In the review by the second authors mentioned here they state that no work to date has looked at addressing the polyphenol rich retained stream which arises from UF, and that no attempts have been made in viewing the overall process in terms of tea solids and polyphenols yields. This section aims to address these issues by way of a bench scale membrane operation for an individual unit operation in a specific operating regime.

It is shown that by application of constant volume diafiltration, (i) the retained stream in the process is converted to a stream of added value in terms of its polyphenolics concentration, (ii) the degree of separation is linked to both the degree of membrane fouling, as well as retentate dilution effects, (iii) that membrane specification is critical for influencing the separation, (iv) that alcohol treatment can be used to enhance the volumetric throughput and minimise the solids loss (enhance yield) over a specified operating duration, so as to partially alleviate the inherent polyphenols loss of the UF process.

7.2 Experimental design

7.2.1 Diafiltration experiments

UF filtration of 1.0 wt.% black tea was carried out in the diafiltration regime using PS25, PS50, PS100 and FP100 membranes over 5 hours at 1.0 bar (PS100 at 3.0 bar also, over 6 hours). To maintain constant dilution conditions, 100 g of RO water was added to the feed tank for every 100 g of permeate had been collected. This was repeated continually until the termination of the experiment. Feed/retentate and permeate streams were sampled after 30 minutes and subsequently after every hour, and analysed for solids content and total polyphenols using the Folin and Ciocalteu assay method described in 4.4.2.2. Further to this, membranes were treated using 50 wt.% ethanol by the method described in 0 and subjected to the same filtration and analysis protocols in order to show that ethanol treatment of polymeric membranes was also influential during diafiltration processing. In addition to analysis of the filtration behaviour and rejection solutes, a full analysis of tea quality indicators (turbidity, lightness and colour) was made to assess the effects of filtration on tea permeate product. The key assessment criteria were the maintenance of permeate product quality, whilst ensuring as higher yield of tea solids and polyphenols as possible.

7.2.2 Application of diafiltration model

In section 4.5.3.2 the initial value problem was derived for a generalised diafiltration scenario. The original un-integrated form describes the stream composition of both retentate and permeate for solutes i over the process duration for a given diafiltration, be it constant or variable volume dilution (for diluent with or without solutes). Since the example in this case was operated with constant volume addition of solute free diluent, eq. 3-31 can be further integrated considering the relationship $u(t) = q(t)$ (i.e. diluent flow rate is equal to permeate flow rate) to give an exact analytical solution.

$$\int_{c_{f,i}(0)}^{c_{f,i}(t)} \frac{1}{c_{f,i}(t)} dc_{f,i}(t) = \int_{0}^{t} \frac{[q(t)R_{app,i}(t) - q(t)]}{V_f(t)} dt \quad \Rightarrow$$

$$c_{f,i}(t) = c_{f,i}(0) e^{\frac{q(t)[R_{app,i}(t)-1]}{V_f(t)}} \tag{6-1}$$

Using eq. 6-1 and with expressions for time and concentration dependant rejection coefficients, time-course composition of the retentate stream could be calculated for a given solute i. After this, utilisation of calculated rejection coefficients allowed concentration of the solute in the permeate stream ($c_{p,i}(t)$) to be defined. Concentration of total residual solids in both feed and retentate was calculated by subtraction of the total polyphenols concentration from the total solids concentration as follows:

$$c_{f,TRS}(t) = c_{f,TS}(t) - c_{f,TP}(t) \tag{6-2}$$

$$c_{p,TRS}(t) = c_{p,TS}(t) - c_{p,TP}(t) \tag{6-3}$$

The separation factor (α) was again used to quantify the degree of separation occurring at a given instance by use of mass fractions for the respective streams. The parameter in this case shows the degree of separation of total polyphenols from total residual solids along the process duration.

7.3 Results and discussion

7.3.1 Diafiltration flux

Data for diafiltration fluxes of PS25 and PS50 is shown in Figure 7-1 complete with data fits for pore blocking mechanisms for the two values of n which fitted best according to the r^2 value. PS25 exhibited the lowest fluxes during operation, the steady value being 6.9 ± 0.2 $Lm^{-2}hr^{-1}$ at 1.0 bar TMP for the untreated membrane. There was a lower but statistically insignificant change to 6.8 ± 0.2 $Lm^{-2}hr^{-1}$ for the 50% ethanol treated membrane. PS50 gave an untreated and treated steady state flux of 19.5 ± 0.3 $Lm^{-2}hr^{-1}$ and 25.2 ± 0.5 $Lm^{-2}hr^{-1}$ respectively.

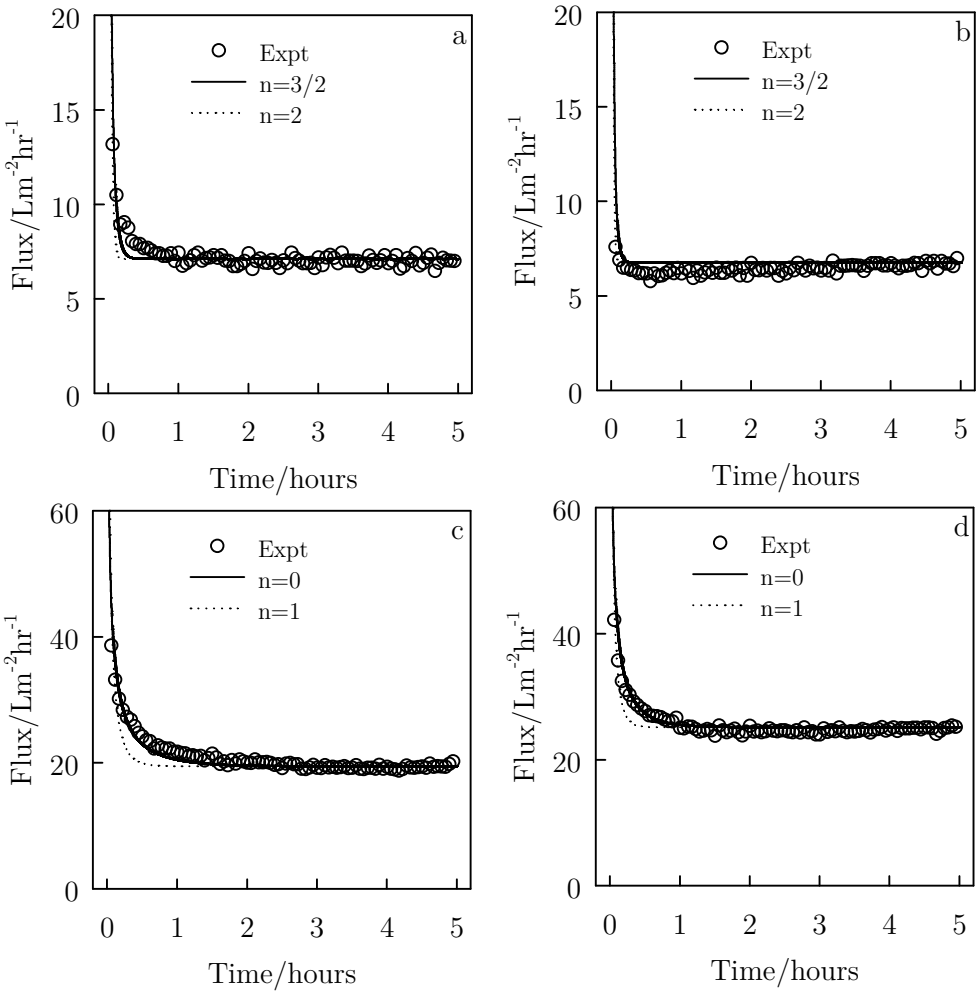

Figure 7-1 - Operating flux and blocking mechanism data fits for diafiltration experiments at 1.0 bar (a) PS25 untreated, (b) PS25 ethanol treated (c) PS50 untreated and (d) PS50 treated

When observing the model fits in Figure 7-1 it is shown that the most suitable mechanism for pore blocking description (best fit according to r^2) for the PS25 membrane comes from when either $n = 3/2$ or $n = 2$ (intermediate and complete pore blocking models respectively). This suggests that both in-pore fouling and flow restriction due to macrosolute accumulating at the pore aperture is occurring. Occurrence of these mechanisms is unlikely exclusive and it would generally be assumed, based on the evidence for tea filtration in this and other sections of this thesis, that filtration reduces to a cake dominated mechanism, especially given the relatively high concentration of feed and absence of a feed pre-treatment stage.

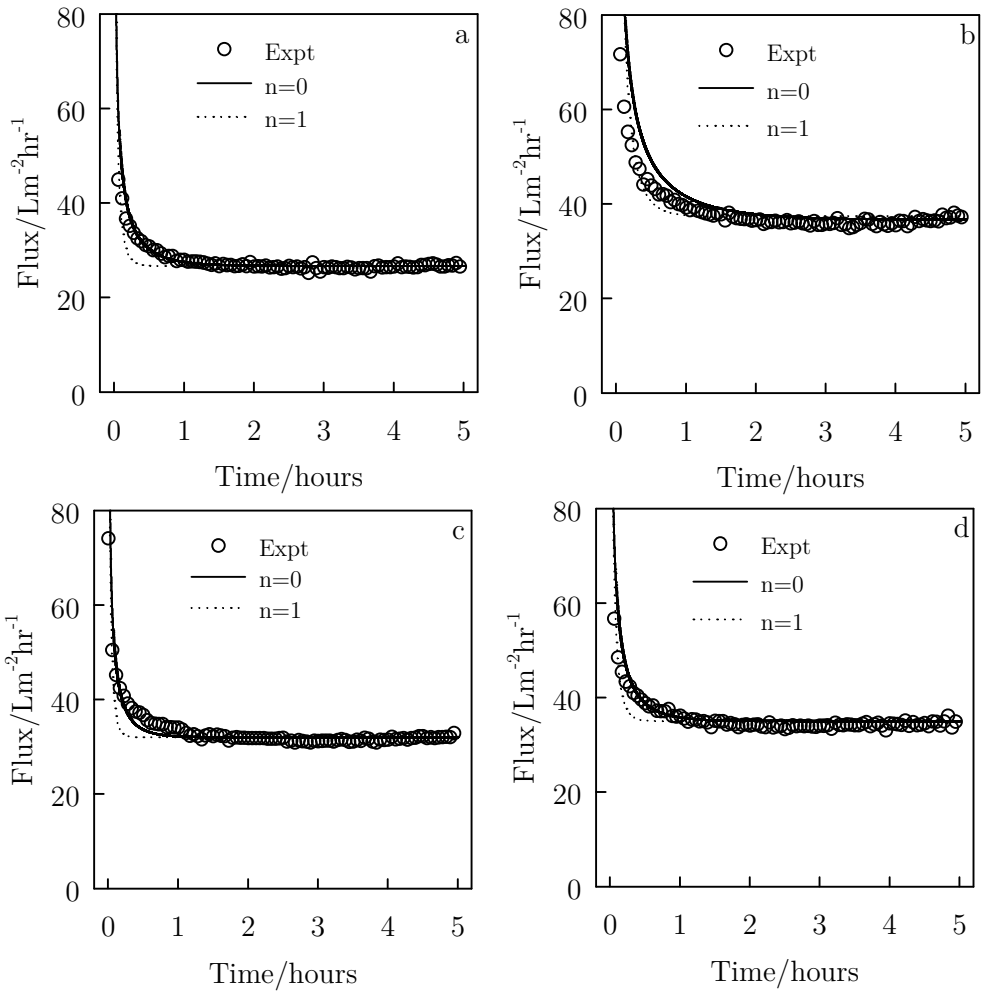

Figure 7-2 - Operating flux and blocking mechanism data fits for diafiltration experiments at 1.0 bar (a) PS100 untreated, (b) PS100 ethanol treated (c) FP100 untreated and (d) FP100 treated

For PS100 (Figure 7-2), the untreated membrane showed a flux of 26.6 ± 0.3 $Lm^{-2}hr^{-1}$. FP100 showed a much greater flux, 32.0 ± 0.3 $Lm^{-2}hr^{-1}$. Differences in flux for similarly specified membranes (in terms of hydrophilicity) were noted by Evans *et al.* (2008) [28] when comparing regenerated cellulose and fluoropolymer membrane. For PS100 there was an uplift after treatment to 37.4 ± 0.5 $Lm^{-2}hr^{-1}$, this resembling a 40% improvement in flux, whereas the FP membrane only showed a 9% rise to 35.0 ± 0.7 $Lm^{-2}hr^{-1}$.

The results confirm that the permeability increases observed are again being converted into the filtration environment as was the case during pressure ramping experiments in Chapter 6, especially for the larger pore size PS membranes. The occurrence of fouling (both cake and pore blocking/plugging) means the relative change observed in terms of pure water permeability cannot entirely be converted to the filtration environment although, given this increased permeability, though the convective transport of solutes through the membrane is in the most part increased, with the only exception being for the PS25 membrane.

7.3.2 Rejection of solutes

Measurement of stream concentrations allowed calculation of rejection coefficients using eq. 3-10. These are displayed in Figure 7-3. In all cases the rejection of total polyphenols was substantially higher than for total residual solids. PS25 (Figure 7-3a) and PS100 (Figure 7-3c) showed the largest discrepancy in these terms and in accordance with previous pressure ramping experiments.

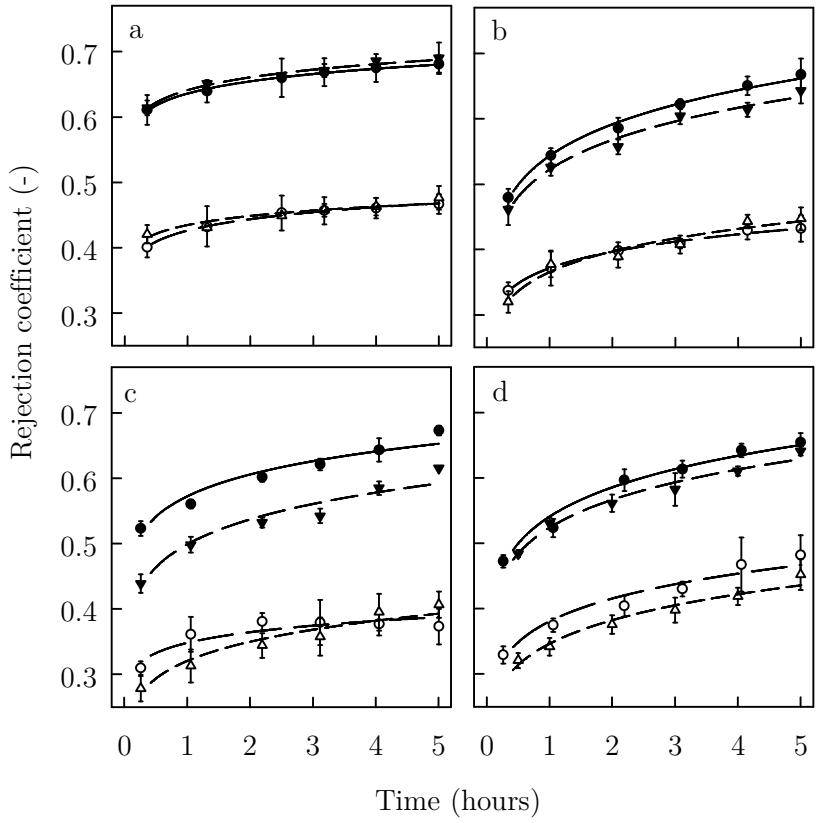

Figure 7-3 - Rejection coefficients for untreated membranes with fitted power law curve for data for (a) PS25, (b) PS50, (c) PS100 and (d) FP100 (filled symbols are for polyphenols, hollow for residual solids, triangles for untreated membranes and circles for treated membranes)

The net charge of the membrane plays a critical role in the transmission of solutes, especially for more strongly charged species. In summary, it is the repulsive mechanism of the negatively charged membrane from the negatively charged phenolate ions which causes high rejection of these species.

Rejection coefficients (both for *TRS* and *TP*) were fitted by a power law approximation of the form: $R_{app} = at^b$ where a and b are non-phenomenological coefficients derived purely for fitting purposes. The fitting of the data in this manner allowed a continuous rejection profile with time to be approximated for both groups of solutes. The advantage of this method over calculations using direct experimental data is that concentration profiles can be corrected to a reference concentration eliminating inter-experimental variability. As was previously the case, the reference concentration was 1.0 wt.% and total polyphenols were

adjudged to account for 26% of this. The fit parameters and determination coefficients are displayed in Table 7-1 noting that all r^2 values exceed 0.94.

Table 7-1 - Fit parameters for rejection coefficient vs. time (*treated membrane)

Membrane	*Total polyphenols*			*Total residual solids*		
	a	*b*	r^2	*a*	*b*	r^2
PS25	0.4518	0.0418	0.9943	0.2647	0.0582	0.9942
PS25*	0.4498	0.0433	0.9757	0.3393	0.0445	0.9444
PS50	0.1999	0.1221	0.9947	0.1729	0.0935	0.9955
PS50*	0.1962	0.1196	0.9859	0.1526	0.1197	0.9789
PS100	0.2934	0.0816	0.9459	0.2253	0.0721	0.9751
PS100*	0.2090	0.1063	0.9492	0.1380	0.1194	0.9471
FP100	0.2116	0.1146	0.9740	0.1547	0.1226	0.9658
FP100*	0.2073	0.1132	0.9802	0.1327	0.1324	0.9746

7.3.3 Polyphenols accumulation in retentate

Figure 7-4a and 6-4b show the disproportionally higher rejection of polyphenols to total residual solids transmission with respect to total filtered volume. There is a definite enrichment in the retained stream.

Progression of diafiltration is considered here as the overall dilution of recycled feed. This implies that high flux membranes allow greater progression. Separation efficiency is defined as there being a larger difference between polyphenols rejection coefficient and total residual solids (higher separation factor).

For FP100 therefore, where separation factor is generally lowest and progression is high, moderate enrichment of the retentate stream can occur with a good yield, though would be improved if polyphenols rejection was greater; something which ethanol treatment worsens. For untreated PS100 membranes, this rejection is greater than for FP100, so despite allowing theoretically faster enrichment, the lower flux results in a lower yield (progression). When the PS100 membrane is ethanol treated, the additional flux allows for greater progression of operation, though the reduction in efficiency means that only a marginal improvement in tea quality is observed. For the PS25 and PS50 membranes, which offer the best separation efficiency, a faster rate of retentate polyphenols accumulation is observed although inferior fluxes mean the yields are poor. The effect of ethanol treated on the overall outcome of the operation is less so than for the larger pore size membranes.

In conclusion, for retention and enrichment of polyphenols it is beneficial to use a tighter pore size membrane though this is at the expense of throughput. Using a larger pore size allow for better recovery of tea in the permeate and faster accumulation of polyphenols in the retentate. Ethanol treatment is sufficient in allowing more polyphenols to transmit meaning that if the permeate stream is the overall target, treatment of membranes would be recommended. If retentate enrichment is favoured, utilising untreated membranes would be the preferred operating strategy.

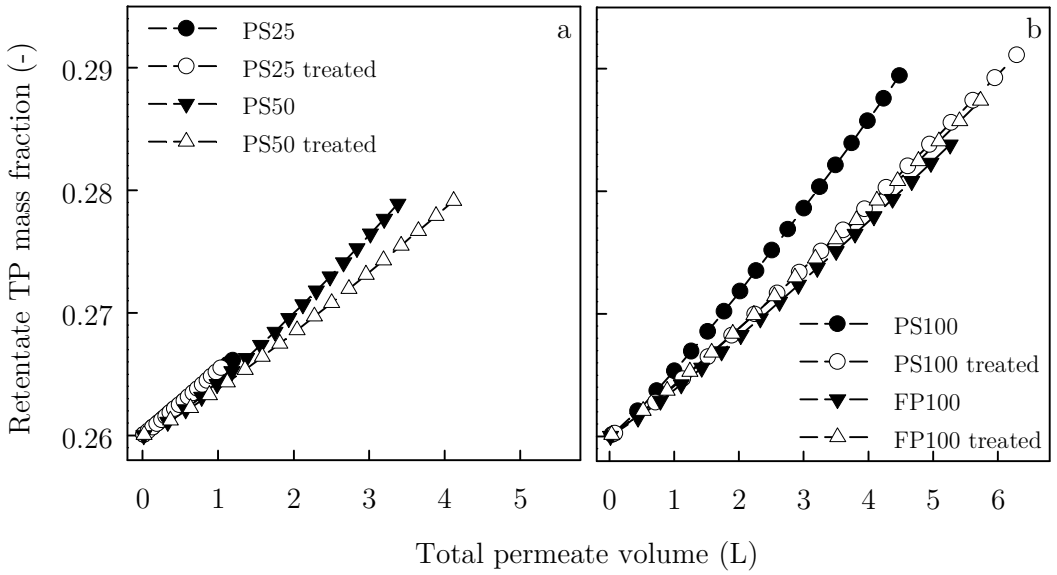

Figure 7-4 - Polyphenols accumulation in the retentate stream as a function of volume filtered for (a) PS25 and PS50, both virgin and treated, and (b) PS100 and FP100, both virgin and treated

Astill *et al.* (2001) [227] reported that black tea total polyphenols ranged from 7.3 to 21.9 %. Balentine *et al.* (1997) [316] said there are 23% polyphenols, of which 3% were 'simple' polyphenols and 12% flavonols, theaflavins and catechins (though some overlap is highly likely). The increase in polyphenols in the retentate (a 12% rise) is thus a major improvement in the quality of the tea in this stream. The application of diafiltration to both maximise yield and utilise the waste stream shows promise for being a viable processing option.

7.3.4 Analysis of separation factor

Figure 7-5 shows the calculated separation factors for the membranes as a function of retentate concentration. Both PS25 (treated and untreated, Figure 7-5a) exhibit similar profiles and show that the feed concentration after 5 hours has only been diluted to a small degree (from 1.0 wt.% to *ca.* 0.94 wt.%). Even though the diafiltration shows minimal progression, the rate of change of the separation factor is significant. This indicates that the rejection of polyphenols is strongly dependant on the foulant build-up over time and less so due to progressive dilution of the feed. This is a key finding as it aids the design and scheduling of an operation. If the foulant build-up is a dominating factor in the polyphenol stripping effect occurring during black tea UF, then the recommendation of operability should be designed towards:

- biasing the operation in favour of filtering over shorter durations by utilising smaller batches and having more frequent membrane regeneration (CIP)
- increasing the membrane area to total feed volume ratio so as to disperse the fouling build-up, thereby remediating the potential losses of polyphenols due to fouling.

Both options would have associated consequences, such as reducing time spent for production, requiring more chemicals spent for CIP and adding to capital expenditure on plant equipment to maximise filtration area.

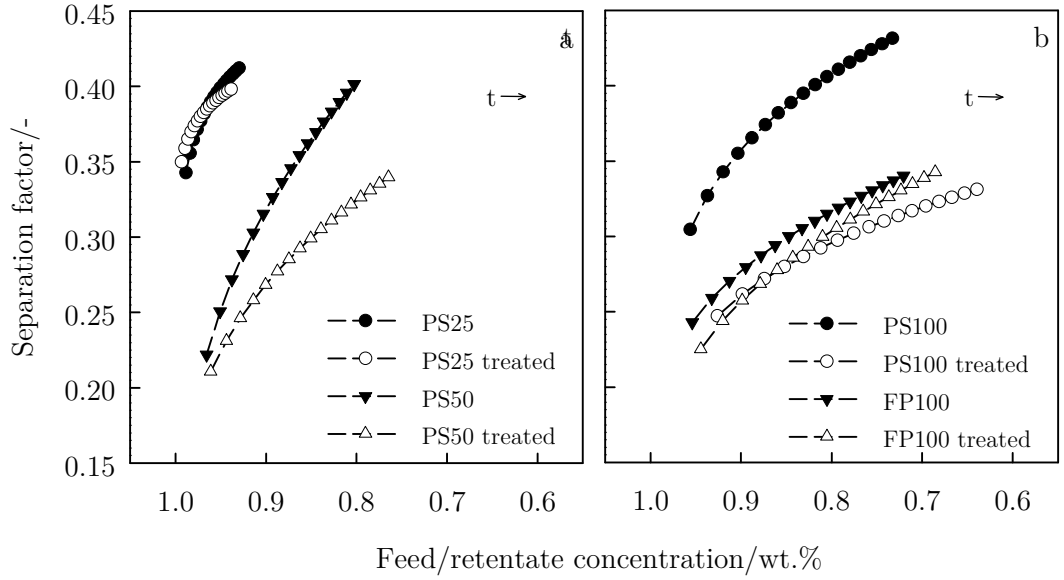

Figure 7-5 - Separation factor for diafiltration experiments as a function of retentate concentration for (a) PS25 and PS50, both virgin and treated, and (b) PS100 and FP100, both virgin and treated

For PS50 (Figure 7-5a) and PS100 (Figure 7-5b) the effects of ethanol pre-treatment are again evident. FP100 shows an insignificant change with ethanol treatment. For PS50 and PS100, the rate of change of separation factor is lower following treatment, meaning that a more consistent permeate is produced in terms of the ratio between polyphenolic and non-polyphenolic species. Ideally for this process, a separation factor of zero would be desirable (or ideally less than 0). This would mean that compositionally speaking, the permeate stream would be the same as the feed stock, or that there is preferential transmission of polyphenols. In conclusion, ethanol treatment shows a positive effect on remediating the fractionation occurring as a result of membrane filtration for PS50 and PS100 membranes.

7.3.5 Tea solids and polyphenolics yield

Figure 7-6 describes the system in terms of total mass processed. For diafiltration, where permeate in the target stream, the objective is to recover as many solids as possible in the permeate stream whilst maintaining the ratio of polyphenols to residual solids present in the feed. Therefore quantifying the performance in overall process yield is a useful comparison to make.

For both solute groups it is shown, as rejection coefficients implied, that the rate of transmission is slowing. These profiles are likely to move into a steady state region if there is a plateau in rejection coefficients. Caution should be taken however in extrapolating

data beyond the experimental duration given that earlier flux charts indicated a flux increase in the latter stages of the operation.

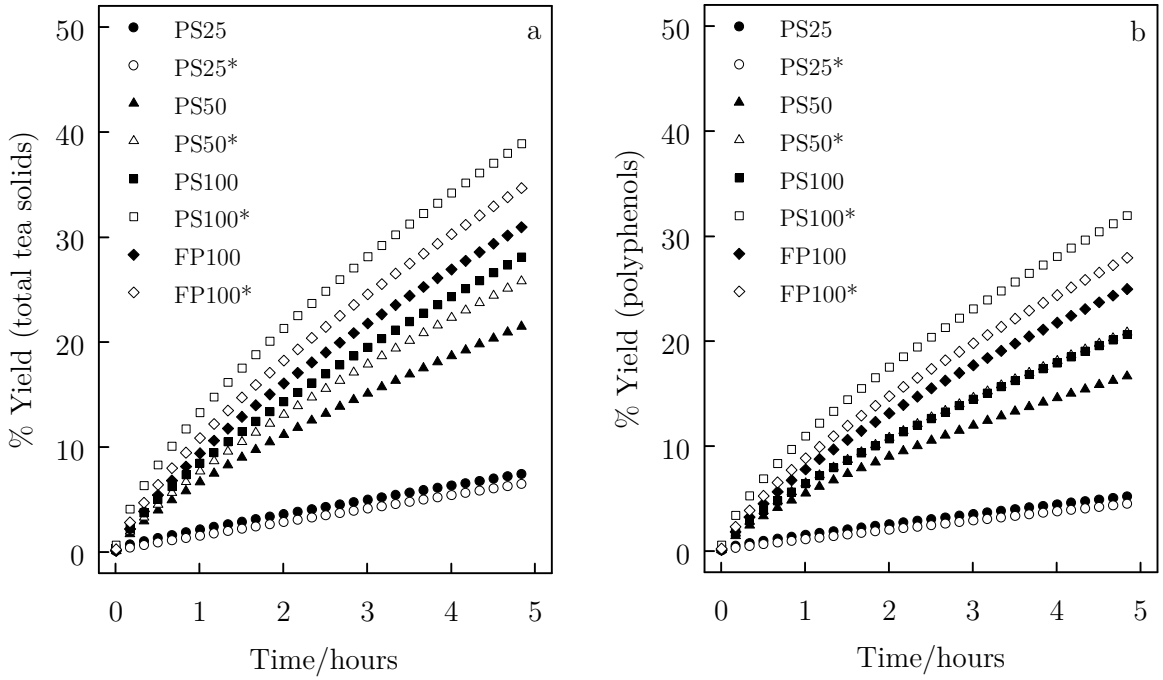

Figure 7-6 - Yields of solutes during 5 hours diafiltration, (a) total solids, and (b) total polyphenols (* denotes ethanol treated membrane)

Table 7-2 shows final yields of solids and polyphenols. The FP100 shows the best performance before treatment for both solids and polyphenols yield criteria, a 25.4 g tea solids yield (from a possible 80 g) and 5.3 g of polyphenols (from a possible 20.8 g).

Table 7-2 - Absolute yield by mass for components

	Total tea solids yield/g (max. 80 g)		*Total polyphenols yield/g (max. 20.8 g)*	
	Untreated	*Treated*	*Untreated*	*Treated*
PS25	6.1	5.3	1.1	1.0
PS50	17.6	21.2	3.5	4.4
PS100	23.0	31.8	4.4	6.8
FP100	25.4	28.4	5.3	5.9

With a treated membrane the best performance arises from using the treated PS100, again a reflection of both the enhanced flux and lowered rejection coefficients; the solids yield is 31.8 g and the polyphenols yield is 6.8 g.

All of the work described was for 1.0 bar TMP operation. Chapter 6 showed that TMP could also influence rejection coefficients significantly. The next section compares a diafiltration experiment conducted at 3.0 bar TMP with the 1.0 bar case for a virgin PS100 membrane. This membrane was selected for analysis as it gave both industrially viable fluxes and strong definition between total residual solids rejection and total polyphenols rejection.

7.3.6 Effect of TMP on diafiltration

7.3.6.1. Diafiltration flux and volumetric throughput

The marginal increase in flux from 1.0 bar to 3.0 bar shows that PS100 is operating at limiting flux as was show in the previous chapter (see Figure 7-7). For 1.0 bar operation the flux plateaued at 26.6 ± 0.3 $Lm^{-2}hr^{-1}$. For 3.0 bar operation, a flux of 29.7 ± 0.8 $Lm^{-2}hr^{-1}$ was recorded. The constant dilution of the retained stream would mean that the pressure at which limiting flux occurs would gradually increase due to lowered concentration of solutes and thus progressive lowering of CP. This would also more generally explain why fluxes for PS50, PS100 and FP100 are all higher during diafiltration than for previous permeate recycle experiments. The fluxes would indeed be even higher if the effects of fouling were not so pronounced during filtration.

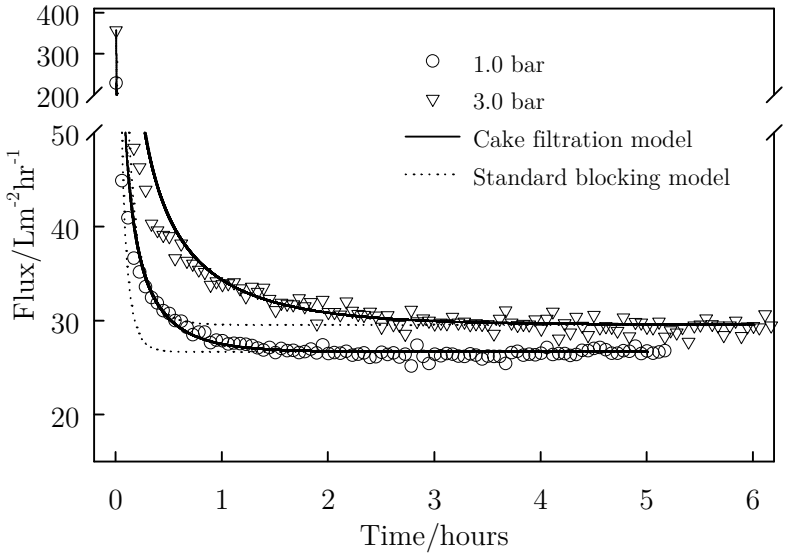

Figure 7-7 - Comparison for 1.0 bar and 3.0 bar TMP diafiltration each with fits for cake filtration and standard pore blocking mechanisms (the two laws describe the data most accurately out of the four blocking mechanisms)

In terms of flux alone, it is assumed to be advantageous to operate at a lower TMP, as the volumetric throughput advantage gained from operating at 3.0 bar over 1.0 bar would not compensate for the additional pumping costs. A full assessment of this assumption cannot be made until mass transfer and energy considerations have been determined.

Fits of the pore blocking power laws show that for both pressures, cake filtration is the dominating fouling mechanism, with determination coefficients of 0.9564 and 0.9573 for 1.0 bar and 3.0 bar respectively, these models fitting best over the standard, intermediate and complete laws by some degree. This suggests that the formation of a secondary layer at the membrane surface is playing a significant role in retarding flux, and is likely to impact on both mass transfer and selectivity.

To contextualise the fluxes measured: at 3.0 bar operation flux was consistently higher than for 1.0 bar, meaning the total specific volume filtered showed a noticeable change; changing from 140.6 ± 3.34 Lm^{-2} at 1.0 bar to 167.8 ± 4.1 Lm^{-2} at 3.0 bar .

7.3.6.2. Rejection coefficients

Stream analysis for this case shows a considerable increase in the proportion of solids and polyphenolics rejected by the membrane with increased TMP (indicated by rejection coefficients in Figure 7-8). The same fitting method for the rejection coefficient profiles was used; parameters are displayed in Table 7-3. Polyphenolics rejection ranged from 0.52 ± 0.01 to 0.67 ± 0.01 at 1.0 bar, and over a range of 0.60 ± 0.02 to 0.74 ± 0.02 at 3.0 bar TMP. This rise was not as significant as was apparent for the solids rejection coefficients over the same diafiltration duration. For 1.0 bar operation the rejection ranged from 0.31 ± 0.01 to 0.37 ± 0.03. For 3.0 bar this rose to a range from 0.42 ± 0.02 to 0.54 ± 0.02. The discrepancy in the spacing between the residual solids rejection coefficient and polyphenols rejection coefficient is lower at any given point during the diafiltration. While from the outset it would appear that a larger proportion of polyphenols can transmit the membrane, the total amount of material transmitting through the membrane is also proportionally less, ensuring a degree of separation comparable with the 1.0 bar case.

Table 7-3 - Fit parameters for rejection coefficient vs. time

PS100	*Total polyphenols*			*Total residual solids*		
membrane	*a*	*b*	r^2	*a*	*b*	r^2
1.0 bar	0.2934	0.0816	0.9459	0.2253	0.0721	0.9751
3.0 bar	0.3316	0.0797	0.9961	0.2196	0.0993	0.9947

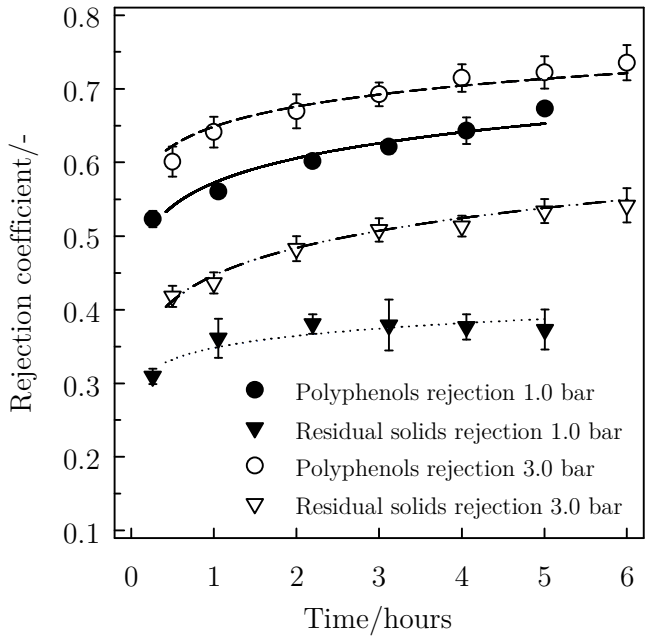

Figure 7-8 - Rejection coefficients for polyphenols and total solids during 1.0 bar and 3.0 bar operation

7.3.6.3. Retentate composition and separation factor

Figure 7-9a shows the rise in polyphenols mass fraction in the retained stream as the diafiltration progresses. The lower discrepancy between the rejection coefficients means the rate of accumulation of polyphenols in the retained stream is less at 3.0 bar than for 1.0 bar filtration. The absolute mass fraction value after 5 hours thus stands marginally lower at 28.7% (for 5.63 L of permeate production) over the 29.1% achieved at 1.0 bar (for 4.73 L of permeate product).

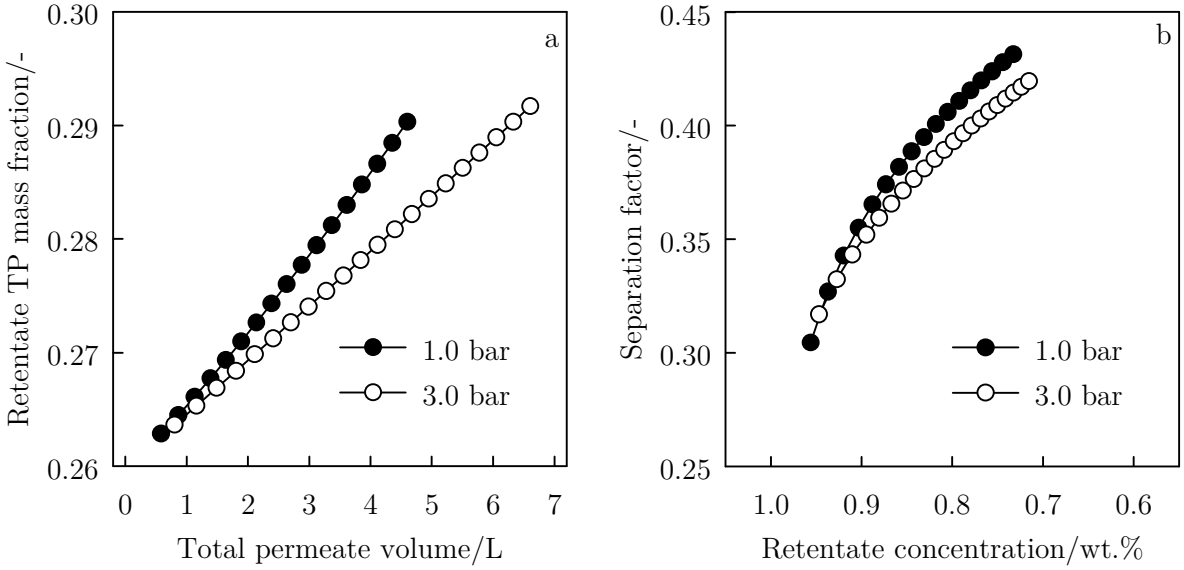

Figure 7-9 - (a) volume filtered vs. retentate polyphenols mass fraction, (b) retentate total solids concentration vs. separation factor

In terms of separation factor (Figure 7-9b) the profiles for both TMPs are similar. This reaffirms the suggestion based on rejection coefficients that there is an insignificant change in the selectivity of the membrane at varied TMP in the range studied. This may not be the case for higher TMP values, as repulsive forces acting between membrane and phenolate ions, fouling layer and phenolate ions, or indeed other factors causing rejection, may be overcome.

7.3.6.4. Yield with TMP variation

The classical trade-off between transmission and flux is demonstrated in Figure 7-10 as was discussed in section 1.4.2. Operating at 3.0 bar gave an increased flux allowing for an increased volumetric throughput of material but at the cost of higher rejection coefficients. When comparing the overall mass yields of solutes, there is an almost identical throughput of material, for both total solids and total polyphenols. This means that it is unquestionable that operating at lower TMP is beneficial, based wholly on the implications relating to energy usage and furthermore, the potentially lower requirement for rinsing and CIP following filtration.

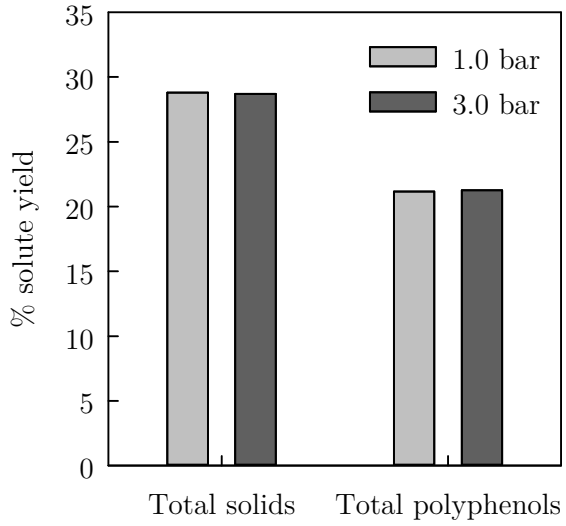

Figure 7-10 - Solute yields for total solids and total polyphenols

Up to this point, no consideration has been made regarding the effect of diafiltration on tea quality, and the effects that ethanol treatment has during this process. The following section focuses on this in an attempt to confirm diafiltration as a valid operational regime.

7.3.7 Appearance of UF diafiltration permeates

7.3.7.1. Lightness and colour

Figure 7-11 shows the lightness (L*) measurements for all membranes. There was a sizeable lightness increase for permeates over the unfiltered tea at comparable concentrations. PS25, as expected, gave the lightest tea permeate and is clearly removing more pigmented molecules than the other membranes when considering that TRs contribute to a darker tea infusion [244].

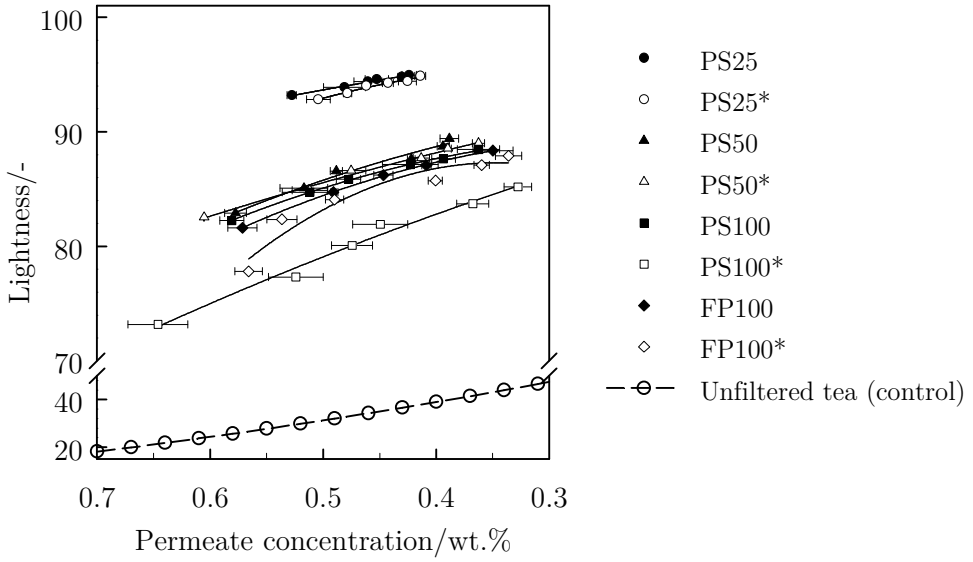

Figure 7-11 - Lightness for diafiltration permeates for all membranes (* denotes ethanol treated membrane) (reverse x-axis indicates progression with time i.e. dilution)

The PS100 membrane following treatment exhibited the darkest filtered tea and is clearly differentiated from the L* profile. This is reinforcing evidence that treatment of the membrane with ethanol had in fact boosted transmission of colour compounds contributing to darkness. Nevertheless, the degree of lightness of the tea, whilst appearing more enticing to the consumer, may be somewhat depleted in terms of flavour. Filtration with ethanol treated membranes goes someway to alleviating this problem.

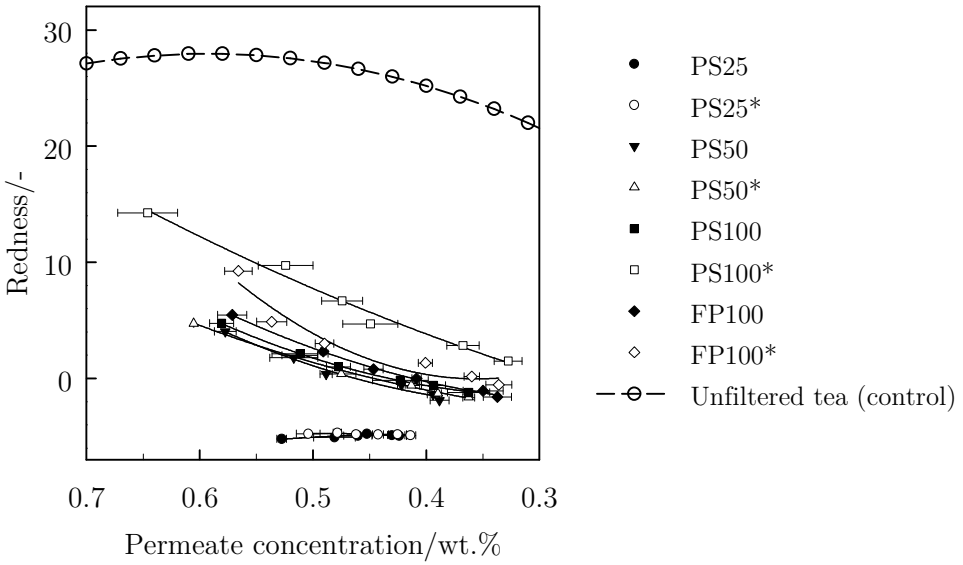

Figure 7-12 - Redness for diafiltration permeates for all membranes (* denotes ethanol treated membrane)

Figure 7-12 shows the redness parameter (a*) measurements. In contrast to the lightness but in full agreement (as lightness can be correlated with decreasing redness), red pigment was being stripped from the tea infusion by the membrane. Redness (like darkness) can be associated with elevated TRs concentration [244]. The FP100 membrane showed the reddest tea for untreated membranes reflecting the better transmission, and more uniform transmission of polyphenols to residual solids. The PS100 shows that when treated, it is able to transmit more red pigmented species for equivalent concentration tea filtered with other membranes.

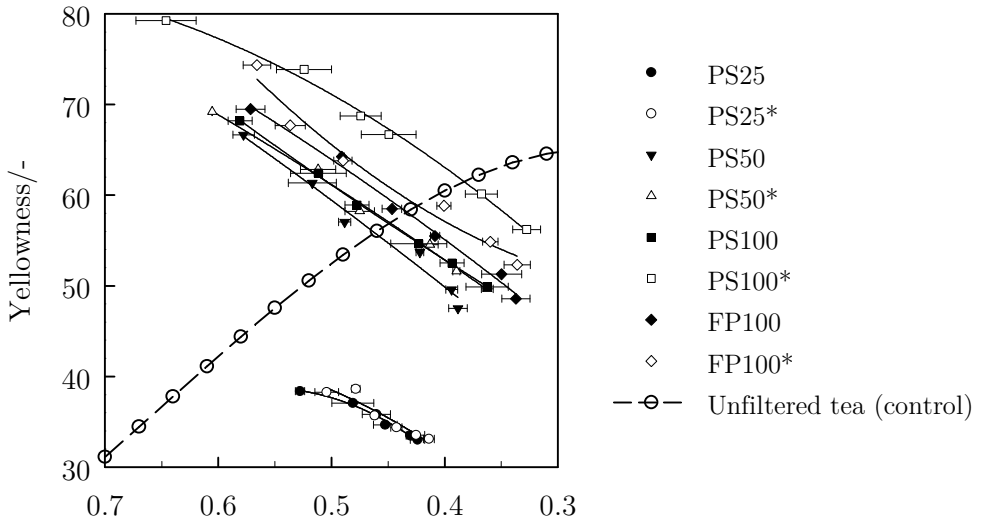

Figure 7-13 - Yellowness for diafiltration permeates for all membranes (* denotes ethanol treated membrane)

According to Liang and Xu (2003) [261], b* is linked to increased concentration in certain TF compounds which, for the four well-defined compounds comprising TF, TF-3-G, TF-3'-G and TF-3-3'-DG, have molecular masses ranging between 564 and 868 $gmol^{-1}$ [317].

The yellowness (b*) (Figure 7-13) shows perhaps the most striking trends. The PS25 membrane shows a loss in yellowness throughout the whole diafiltration. For all other membranes however, there is a gain in b* over unfiltered tea for the majority of the process. With decreasing permeate concentration and in contrast to the unfiltered tea, permeates show an increase in b*, even when the permeates have been shown to be increasing in lightness. At some point during the diafiltration the b* values become lower than that of the unfiltered tea. The rate at which this occurs is high, and similar for all membranes, excluding PS25.

As was shown for the PS25, the separation factor showed a substantial rate of change across the duration of filtration, and indeed the yellowness for PS25 shows a stronger rate of change than a* data showed. From this information a number of inferences can be made.

The first is that as already mentioned, fouling causes a decrease polyphenols transmission. At first, it is likely that this is due to the red species being retained by the membrane. Wu and Bird (2007) [33] showed that the presence of TRs had a negative impact on the transmission of TFs for a 30 kDa PS membrane. Results here indicate the same effect. Another point to consider is that for the larger pore size membranes, the redness transmission starts to diminish over the experimental duration (although to what degree relative to the unfiltered tea it is hard to tell). It would be assumed that if the yellow species are being rejected more substantially at the end of the filtration more so than the beginning, then so are the red pigments (TRs) to an equal or greater degree.

It was shown in Figure 7-1 and Figure 7-2 that the dominant mechanism of fouling is the formation of a cake, at least after the substantial flux decline during the first 5 – 20 minutes of filtration. This would mean the deposition and aggregation of tea solutes at the membrane surface is substantial. This would in-effect form a tea-cream phase due to the excessive concentration i.e. a supersaturated solution creates an insolubilised zone. This would have the effect of even greater increased solute rejectio, and could be initiated by TR aggregation in the early stages of filtration by observation that there is constant a* and decreasing b* for PS25. For larger pore sizes, more red species (and aggregates thereof) would transmit to begin with though the same effect eventually ensues. This is not dissimilar to the mechanism of humic acid fouling, as described by Yuan and Zydney (1999) [318], who suggest that aggregation of these polyphenol substances is formed by intermolecular hydrophobic interactions; the chemistry of humic acids being alike to the structure of complex TRs given the in-common occurrence of phenol, catechol and quinone groups.

7.3.7.2. Turbidity

Figure 7-14 shows the haze of permeates for (a) untreated and (b) treated membranes. There is no defining trend observable from the data although it would seem that the PS25 membrane gives the best overall haze reduction, as the measures and errors were, on the whole, lower. This further indicates that removal of the red and yellow species is a necessary consequence of highly efficient haze removal and that exclusion using small pore sizes to retard the formation of aggregates is required for turbidity free RTD teas.

The maximum haze value occurred arbitrarily at 1.99 ± 0.51 NTU for the FP100 membrane after 3.2 hours. Despite this arbitrary point, globally speaking, all data shows excellent haze removal over the unfiltered raw feed stock.

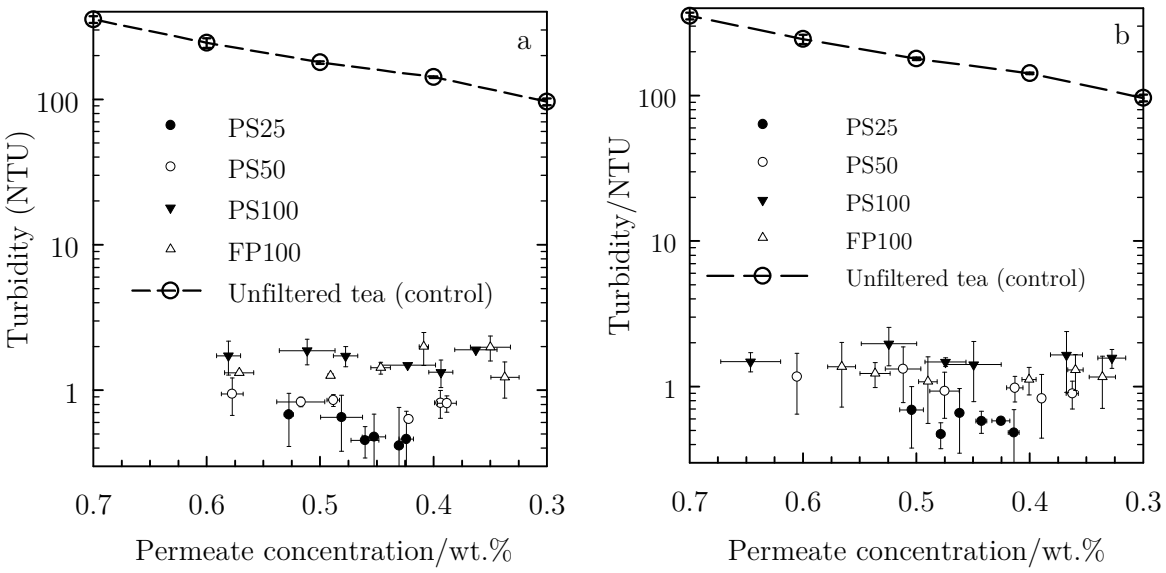

Figure 7-14 - Turbidity of permeates and unfiltered turbidity profile with respect to total solids concentration for a) untreated, and b) - treated membranes

7.3.8 Conclusions

Constant volume diafiltration was carried out as a progression of prior observations concerning the disproportional transmission of polyphenols to all other tea solids through UF membranes. It has been shown that there is a progressive enrichment of polyphenols (in terms of mass fraction) in the retained stream of the process, although at ever decreasing concentration. This arises through the difference in rejection coefficients which occurs especially for PS membranes. It is shown that the influence of fouling on the membranes plays an integral role in limiting the transmission of polyphenolic species into the permeate. This is likely to start through a repulsive mechanism; however due to the inclination of species to accumulate at the membrane surface and form a cake layer, as shown by power-law fits for pore blocking mechanisms, the additional aggregation and build-up of foulant, which at first limits the transit of TRs through the membrane, exacerbates the transmission of the smaller TF molecules in the later stages of filtration. This is further worsened by concentration polarisation effects of small molecules which have higher diffusion coefficients. It is shown that the permeate product gained across the duration of the experiment is below 2.0 NTU for all experimental cases meaning highly efficient haze removal. The smallest cut-off (PS25 membrane) indicating that the haze removal may be strongly dependant on removal of species that are darker and redder.

Alcohol treatment was shown to be beneficial when applied to PS membranes with pores that are considered to be at the upper end of the UF classification (50 kDa and 100 kDa). The positive permeability responses are converted to the filtration environment i.e. improved fluxes are observed in most cases. This has positive effects upon both the total solids and polyphenols yields given both the greater convective mass transport (due to increased fluxes and thus increased solute flux) and the lowered rejection of polyphenols compared to all other constituents. In summary the effects of ethanol pre-treatment for PS50 and PS100 membranes (and marginally for FP100) improves the product yield when conducting UF of black tea.

8. Ethanol pre-treated membranes: Black tea liquor filtration over multiple cycles

8.1 Introduction

Multiple fouling and cleaning of membranes is an often overlooked yet fundamentally important area of research, be it for membrane materials, modification to membranes or applications of membrane processes involving new feeds or operating regimes.

For membrane systems, the performance of a cleaning protocol, and thus the benchmark for the chemical engineer is normally defined by the ability of the regime to return the membrane to its condition as new, in terms of permeability. This is typically specified as a percentage flux recovery [268]. There are three main strategies for reducing the impact of fouling, and the associated flux losses, aside from optimisation of operating conditions as indicated by Field *et al.* (1995) [117]:

1. Hydrodynamic changes: this can influence foulant build-up by subjecting the membrane surface to various flow regime changes.
2. Optimisation of cleaning thermo-hydraulics, detergent concentration and cleaning frequency. This minimises plant downtime in so maximising productivity [268].
3. Pre-treatment: this can be applied directly to the membrane or to the feed solution in order to influence solute-membrane interactions.

As has been the theme of previous sections, this section focuses on pre-treatment of the membrane using alcohol solutions. The criteria of maximum regeneration of the virgin PWF was been adopted here, which enabled quantification of the effects of alcohol treatment over multiple cycles by using a standard fouling and cleaning protocol.

The way in which membranes age, as a result of repetitive fouling and cleaning, can influence membrane behaviour, due to changes in surface chemistry. Property modifications such as hydrophobicity change and charge alteration are commonly known to influence fouling propensity both on membrane surfaces and inside pores. This was of particular relevance during the UF of tea for Evans *et al.* (2008) [28] who showed that FP membranes fouled by tea inherited the negative charge associated with tea constituents, before cleaning retuned them to a lower magnitude of charge. That charge however was between that of the virgin membrane and fouled membrane. This was particularly apparent for 10 kDa and 30 kDa FP membranes and noticeable to a degree for 100 kDa FP membranes. In a separate study, the progressive hydrophilisation of an FP 30 kDa membrane was shown after repetitive fouling and cleaning cycles, shown by a reduction in contact angle from 65° to

52° after 23 consecutive foul/clean cycles [25]. This study showed the action of fouling with tea and cleaning with NaOH could result in modification of membranes from a moderate hydrophilic state when pristine, to a more hydrophilic state. Also contained within the aforementioned studies were details of how membrane material significantly influences the UF of black tea.

By testing membranes this section aims to show that:

- Membranes are modified substantially by repetitive fouling and cleaning cycles using black tea as the foulant and NaOH as a cleaning agent.
- There is a synergy between the surface chemistry aspects of the membrane and the resulting tea permeate product when subjected to multiple foul-clean cycles.
- The influence of surface chemistry and water permeability brought about by alcohol treatment of PS membranes as detailed in Chapter 5 is observed through membrane performance over multiple cycles.

8.2 Experimental design

A 3^3 experimental design was employed in order to test the effects of ethanol concentration for 3 different PS membranes of varying specification (see Table 8-1). Due to limiting flux studies performed for a range of pressures and concentrations (as detailed in 6.3.2), the PS25 membrane was excluded given the low recorded fluxes and high solids rejection coefficients. In order to test 3 membranes, the MFG1 was used as an alternative; bridging the gap between UF and MF processes. This membrane was introduced comparatively late in the study and was hence less well characterised than other membranes. In terms of characterisation completed, it was generally comparable to the PS100 in terms of pore size distribution and hydrophilicity, wetting properties with ethanol, as well as water permeability.

Table 8-1 -Experimental program for black tea filtration over multiple cycles

Treatment type	*Membrane type*		
	PS50	*PS100*	*MFG1*
No treatment	4 × foul, 4 × clean	5 × foul, 5 × clean	4 × foul, 4 × clean
50 wt.% ethanol treatment	4 × foul, 4 × clean	5 × foul, 5 × clean	4 × foul, 4 × clean
100 wt.% ethanol treatment	4 × foul, 4 × clean	5 × foul, 5 × clean	4 × foul, 4 × clean

Membranes were assessed for their performance in terms of virgin water permeability and tea filtration fluxes over 60 minutes, with 0.5 wt.% tea. A 0.5 wt.% feed concentration was selected so as to maximise the definition between untreated and treated membranes. Total solids, total polyphenols, colour and haze of permeates were measured at the 15, 30, 45 and 60 minute points during filtration. A standard rinsing and cleaning protocol was employed (15 minutes rinse at room temperature followed by 10 minutes cleaning with 0.5 wt.% NaOH at 60°C). Relevant resistances were measured via PWF measurements between fouling and cleaning events. This also enabled quantification of the cleaning efficiency. Membrane hydrophobicity and charge was measured after 4 × foul and 4 × clean cycles

(4F4C) (or 5F5C for PS100), complementing values measured for virgin membranes (V) after hot water conditioning, after 1F, and after 1F1C.

8.3 Results and discussion

8.3.1 Filtration performance

8.3.1.1. Pure water permeability

As has been shown in previous chapters, increases in relative PWF of all membranes following ethanol treatment have again been noted. Figure 8-1 shows the relative increases for membranes specific to this section. For PS50, 50 wt.% and 100 wt.% ethanol treatment yielded respective relative flux increases of 1.32 ± 0.01 and 2.32 ± 0.04. For PS100, these treatments gave increases of 3.75 ± 0.11 and 3.84 ± 0.06; representing the most pronounced increases, and in agreement with previously presented results. MFG1 gave a larger increase over for PS50 membrane for 50% ethanol treatment (2.09 ± 0.04) but the lowest overall relative flux increase for all membrane when treated with 100% ethanol (2.13 ± 0.03).

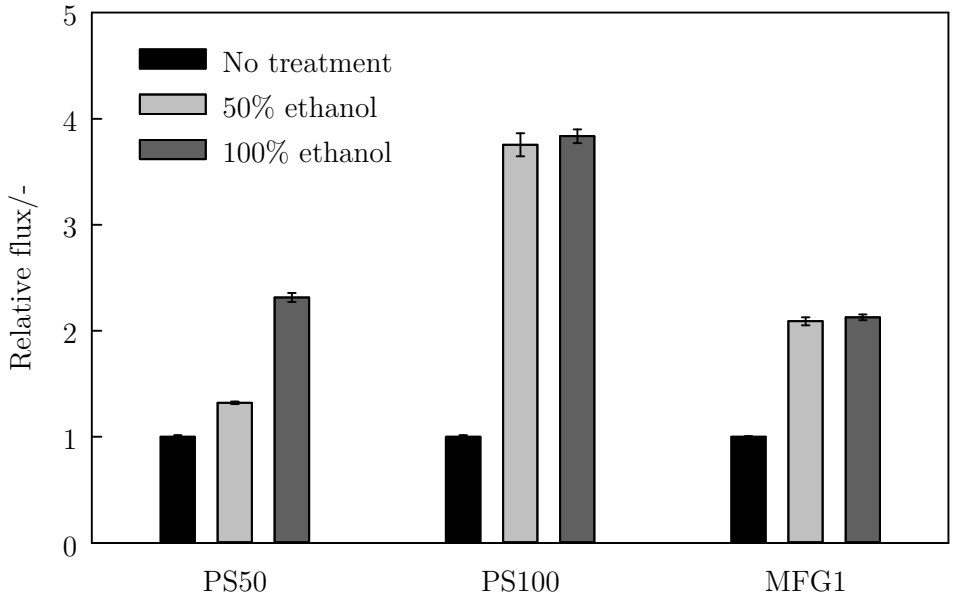

Figure 8-1 - Relative PWF for membranes with differing treatment

The smaller discrepancy of the larger cut-off membranes between 50 wt.% and 100 wt.% ethanol is again shown here, in contrast to the greater flux increase observed between comparable treatments for the PS50 membrane.

8.3.1.2. Filtration flux

The advantage of using ethanol treatment as a strategy to improve membrane filtration operation is again seen. Figure 8-2 shows the filtration fluxes for the PS50 membrane with varied treatment type. As was true for the PWFs measured, generally the greatest improvement in flux was observed when comparing the 50 wt.% ethanol to the 100 wt.% ethanol experiments over the discrepancy between 0 wt.% and 50 wt.% ethanol. For the untreated PS50, the first relative fouling flux was 0.255 ± 0.010 and rose to 0.304 ± 0.011

after 4F3C. Whilst this membrane and treatment scenario showed increases, the 100% ethanol case showed a drop off through the same operational scheme, a fall from 0.455 ± 0.016 to 0.380 ± 0.13. If these fluxes are quantified in terms of a percentage improvement, the 50 wt.% ethanol treatment gave a 21% improvement during 1F and fell to a 6% flux improvement after 4F3C. For the 100 wt.% ethanol treated PS50, the initial improvement was a 79% gain which fell to a 25% enhancement after 4F3C. Generally, ethanol treatment made a prolonged improvement to the filtration flux over 4F3C cycles. Whilst the effect of 50 wt.% ethanol treatment diminished to similar values shown by the untreated membrane, the 100% ethanol treated PS50 continued to offer much greater flux gains, although the effect was lessened with each foul-clean cycle.

The initial flux improvement can be regarded as a hugely significant result but the steep drop in the advantage gained by ethanol treatment over these multiple foul-clean experiments is less promising.

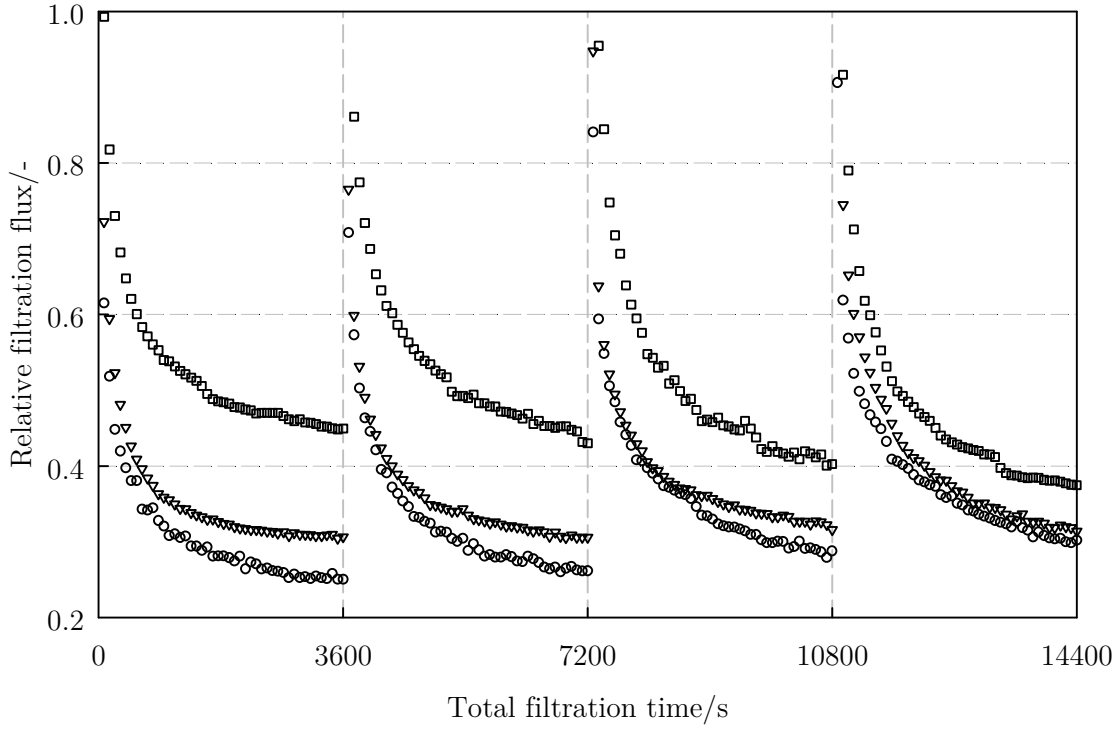

Figure 8-2 - Filtration fluxes over 4 cycles for PS50, ○ - untreated membrane, ∇ - 50% ethanol treated, □ - 100% ethanol treated

Figure 8-3 shows the data collected for the PS100 membrane subjected to the same treatments and protocol. The less significant flux improvement compared to the PS50 data is immediately obvious. The same trends still emerge in terms of the ethanol treated membranes showing depleted performance over consecutive cycles, whereas the untreated membrane offered minimal improvements. It is also apparent is that the fouling data mirrors the PWF results. For PS50 it was seen that the largest improvement in flux was apparent between treatments with 50% ethanol and 100% ethanol, for PS100, the effect of

50% ethanol was shown to have the largest effect on flux improvement, whereas 100% ethanol did not show a distinct improvement.

Figure 8-4 shows the result for the MFG1 membrane. This membrane repeats the performance of the PS100 membrane, although the flux gains are less significant, again reflecting the PWF data. The absolute relative flux change is also in agreement with the PWF data, given the effect of ethanol upon the MFG1 membrane was less apparent than for the PS100.

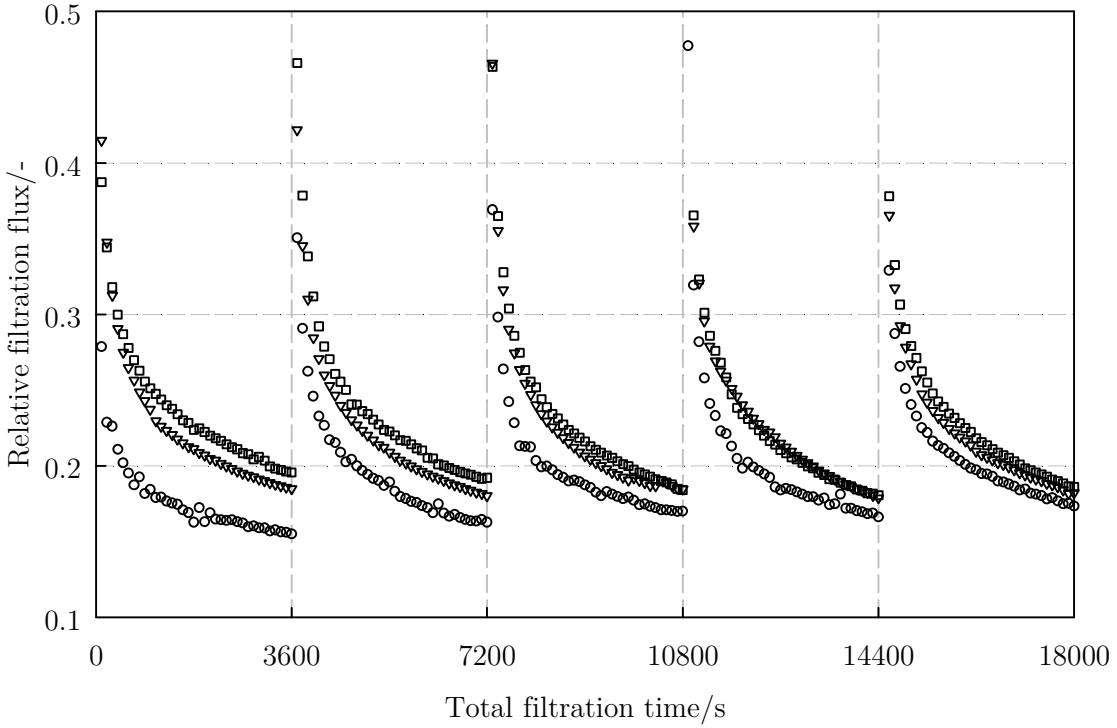

Figure 8-3 - Filtration fluxes over 4 cycles for PS100, ○ - untreated membrane, ∇ - 50% ethanol treated, □ - 100% ethanol treated

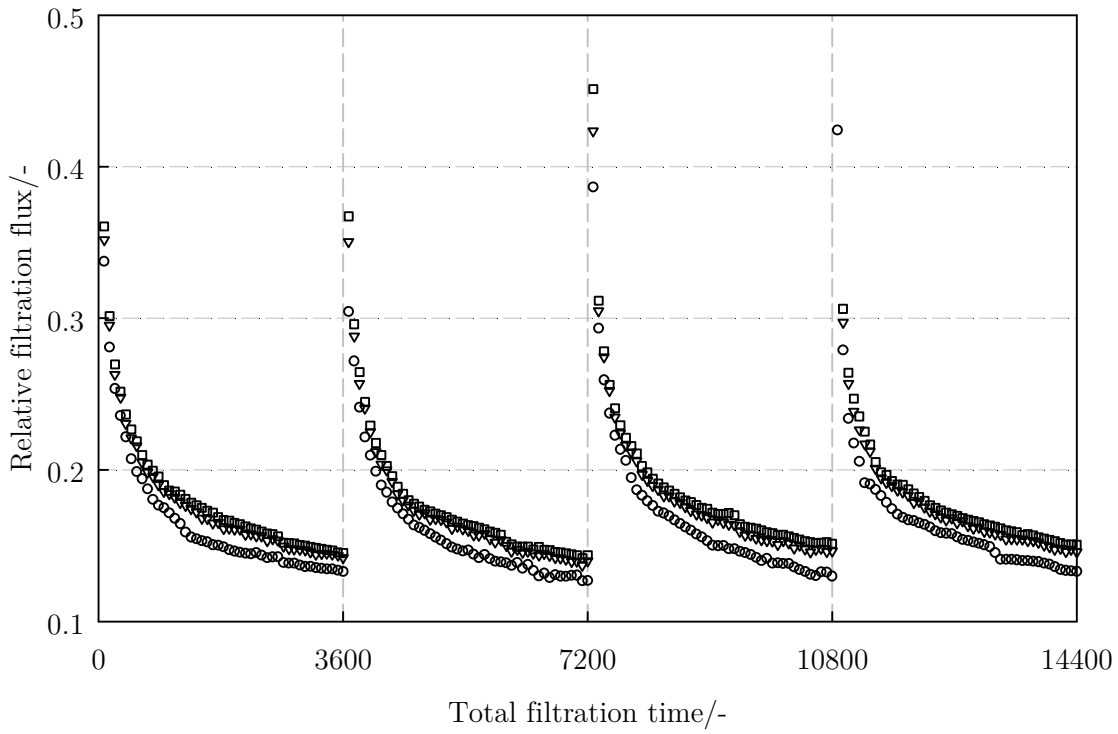

Figure 8-4 - Filtration fluxes over 4 cycles for MFG1, ○ - untreated membrane, ∇ - 50% ethanol treated, □ - 100% ethanol treated

The occurrence of a surface cake layer and effects such as CP during 1.0 wt.% tea filtration was shown to restrict fluxes to a limiting value when filtering at around 2.0 bar TMP, though little variation was seen when operating in the range above 1.0 bar (Chapter 6). It was expected that a reduction in feed concentration would enable amplification of the ethanol treatment's effects. Reducing the feed concentration used for these experiments would raise the limiting flux to higher values for a given TMP as fouling and CP would be reduced. This would mean that the operating regime would be firmly shifted to within the pressure dependant region (i.e. when flux is linearly correlated with TMP), when referring to the three operating regimes as described in the literature [117, 319]. If this is the case, then the marked improvements in permeability would show direct conversion to the filtration environment. Considering these thoughts it would be assumed further that the PS100 membrane would show the greatest improvements in relative flux. This is not the case; the modifications offer less improvement to the PS100 when carrying out tea filtration; further analysis and experimentation has been carried out to elucidate this.

8.3.2 Resistance-in-series analysis

Figure 8-5 shows the steady state resistances divided into intrinsic membrane resistance (R_m), irreversible and reversible fouling (R_r and R_i respectively), and resistance due to CP (R_{cp}), calculated as explained in 4.5.1. Noticeable is the overall size of the bars for the membranes in which ethanol treatment has been applied, this being attributed to reductions in nearly all resistance categories. It comes in part as a result of a reduced R_{cp} term. This could be an effect of the greater convective transport through the membrane

and thus reduced accumulation of solutes at the membrane surface, acting to reduce the back diffusion in the CP boundary layer.

A reduction in R_r following treatment is shown. To exemplify this, during the first fouling cycle for the untreated PS50, R_r equates to 2.46 × 10^{12} m^{-1}, for the 50 wt.% ethanol treatment membrane; this is reduced to 1.70 × 10^{12} m^{-1}, and for 100 wt.% ethanol treatment it is further reduced to 1.38 × 10^{12} m^{-1}. It suggests that foulant is bound to the surface more strongly following ethanol treatment, as was elucidated for protein fouling in Chapter 5. Another observation is that the untreated membrane tends to improve as it ages. This is shown by slight increases in R_m but countered by large reductions in R_i, whereas for treated membranes, there is a tendency for R_i to increase. The trend is most apparent for the 100 wt.% ethanol treated membrane. It means that cycle on cycle, the propensity for fouling is increasing following ethanol treatment contrasting the untreated membrane fouling propensity which decreases with each foul-clean cycle repetition.

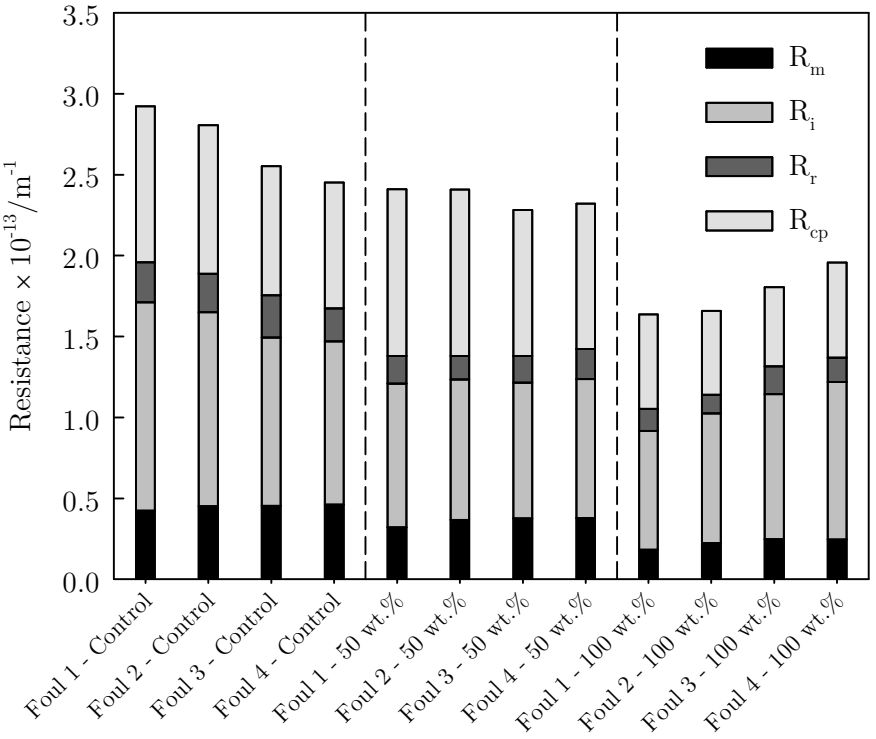

Figure 8-5 - Resistance breakdown for PS50 membranes over multiple cycles following varied ethanol treatment (treatment type separated by dashed lines)

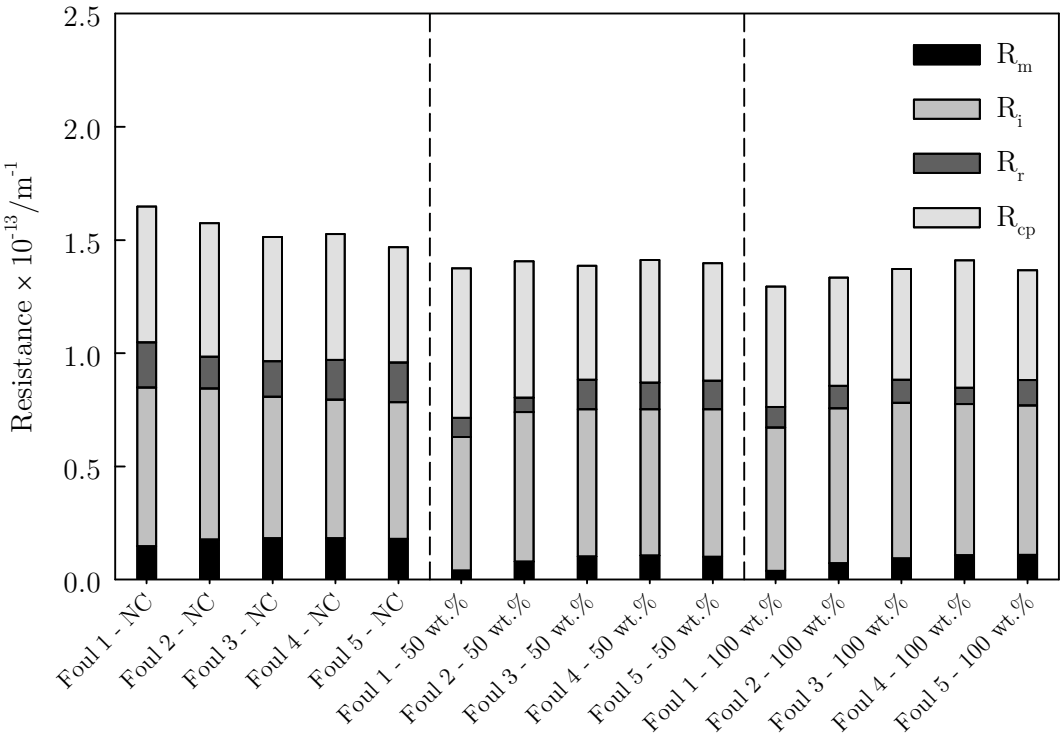

Figure 8-6 - Resistance breakdown for PS100 membranes over multiple cycles following varied ethanol treatment (treatment type separated by dashed lines)

Again the PS100 indicates the same trends as shown in Figure 8-6. The three treatments for the PS50 all showed distinct differences, whereas the characteristics of the PS100 resistance breakdown showed the closest similarities between that of the 50% and 100% ethanol treatment membranes, as was the case with PWFs and filtration fluxes. R_r increased with each consecutive foul-clean cycle for the treated membranes, whilst it stayed reasonably consistent for the no ethanol treatment case. Again though, R_i showed a progressive decrease from $7.01 \times 10^{12}\,m^{-1}$ at 1F1C to $6.04 \times 10^{12}\,m^{-1}$ after 5F5C. It would suggest that whilst overall foulant binding to the surface is lessened, or at least cancelled out slightly by the increased permeability, the foulant is more persistent and is harder to remove by mechanical action alone. This is complimentary to AFM measurements shown in Chapter 5 showing stronger binding and more long range interactions between BSA and a treated surface. The foulants in this instance are far less chemically uniform however.

The overall total resistance attributed to fouling ($R_r + R_i$) is an interesting value to compare. During 1F for the untreated PS100 membrane, this value was $9.01 \times 10^{12}\,m^{-1}$, after 100% ethanol treatment it was $7.24 \times 10^{12}\,m^{-1}$. Similarly for the MFG1 membrane (data shown in Figure 8-7), the total fouling resistance was $8.39 \times 10^{12}\,m^{-1}$ for the virgin untreated membrane, which fell to $7.56 \times 10^{12}\,m^{-1}$ and $6.48 \times 10^{12}\,m^{-1}$ for respective 50% and 100% ethanol treatments. Generally speaking for the MFG1 membrane, the differences in resistances were less distinguishable than for the other membranes tested. Likely a reflection of the lower gains in filtration fluxes and PWF uplifts.

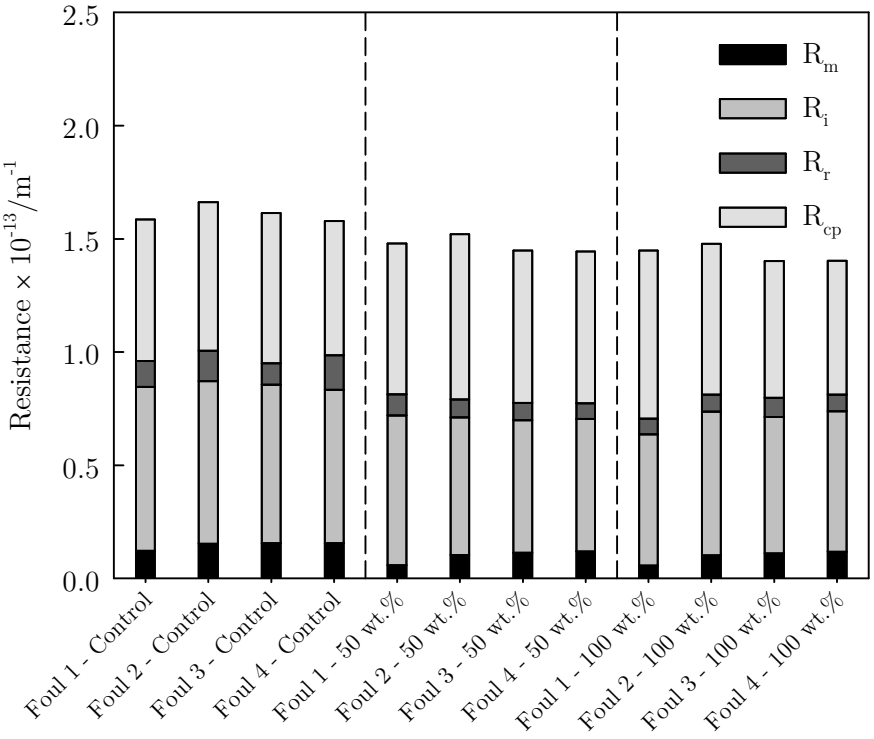

Figure 8-7 - Resistance breakdown for MFG1 membranes over multiple cycles following varied ethanol treatment (treatment type separated by dashed lines)

With reference to the total resistance (R_T) of the membranes; the PS100 begins to outperform the MFG1 membrane after the first foul-clean cycle when untreated (R_T was recorded at for $1.65 \times 10^{13}\,m^{-1}$ for PS100 and 1.59×10^{13} for MFG1, by 4F4C these values were $1.53 \times 10^{13}\,m^{-1}$ for PS100 and $1.58 \times 10^{13}\,m^{-1}$ MFG1). When ethanol treatment was applied, the response of the membrane was such that the PS100 immediately outperformed the MFG1 membrane despite the MF membrane having a superior PWF when in the virgin untreated state; the PS100 operated with an R_T of $1.33 \times 10^{13}\,m^{-1}$ following 100 wt.% ethanol treatment, compared to the MFG1 value of R_T of $1.45 \times 10^{13}\,m^{-1}$. This is significant as it shows the UF membrane has been modified to offer the same performance in terms of throughput than that of an MF classified membrane.

8.3.3 Flux recovery after cleaning

As already mentioned, flux recovery is a benchmark value used to assess efficiency of the cleaning process. For this analysis, a value of 100% would mean that a membrane has been returned to its PWF as new, quantified here following hot water conditioning.

Figure 8-8 shows the recovery of the PS50 after each fouling cycle. For the untreated membrane, the best flux recovery came after 1F1C (94% ± 6%), this fell to 93% ± 5% after 4F4C as represents a statistically consistent recovery upon membrane cleaning. When treated by 50 wt.% ethanol, a recovery of 116% ± 5% after F1C1, falling to 111% ± 2% after 4F4C (considering the treated flux was 132% ± 1% of the untreated flux). For 100% ethanol, after 1F1C there was a 188% ± 13% recovery (compared to the 213% ± 4% PWF following treatment), and after 4F4C this value fell to 166% ± 9%. It indicates that the

ethanol treatment protocol is not effective in sustaining the flux uplifts over multiple cycles, although there is still a profound improvement after 4 foul-clean cycles, and in fact, all of the post foul-clean values gathered showed an overlap when comparing the error bars for 100 wt.% ethanol treatment.

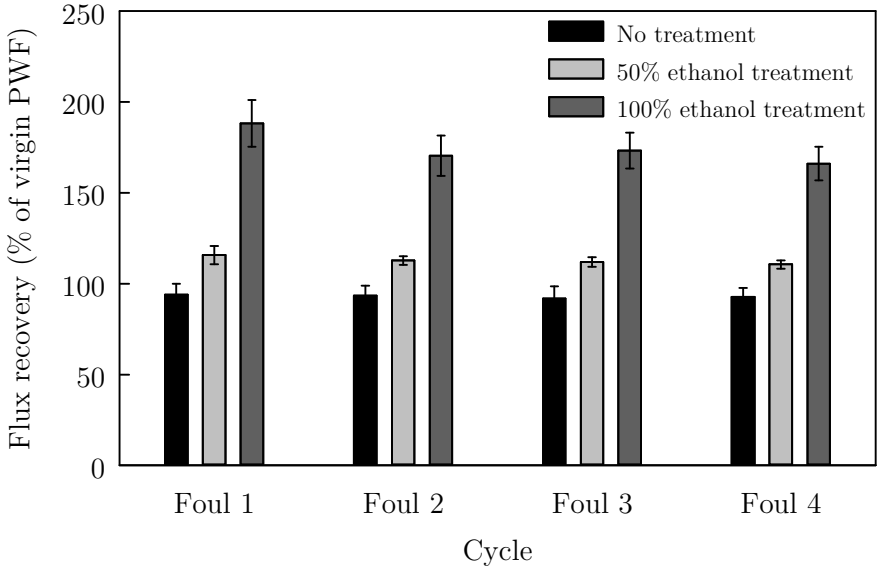

Figure 8-8 - Recovery of PWF (relative to pre-treated virgin PWF) following subsequent foul/clean cycles for PS50

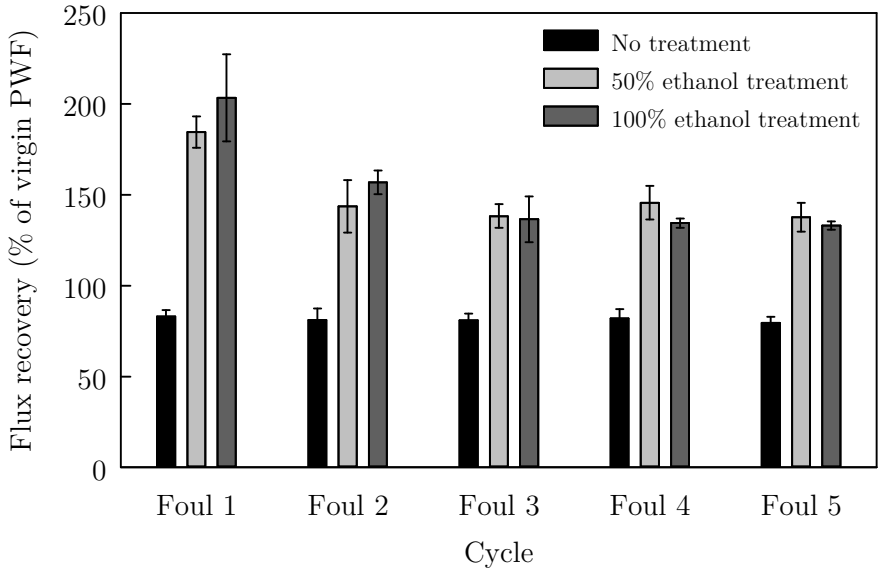

Figure 8-9 - Recovery of PWF (relative to pre-treated virgin PWF) following subsequent foul/clean cycles for PS100

For the PS100 membrane, the recovery showed a more defined trend for both 50 and 100 wt.% ethanol treated membranes (Figure 8-9). The drop-off from the PWF uplifts shown following treatment are clear (375% ± 11% for 50 wt.% ethanol, 384% ± 6% for 100 wt.% ethanol). During repeated foul-clean cycles, the untreated membrane showed only partial (yet consistent) flux recovery, with recovery not of the same magnitude as the PS50; recording PWFs of 83% ± 3% and 80% ± 3% for 1F1C and 5F5C respectively. When

measured following treatment, the 1F1C values were 185% ± 9% and 203% ± 24% for respective 50 and 100 wt.% ethanol treatments; these values represent the largest flux recoveries seen and offer two-fold improvements over untreated membranes. The values for 5F5C fell to 137% ± 8% and 133% ± 2%.

Figure 8-10 shows comparable data for the MFG1 membrane. It shows that when the membrane is untreated it is the least well regenerated out of the three tested; offering only 77 – 79% returns from the original PWF. After treatment, 209% ± 4% and 213% ± 3% PWFs following treatment were reduced to 118% ± 12% and 120% ± 5% of the virgin PWF for 50 and 100 wt.% ethanol treatment respectively (for 1F1C); the values after 4F4C were 98% ± 8% and 94% ± 5%. This was the first instance in which membranes, which had undergone ethanol treatment, had fallen to a value below that of the original membrane PWF.

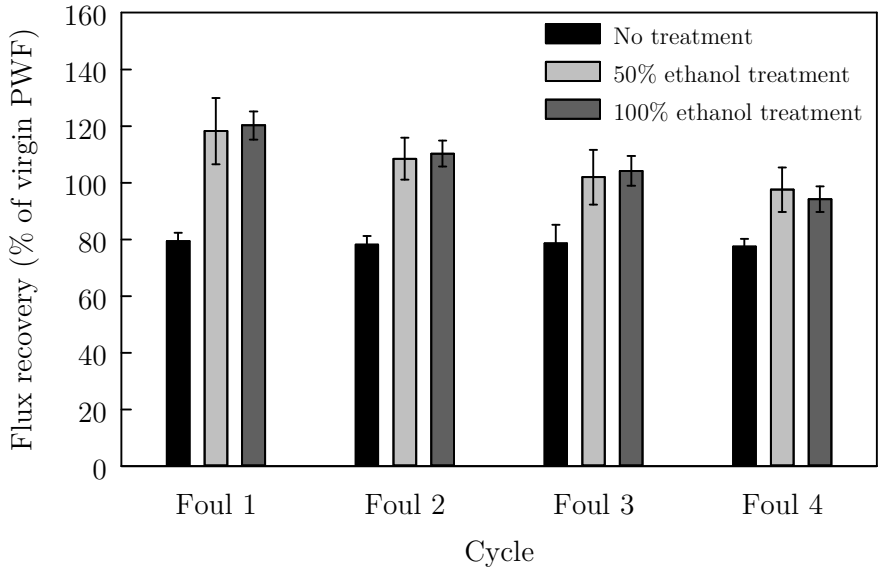

Figure 8-10 - Recovery of PWF (relative to pre-treated virgin PWF) following subsequent foul/clean cycles for MFG1

Given that cleaning does not achieve PWF regeneration to values equal to the treated virgin PWFs, and additionally that regeneration is lowered with each successive foul-clean cycle, it is clear that ethanol treatment does not succeed in permanently modifying the membrane, but does have lasting effects.

8.3.4 Convergence analysis of terminal filtration flux

Figure 8-11 shows the extrapolation of terminal flux values (taken as the average flux over the last 10 minutes of the filtration experiment) over a number of cycles. This gives an indication as to how many foul-clean cycles in may take for the effects of alcohol treatment to diminish to a point at which no advantage is realised in terms of throughput.

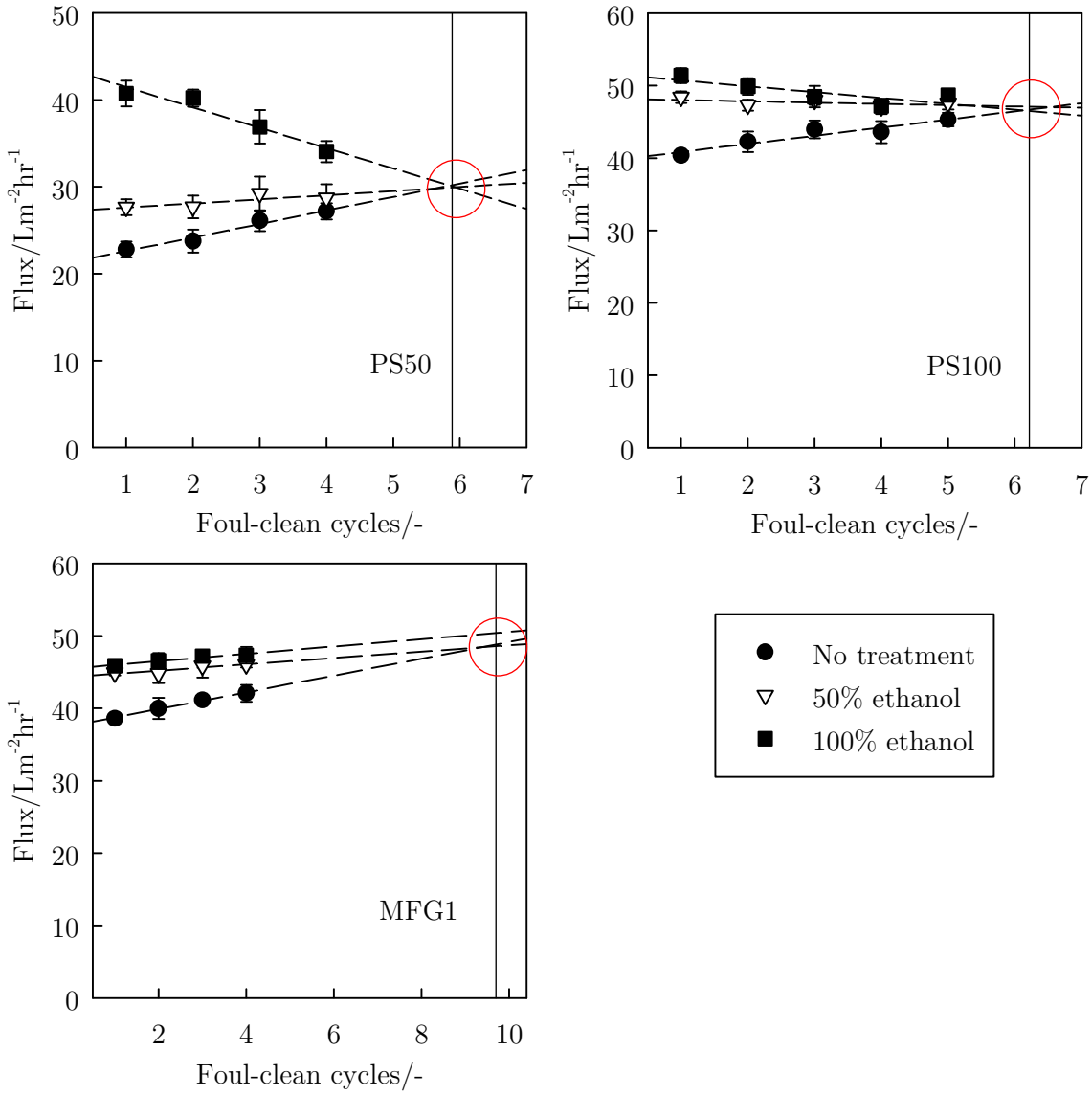

Figure 8-11 - Convergence of terminal fluxes versus number of fouling runs. Circles denote approximate point of convergence and thus where ethanol treatment is potentially non-beneficial

The PS50 membrane, which showed the largest improvements in terminal flux, gave the sharpest decline in performance gain. At this rate of decline, convergence would occur at approximately the 6F6C point for both 50 and 100 wt.% ethanol treatment. For PS100 the effects are similar with convergence also happening between the 6F and 7F point. For MFG1, although the terminal flux gains were the least prolific, the fluxes for treated membranes increased similarly to the untreated membrane. There is no convergence for the 100 wt.% ethanol treatment case; the 50 wt.% membrane shows cross-over with the untreated membrane at approximately 10F10C. The reliability of such a long range extrapolation is questionable given that the extension is more than twice the sample range. Also the extrapolation has been assumed linear. This can be applied with reasonable confidence for the PS50 and PS100 cases. If the effect is that of membrane degradation however, the trend would likely be more closely allied to an exponential decay than a fitting

of a negative linear correlation. Nevertheless the analysis gives some indication as to the longevity of ethanol treatment.

8.3.5 Membrane surface aspects

Surface analysis techniques were carried out on a simplified range of samples: PS50 with no treatment and 100 wt.% ethanol treatment, and PS100 also with no- and 100 wt.% ethanol treatment[4]. The sample range was selected due to their being limited scope for measurement at all stages of the filtration cycle given the unfeasibility of sample preparation. The membranes were chosen as they gave the most variability in performance in terms of the flux data observed, and would thus potentially show the most striking changes when analysing hydrophobicity and ζ potential.

8.3.6 Contact angle

Contact angle (measured using the sessile drop method) was recorded for the surface of both untreated and treated membranes. For the PS50 membrane the values are shown in Table 8-2. After hot-water conditioning, the virgin membrane was found to be moderately hydrophilic, and when treated, hydrophobicity increased somewhat (data for a range of alcohol treatments was also displayed in section 5.4). This again implied that the fouling propensity was increased as shown for BSA and by other authors [320, 321].

Table 8-2 - Static contact angles of PS50 membranes at various points during the filtration cycles

Treatment type	*Contact angle (sessile drop)*				
	V	*1F*	*1F1C*	*4F3C*	*4F4C*
No treatment	74° ± 2°	36° ± 3°	67° ± 2°	38° ± 4°	65° ± 2°
100% ethanol treatment	85° ± 2°	29° ± 2°	74° ± 4°	33° ± 5°	72° ± 2°

When measuring the fouled membrane (1F and 4F3C), a more hydrophilic surface was the result with little variation between cycle number. Evans and Bird (2006) [25] observed the effect for fluoropolymer (FP) and regenerated cellulose (RC) membranes (both 30 kDa nMWCO) when filtering 1.0 wt.% black tea liquor at the 1F point. In this article, fouling resulted in respective contact angles of 43° ± 3.5° and 50° ± 2.3° (virgin hot water conditioned surfaces were 62° ± 1.5° and <15°). Wu and Bird (2007) [33] also showed that a PS membrane (30 kDa) contact angle was reduced from 61.6° ± 3.6° to 37.2° ± 4.4° for virgin and 1F states respectively (fouled with tea protein and model theaflavin in this instance). The FP membrane values in the studies of the aforementioned work were most closely matched to the PS50 membrane studied here, thus it is likely that the fouling behaviour would be comparable.

[4]Measurement of contact angle was made on the MFG1 membrane though reliability and reproducibility was poor due to permeation of water droplets though the membrane.

When the membrane was cleaned, the untreated sample returned to a value between that of the virgin and fouled surfaces, which suggests incomplete removal of foulant. This was also the case for the treated membrane although such an effect is countered by the initial hydrophobisation as a result of treatment. After 4F4C, the values for both treated and untreated membranes were within the respective error bars for the 1F1C measurements, implying that any modification seen as a result of the first foul-clean cycle had not been further modified. Also noteworthy is that the contact angle of the 1F1C and 4F4C treated membrane returned values similar to that of the untreated virgin membrane. It is not possible to deduce whether the results gained are hydrophilisation by surface active species or merely the diminishing of the initial modification back to its unmodified state as a result of incomplete foulant removal i.e. the apparent not intrinsic hydrophilicity.

Table 8-3 - Static contact angles of PS100 membranes at various points during the filtration cycles

Treatment type	Contact angle (sessile drop)			
	V	1F	1F1C	5F5C
No treatment	66° ± 2°	(22° ± 4°)*	70° ± 3°	69° ± 3°
100% ethanol treatment	74° ± 2°	(16° ± 6°)*	72° ± 3°	70° ± 2°

*denotes low contact angle due to excessive hydrophilisation, difficulty in accurate measurements is confirmed by large errors

Table 8-3 shows data for the PS100 membrane. The membrane is moderately more hydrophilic than the PS50 membrane, and shows more resemblance to the already quoted PS25 membrane value in section 5.4 (62.4° ± 2.0°). When treated with alcohol, again there is hydrophobisation of the surface bringing it into the range of the untreated PS50. Upon fouling, the treated membrane exhibits a lower contact angle than that of the untreated PS50 despite the similar virgin values. These observations highlight that other factors such as charge and morphology can play a key role in fouling propensity.

From literature data and that collected here, the following deductions can be made. There is hydrophilisation of more hydrophobic surfaces, and hydrophobisation of more hydrophilic surfaces upon fouling. In addition, the amount of hydrophilisation that occurs as a result of fouling for a given membrane is increased by the initial hydrophobicity.

In order to explain this deduction certain aspects must be considered. Hydrophobic species present in tea e.g. moderately insoluble caffeine and other alkaloids, or certain tea protein residues, may adsorb more readily to the hydrophilic surface creating an apparent hydrophobicity. This hypothesis was offered by Evans and Bird (2006) [25] yet seems unlikely. If a surface is strongly hydrophilic, a well-adhered film of water would be present over the surface which would exclude such foulants from adherence to the membrane surface. This would be especially true for a species such as caffeine which is known to associate through hydrophobic interactions [322]. More likely is that the deposition of a cake layer covers the membrane surface substantially to ensure the surface properties of the membrane are masked (to an extent). The contact angle measurement is simply a

measurement of the bulk fouling layer and thus an average for all tea species present. Components in tea generally have good solubility; comprising high levels of highly hydroxylated polyphenols. This would have the effect of membrane surface hydrophilisation of moderately hydrophilic membranes. For the RC membrane, as detailed by Evans and Bird (2006) [25], the bulk fouling layer would again mask the hydrophilic nature of the membrane. This would bring the contact angle to somewhere close to that of the results shown in this chapter and other such systems e.g. FP membranes.

In summary, the apparent fouled membrane contact angle is not solely dependent on the underlying membrane wetting properties though it is not to say that the magnitude of foulant adhesion can vary. The influence of the membrane wetting properties can influence the contact angle measured, although there is a point at which the fouling layer dominates this measurement with negligible influence from the underlying membrane surface. When a virgin membrane surface is more hydrophobic, the net effect is deposition of more foulant, which in the case of tea fouling, causes a more hydrophilic surface than the equivalent situation for a less hydrophobic membrane. This reaffirms the conclusions of Evans *et al.* (2008) [28] in that use and subsequent modification of more hydrophobic surfaces to a more hydrophilic state is beneficial for tea filtration. It also supports one of the overarching theme presented in this thesis, given that alcohol imparts hydrophobicity to the membrane surface.

8.3.7 Apparent zeta potential

Through-pore streaming potential measurements were made using the same sample set as in 8.3.6. Samples for this study were prepared in the dead-end cell as described in 4.1.3 using a constant stirring speed of 800 rpm under equivalent TMPs, temperatures and solute concentrations.

Data are not strictly comparable given inner pore surfaces and membrane top-surface measurements could display different properties though they can be used complimentarily with contact angle measurements to develop a picture of the membrane.

Figure 8-12 shows the measurements for the PS50 membrane. The untreated membrane was the most negatively charged out of the two in its virgin state, this also showed the greatest down-modification after treatment (to values consistently below -4.5 mV) over the pH range. The implication of this would be a greater fouling tendency by negatively charged phenolate ions (dissociated polyphenol species) due to lower negative charge repulsion.

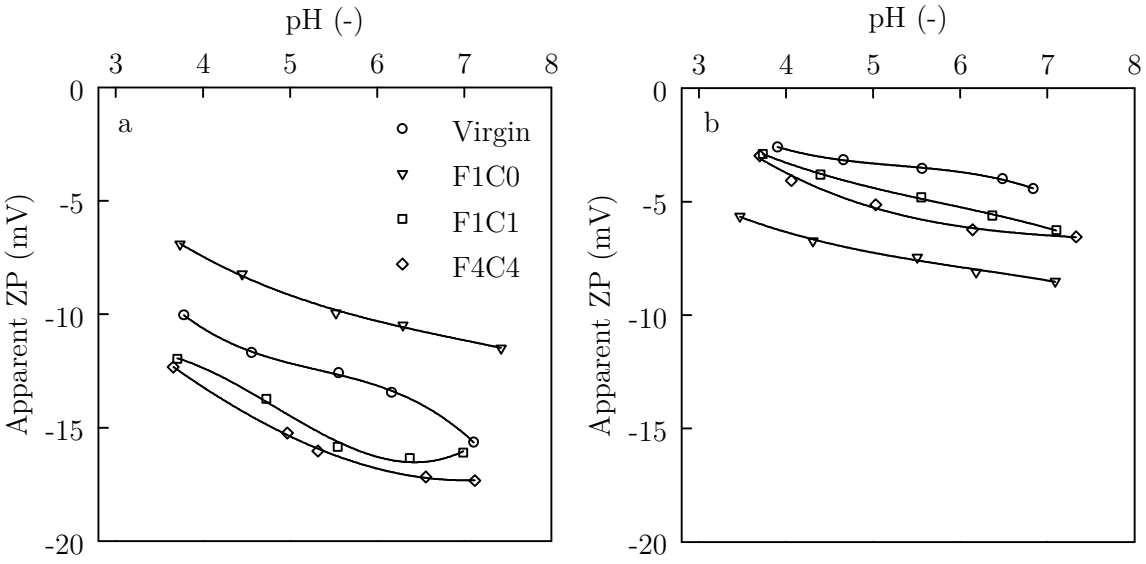

Figure 8-12 - Apparent zeta potential for PS50 membrane, (a) untreated membrane, and (b) treated membrane (legend in (a) refers to both figures)

When fouled, the untreated PS50 membrane was reduced in charge, before cleaning returned it to a state of greater magnitude negative charge than was shown prior to fouling. This was also true after 4F4C cycles. After the treated membrane was fouled, it became more charged, approaching the values for the untreated fouled membrane. These results show that the foulant acts to mask the underlying surface charge, as was discussed in 8.3.6. However this time, the measurement relates to the in-pore environment. The reason why the fouled membrane charge values were not of the same magnitude could be because an electrical double layer overlap exists in the pores, and thus a highly charged environment may mean that the measurement of the fouled untreated membrane was still heavily contributed to by the membrane charge. When treated, the charge was diminished and therefore a lesser influence from the underlying membrane was apparent.

If the PS100 membrane is now considered (Figure 8-13) essentially the same pattern is observed as was shown for the PS50. In this instance however, the foulant imparted an apparent ζ potential similar to that of the virgin membrane. When the membrane was treated, the charge was lowered to values between -1.7 mV and -3.9 mV (between pH 3.5 and pH 7 respectively). Upon fouling the membrane gained negatively charged species, which raised the ζ potentials to values almost identical to the untreated fouled membrane. When taking into account that overall ζ potentials are lower for this membrane, and the pores are larger (lower apparent charge likely being attributed in part to wider pores), the charge masking which would result upon fouling would be greater, and thus the apparent ζ potentials for treated and untreated membranes would result in more comparable readings. This is to say that both are a result of the predominance of the charge attributed to the foulant, and not so much the influence of membrane pore walls. Since the PS100 membrane in both cases was lower than for the analogous experiments on PS50 membranes, it is thought that the influence of the underlying membrane shows more presence in the PS50 reading, a direct result of the initial virgin membrane negative charge being greater.

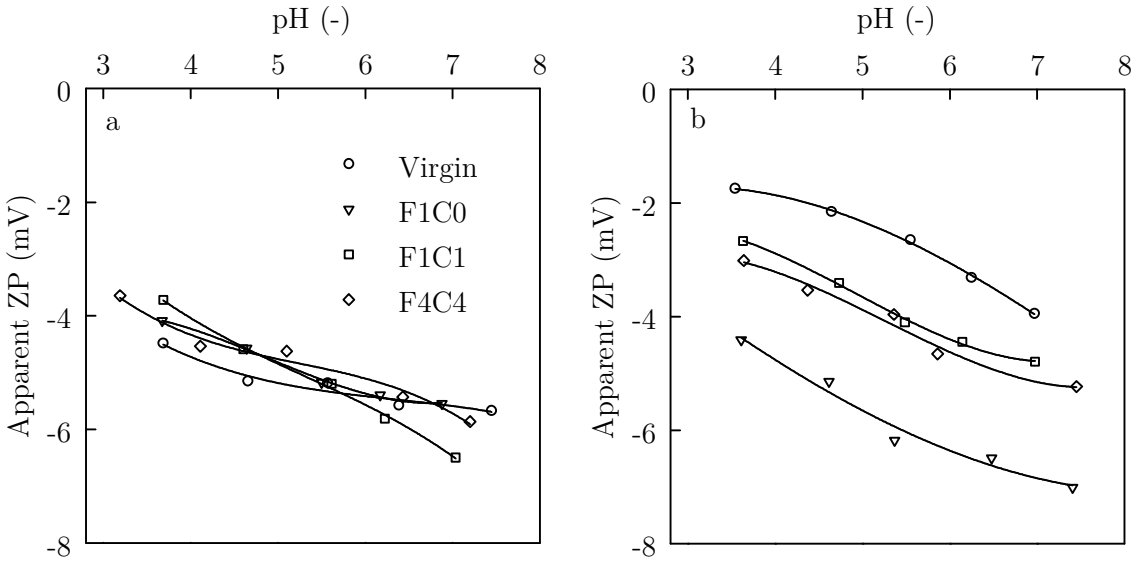

Figure 8-13 - Apparent zeta potential for PS100 membrane, (a) untreated membrane, and (b) treated membrane (legend in (a) refers to both figures)

When cleaning was performed, the untreated membrane remained at a similar magnitude of negative charge at both the F1C1 and F4C4 points. This supports the contact angle data in Table 8-3, given that upon cleaning, the membrane was returned to a similar state. When treated, the charge of the F1C1 membrane shows a moderate re-adjustment back towards the virgin state, the value lying between the virgin treated state and the virgin untreated state. This result may be interpreted in a number of ways:

- As a reduction in the amount of negatively charged foulant attached to the membrane. This assumes that there was incomplete removal from the untreated membrane using the cleaning protocol employed.
- As incomplete removal of foulant from the treated membrane and thus only a partial return of the membrane to its treated state. This assumes there is no degradation in performance as a result of alcohol treatment.
- As a result of the degradation of the effects of alcohol treatment. Performance losses for both repetitively fouled membranes and membranes stored following treatment have both shown the effects of alcohol to diminish slightly. It could be argued that degradation of the effects of alcohol treatment occurs, and thus an increase in charge back towards to the virgin untreated state resulted. Then it would be assumed that the membrane would also adsorb a lesser amount of negatively charged material since it is more negatively charged itself.

After 4F4C, there appears to be a small increase in the magnitude of negative charge away from the isoelectric axis which further equally supports all of the aforementioned theories.

8.3.8 Solute transmission and tea quality

8.3.8.1. Total solids transmission

In addition to the fouling and surface chemistry phenomena shown previously, observations regarding the transmission of species were also recorded.

Figure 8-14 shows the treatments effects on total solids transmission of 0.5 wt.% tea over multiple cycles. For the PS50 (Figure 8-14a) there was no apparent change in total solids transmission concerning both treatment type or filtration number. Thus the alcohol treatment can be deemed beneficial in terms of flux gained.

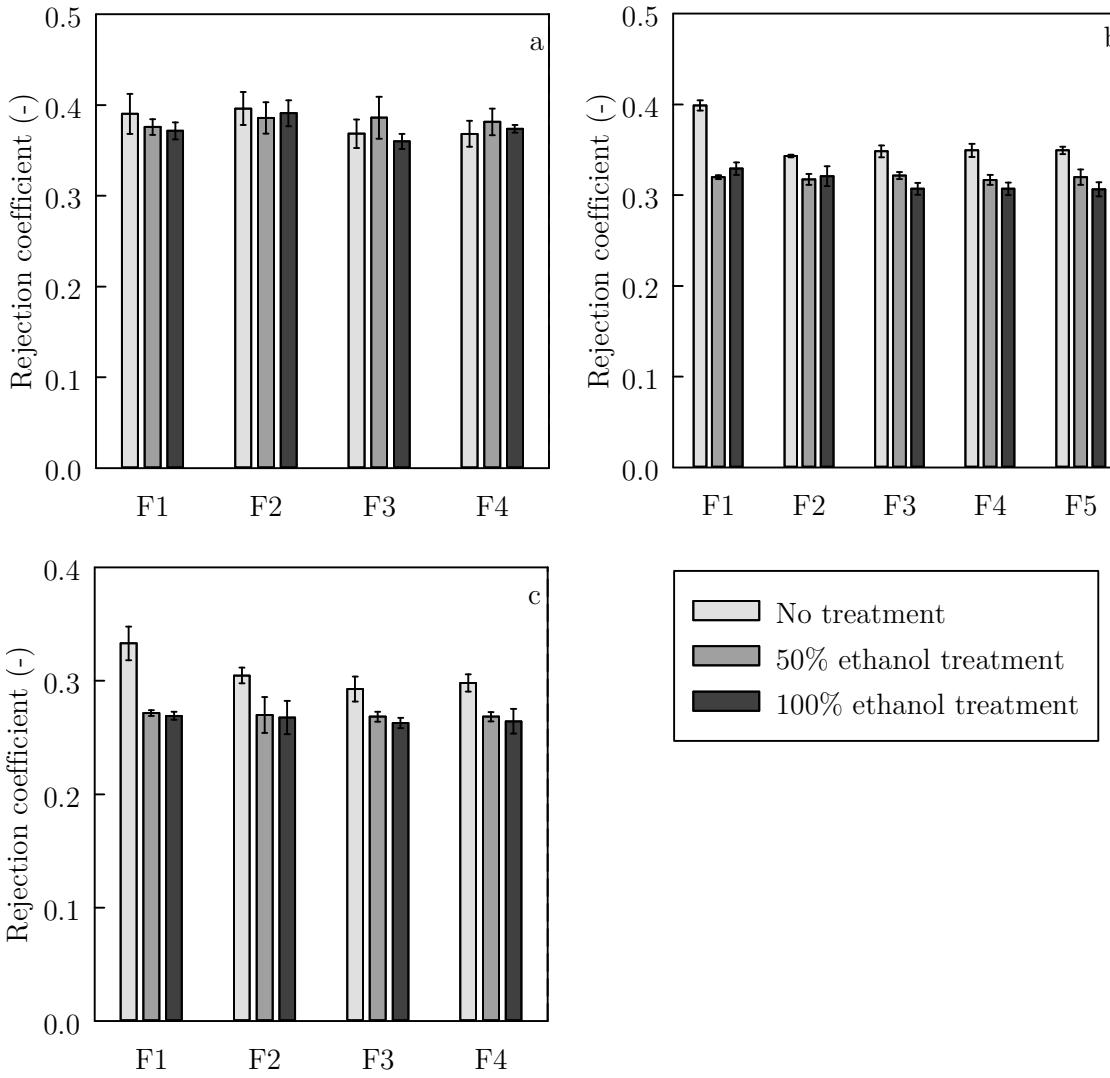

Figure 8-14 - Total tea solids transmission for (a) PS50, (b) PS100, and (c) MFG1 membranes over multiple foul-clean cycles

When PS100 data are considered (b), a large drop in R_{app} was seen between F1 and subsequent fouling cycles for the untreated membrane, this feature was repeated by a similar magnitude for the MFG1 membrane (c). It suggests further that there is remaining foulant present after cleaning and that the membrane is both developing a layer of anti-

foul protection as a result of the initial foul-clean cycle (shown by flux improvements cycle-on-cycle), but also this anti-foul layer is allowing preferential transmission of solutes. The effect is sustained for the remaining 3/4 foul-clean cycles. The step down in rejection coefficient after F1 was not indicated by flux or surface chemistry measurements for the instances reported.

8.3.8.2. Total polyphenols transmission

Total polyphenols concentration of each stream was measured as per the method described in 4.4.2.2. Figure 8-15 and Figure 8-16 show the data for PS50 and PS100 membranes respectively.

The untreated PS50 (Figure 8-15a) shows a step change similar to the solids transmission of the untreated PS100 and MFG1 membranes from 1F to 2F1C. After this step-down in rejection, R_{app} values show little difference considering the magnitude of the errors (standard deviation for $n = 8$ absorbance measurements for duplicate samples). All R_{app} values after 15 minutes filtration measured between 0.44 and 0.48, and after 60 minutes, between 0.48 and 0.51. This is compared to the initial rejections of between 0.55 and 0.62 for 15 and 60 minute marks respectively during 1F. By taking the normalised permeate concentrations (C_p); the tea at 4F3C has 24.9% ± 1.2% improved polyphenol content over that of 1F (calculation shown by eqs. 7-1 and 7-2).

$$polyphenol\ increase\ (\%) = \frac{C_{p_{1\mathrm{F}}}}{C_{p_{\mathrm{nFnC}}}} \times 100 \tag{7-1}$$

and:

$$\frac{C_{p_{1\mathrm{F}}}}{C_{p_{\mathrm{nFnC}}}} = \frac{(1 - R_{app_{1\mathrm{F}}})C_{b_{1\mathrm{F}}}}{(1 - R_{app_{\mathrm{nFnC}}})C_{b_{\mathrm{nFnC}}}} \tag{7-2}$$

This comparison also provides a useful indication as to the reduction in polyphenol loss as a result alcohol treatment to membranes compared to untreated counterparts, as will be later discussed.

Untreated PS100 membranes (Figure 8-16a) shows a more incremented step down in rejection coefficient. During 1F, R_{app} at 15 and 60 minutes respectively were 0.53 ± 0.02 and 0.57 ± 0.02; this dropped to 0.41 ± 0.01 0.45 ± 0.02 after 5F4C. The fractional increase as calculated by the above equations was 27.3% ± 1.3%. Despite some error overlap, there are well-defined increments between consecutive fouling curves providing insight and showing that, whilst there was no change between the charge of the membrane after 1F1C and 4F4C (and no obvious change in hydrophilicity), the rejection of species varied significantly.

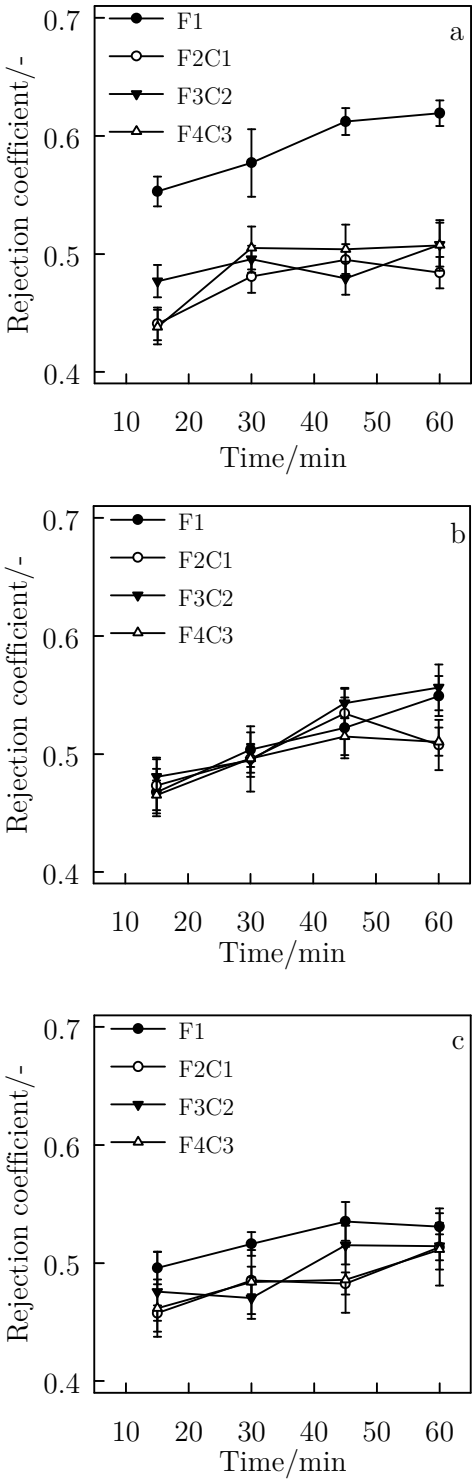

Figure 8-15 - PS50 polyphenols rejection coefficient (R_{app}) for (a) untreated, (b) 50 wt.% ethanol treated and (c) 100 wt.% ethanol treated

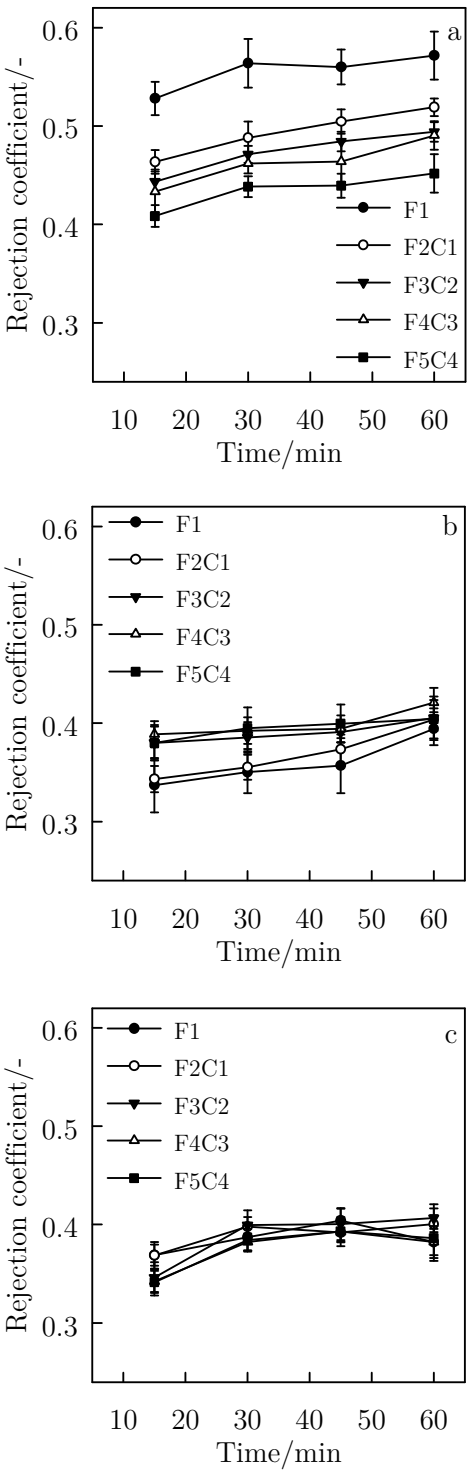

Figure 8-16 - PS100 polyphenols rejection coefficient (R_{app}) for (a) untreated, (b) 50 wt.% ethanol treated and (c) 100 wt.% ethanol treated

When the ethanol treated membranes are compared, it is apparent that R_{app} values are substantially lower than for untreated membrane. For the PS50 with 50 wt.% ethanol treatment (Figure 8-15b), the polyphenols rejection values make an immediate and permanent shift to the approximate values at which the untreated membranes displayed after F1. This was repeated for the PS50 with 100 wt.% ethanol treatment membrane and gave rise to similar R_{app} values (Figure 8-15c). For 50 wt.% and 100 wt.% ethanol treated PS100 membranes (Figure 8-16a and b respectively), all values for both treatments are, in the most part, shifted to below 0.4 (all untreated rejection coefficients were greater than this value). There is an increase in rejection for treated membranes towards the values achieved after 4F4C (or 5F5C for PS100).

Figure 8-17 shows the coefficients for the MFG1 membrane with various treatments. The untreated membrane again showed the incremental R_{app} decrease as foul-clean cycle number increases, with considerable likeness to the PS100 trends shown previously, as would be expected given the greater similarity in membrane properties. Interestingly, the lowest R_{app} values for the untreated membrane (Figure 8-17a, 4F3C) showed lower rejection of polyphenols than for any membrane of any treatment type at all stages of the foul-clean regime. The R_{app} values achieved here were 0.34 ± 0.01 at 15 minutes and 0.32 ± 0.01 after 60 minutes. Comparing these figures to the average solids transmission over the 60 minute filtration (0.30 ± 0.01) shows that there is a near proportional transmission of polyphenols to total solids for this filtration. Also apparent is the occurrence of a downward trend for this data set, implying that polyphenols started to transmit through the membrane more preferentially as foulants have built up; contrasting with observations seen for all other experiments. This is discussed further in 8.3.9.

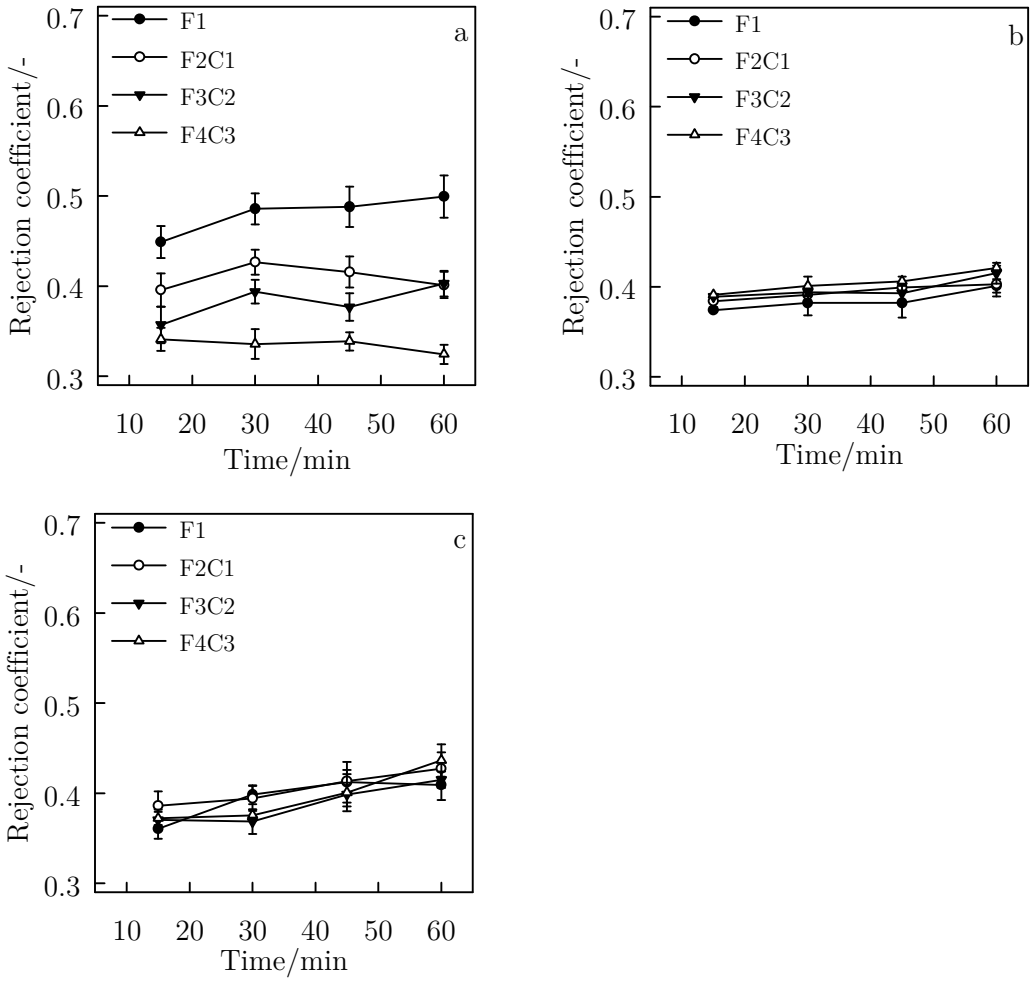

Figure 8-17 - MFG1 polyphenols rejection coefficient (R_{app}) for (a) untreated, (b) 50% ethanol treated and (c) 100% ethanol treated

When the MFG1 membrane was treated with ethanol, both 50% (Figure 8-17b) and 100% (Figure 8-17c) ethanol treatment gave rise to a similar level of enhanced transmission for 1F over the untreated membrane. After foul-clean repetition, rejection values remained consistent with the 1F values for both treatment types suggesting that little modification was occurring to the surface or inside the pores during cycling. This is consistent with the solids transmission data presented in Figure 8-14c.

8.3.8.3. Colour

Tea colour was measured for all permeate samples collected. Generally, the tea permeates showed substantial changes in all colour parameters (lightness, redness and yellowness). All membranes (for all treatment types) showed some common trends (data displayed in Figure 8-18 andFigure 8-20):

- Tea permeates were darker following ethanol treatment, with increased alcohol concentration during treatment giving darker permeates.
- Redness and yellowness were increased with alcohol treatment. Again the effect of alcohol concentration increase was sufficient in producing increases in red and yellow pigment in the permeate products.
- A progressive enhancement in red and yellow and progressive darkening of permeates with increased foul-clean cycle number was seen for all membranes regardless of treatment type. This suggests repetitive fouling is beneficial to TFs and TRs transmission, and thus gives positive outcomes in the filtered tea product stream.
- All membrane surfaces with all treatments showed lightness increase, redness decrease, and yellowness decrease along the duration of a single filtration experiment. This implies, as was stated in 8.3.8.2, that foulant build-up leads to rejection of key polyphenolic species before membrane cleaning alleviates this effect.

Figure 8-18 shows the PS50 colour data. The numbers reflect the polyphenol transmission data to a degree in that the separation between the foul-clean cycle numbers is greater for no treatment and 100 wt.% ethanol treatment than for 50 wt.% treatment (lightness for 50% ethanol treatment was almost identical for all cycles. The membrane produced the lightest tea permeates of all membranes, as well as the lowest readings for red and yellow - the red reading fell below 0 for all treatment types. The only other instance of this was for the untreated PS100). This is in agreement with polyphenol rejection data and shows that the membrane with the smallest pores and highest through-pore charges was rejecting polyphenol species more substantially than the PS100 and MFG1 membranes.

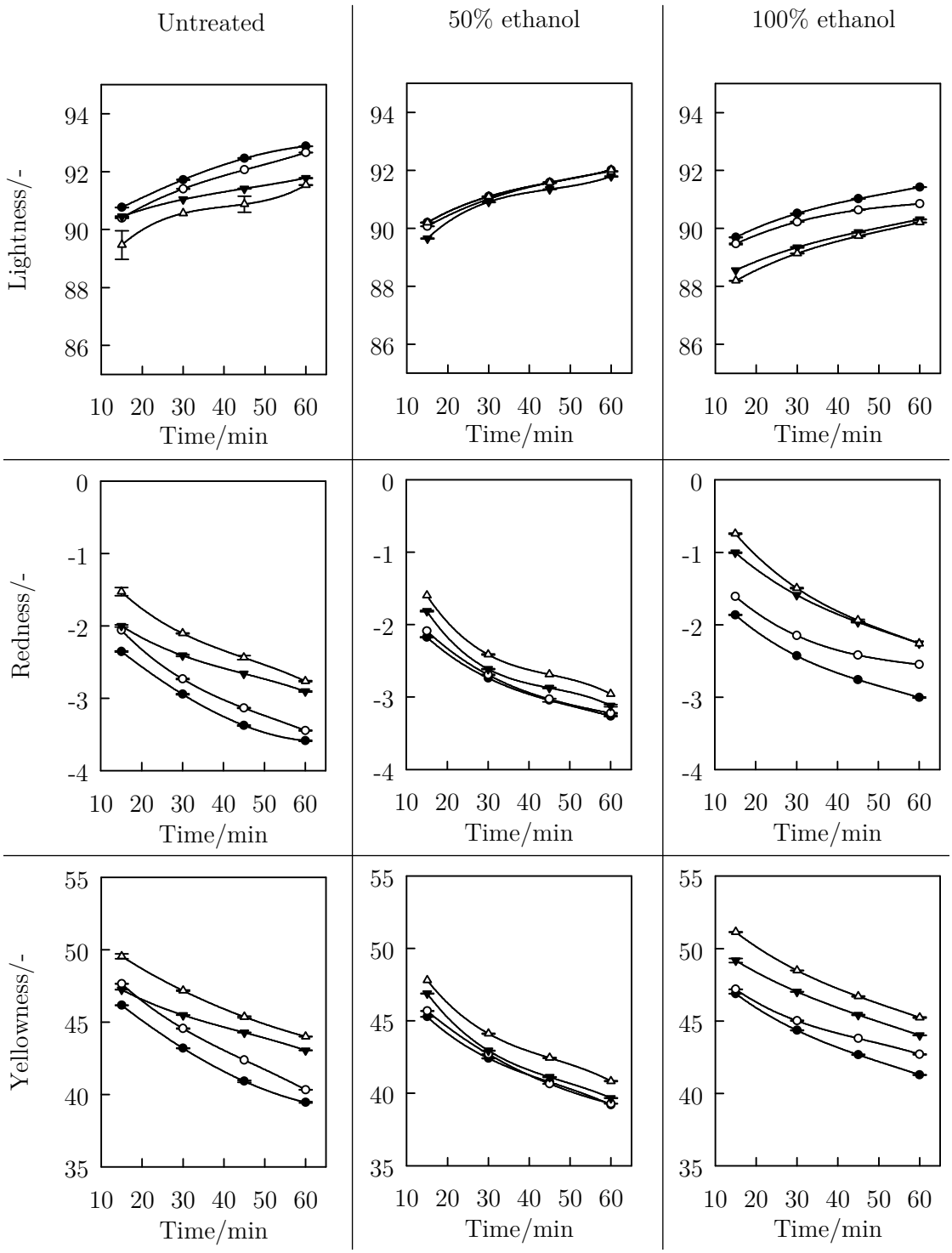

Figure 8-18 - Lightness (row1), redness (row 2) and yellowness (row 3) of tea permeates from untreated, 50% ethanol treated and 100% ethanol treated PS50 membranes

Figure 8-19 shows the data collected for the PS100. This membrane, as with the MFG1 (Figure 8-20), gave the highest red and yellow intensities for all permeates, this being coupled with a darker product. The highest red and yellow intensity was shown for the PS100 membrane with 100% ethanol treatment during the 5F4C filtration; the permeate

having an initial redness of 7.26 ± 0.01 (at 15 minutes) which fell to 4.85 ± 0.35, the yellowness was initially 69.18 ± 0.05 falling to 63.06 ± 0.10 (after 60 minutes).

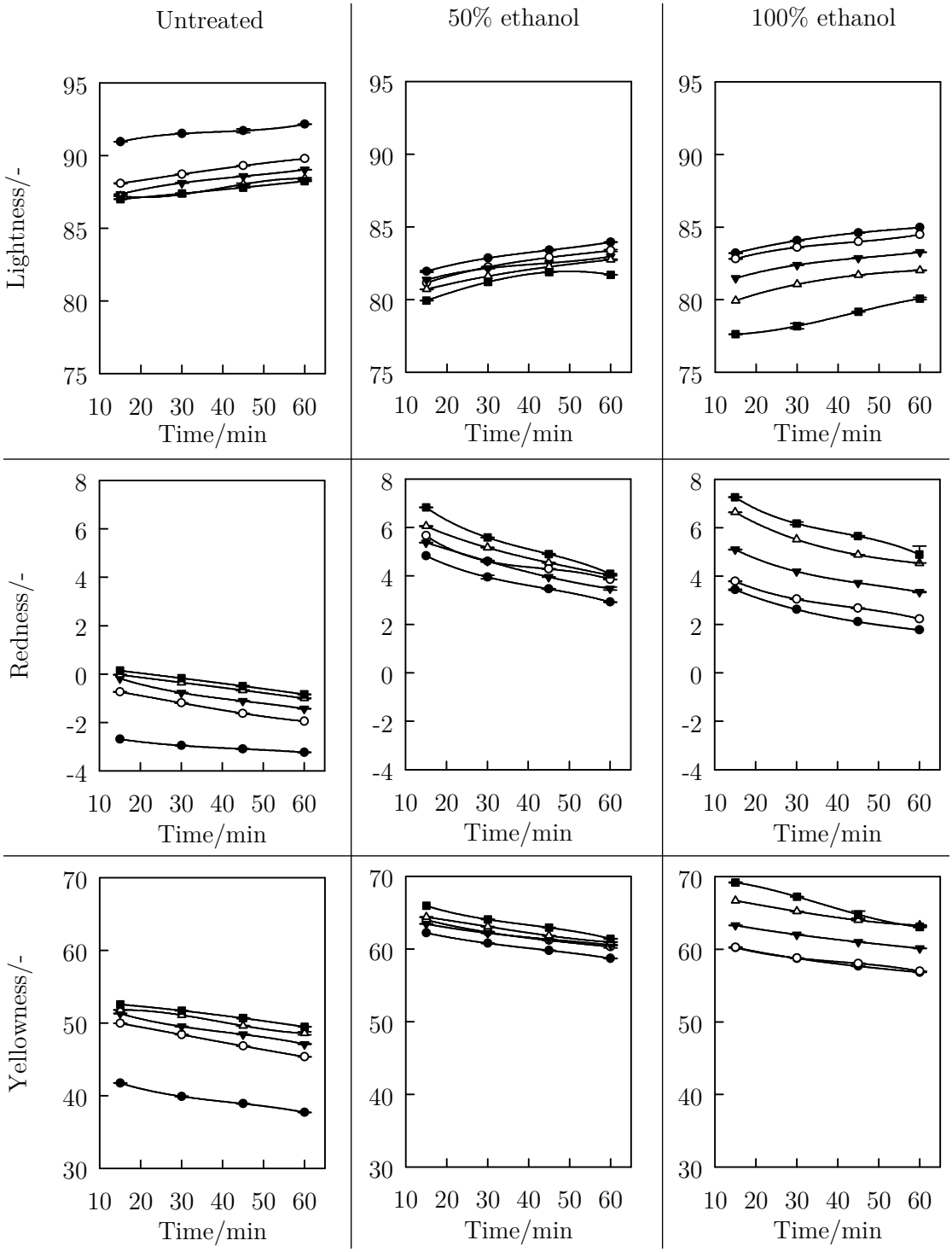

Figure 8-19 -Lightness (row1), redness (row 2) and yellowness (row 3) of tea permeates from untreated, 50% ethanol treated and 100% ethanol treated PS100 membranes

Observing the MFG1 membrane data shows that the least change was brought about by ethanol treatment in terms of tea permeate appearance. This is in agreement with the total polyphenols rejection data in Figure 8-17 .

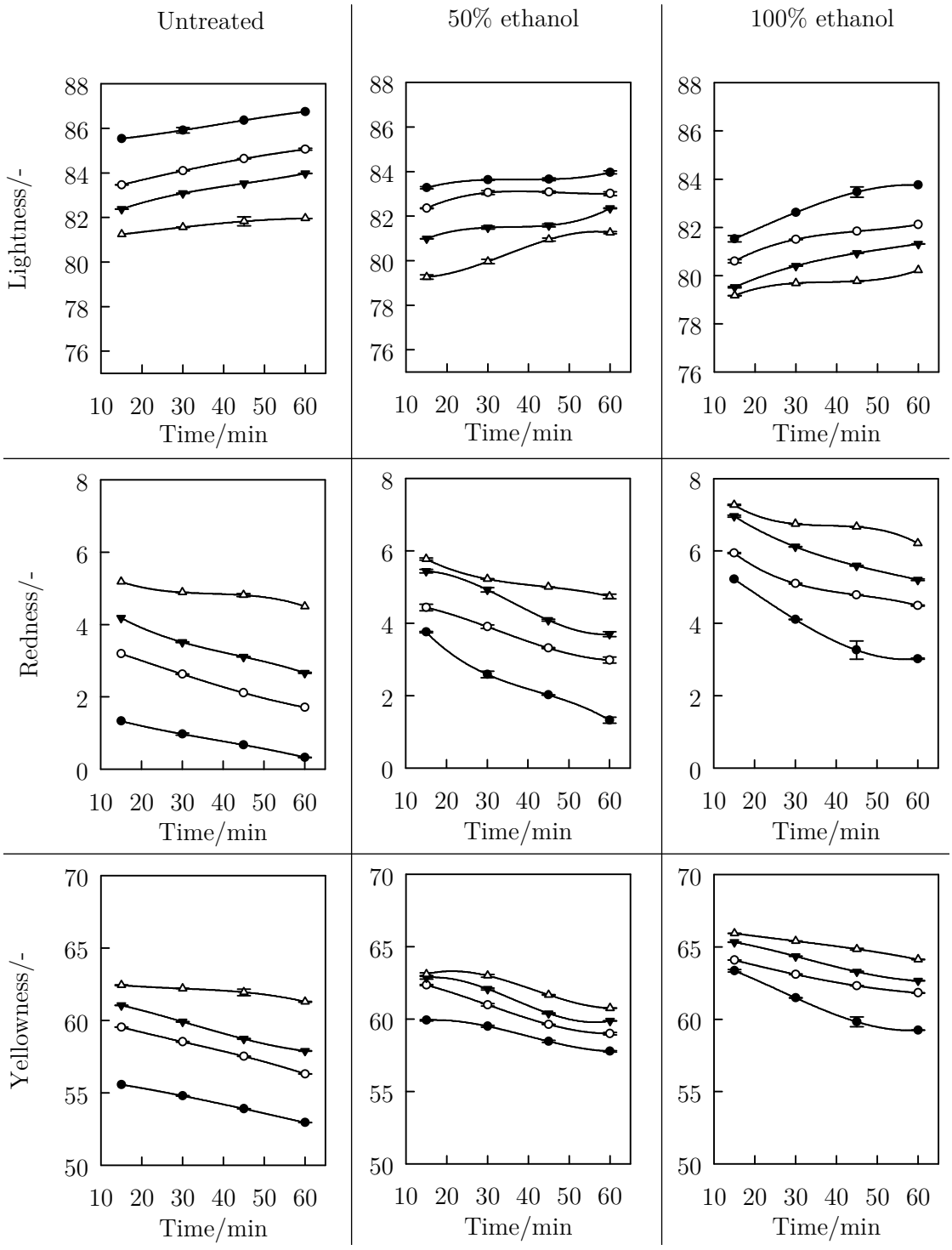

Figure 8-20 - Lightness (row 1), redness (row 2) and yellowness (row 3) of tea permeates from untreated, 50% ethanol treated and 100% ethanol treated PS100 membranes

8.3.9 Foulant build-up, preferential rejection and foul-clean synergy

It was mentioned previously in sections 8.3.8.2 and 8.3.8.3 that rejection of polyphenolic species increases as fouling builds up. This was also a point of discussion in Chapter 7 where long duration filtrations with dilution caused accelerated build-up of polyphenols on the retained side of the membrane.

After each successive fouling run the rejection coefficient (and red colour) is shifted to a state where the species are able to transmit more favourably. This is true until inevitable fouling builds up such that the rejection increases positively (or redness decreases). Upon cleaning, the rejection coefficient trend then begins at a point below the previous cycle's initial rejection coefficient (or above for redness); this initial point is termed the 'offset' point. Further fouling then increases this value in a similar linear trend though absolute rejection values are shifted upwards. This shift is repeated after each cleaning run but from a new offset point. The phenomenon is well-illustrated by the data obtained for the PS100 membrane with no treatment (Figure 8-21).

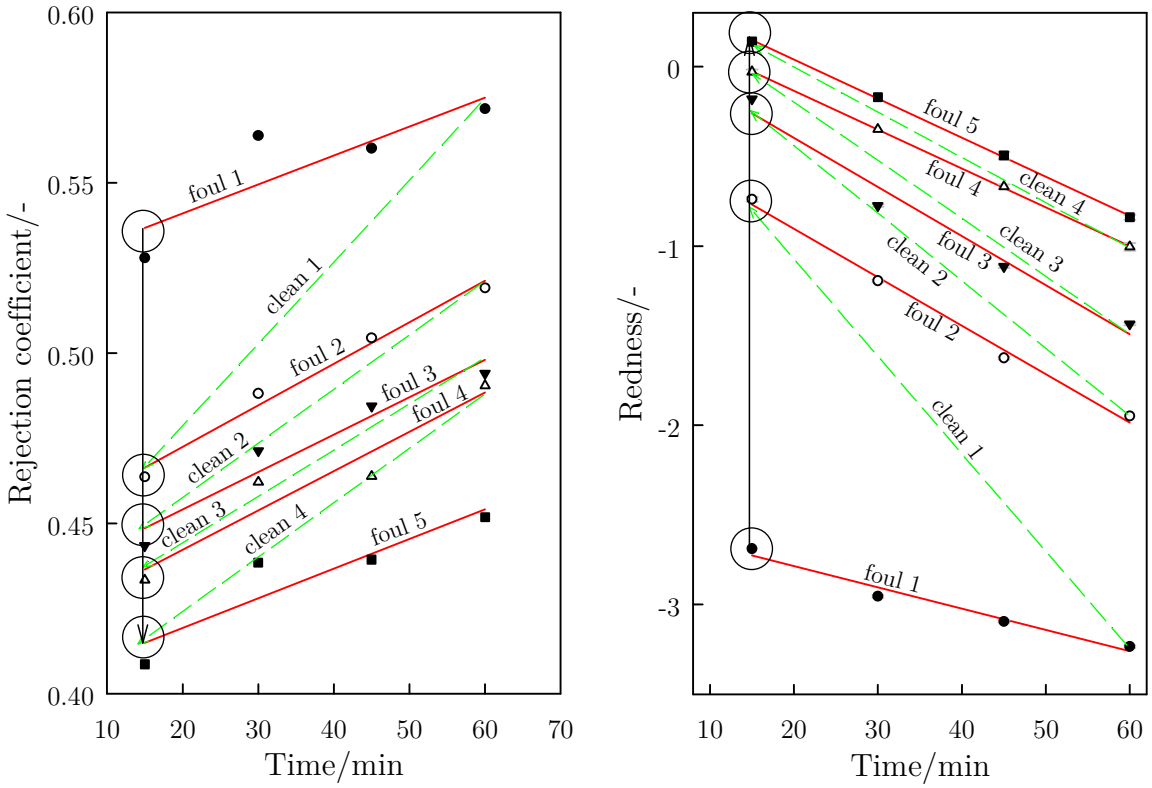

Figure 8-21 - Illustration of the competing effects of fouling and cleaning with varied solute transmission as deduced by permeate properties. Left is polyphenols rejection for untreated PS100, right is redness for the same experimental data set. Red lines denote correlations during fouling for respective measurement; dashed green arrows denote the direction in which cleaning and re-fouling effects the 'offset' point (circles) for the measurement (error bars removed to aid visualisation).

These observations show that a cleaning agent-foulant interaction is playing a key role in the transmission of key species. The greatest shift comes following the first cleaning cycle. It would imply that there is some chemical modification occurring on the membrane, or inside the pores, which is functionalising the surface to allow enhanced species transmission. It cannot be ruled out however that there is incomplete removal of cleaning agent from the membrane matrix and the resulting pH modification of contact between sodium hydroxide solution with tea would in this case result in the deprotonation and thus enhanced solubility of certain polyphenol species e.g. catechin [323]. There is also the possibility that any aggregates (tea cream) which formed in the vicinity would also be solubilised if a variation in local pH occurred. The effect of pH on tea cream moiety size being shown by Liang and Xu (2001) [239]. It would seem likely that given the incremental step down, there is certainly some membrane modification occurring.

8.3.10 Haze removal

As has been the case in previous chapters, haze removal by the membranes has been highly efficient (see Figure 8-22). Generally neither membrane type nor treatment type had any statistical benefit or detriment over any other. All permeates from 15 minutes to 60 minutes were averaged, the maximum average occurring for the untreated MFG1 membrane during the F1 cycle though this is thought to be an arbitrary occurrence given the size of standard deviations. It is the again the case that improvements in haze removal cannot be made as they are already highly efficient however the benefits of alcohol conditioning are realised given the improvements in permeate quality and membrane flux.

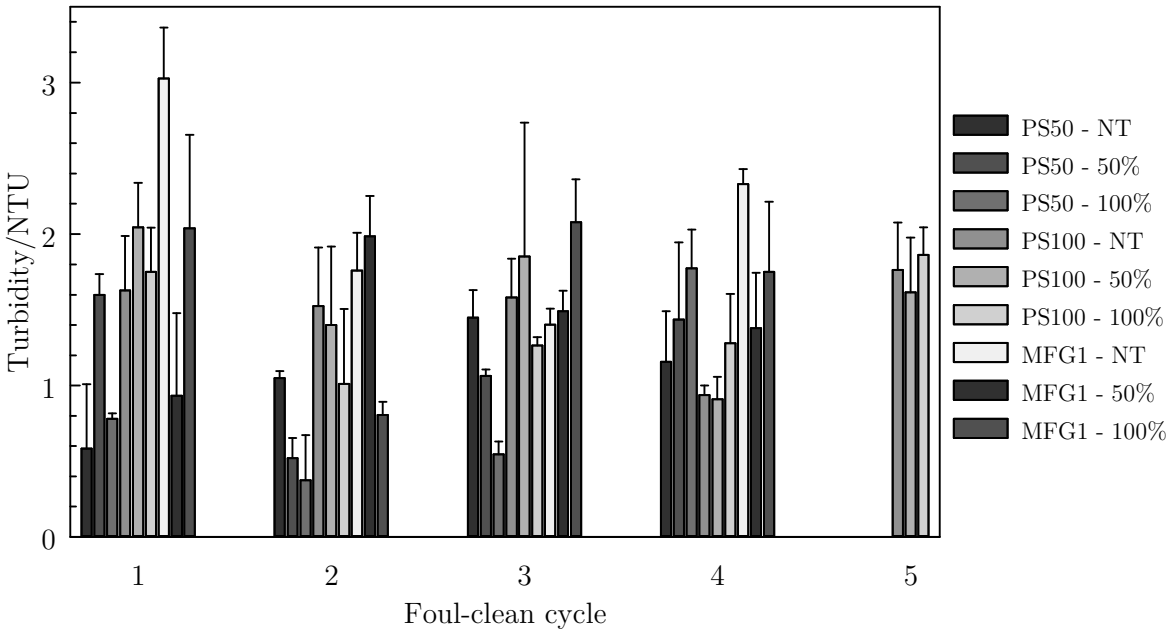

Figure 8-22 - Permeate turbidity (average over total filtration time)

8.4 Conclusions

The study has shown that the application of 50 wt.% and 100 wt.% ethanol treatment to commercially available polysulfone membranes is capable of simultaneously giving flux uplifts in terms of both PWF and filtration flux, and is able to mitigate the preferential rejection of polyphenols from the membrane when filtering black tea liquor.

It has been shown that the PS50 tested showed the highest gains in filtration fluxes following treatment, with 100 wt.% ethanol resulting in a significantly larger flux increase than for 50 wt.% ethanol. The application of the repetitive fouling and cleaning regime diminished the beneficial effects in terms of tea permeate flux though gains will still observed after up to 5 foul-clean cycles. When looking at membrane fouling resistances, it was observed that reversible fouling was lowered, implying that foulant bound more strongly to the membrane surface. This effect decreased with increased fouling number. The result was reinforced by the fact that the membrane became more hydrophobic after treatment; the ζ potentials of the membrane also showing a reduction in charge which implies greater fouling propensity.

Apparent was an incremental step-down in the transmission of polyphenols with repeated cycles, this also being shown by intensity increases in redness and yellowness of permeates. The solids transmission data did not show similar trends which suggests that the effect of fouling and caustic cleaning is bringing about a chemical and/or physical change to the membrane. It can be speculated therefore that there was no chemical structure modification to the membrane though it is still likely that physical changes could have occurred, either by charge modification or otherwise. Perhaps ζ potential measurements did not have suitable resolution to detect more subtle changes.

The work has shown that a membrane can potentially be tailored to allow for specific transmission requirements, though the improvement in behaviour of membranes in more realistic industrial scenarios is likely to be more sporadic and unpredictable. For the specific instances shown here, the net result of increased foul-clean cycle number was generally a movement in a positive direction, with no damaging effects upon the haze removing ability of the membrane.

9. Filtration of high concentration black tea streams for haze removal using polymeric microfiltration membranes

9.1 Introduction

Haze is a recurrent problem in beverages, particularly those with both protein and polyphenolic constituents where chemical interactions have been shown to cause 'creaming' of products post-processing and thus limiting shelf-life [248]. Whereas work in the UF regime has focussed on the modification of membrane properties for filtration, with the encompassing goal of removal of haze from low concentration (0.5 – 1.0 wt.%) tea streams, the MF experiments presented here concern the removal of haze from high concentration (~10 wt.%) feed streams. The requirement for high solids load filtration lies with the need to minimise processing loads so as to attain more highly intensified processes and so reduce capital expenditure on plant equipment.

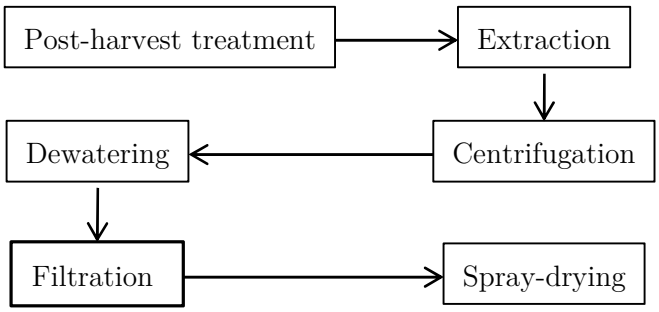

Figure 9-1 – Process overview for CWS tea production

The case presented here was industrially motivated. The project sponsors required a haze removal operation in their tea powder preparation process in order avoid chemical solubilisation by sodium hydroxide addition. The new unit operation can be seen inserted into the process flow chart shown in Figure 9-1.

The addition of sodium hydroxide up-modifies the pH from the natural state (~pH 4.5) so by reducing protein-polyphenol interactions shown to be at optimum conditions when at pH 4.0 [248]. The problem with pH modification is the uncontrollable formation of acid salts (sodium citrates) upon re-modification of pH with citric acid, used as a souring

agent in many beverage formulations. Sodium citrates (E331) are by no means a harmful by-product. On the contrary, they contribute to increased antioxidant activity in the bottle and the human body, regulate acidity, and have anti-coagulant properties with regard to blood clotting [324]. For these reasons they are approved for usage *quantum satis* by the European Parliament (European Parliament and Council Directive No. 95/2/EC). It is the uncontrollable excess salt formation which could begin to affect flavour and health giving properties in negative ways.

The work presented is a feasibility study of the potential for polymeric membrane MF to be applied as an alternative technology to traditional solubilisation as described previously. The relevance was clear as it supplied the company with useful information to further their research and development endeavour with regards to their process. The study was scientifically relevant as it presents findings for MF of high solids food streams, which are often overlooked. This fact is noticeable given the relatively low frequency of articles in the subject area.

9.2 Experimental aims and scope

There is an inherent haze in this stream; clarifying this was the main objective of the experimentation. Larger pore size membranes in the MF range were used for this study over UF membranes, namely PS05, PS09, PS15 (0.5 µm, 0.9 µm and 1.5 µm respectively).

The aim of the study was to investigate a range of operating parameters with a view to refining some optimum conditions for future development. Both tea quality and processing performance required assessment. Tea quality indicators were the turbidity of the filtered teas, the colour and total polyphenolics concentration. Process performance was assessed by filtration fluxes, total solids transmission, and the flux recovery after cleaning. In addition, resistance break-downs and mechanisms of fouling gave an insight into how fouling affects the process, which enables better strategic planning for future operations.

In a commercial environment, spiral wound modules would typically be used for large scale filtrations in which polymeric membranes are used. The results highlight the potential outcomes that these modules would have, but the study has employed a flat-sheet system to enable greater number of experiments.

9.3 Unfiltered tea properties

9.3.1 Turbidity of unfiltered tea

Turbidity was measured for the unfiltered tea to ascertain a benchmark for filtrations (Figure 9-2). 10 wt.% tea was diluted with a 3.0 wt.% citric acid stock solution to give a final acid concentration of 0.3 wt.% and 0.3 wt.% tea solids. The turbidity was found to be 86 ± 8 NTU. After storage with 0.01 wt.% sodium azide at RT, the turbidity increased to 117 ± 11 NTU after 2 weeks and 187 ± 32 NTU after 4 weeks. The

manufacturer highlighted a turbidity limit of 50 NTU as a requirement for the filtered tea.

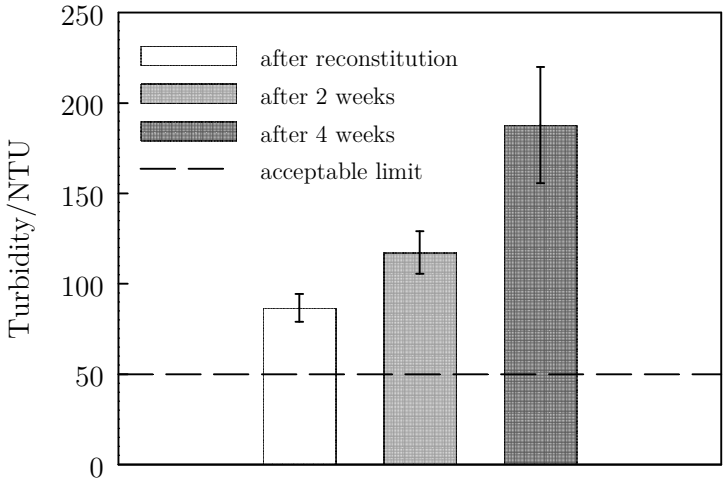

Figure 9-2 - Unfiltered tea turbidity

9.3.2 Colour of unfiltered tea

Tea was diluted from a range of concentrations (1.0 – 10.0 wt.%) to 0.3 wt.% with citric acid in the same ratio as in 9.3.1 before L*, a* and b*colour coordinate measurement. It was important to confirm that the diluted tea appearance was independent of initial concentration.

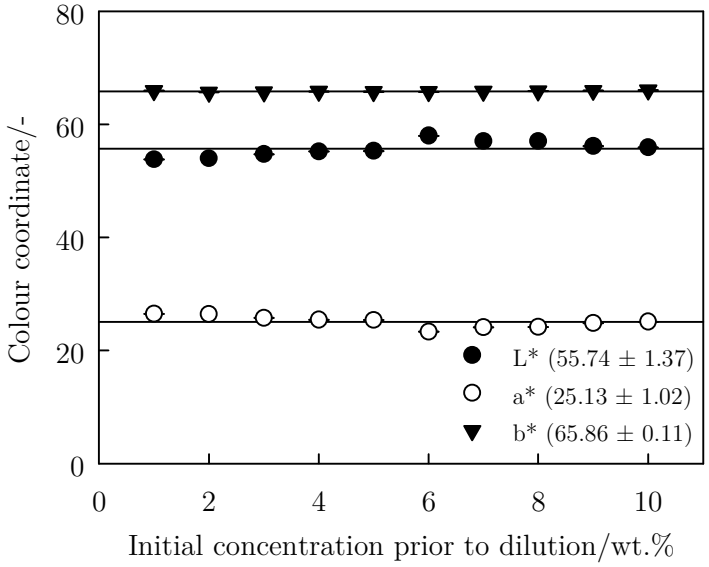

Figure 9-3 - Colour coordinates of 0.3 wt.% tea diluted from various concentrations

Figure 9-3 shows that the tea colour is consistent when diluted to the required strength from various stock solution concentrations. This shows that sample to sample error is eliminated with respect to varying dilutions and that variability in the partitioning of the cream and non-cream phases does not affect the colour significantly. Global averages and errors of the sample are shown in the legend to the right of the figure.

9.4 Results and discussion

9.4.1 Membrane performance

9.4.1.1. Flux change with TMP variation

Quasi-steady-state fluxes were measured across a 1.0 to 4.0 bar TMP range after 60 minutes in the laminar regime at 1.0 ms^{-1} ($Re = 1020$) for 10 wt.% tea and are shown in Figure 9-4. Limiting fluxes were approached for all membranes at 4.0 bar, the limiting values being approximately 10, 17 and 21 $Lm^{-2}hr^{-1}$ for PS05, PS09 and PS15 membranes respectively.

Field *et al.* (1995) [117] and Howell (1995) [319] describe the situation in which the flux-pressure relationship is divided into three regions, namely (i) sub-critical operation where flux increase is dependent on TMP and independent of membrane fouling related effects, (ii) TMP is above a certain critical pressure and there is time dependant flux, and (iii) where TMP far exceeds the critical pressure and severe cake formation limits fluxes. During constant flux operation; operating at sub-critical flux is thus accompanied by no change in TMP, whereas when operating above this critical point, a TMP rise is shown due to the onset of fouling. Brans *et al.* (2004) [325] state that in region (ii), flux is independent of pore size, which is not the case here; however the flux-pressure trend is not linear as would be the case in region (i). The results suggest that the working region is somewhere in the transition zone between (i) and (ii).

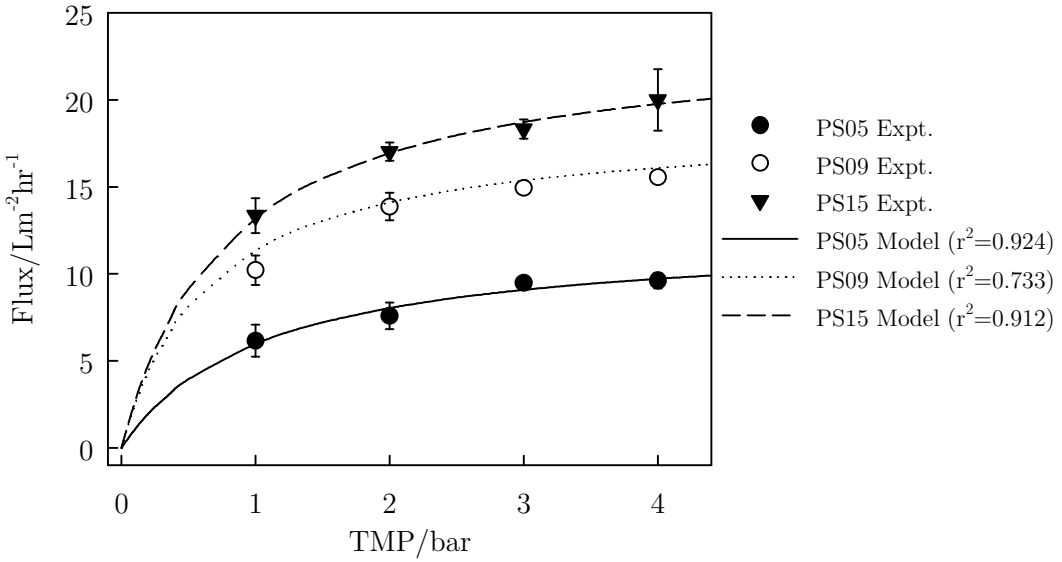

Figure 9-4 - Variation in flux with TMP

Thus there is a both a flux-pressure dependency and fouling onset has occurred, with the formation of a dynamic cake limiting the flux increase, which can be described by back-transport or gel filtration models [325]. The fluxes are still highly pore-size dependant, implying cake filtration is not the sole or even dominating mechanism causing declined fluxes.

Data fits have employed the resistance model, with the resistance causing flux decline expanded to account for back diffusion (CP) and fouling layer build-up (cake formation) as shown in equation 2-23. The expansion has been deemed suitable given the laminar flow regime, these flow dynamics are unlikely to prolifically disturb the cake settling and resulting solute accumulation/deposition on the membrane surface. Also given the high solids concentration, indication that back-diffusion from the cake/CP interface across the CP boundary layer, and the associated resistance, is substantial.

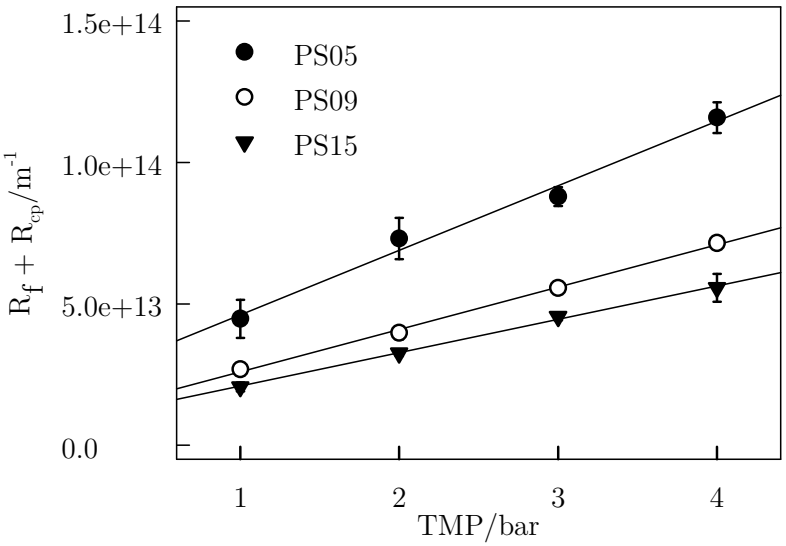

Figure 9-5 - Combined resistance caused by fouling and concentration polarisation with varied TMP

By subtraction of R_m from the total resistance R_T, $R_f + R_{cp}$ can be determined. The expanded resistance term is shown graphically in Figure 9-5. The combined resistance shows a linear increase with TMP. The quantitative breakdown of this term is discussed later.

9.4.1.2. Solids transmission

Total solids transmission by dry weight measurement of feed and permeate samples was carried out after 1 hour of filtration (at the same time as quasi-steady state flux assumption). The trend observed is that of a negative linear correlation with TMP ranging from ~79% solids transmission at 1.0 bar to ~69% transmission at 4.0 bar for the PS15 membrane, and in the worst case, 61% to 42% over the same pressure range for PS05 membranes (see Figure 9-6).

The observation of increased rejection of solutes with TMP has been noted by a number of authors. Blanpain *et al.* (1993) [326] reported that a rejection increase over both processing time and TMP increase was significant during MF of ~12 nm silica colloids. Penders *et al.* (1998) [327] also noted that when TMP was stepped from 10 kPa to 100 kPa, increased rejection was recorded for MF of lager beer solutes, although for the filtration scheme in this article (dead-end stirred), the effects of retentate concentration cannot be ruled out as affecting the rejection, despite the presence of an excess feed

reservoir. These finding are indicative of this process, with both authors pointing towards the theoretical hypothesis that in the early stages of filtration, pore plugging (through a standard blocking mechanism) acts to reduce the effective pore diameter (internal fouling), followed by the onset of a surface cake acting as a composite membrane (external fouling) due to protein-membrane interactions [327]. With higher pressures, cake layer compaction occurs and increased CP is in effect, resulting in a raised rejection of the composite membrane given the now effective 'tighter pores'.

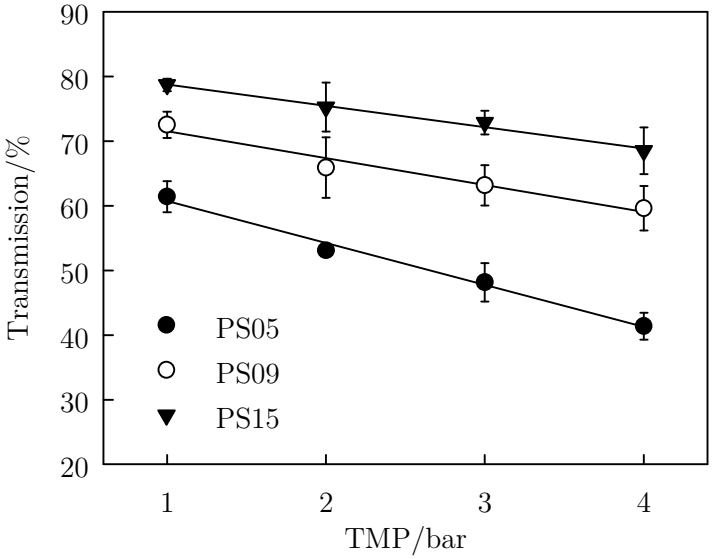

Figure 9-6 - Transmission of total solids

9.4.1.3. Mass transfer

Concentration was varied in order to determine experimental mass transfer coefficients (MTCs) for total solids with a view to aiding future process design. 1.0, 5.0 and 10.0 wt.% solutions were filtered through PS09 and PS15 membranes with solids transmission being monitored at the quasi-steady state point. PS05 was excluded from this experimentation due to the unacceptable loss of solutes recorded during flux-TMP experimentation.

By calculation of apparent rejection coefficients R_{app} and flux J, the integrated form of the boundary layer model (eq. 8-1) can be used to deduce the MTC, k, by plotting J against $\ln[R_{app}/(1-R_{app})]$ (see Figure 9-7). The same method was followed by Evans (2008) [176], which also describes membrane filtration of tea, but in that instance, UF of low concentrations (0.5 – 1.5 wt.%) was carried out. The inverse of the slope gives the experimentally measured MTC, and the intercept and subsequent rearrangement gives an estimate of the maximum concentration at the membrane surface (C_m). The experimentally measured and derived values are displayed in Table 9-1.

$$ln\left(\frac{R_{app}}{1-R_{app}}\right) = ln\left(\frac{R_{max}}{1-R_{max}}\right) + \frac{J}{k} \qquad (8\text{-}1)$$

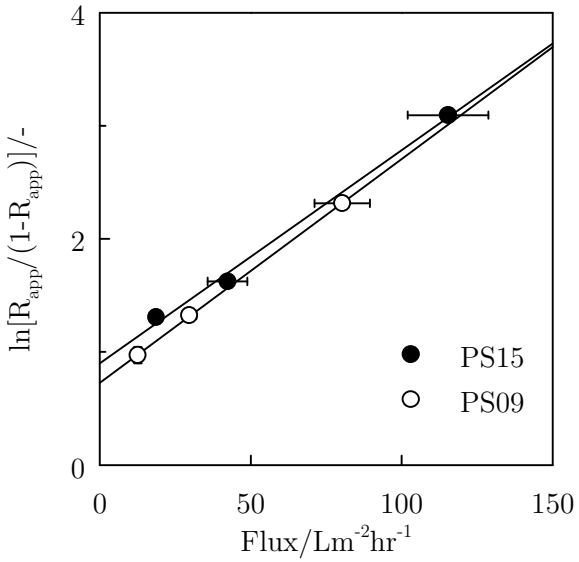

Figure 9-7 – Linearised plot of equation 8-1 for MTC determination

The calculations in Table 9-1 show that there is marginally better mass transfer across the PS15 membrane as can also be deduced from rejection coefficients. The relationship $k = D/\delta$ must be considered where D is the diffusion coefficient and δ is the CP boundary layer thickness. For constant diffusion and mass transfer i.e. at steady state conditions, boundary layer thickness will be slightly greater for the PS09 than PS15 membrane meaning performance is hindered more due to CP for the smaller pore size membrane. This is thus a causation for the lower observed fluxes, even though the driving force (concentration gradient) in the boundary layer is greater for the PS15 membrane. Overall, the findings provide evidence that a concentration gradient over a boundary layer at the membrane service is evident and that CP plays an important role in limiting the fluxes. For these reasons it is advantageous to work at sub-critical (lower) fluxes. This was also the case when operating in the UF regime (section 5.9). In order to specifically determine these values, a study operating at constant flux would be required.

Table 9-1 - Maximum rejection coefficients, membrane surface concentration and MTCs

Membrane	J/ $Lm^{-2}hr^{-1}$	C_b/ *wt.%*	C_p/ *wt.%*	R_{app}/ -	R_{max}/-	C_m/ *wt.%*	k $\times 10^{-5}$/ ms^{-1}
PS09	80.3 ± 9.2	2.01	1.83	0.090	0.326	2.59	1.40
	29.7 ± 2.3	4.99	3.94	0.210		5.54	
	12.6 ± 0.5	9.54	6.92	0.275		9.74	
PS15	115.4 ± 13.3	1.95	1.86	0.043	0.289	2.62	1.47
	42.3 ± 6.5	5.12	4.28	0.165		6.02	
	18.7 ± 1.7	9.76	7.68	0.213		10.81	

9.4.1.4. Resistance calculations

Resistance break-downs were quantified by recording the flux at various points during the fouling and rinsing process. Calculations show that resistances during fouling were dominated by concentration polarisation for all membranes as shown in Figure 9-8. An increase from $1.57 \times 10^{13} \pm 1.92 \times 10^{12}$ to $8.19 \times 10^{13} \pm 3.24 \times 10^{12}$ for the PS05 membrane between 1.0 bar and 4.0 bar; this representing over a 5-fold increase. This proportion of increase was repeated for PS09 and PS15 also.

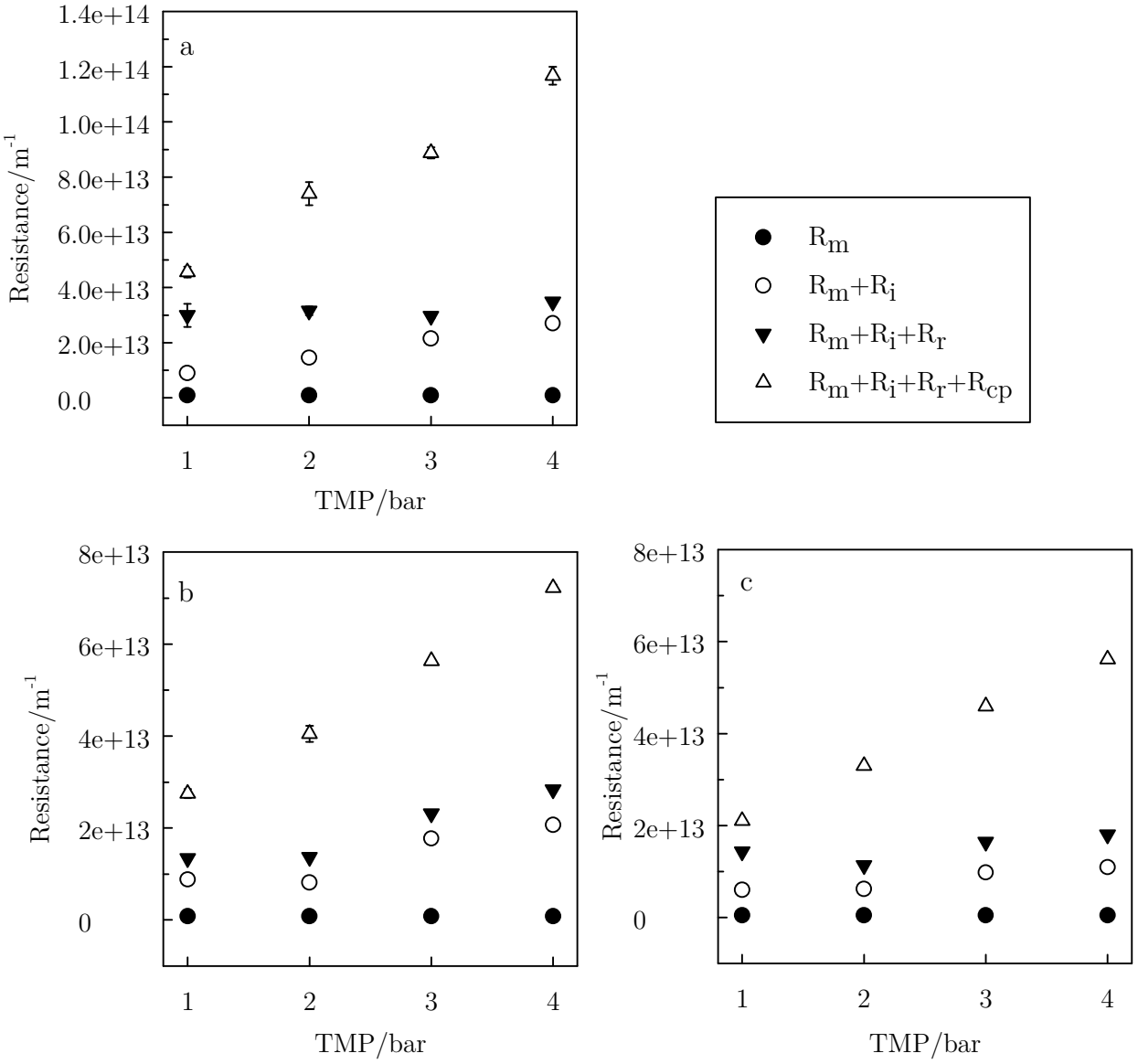

Figure 9-8 - Resistance break-down for membranes (a) PS05, (b) PS09 and (c) PS15

Another trend worth noting is that of the transition from rinsable fouling at lower TMP to irreversible fouling at higher TMP. The ratio of reversible to irreversible fouling (as a total of R_f) shifts from 0.28:0.72 to 0.77:0.23 for the PS05 membrane over the TMP range, for PS09 this change is from 0.64:0.36 to 0.72:0.28 and for PS15: 0.4:0.6 to 0.6:0.4. The additional TMP compacts the deposited cake layer, which reduces the amount of foulant removable with shear forces present at the membrane surface during rinsing.

9.4.1.5. Effect of cross-flow velocity

Cross-flow velocity was varied in the workable range from 0.5 – 1.5 ms^{-1} at 1.0 bar TMP. Additional CFV was successful in boosting steady state fluxes from 7.3 ± 1.1 $Lm^{-2}hr^{-1}$ to 12.2 ± 0.5 $Lm^{-2}hr^{-1}$ for PS09, and 8.5 ± 0.9 $Lm^{-2}hr^{-1}$ to 16.4 ± 2.0 $Lm^{-2}hr^{-1}$ for the PS15 as shown in Figure 9-9a. Increases in CFV are known to induce greater shear forces on the membrane or surface layer acting to mediate cake growth. In this instance,

a rise from 0.5 ms^{-1} to 1.5 ms^{-1} results in an increased wall shear stress from 5.4 to 16.3 Nm^{-2} (assuming Newtonian fluid behaviour) (See Appendix C5).

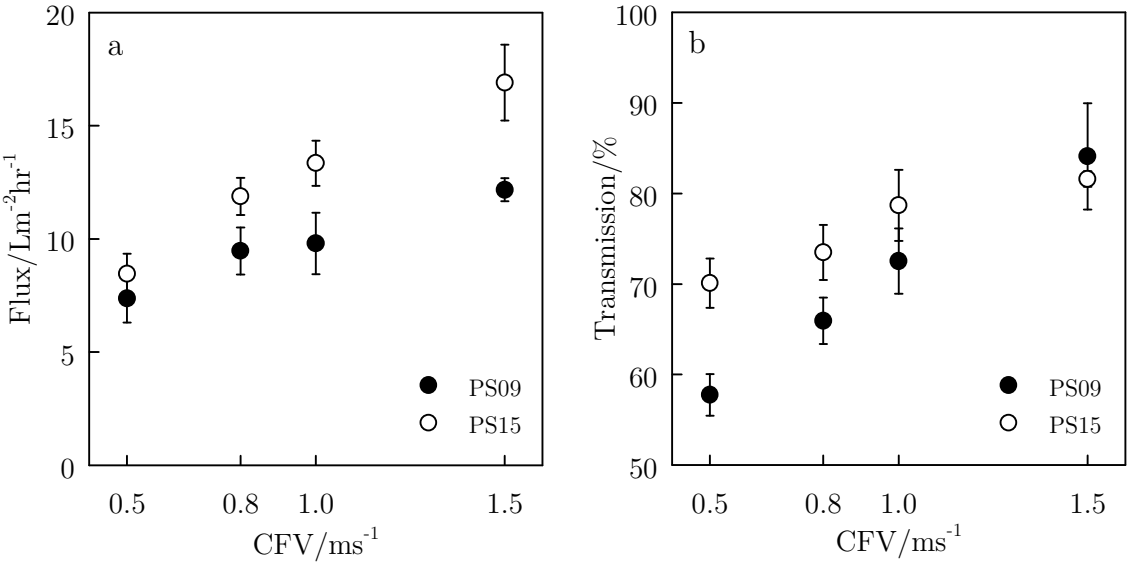

Figure 9-9 –Flux vs. CFV plots for (a) PS09 and b) PS15

Also in effect is the increased solids transmission, ranging from 58 ± 2% to 84 ± 6% and 70 ± 3 to 81 ± 1% for PS09 and PS15 respectively. Head and Bird (2013) [59] indicated the same effect when filtering high solids content milk protein isolate for the removal of spores, noticing a solids transmission increase from 6.4% to 10.7% and also an increased protein transmission of 15% to 19% when filtering with a 1.4 µm ceramic membrane at 0.7 and 1.4 ms^{-1} CFV. Van der Berg *et al.* (1989) [127] state that $k \propto CFV^{0.33}$ when operating in the laminar regime as is the case here (Reynolds numbers of between 510 and 1531). The changes in flux monitored here suggest changing the CFV will affect performance significantly. Apparatus modification would have been required to gain CFVs whereby the flow regime is in the turbulent region i.e. Re > 2300.

9.4.2 Fouling mechanism determination

The cross flow filtration blocking laws as described by Field *et al.* (1995) [117] were applied to the flux data in MATLAB® using the methodology of De Barros *et al.* (2003) [119] to understand the mechanism of fouling in the early stages of filtration and what affect pressure may have. The authors analysed the flux decline data produced from the UF of pineapple juice and found strong dependency on both complete blocking (where $n = 2$) and cake filtration (where $n = 0$), with the complete blocking mechanism dominating the first 0 – 20 minutes of fouling time and cake filtration (and in fact all) mechanisms converging to a limiting flux value by final stages of filtration. They affirm that complete pore blockage was the dominant mechanism when comparing SSR values of model fits.

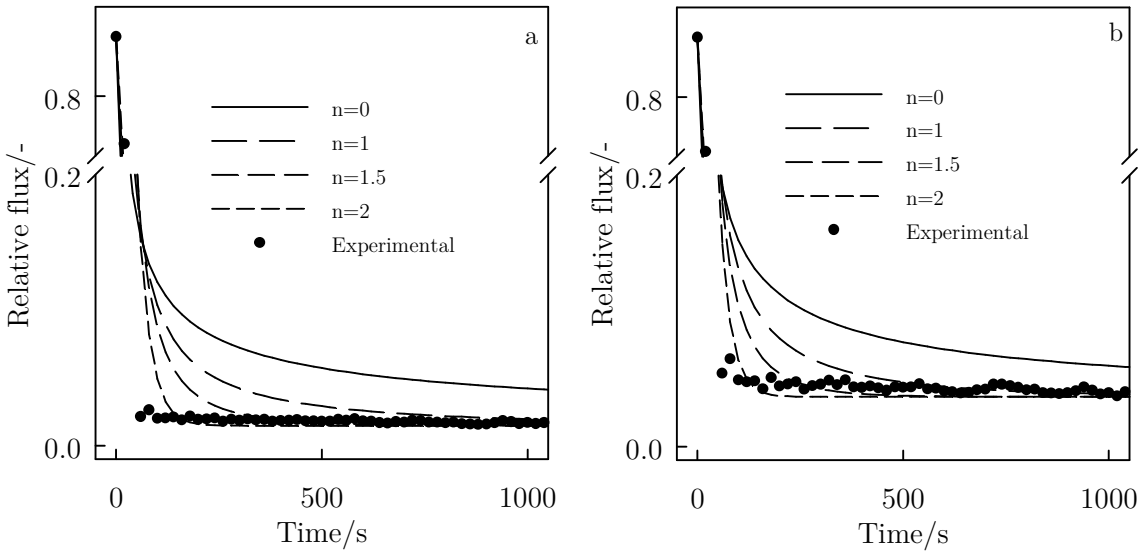

Figure 9-10 - Fitted pore blocking models for (a) PS05 at 1.0 bar TMP. (b) PS05 at 4.0 bar TMP

For PS05 membranes in this study, generally all models fitted the data reasonably well (see Figure 9-10 and Table 9-2) considering the SSR and r^2 fitting criteria. However, due to the prolific and almost instantaneous flux decline, models were deemed only partially sufficient in describing the flux behaviour in terms of specific blocking laws. It is shown that for greater TMPs and larger pore sizes, the models statistically fit the flux data better due to the lower relative flux decline.

This is potentially a topic of further investigation as it would seem that there is an almost instant cake formation restricting the membrane permeability from <40 seconds after the commencement of filtration for 10.0 wt.% feed concentration. It would seem that a firm theoretical understanding of this is missing from the literature. It could be speculated that given the high solids load in the feed, the rapid accumulation of solutes at the surface could push the boundary layer concentration to one exceeding the solution saturation point for the tea/water system, thus depositing solute on the surface.

Table 9-2 - Fit parameters, SSR and determination coefficients for blocking mechanism models at various TMPs

Membrane	*TMP*	$n = 0$ *(cake filtration)*			$n = 2$ *(complete blocking)*		
		$k_c \times 10^{-1}$	$SSR \times 10^{-1}$	r^2	$k_b \times 10^{-1}$	$SSR \times 10^{-1}$	r^2
PS05	1.0	3.69	3.26	0.690	0.42	0.08	0.993
	2.0	4.05	0.75	0.927	0.51	0.02	0.998
	3.0	3.77	1.04	0.900	0.46	0.05	0.996
	4.0	3.77	0.95	0.909	0.46	0.04	0.996
PS09	1.0	2.10	7.81	0.303	0.22	2.30	0.853
	2.0	2.57	2.37	0.779	0.35	0.35	0.971
	3.0	2.48	2.43	0.774	0.34	0.40	0.968
	4.0	2.53	2.00	0.813	0.36	0.27	0.978
PS15	1.0	3.93	0.73	0.930	0.51	0.03	0.997
	2.0	2.73	1.69	0.842	0.37	0.12	0.990
	3.0	2.41	3.06	0.719	0.28	0.74	0.946
	4.0	2.59	2.09	0.805	0.36	0.26	0.978

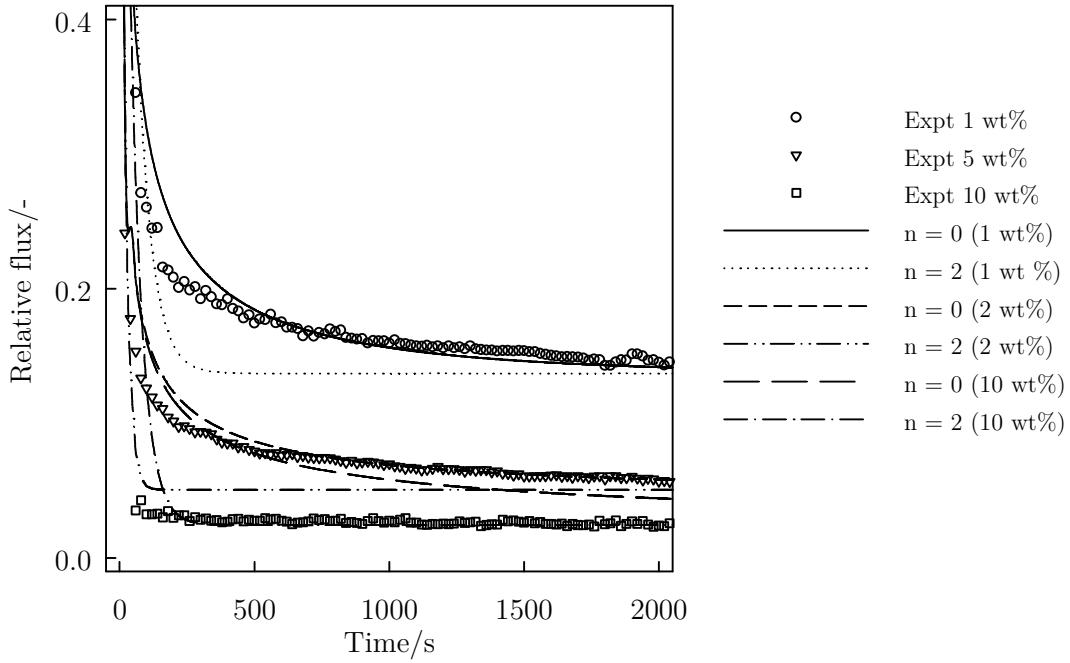

Figure 9-11 - Flux decline models for various concentrations of tea for PS09 membrane

Data fits for varied concentration experimentations were also carried out as shown in Figure 9-11 and Figure 9-12. For 1.0 wt.% tea, data for both PS09 and PS15 follow a good correlation with the cake filtration model ($r^2 > 0.94$ in all cases as noted in Table 9-3), with arguably initial fluxes for the PS09 membrane fitting the complete pore blocking model accurately until a transition to the cake region takes place (region between *ca.* 100 and 500 seconds). The apparent transition between mechanisms is repeated for 5.0 wt.% tea but appears to begin earlier and at a much lower relative flux i.e. the cake build up is more rapid. It follows that for 10.0 wt.% tea, cake formation could be almost instantaneous.

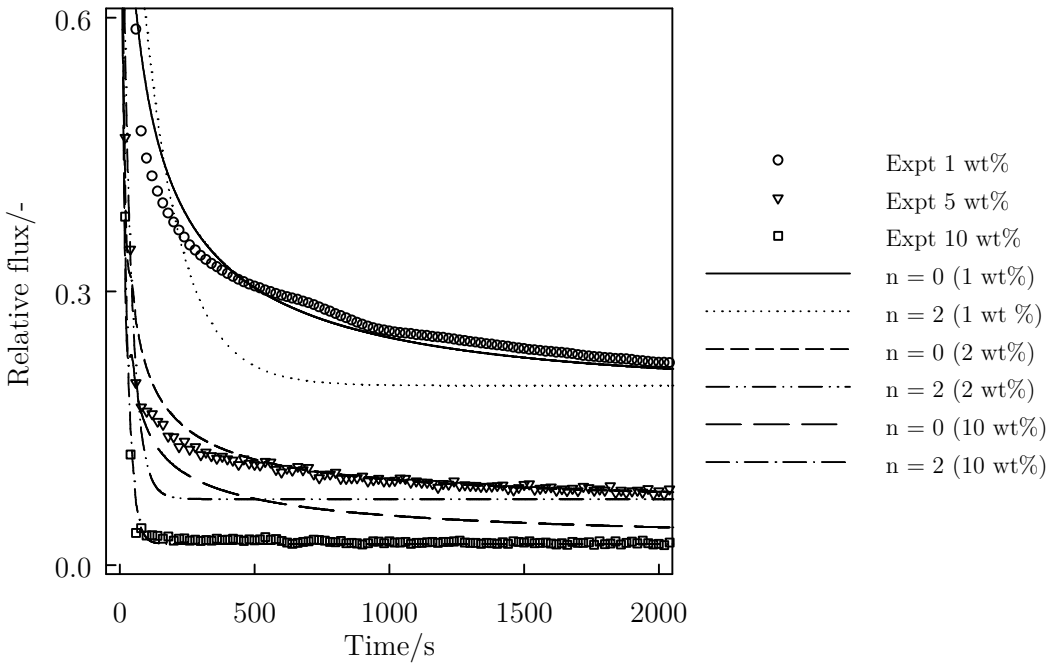

Figure 9-12 - Flux decline models for various concentrations of tea for PS15 membrane

Table 9-3 - Fit parameters, SSR and determination coefficients for blocking mechanism models at various feed concentrations

Membrane	*Conc.*	$n = 0$ *(cake filtration)*			$n = 2$ *(complete blocking)*		
	wt.%.	$k_c \times 10^{-1}$	$SSR \times 10^{-1}$	r^2	$k_b \times 10^{-1}$	$SSR \times 10^{-1}$	r^2
PS09	1.0	2.28	0.07	0.994	0.59	0.92	0.907
	5.0	0.65	0.70	0.942	0.19	0.97	0.930
	10.0	2.10	7.81	0.303	0.22	2.30	0.853
PS15	1.0	0.19	0.93	0.950	0.07	4.18	0.824
	5.0	1.34	0.22	0.981	0.32	1.06	0.910
	10.0	3.93	0.73	0.930	0.24	4.95	0.675

As a consequence of the severe flux decline, data for the larger pore size membranes appears to fit the complete pore blocking model most consistently across the duration of the filtration, as this form of the equation will tend to describe the more 'sharp' flux decline, even when in fact a cake layer was visibly present. The cake layer model offers a generally unsatisfactory representation for the large relative flux declines with high solids load feeds in the early stages of filtration. In retrospect and despite the modelling outcomes, it would be safe to assume that in-pore and surface fouling would both be contributing factors for the high solids load filtrations, though what mechanism dominates can only be speculated using the evidence from these examples.

9.4.3 Tea quality upon filtration

9.4.3.1. Haze reduction

Haze was measured to see the effect of MF. Results show that for tea filtered and measured immediately following dilution to 0.3 wt.%, haze removal is superior for PS05 membrane over PS09 and PS15 membranes (Figure 9-13). This would be expected given the smaller pore diameter and thus better efficiency in separating out haze aggregates.

There was no significant change in the haze for all TMPs tested for PS05. Observable is that operating at a lower TMP acted to reduce haze more effectively than at higher TMPs. This is as expected and be would be implied if only solids transmission data was considered. These findings suggest that haze causing aggregates can transmit through the membrane (and cake layer) more readily than other solutes with these pore sizes.

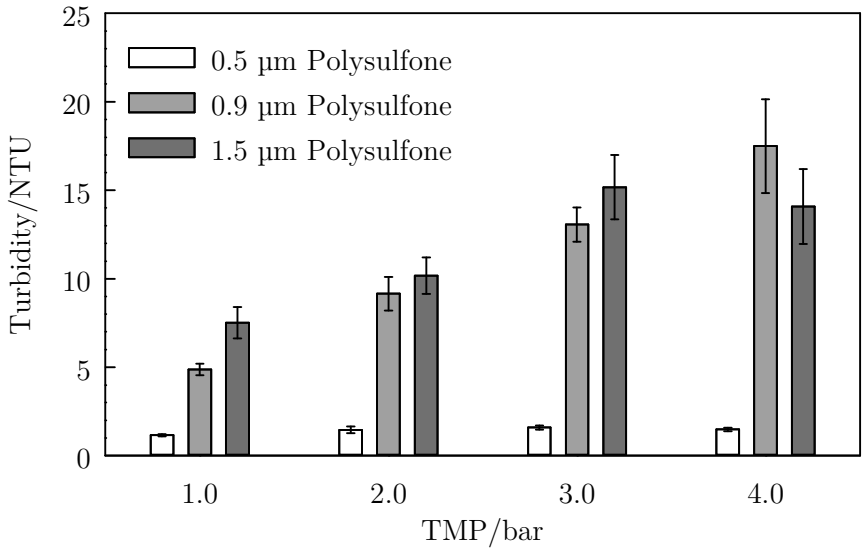

Figure 9-13 - Haze removal at various TMPS directly after filtration

The reasoning for this is that aggregates (protein-polyphenol, protein-caffeine interactions, and other interactions stabilised by metal cations) would be transmitted to the membrane surface through convective flow, as like any other solutes. With the formation of the CP boundary layer, diffusion of these larger aggregates would be lower than smaller un-associated molecules. This would result in a proportionally greater concentration at the membrane surface of aggregates to unbound solutes, and thus a better chance of transmission is presented. Given that CP is increased with TMP, the effect would be more pronounced at greater pressures. Also, upon aggregation, charge neutralisation between associating species would occur thus reducing solute-solute and solute-membrane charge interactions. These theories would suggest that the PS05 membranes creates a more robust barrier (through steric exclusion) to the tea than the PS09 and PS15 counterparts and that haze removal performed by PS09 and PS15 is due more to the composite foulant layer formed than by the membrane itself. Liang and Xu (2001) [239] show that when extracting black tea from fermented leaves, tea-cream particle size measured with light scattering (for pH 1.2, 3.0 and 9.0) showed a major size peak between 0.2 and 0.8 µm (and another smaller peak between 5 and 50 µm), with the greater peak intensity (in terms of volumetric fraction) appearing for the 0.2 to 0.8 µm pH 3.0, the closest to pH of the tea in this instance (around pH 5.5 - 6.0).

Tea was left in cold-storage and turbidity was measured again after 2 and 4 weeks in order to gain insight into how haze reforms, an indication of shelf-life improvement. Figure 9-14 shows an image of filtered and unfiltered tea. These images show that after MF (top right) a much lighter, brighter and clearer tea is produced. This means a more

visually appealing product from a consumer perspective over the unfiltered tea is produced.

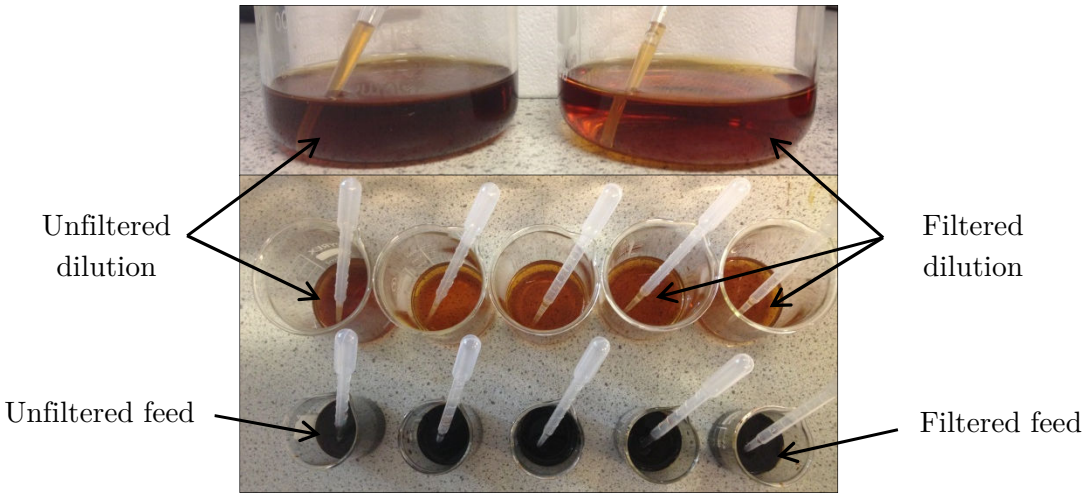

Figure 9-14 – Tea appearance change upon filtration

Figure 9-15 shows the quantitative analysis of haze reformation over time at various TMPs. Haze reformation for PS05 membrane remains low after 4 weeks in comparison to PS09 and PS15. The sample with most clarity (1.0 bar TMP for PS05) rises from 1.1 ± 0.1 NTU to 6.0 ± 0.7 NTU and the 4.0 bar (lowest initial clarity for PS05) rises from 1.5 ± 0.1 NTU to 7.7 ± 0.9 NTU. Haze reformation is greatly increased as pore size increases. In the least effective instances (at 4.0 bar for PS09 and PS15) haze rises from 17.5 ± 2.7 NTU and 14.1 ± 2.1 NTU to 50 ± 4 NTU and 55 ± 11 NTU for the respective membranes. These results would be deemed insufficient by comparison to the manufacturer's requirements. The PS09 and PS15 membranes do perform to an adequate standard at lower TMPs, where turbidity rises from 4.9 ± 0.3 NTU to 29.4 ± 4.3 NTU (for PS09) and 7.5 ± 0.9 NTU to 36.5 ± 9 NTU for PS15 (both changes being for 1 bar TMP).

Time course formation of haze has been shown for various foods. Results for grape juice, cranberry juice and apple juice show a plateau phase over the initial time course (~20 days) and then a sharp increase in turbidity [255]. McMurrough *et al.* (1992)[263] show that with lager beer this plateau region is shorter and chill haze formation begins much earlier (within 2 days).

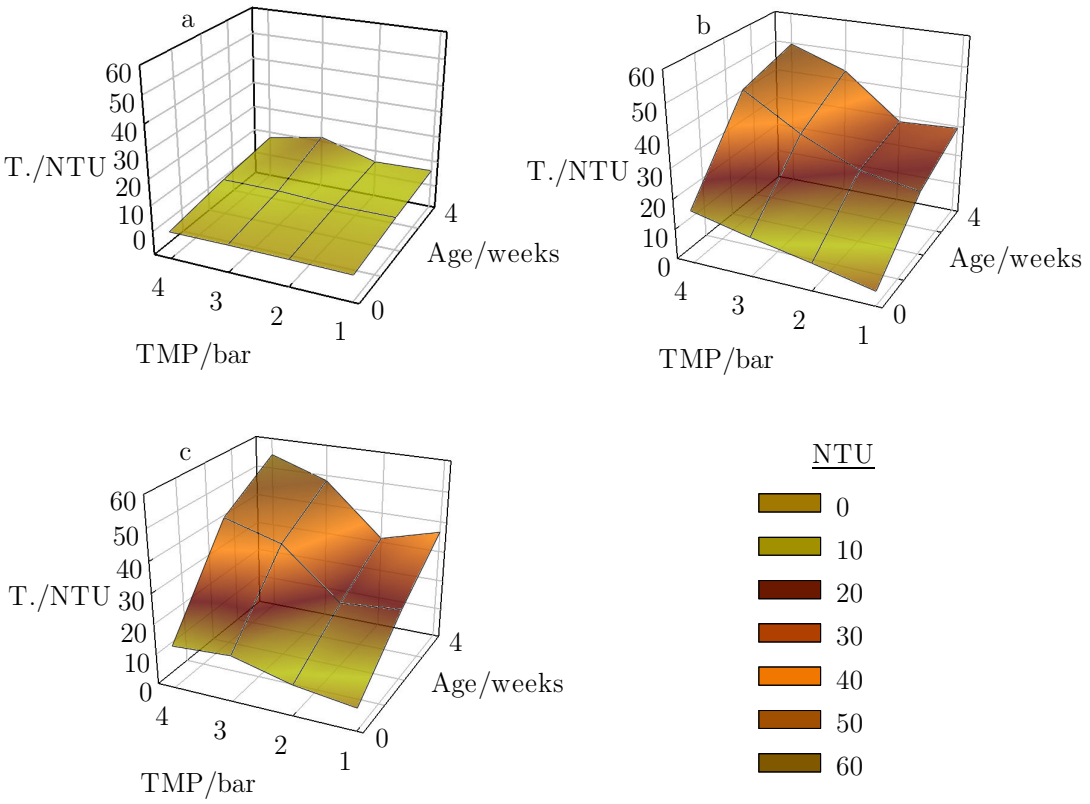

Figure 9-15 - Surface plots showing haze reformation for teas filtered with (a) PS05, (b) PS09 and (c) PS15 membrane over time at various TMPs

The data collected suggests that there appears to be a critical maximum turbidity value at which haze reformation is substantially reduced - achievable with the PS05 membrane. This value occurring around 2 – 3 NTU for freshly filtered tea streams and above which, haze reformation occurs more prolifically over time. This critical value, if significant, would require more refinement by reducing the mesh size for the experimental procedure and likely requiring the introduction of more process variables. This however was not within the scope of this study. Understanding how this value can be related to the chemistry of the constituents would require a more rigorous understanding of the binding capabilities of the given components, aggregate growth kinetics, and the resulting partitioning characteristics of the cream phase and soluble phase.

Penders *et al.* (1998) [328] showed from their light scattering studies of tea-cream that hydrodynamic radius of particles increase over time implying small tea cream particles accumulate in size over time. With this in mind, expulsion of already formed tea-cream particulates from the permeate side of the membrane will not only reduce haze in the short-term, but retard the long-term formation. Results from this study (for PS05) reinforce these findings.

9.4.3.2. Lightness and colour

Colour results show that after dilution of the tea, lightness was higher for permeate of the smaller pore size membranes (Figure 9-16). Liang and Xu (2003) [261] attributed a darker tea to a better quality product with more total TFs present. The lightness data collected here shows progressive lightening with increased TMP indicating that tea filtered at higher pressure has a greater proportion of TFs removed. Also noteworthy is the lightness increase over the duration of the filtrations. This indicates that as foulant built up on the surface of the membrane, lower transmission of TFs occurred. This effect was shown in analogous experiments using UF membranes, different tea infusions, and lower concentrations meaning the effect is non-system specific.

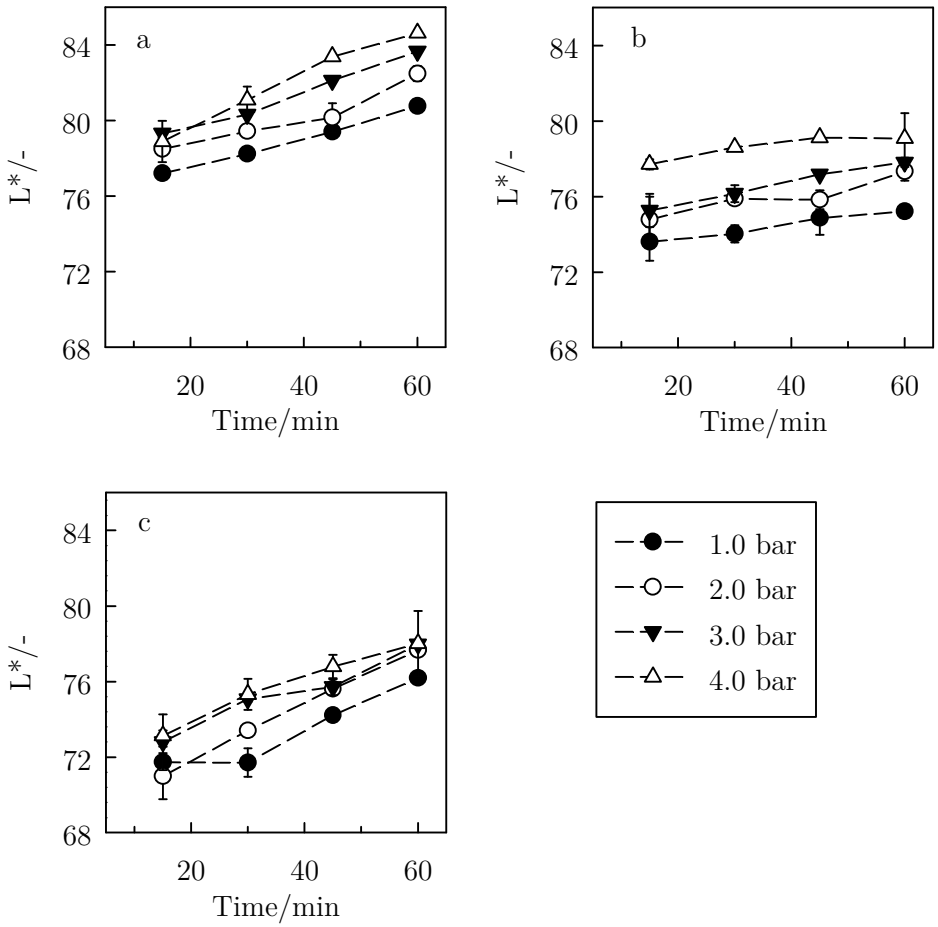

Figure 9-16 - Lightness (L*) after MF (a) PS05, (b) PS09 and (c) PS15

It has been found that redness and yellowness is also correlated to TFs content [261] (or more generally orange colour [244]). In a sensory evaluation performed by Liang and Xu (2003) [261], positive correlations were drawn between appearance and quality (TFs content shown to be an indicator of this) as well as greater TFs concentration giving higher scores for aroma and taste perception. Figure 9-17 shows a* and b* colour coordinates measured for MF permeates. Generally, there is an overall loss in red and an increase in yellow for all permeates. Scharbert *et al.* (2004) [244] also indicate that

TRs produce the red-brown pigmentation in tea brews, which would contribute to a darkening of the tea brew. Wu and Bird (2007) [33] showed that when fouling tea component mixtures, TRs led to higher levels of fouling of UF membranes and greater levels of TFs rejection as a result. This observation *a posteriori* would lead to a more yellow, less red and lighter tea due to selective transmission of species.

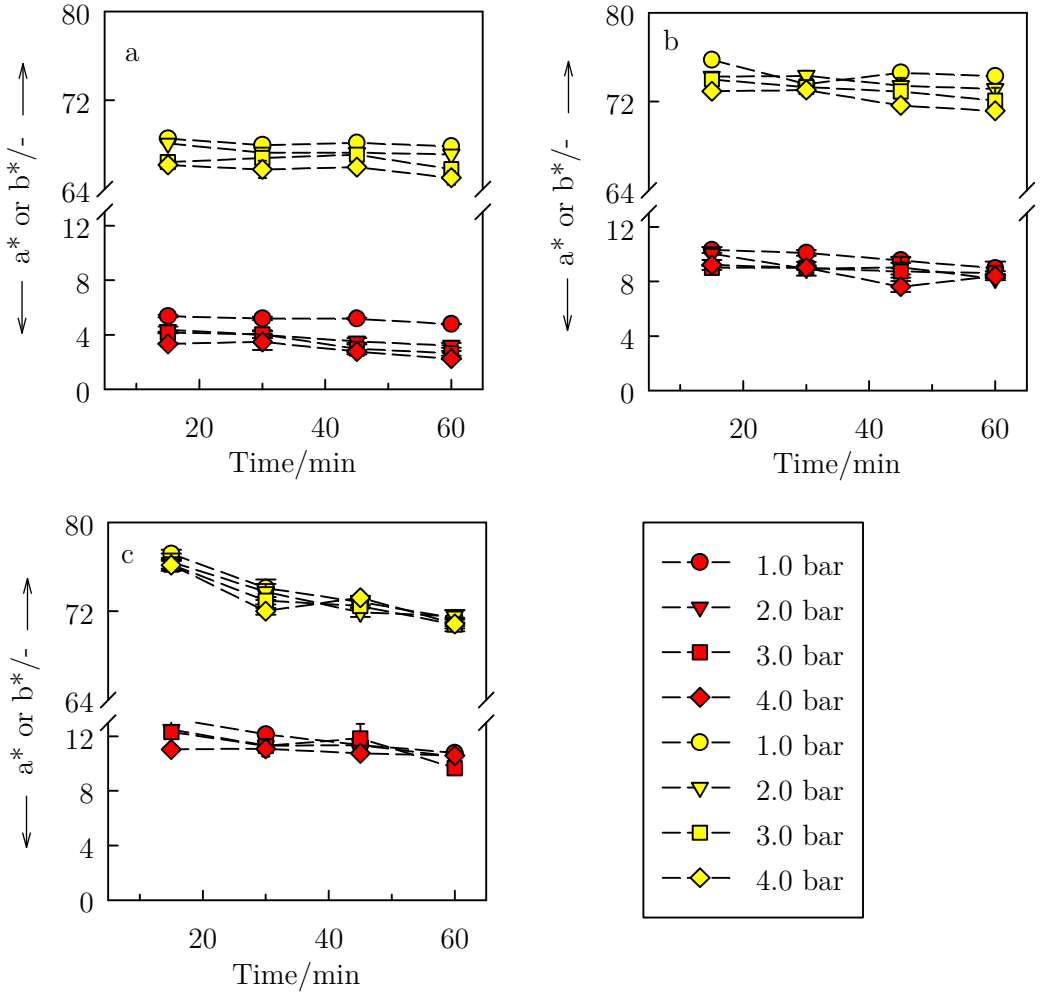

Figure 9-17 - Redness (a*) and yellowness (b*) for (a) PS05, (b) PS09 and (c) PS15

9.4.3.3. Total Polyphenols

Total polyphenols was measured as a complimentary technique to monitor tea quality in reinforcement to the colour losses found. The findings presented in Figure 9-18 show that there is disproportionately less polyphenols transmitting through the membrane, especially at lower pore size. In the worst case (PS05 at 4.0 bar) only 26.3 ± 3.1% are transmitted, this compared to 42% of solids. For PS09 and PS15 membranes, 61.2 ± 2.9% and 56.7 ± 3.0%' of total polyphenols are transmitted (in comparison to 73% and 79% of solids. The results again demonstrate that there is a preference for non-polyphenolic species to transmit the membrane even when polyphenols have generally lower molecular weights (especially gallo-catechins and TFs) than other solutes present in black tea such as proteins, polysaccharides and cellulosic plant matter. It was postulated by Wu and Bird (2007) [33] when conducting UF experiments with TF/tea

protein mixtures that the aggregation of the proteins and polyphenols species dominated the charge at the membrane surface, and upon cake layer deposition, increased the negative charge of the system to one greater than a membrane fouled solely by tea protein alone, thus restricting further polyphenol and protein transmission. The authors also indicate that unbound TFs filtration fluxes displayed signs of strong concentration polarisation, another indicator for the preferential transmission of non-polyphenolic solutes.

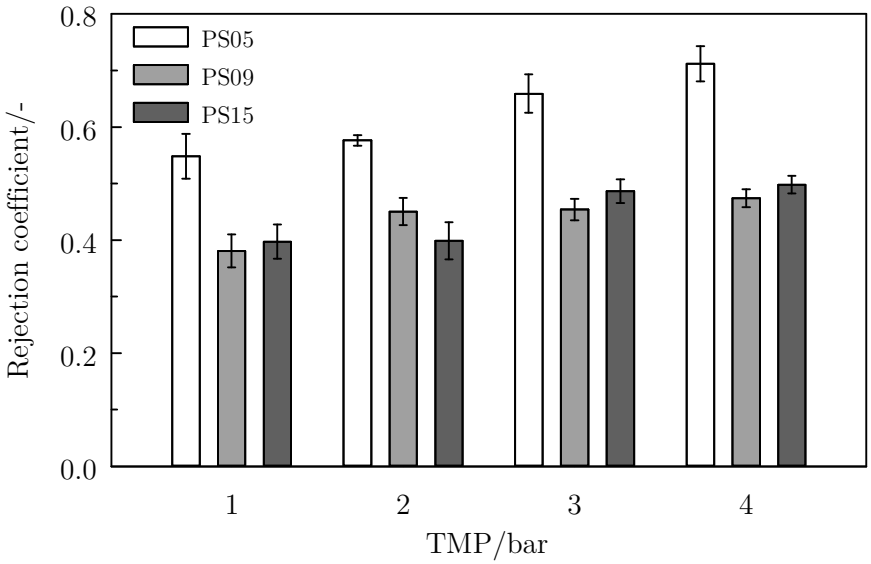

Figure 9-18 - Total polyphenols for tea permeates

Aside from the PS05 membrane, there was a marginal but insignificant increase in rejection between TMPs suggesting that factors such as cake layer deposition, cake growth and CP may not be entirely responsible for the rejection of the majority of polyphenols, and that interactions between the species and the membrane material itself are possibly the significant factors. These findings indicate that modification to membrane properties such as hydrophobicity and charge could help to reduce the shortfall in solute transmission and thus reduce the quality of the tea product with regard to key polyphenolic species. These are significant results as they show that MF membranes may be selective on a charge basis when traditionally their separation performance is thought to be that of size exclusion alone.

9.4.4 Conclusions

MF has been shown to be effective in the haze removal and haze prevention of high solids concentration tea solutions. Filtrations showed variability in product quality, typically with a trade-off between acceptable solids transmission and haze reduction and flux. For all membranes examined, there was sufficient haze removal to satisfy the producer's requirements, and the haze reoccurrence was significantly reduced.

Given the high concentration of the feed, both CP and cake filtration played dominant roles in reducing flux, as was expected. Nevertheless, fluxes at the lower end of what

would be deemed industrially acceptable were gained. In efforts to maximise these fluxes by use of larger pore size membrane, haze reduction efficiency and increase in haze reoccurrence was sacrificed somewhat. The PS05 membrane showed greatest promise in terms of haze reduction although the high solids rejection meant that the total product loss was unacceptable.

Looking to the future – regimes for minimisation of product loss such as constant and variable volume diafiltration would be promising candidates for this if the strict requirement for such a concentrated feed could be relaxed. Studies for multiple tea fouling and cleaning of polymeric membranes have shown that flux increases and solute transmission are improved with membrane age (as detailed in this thesis) and would thus need investigation. Other aspects for batch processing operation are the application of tubular ceramic membranes operated at high CFV. These membranes are suitable for high solids load feeds as was demonstrated by Head and Bird (2013) [59] for milk protein isolate, and in combination with backwashing [189]. CFV variation results in this study showed promise as a useful strategy in both maximising flux and minimising product loss. These strategies are likely to produce an improvement in the solids transmission values achieved in this study. The fouling aspects would also be of interest as limited work has been carried out to date using ceramic membranes (only Todisco *et al.* (2002) [30] to date).

10. Conclusions, recommendations and future developments

It was the intention in this thesis to conclude each experimental section individually based on their relative scientific merits. It leaves this chapter with more simplistic function – to draw together the more general findings from the aforementioned chapters, and to conclude the overall thesis narrative.

A summary of the key findings are:

- Industrial PS membranes are modified by alcohol giving performance uplifts in terms of permeability with pure water.
- Mechanisms of modification are varied and encompass swelling related effects, apparent polymer surface modification and leaching of pore forming agents.
- The result of these modifications are changes to the surface chemical and physical properties of the membrane, namely hydrophobisation (likely due to leaching of PVP), net through-pore zeta potential reduction, mechanical modification through polymer plasticisation, and leaching of sub-surface material.
- Whilst being apparently detrimental to the operation in terms of fouling susceptibility, modification resulted in uplifts in performance (flux and species rejection) outweighing the identified negative attributes. This was shown by enhanced dewatering or protein solution and by filtration of black tea for haze removal.
- A distinct interplay between the surface properties gained as a result of treatment and the transmission of tea species, particularly polyphenols, was realised. The effect being that polyphenols transmission was enhanced due to negative-negative charge repulsion reduction from the charge neutralised membrane and the removal of PVP (a known hindrance for polyphenols transmission of membranes).
- A diafiltration process was demonstrative showing the differential transmission of polyphenol species over all other constituents. The operating regime showed that polyphenols could be accumulated in the retentate side of the membrane creating a polyphenol-enriched tea product.
- The effect of ethanol during diafiltration allowed modification of the process so as to allow more uniform rejection of polyphenols and other constituents coupled with enhanced fluxes. This showed that total process yield of both group of species was improved.
- The overall impact of alcohol treatment had an insignificant effect on the haze removal efficiency of membranes meaning for this purpose, the recommendation

of using alcohol pre-treatment is made to reduce polyphenols loss (this on the basis of positive outcomes of long term ethanol exposure tests)

- Finally, as an alternative processing perspective to UF, MF showed promise as a means to remove haze from high solids load streams. This process could be used as a pre-filtration step prior to UF.

Already mentioned was the mitigation of polyphenols loss during clarification, which was improved as a result of treatment by 100 wt.% ethanol. The PS100 membrane offered the best enhancement in polyphenols transmission in this case, though the PS50 membrane offered far superior flux uplifts. Since haze removal efficiency was excellent, it would generally be concluded that utilisation of the PS100 would be a recommendation based on findings in this work. As for further recommendations to users of ethanol treated membrane; operation at sub-limiting flux only will produce flux improvements of note. Since flux is limited by cake deposition and CP, the classical dependence of membrane filtration efficiency on mass transfer over transmembrane pressure remains apparent and flux improvements are admittedly limited. Having said this, if high value transmission of negatively charged products is the main driver for the filtration, treatment with ethanol prior to membrane usage improves their recovery. This has particular relevance for pharmaceutical manufacture where high value protein and bioactive compound filtration is often required. The thesis has shown this remediation in the context of food processing, though in theory, any industrial sector, could employ a similar philosophy. Product loss must always be minimised.

10.1 Research continuation within this area

In terms of future work, an interesting area of study came to light through preliminary experimentation, some data of which is presented. The work shown indicates that certain modifiers can used as pre-treatment agents, again through a 'pre-treatment in place' method, to enhance separations.

Experiments were conducted in order to investigate the hypothesis that using readily available phenolic acids as pre-treatment agents could influence membrane selectivity. It was indicated in the literature review that association of polyphenols and proteins was a major factor in tea cream make-up. Also apparent was that polyphenols transmission was reduced by alcohol treatment, and that the susceptibility to polyphenols attachment was greatest for unconditioned membranes. Considering these factors it was hypothesised that by coating the surface with phenolic and polyphenolic species, a stronger association of protein onto the membrane would occur. In effect this would create a model 'tea cream' mechanism of attachment to the surface. This may sound illogical as fouling should normally be reduced. However, by using this mechanism of attachment, it was thought that rejection of protein could be enhanced, and thus dewatering of protein solutions using membranes with pore sizes that should allow facile transmission of species could be achieved.

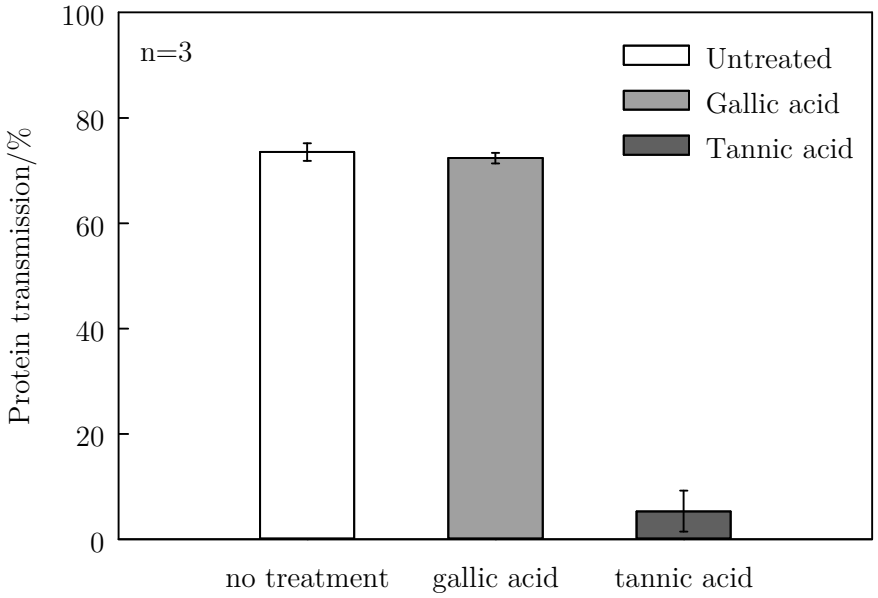

Figure 10-1 - Effect of pre-treatment method on transmission of protein when filtered through PS100 membranes (certain experimental details have been omitted before future confirmation and discussion)

Experiments examining the performance of PS100 membranes for dewatering of 0.2 $mgmL^{-1}$ BSA solutions were conducted to investigate whether gallic acid (a phenolic acid) and tannic acid (an ill-defined polyphenolic acid) indicated the expected results. Figure 10-1 shows these results; the definition is striking. The retention of BSA is improved nearly 15-fold, which shows that the membranes undergo a performance modification as a result of polyphenol species attachment. The tannic acid shows that the poly-cyclic structure of polyphenols is integral in creating the expected interaction. This is affirmed given the ineffectual performance of the mono-cyclic gallic acid as control treatment agent.

Another preliminary investigation conducted was that of utilising tea species as pre-treatment agents. TF-3-3'-DG was utilised as a model tea component as this was identified as a key foulant during UF by Evans *et al.* (2009) [29]. This was also compared with tannic acid as a more general model polyphenolic pre-treatment solute. The results shown in Figure 10-2 show that whilst tannic acid imparts a moderate hydrophilisation onto the membrane, the model tea component hydrophilises the membrane with great effect, reducing the contact angle from 74.2° ± 1.9° to 22.0° ± 4.9°.

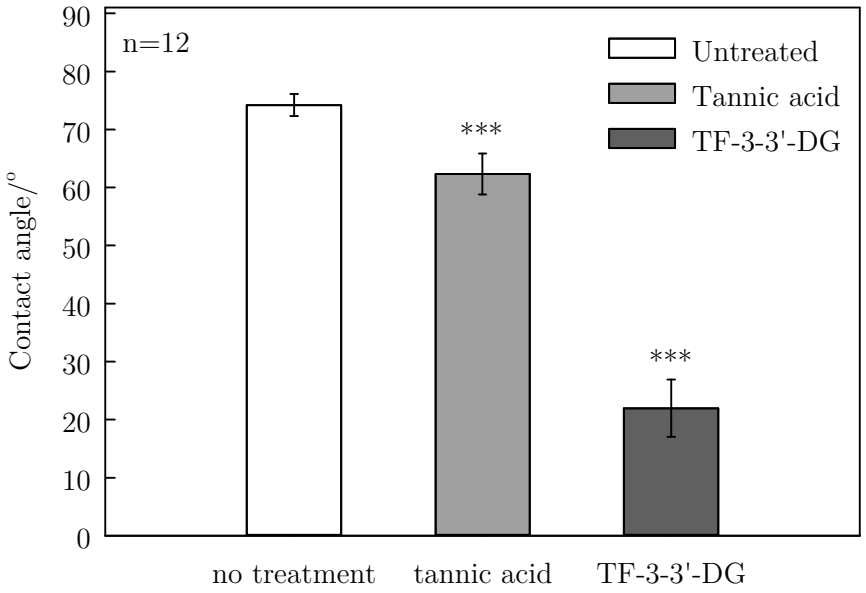

Figure 10-2 - Effect of pre-treatments on membrane contact angle

This result should imply that the surface fouls less readily. When treated however, membranes which are exposed to tea (via static adsorptive tests of foulants) show results that are not consistent with the expected case. Figure 10-3 shows that the pure water flux following treatment is unchanged following tannic acid treatment and significantly reduced after TF-3-3'-DG treatment. After adsorptive fouling is applied (90 minutes immersion at 50 °C), the PWF for the membranes are modified depending on treatment type. Tannic acid treatment results in the PWF being increased when compared to the control implying that an anti-foul type protection is made. This is not the case with TF-3-3'-DG which shows an overall loss in PWF, likely a result of the severe drop-off in relative flux due to treatment.

The mechanisms of attachment here, or more generally phenomena effecting membrane rejection and loss of flux, have been inspired from working on black tea membrane filtration. It shows that certain foulant species can have drastic effects on the performance of membranes. Furthering this research would not only open up new possibilities for membrane functionalisation, but would feed in to informing mechanism of species rejection for membrane filtration of tea and other polyphenol or protein containing feed stocks.

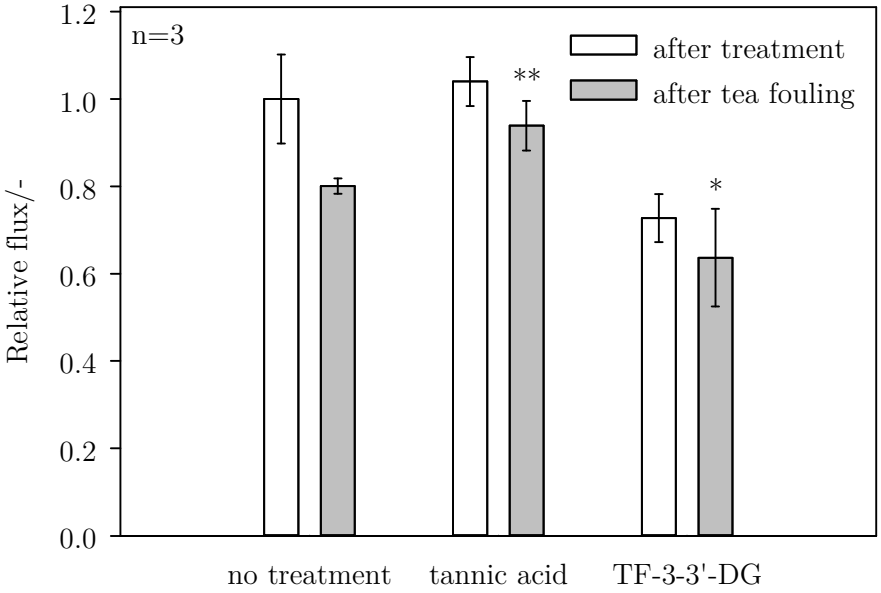

Figure 10-3 - Effect of pre-treatments on adsorptive fouling of black tea as measured by pure water flux. *p<0.05, **p<0.01 (significance levels apply to comparison of each treatment after fouling to the 'after fouling' control)

10.2 Final words

It is the belief that this thesis has continued to reinforce the fundamental membrane science theories surrounding surface chemical analysis and structure, and its impact on both membrane selectivity and fouling within food processing. Figure 10-4 has attempted to distil the key concepts and observations into a single diagram. It is appreciable that one treatment method can have far reaching and complex impacts on the membrane and performance thereof. It also becomes difficult to characterise what are causes, and what are effects, though an attempt has been made. What is apparent are that there are some fundamental root causes, such as PVP leaching and swelling, which have far reaching impact on other parameters measured.

The interrelation of properties is quite clear. While experimental techniques are advancing to enable accurate qualitative interpretation of many situations, control of experiments, development of correlations, and deriving a firm theoretical quantitative understanding is the obvious direction in which research, and particularly research into membrane filtration, strives. Full incorporation of the factors investigated here, and their relative contributions, into a generalised filtration model would constitute something of a shift in the current capabilities of theorists. The endeavour may be best left to the experimentalist.

What is clear is that membrane performance and its strong association with fouling can be remediated. The thesis has aimed to highlight that this can be done by relatively simple and low cost means such as the *pre-treatment in place* method described here. The modifications could however be potentially damaging to the membranes and further research is required to elucidate if long-term or multiple exposure to alcohols (or other

treatment agents) can impact negatively on membrane performance. Certainly the work presented here can have direct industrial impact in general membrane filtration and specifically to that of tea.

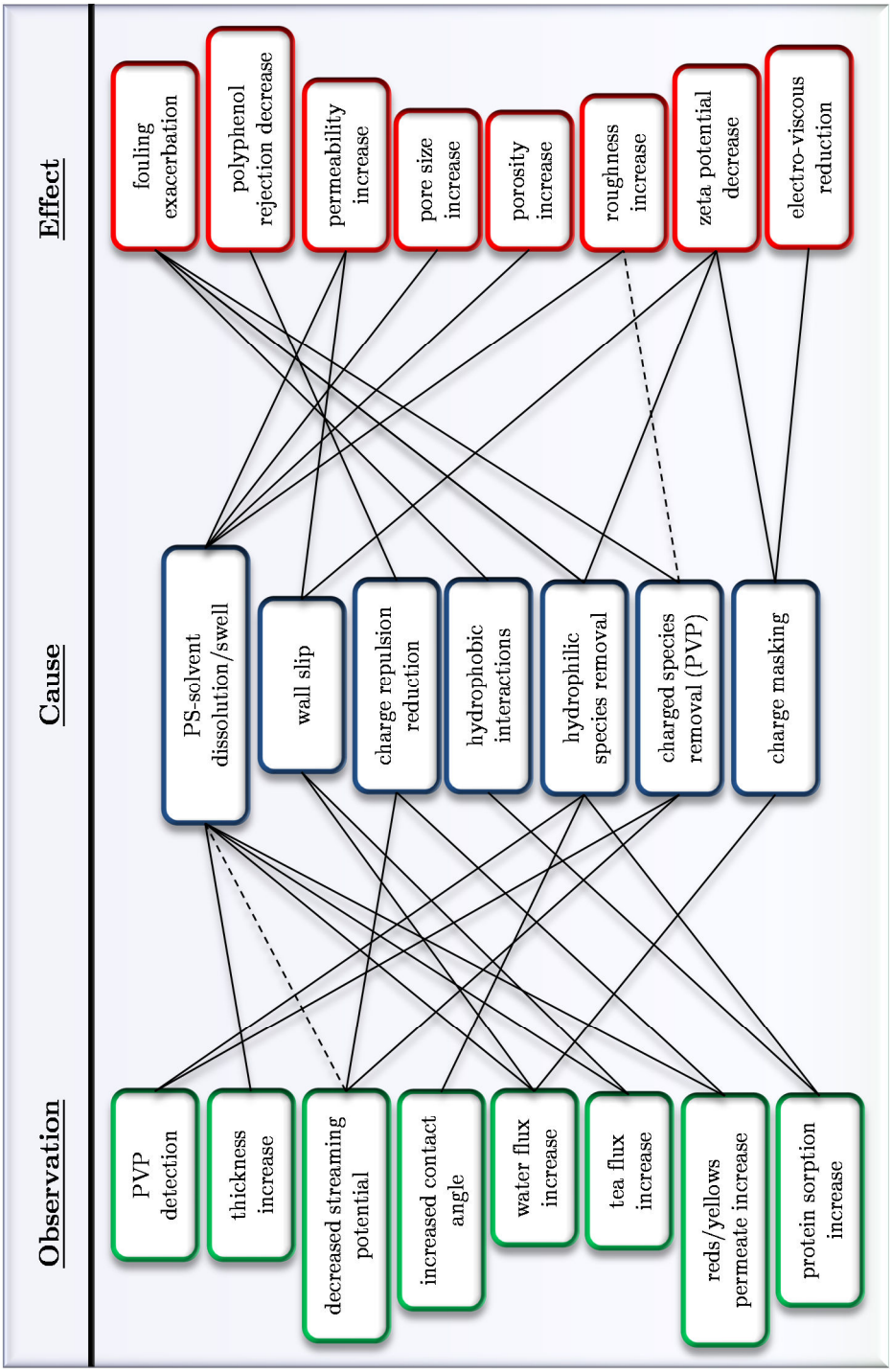

Figure 10-4 - Observation, cause and effect diagram for alcohol treatment of PS membranes. Dotted lines represent speculative mechanisms.

11. Bibliography

1. Li, S., C.-Y. Lo, M.-H. Pan, C.-S. Lai, and C.-T. Ho, Black tea: chemical analysis and stability. *Food & Function*, 2013. 4(1): p. 10-18.
2. Hicks, A., Current status and future development of global tea production and tea products. *Au J*, 2009. 12(4): p. 251-264.
3. FAO. Current situation and medium term outlook for tea. in *Twentieth Session of the Intergovernmental Group on Tea*. 2012: FAO.
4. FAO, Food outlook: Biannual report on global food markets, FAO, Editor. 2013.
5. Euromonitor, Global soft drinks: has the world finally acquired a taste for RTD tea? *Euromonitor International*, 2009.
6. Euromonitor. Soft Drinks: Euromonitor from trade sources/national statistics. 2014 [cited 2013 29/06/14]; Available from: http://www.portal.euromonitor.com.
7. Tanui, J.K., W. Fang, W. Feng, P. Zhuang, and X. Li, World Black Tea Markets: Relationships and Implications for the Global Tea Industry. *Journal of International Food & Agribusiness Marketing*, 2012. 24(2): p. 148-168.
8. Del Rio, D., L. Calani, F. Scazzina, L. Jechiu, C. Cordero, and F. Brighenti, Bioavailability of catechins from ready-to-drink tea. *Nutrition*, 2010. 26(5): p. 528-533.
9. Menrad, K., Market and marketing of functional food in Europe. *Journal of Food Engineering*, 2003. 56(2): p. 181-188.
10. Roberfroid, M.B., A European consensus of scientific concepts of functional foods. *Nutrition*, 2000. 16(7): p. 689-691.
11. Siro, I., E. Kapolna, B. Kapolna, and A. Lugasi, Functional food. Product development, marketing and consumer acceptance—A review. *Appetite*, 2008. 51(3): p. 456-467.
12. Hilliam, M., Functional Food–How big is the market. *The World of Food Ingredients*, 2000. 12(50-52).
13. Jensen, J. and S. Smed, The Danish tax on saturated fat. Short run effects on consumption and consumer prices of fats. *Institute of Food and Resource Economics, University of Copenhagen, working paper*, 2012. 14.
14. Bearth, A., M.-E. Cousin, and M. Siegrist, The consumer's perception of artificial food additives: Influences on acceptance, risk and benefit perceptions. *Food Quality and Preference*, 2014.
15. Kärkkäinen, M., Increasing efficiency in the supply chain for short shelf life goods using RFID tagging. *International Journal of Retail & Distribution Management*, 2003. 31(10): p. 529-536.
16. Gardner, E., C. Ruxton, and A. Leeds, Black tea–helpful or harmful? A review of the evidence. *European journal of clinical nutrition*, 2006. 61(1): p. 3-18.

17. Leung, L., Y. Su, R. Chen, Z. Zhang, Y. Huang, and Z. Chen, Theaflavins in black tea and catechins in green tea are equally effective antioxidants. *Journal of Nutrition*, 2001. 131(9): p. 2248.
18. Sharma, V. and L. Rao, A thought on the biological activities of black tea. *Critical reviews in food science and nutrition*, 2009. 49(5): p. 379-404.
19. Tscharntke, T., Y. Clough, T.C. Wanger, L. Jackson, I. Motzke, I. Perfecto, J. Vandermeer, and A. Whitbread, Global food security, biodiversity conservation and the future of agricultural intensification. *Biological Conservation*, 2012. 151(1): p. 53-59.
20. Godfray, H.C.J., J.R. Beddington, I.R. Crute, L. Haddad, D. Lawrence, J.F. Muir, J. Pretty, S. Robinson, S.M. Thomas, and C. Toulmin, Food security: the challenge of feeding 9 billion people. *Science*, 2010. 327(5967): p. 812-818.
21. Kearney, J., Food consumption trends and drivers. *Philosophical transactions of the royal society B: biological sciences*, 2010. 365(1554): p. 2793-2807.
22. Yanniotis, S., P. Taoukis, N.G. Stoforos, and V.T. Karathanos, Advances in Food Process Engineering Research and Applications. 2013: Springer.
23. Schuchmann, H.P., K. Köhler, M.A. Emin, and H. Schubert, Food Process Engineering Research and Innovation in a Fast Changing World: Paradigms/Case Studies, in *Advances in Food Process Engineering Research and Applications*. 2013, Springer. p. 41-59.
24. Pouliot, Y., Membrane processes in dairy technology—from a simple idea to worldwide panacea. *International Dairy Journal*, 2008. 18(7): p. 735-740.
25. Evans, P.J. and M.R. Bird, Solute-Membrane Fouling Interactions During the Ultrafiltration of Black Tea Liquor. *Food and Bioproducts Processing*, 2006. 84(4): p. 292-301.
26. Evans, P.J. and M.R. Bird, The role of black tea feed conditions upon the ultrafiltration performance during membrane fouling and cleaning. *Journal of Food Process Engineering*, 2010. 33(2): p. 309-332.
27. Evans, P.J. and M.R. Bird, The role of black tea feed conditions upon ultrafiltration performance during membrane fouling and cleaning. *Journal of Food Process Engineering*, 2010. 33(2): p. 309-332.
28. Evans, P.J., M.R. Bird, A. Pihlajamaki, and M. Nystrom, The influence of hydrophobicity, roughness and charge upon ultrafiltration membranes for black tea liquor clarification. *Journal of Membrane Science*, 2008. 313(1-2): p. 250-262.
29. Evans, P.J., M.R. Bird, D. Rogers, and C.J. Wright, Measurement of polyphenol-membrane interaction forces during the ultrafiltration of black tea liquor. *Colloids and Surfaces A: Physicochemical and Engineering Aspects*, 2009. 335(1-3): p. 148-153.
30. Todisco, S., P. Tallarico, and B. Gupta, Mass transfer and polyphenols retention in the clarification of black tea with ceramic membranes. *Innovative Food Science & Emerging Technologies*, 2002. 3(3): p. 255-262.

31. Chandini, S.K., L.J. Rao, and R. Subramanian, Membrane Clarification of Black Tea Extracts. *Food and Bioprocess Technology*, 2013. 6(8): p. 1926-1943.
32. Subramanian, R., C.S. Kumar, and P. Sharma, Membrane clarification of tea extracts. *Critical reviews in food science and nutrition*, 2013(accepted manuscript).
33. Wu, D. and M. Bird, The fouling and cleaning of ultrafiltration membranes during the filtration of model tea component solutions. *Journal of Food Process Engineering*, 2007. 30(3): p. 293-323.
34. Mérian, T. and J.M. Goddard, Advances in Nonfouling Materials: Perspectives for the Food Industry. *Journal of agricultural and food chemistry*, 2012. 60(12): p. 2943-2957.
35. Kochan, J., T. Wintgens, R. Hochstrat, and T. Melin, Impact of wetting agents on the filtration performance of polymeric ultrafiltration membranes. *Desalination*, 2009. 241(1-3): p. 34-42.
36. Machado, D., D. Hasson, and R. Semiat, Effect of solvent properties on permeate flow through nanofiltration membranes. Part I: investigation of parameters affecting solvent flux. *Journal of Membrane Science*, 1999. 163(1): p. 93-102.
37. Lencki, R.W. and S. Williams, Effect of nonaqueous solvents on the flux behavior of ultrafiltration membranes. *Journal of Membrane Science*, 1995. 101(1–2): p. 43-51.
38. Geens, J., K. Peeters, B. Van der Bruggen, and C. Vandecasteele, Polymeric nanofiltration of binary water-alcohol mixtures: Influence of feed composition and membrane properties on permeability and rejection. *Journal of Membrane Science*, 2005. 255(1-2): p. 255-264.
39. Geens, J., B. Van der Bruggen, and C. Vandecasteele, Transport model for solvent permeation through nanofiltration membranes. *Separation and Purification Technology*, 2006. 48(3): p. 255-263.
40. Nguyen, Q., P. Aptel, and J. Neel, Characterization of ultrafiltration membranes:: Part I. Water and organic-solvent permeabilities. *Journal of Membrane Science*, 1979. 5: p. 235-251.
41. Shukla, R. and M. Cheryan, Performance of ultrafiltration membranes in ethanol-water solutions: effect of membrane conditioning. *Journal of Membrane Science*, 2002. 198(1): p. 75-85.
42. Roh, I.J., S.Y. Park, J. Kim, and C. Kim, Effects of the polyamide molecular structure on the performance of reverse osmosis membranes. *Journal of Polymer Science Part B: Polymer Physics*, 1998. 36(11): p. 1821-1830.
43. Mehta, A. and A.L. Zydney, Permeability and selectivity analysis for ultrafiltration membranes. *Journal of Membrane Science*, 2005. 249(1): p. 245-249.
44. Freeman, B.D., Basis of permeability/selectivity tradeoff relations in polymeric gas separation membranes. *Macromolecules*, 1999. 32(2): p. 375-380.
45. Mulder, M., Basic principles of membrane technology. 1996: Springer.
46. Cheryan, M., Ultrafiltration and microfiltration handbook. 1998: CRC press.

47. Osada, Y. and T. Nakagawa, Membrane science and technology. 1992: CRC Press.
48. Belfort, G., R.H. Davis, and A.L. Zydney, The behavior of suspensions and macromolecular solutions in crossflow microfiltration. *Journal of Membrane Science*, 1994. 96(1): p. 1-58.
49. Belfort, G., Membrane modules: comparison of different configurations using fluid mechanics. *Journal of Membrane Science*, 1988. 35(3): p. 245-270.
50. Pörtner, R., S. Nagel-Heyer, C. Goepfert, P. Adamietz, and N.M. Meenen, Bioreactor design for tissue engineering. *Journal of bioscience and bioengineering*, 2005. 100(3): p. 235-245.
51. Morgan, S.M., S. Tilley, S. Perera, M.J. Ellis, J. Kanczler, J.B. Chaudhuri, and R.O. Oreffo, Expansion of human bone marrow stromal cells on poly-(dl-lactide-co-glycolide) hollow fibres designed for use in skeletal tissue engineering. *Biomaterials*, 2007. 28(35): p. 5332-5343.
52. Nevell, J.M. and S.P. Perera, Novel adsorbent hollow fibres for oxygen concentration. *Adsorption*, 2011. 17(1): p. 273-283.
53. Baker, R.W., Membrane technology. 2000: Wiley Online Library.
54. Yampolskii, Y.P., I. Pinnau, and B.D. Freeman, Materials science of membranes for gas and vapor separation. 2006: Wiley Online Library.
55. Greenlee, L.F., D.F. Lawler, B.D. Freeman, B. Marrot, and P. Moulin, Reverse osmosis desalination: water sources, technology, and today's challenges. *Water research*, 2009. 43(9): p. 2317-2348.
56. Van der Horst, H. and J. Hanemaaijer, Cross-flow microfiltration in the food industry. State of the art. *Desalination*, 1990. 77: p. 235-258.
57. Madaeni, S., M. Yasemi, and A. Delpisheh, Milk sterilization using membranes. *Journal of Food Process Engineering*, 2011. 34(4): p. 1071-1085.
58. Bird, M. and M. Bartlett, Measuring and modelling flux recovery during the chemical cleaning of MF membranes for the processing of whey protein concentrate. *Journal of Food Engineering*, 2002. 53(2): p. 143-152.
59. Head, L.E. and M.R. Bird, The removal of psychrotropic spores from Milk Protein Isolate feeds using tubular ceramic microfilters. *Journal of Food Process Engineering*, 2013. 36(1): p. 113-124.
60. Jones, S., Y. Chew, D. Wilson, and M.R. Bird, Fluid dynamic gauging of microfiltration membranes fouled with sugar beet molasses. *Journal of Food Engineering*, 2011.
61. Boissier, B., F. Lutin, M. Moutounet, and A. Vernhet, Particles deposition during the cross-flow microfiltration of red wines—incidence of the hydrodynamic conditions and of the yeast to fines ratio. *Chemical Engineering and Processing: Process Intensification*, 2008. 47(3): p. 276-286.
62. Ulbricht, M., W. Ansorge, I. Danielzik, M. König, and O. Schuster, Fouling in microfiltration of wine: The influence of the membrane polymer on adsorption of polyphenols and polysaccharides. *Separation and Purification Technology*, 2009. 68(3): p. 335-342.

63. Czekaj, P., F. López, and C. Güell, Membrane fouling during microfiltration of fermented beverages. *Journal of Membrane Science*, 2000. 166(2): p. 199-212.
64. Lopez, F., P. Pescador, C. Güell, M. Morales, M. Garcia-Parrilla, and A. Troncoso, Industrial vinegar clarification by cross-flow microfiltration: effect on colour and polyphenol content. *Journal of Food Engineering*, 2005. 68(1): p. 133-136.
65. Gan, Q., J. Howell, R. Field, R. England, M. Bird, C. O'Shaughnessy, and M. MeKechinie, Beer clarification by microfiltration—product quality control and fractionation of particles and macromolecules. *Journal of Membrane Science*, 2001. 194(2): p. 185-196.
66. van der Sman, R., H. Vollebregt, A. Mepschen, and T. Noordman, Review of hypotheses for fouling during beer clarification using membranes. *Journal of Membrane Science*, 2012.
67. Freeman, G. and M. McKechnie, Filtration and stabilization of beers, in *Fermented Beverage Production*. 2003, Springer. p. 365-392.
68. Taddei, C., P. Aimar, J.A. Howell, and J.A. Scott, Yeast cell harvesting from cider using microfiltration. *Journal of Chemical Technology and Biotechnology*, 1990. 47(4): p. 365-376.
69. Nandi, B., B. Das, and R. Uppaluri, Clarification of orange juice using ceramic membrane and evaluation of fouling mechanism. *Journal of Food Process Engineering*, 2010.
70. Yazdanshenas, M., S.A.R. Tabatabaee-Nezhad, M. Soltanieh, R. Roostaazad, and A.B. Khoshfetrat, Contribution of fouling and gel polarization during ultrafiltration of raw apple juice at industrial scale. *Desalination*, 2010. 258(1): p. 194-200.
71. de Oliveira, R.C., R.C. Docê, and S.T.D. de Barros, Clarification of passion fruit juice by microfiltration: Analyses of operating parameters, study of membrane fouling and juice quality. *Journal of Food Engineering*, 2012.
72. Cassano, A., A. Figoli, A. Tagarelli, G. Sindona, and E. Drioli, Integrated membrane process for the production of highly nutritional kiwifruit juice. *Desalination*, 2006. 189(1-3): p. 21-30.
73. Laorko, A., S. Tongchitpakdee, and W. Youravong, Storage quality of pineapple juice non-thermally pasteurized and clarified by microfiltration. *Journal of Food Engineering*, 2013. 116(2): p. 554-561.
74. Kawakatsu, T., T. KoBAYAsH, Y. Sano, and M. Nakajima, Clarification of Green Tea Extract by Microfiltration and Ultrafiltration. *Biosci. Biotech. Biochem*, 1995. 59(6): p. l0l&l020.
75. Decloux, M., M. Dornier, and I. Gratius, Crossflow microfiltration of gum arabic solutions: Comparison of the classical system with the co-current permeate flow system. *International Journal of Food Science & Technology*, 1996. 31(2): p. 153-166.

76. Fontes, S.R., Mass transfer in microfiltration with laminar and turbulent flow of macromolecular solutions. *Journal of Membrane Science*, 2005. 249(1): p. 207-211.
77. Lu, W.-M., K.-L. Tung, C.-H. Pan, and K.-J. Hwang, Crossflow microfiltration of mono-dispersed deformable particle suspension. *Journal of Membrane Science*, 2002. 198(2): p. 225-243.
78. Mohammad, A.W., C.Y. Ng, Y.P. Lim, and G.H. Ng, Ultrafiltration in food processing industry: review on application, membrane fouling, and fouling control. *Food and Bioprocess Technology*, 2012. 5(4): p. 1143-1156.
79. Guadix, A., J.E. Zapata, M.C. Almecija, and E.M. Guadix, Predicting the flux decline in milk cross-flow ceramic ultrafiltration by artificial neural networks. *Desalination*, 2010. 250(3): p. 1118-1120.
80. Catarino, I., A.P. Martins, E. Duarte, E.S. Prudêncio, and M.N. de Pinho, Rennet coagulation of sheep milk processed by ultrafiltration at low concentration factors. *Journal of Food Engineering*, 2013. 114(2): p. 249-254.
81. Arunkumar, A. and M.R. Etzel, Fractionation of α-lactalbumin and β-lactoglobulin from bovine milk serum using staged, positively charged, tangential flow ultrafiltration membranes. *Journal of Membrane Science*, 2014. 454: p. 488-495.
82. Loginov, M., K. Loginova, N. Lebovka, and E. Vorobiev, Comparison of dead-end ultrafiltration behaviour and filtrate quality of sugar beet juices obtained by conventional and "cold" PEF-assisted diffusion. *Journal of Membrane Science*, 2011. 377(1): p. 273-283.
83. Mondal, S., C. Rai, and S. De, Identification of fouling mechanism during ultrafiltration of stevia extract. *Food and Bioprocess Technology*, 2013. 6(4): p. 931-940.
84. de Bruijn, J., J. Martínez-Oyanedel, C. Loyola, J. Seiter, F. Lobos, and R. Pérez-Arias, Fractionation of Sauvignon wine macromolecules by ultrafiltration and diafiltration: impact of protein composition on white wine haze stability. *International Journal of Food Science & Technology*, 2011. 46(8): p. 1691-1698.
85. Resende, A., S. Catarino, V. Geraldes, and M. de Pinho, Separation and Purification by Ultrafiltration of White Wine High Molecular Weight Polysaccharides. *Industrial & Engineering Chemistry Research*, 2013. 52(26): p. 8875-8879.
86. Mondal, S., A. Cassano, F. Tasselli, and S. De, A generalized model for clarification of fruit juice during ultrafiltration under total recycle and batch mode. *Journal of Membrane Science*, 2011. 366(1): p. 295-303.
87. Bahçeci, K.S., Effects of pretreatment and various operating parameters on permeate flux and quality during ultrafiltration of apple juice. *International Journal of Food Science & Technology*, 2012.
88. Destani, F., A. Cassano, A. Fazio, J.-P. Vincken, and B. Gabriele, Recovery and concentration of phenolic compounds in blood orange juice by membrane operations. *Journal of Food Engineering*, 2013. 117(3): p. 263-271.

89. Domingues, R.C.C., A.A. Ramos, V.L. Cardoso, and M.H.M. Reis, Microfiltration of passion fruit juice using hollow fibre membranes and evaluation of fouling mechanisms. *Journal of Food Engineering*, 2014. 121: p. 73-79.
90. Rao, L., K. Hayat, Y. Lv, E. Karangwa, S. Xia, C. Jia, F. Zhong, and X. Zhang, Effect of ultrafiltration and fining adsorbents on the clarification of green tea. *Journal of Food Engineering*, 2011. 102(4): p. 321-326.
91. Lalia, B.S., V. Kochkodan, R. Hashaikeh, and N. Hilal, A review on membrane fabrication: Structure, properties and performance relationship. *Desalination*, 2013. 326: p. 77-95.
92. Strathmann, H., K. Kock, P. Amar, and R. Baker, The formation mechanism of asymmetric membranes. *Desalination*, 1975. 16(2): p. 179-203.
93. Zheng, Q.-Z., P. Wang, Y.-N. Yang, and D.-J. Cui, The relationship between porosity and kinetics parameter of membrane formation in PSF ultrafiltration membrane. *Journal of Membrane Science*, 2006. 286(1): p. 7-11.
94. Smolders, C., A. Reuvers, R. Boom, and I. Wienk, Microstructures in phase-inversion membranes. Part 1. Formation of macrovoids. *Journal of Membrane Science*, 1992. 73(2): p. 259-275.
95. Liu, Y.-L., C.-H. Yu, and J.-Y. Lai, Poly (tetrafluoroethylene)/polyamide thin-film composite membranes via interfacial polymerization for pervaporation dehydration on an isopropanol aqueous solution. *Journal of Membrane Science*, 2008. 315(1): p. 106-115.
96. Chakrabarty, B., A. Ghoshal, and M. Purkait, Effect of molecular weight of PEG on membrane morphology and transport properties. *Journal of Membrane Science*, 2008. 309(1): p. 209-221.
97. Chuang, W.-Y., T.-H. Young, W.-Y. Chiu, and C.-Y. Lin, The effect of polymeric additives on the structure and permeability of poly (vinyl alcohol) asymmetric membranes. *Polymer*, 2000. 41(15): p. 5633-5641.
98. Lafreniere, L.Y., F.D. Talbot, T. Matsuura, and S. Sourirajan, Effect of poly (vinylpyrrolidone) additive on the performance of poly (ether sulfone) ultrafiltration membranes. *Industrial & Engineering Chemistry Research*, 1987. 26(11): p. 2385-2389.
99. Ochoa, N., P. Pradanos, L. Palacio, C. Pagliero, J. Marchese, and A. Hernandez, Pore size distributions based on AFM imaging and retention of multidisperse polymer solutes: characterisation of polyethersulfone UF membranes with dopes containing different PVP. *Journal of Membrane Science*, 2001. 187(1): p. 227-237.
100. Marchese, J., M. Ponce, N. Ochoa, P. Prádanos, L. Palacio, and A. Hernández, Fouling behaviour of polyethersulfone UF membranes made with different PVP. *Journal of Membrane Science*, 2003. 211(1): p. 1-11.
101. Hildebrand, J.H., Solubility. *Journal of the American Chemical Society*, 1916. 38(8): p. 1452-1473.

102. Scatchard, G., Equilibria in Non-electrolyte Solutions in Relation to the Vapor Pressures and Densities of the Components. *Chemical Reviews*, 1931. 8(2): p. 321-333.
103. Hildebrand, J.H., Solubility of Non-electrolytes. 1936.
104. Hansen, C.M., The three dimensional solubility parameter. *Danish Technical: Copenhagen*, 1967: p. 14.
105. Hansen, C.M., Hansen solubility parameters: a user's handbook. 2012: CRC press.
106. Milliman, H.W., D. Boris, and D.A. Schiraldi, Experimental Determination of Hansen Solubility Parameters for Select POSS and Polymer Compounds as a Guide to POSS–Polymer Interaction Potentials. *Macromolecules*, 2012. 45(4): p. 1931-1936.
107. Nyström, M., Fouling of unmodified and modified polysulfone ultrafiltration membranes by ovalbumin. *Journal of Membrane Science*, 1989. 44(2-3): p. 183-196.
108. Sing, K., D. Everett, R. Haul, L. Moscou, R. Pierotti, J. Rouquerol, and T. Siemieniewska, Reporting physisorption data for gas/solid systems. *Pure Appl. Chem*, 1982. 54(11): p. 2201.
109. Singh, S., K. Khulbe, T. Matsuura, and P. Ramamurthy, Membrane characterization by solute transport and atomic force microscopy. *Journal of Membrane Science*, 1998. 142(1): p. 111-127.
110. Nakao, S.-i., Determination of pore size and pore size distribution: 3. Filtration membranes. *Journal of Membrane Science*, 1994. 96(1): p. 131-165.
111. Yan, L., Y.S. Li, C.B. Xiang, and S. Xianda, Effect of nano-sized Al_2O_3 particle addition on PVDF ultrafiltration membrane performance. *Journal of Membrane Science*, 2006. 276(1): p. 162-167.
112. Sanz, J., R. Peinador, J. Calvo, A. Hernández, A. Bottino, and G. Capannelli, Characterization of UF membranes by liquid–liquid displacement porosimetry. *Desalination*, 2009. 245(1): p. 546-553.
113. Peinador, R.I., J.I. Calvo, P. Prádanos, L. Palacio, and A. Hernández, Characterisation of polymeric UF membranes by liquid–liquid displacement porosimetry. *Journal of Membrane Science*, 2010. 348(1): p. 238-244.
114. Morison, K., A comparison of liquid-liquid porosimetry equations for evaluation of pore size distribution. *Journal of Membrane Science*, 2008. 325(1): p. 301-310.
115. Hernández, A., J. Calvo, P. Prádanos, and F. Tejerina, Pore size distributions in microporous membranes. A critical analysis of the bubble point extended method. *Journal of Membrane Science*, 1996. 112(1): p. 1-12.
116. Darcy, H., Les fontaines publiques de la ville de Dijon, 1856. *Dalmont, Paris*, 1856. 70.
117. Field, R., D. Wu, J. Howell, and B. Gupta, Critical flux concept for microfiltration fouling. *Journal of Membrane Science*, 1995. 100(3): p. 259-272.

118. Ho, C. and A. Zydney, Transmembrane pressure profiles during constant flux microfiltration of bovine serum albumin. *Journal of Membrane Science*, 2002. 209(2): p. 363-377.
119. De Barros, S., C. Andrade, E. Mendes, and L. Peres, Study of fouling mechanism in pineapple juice clarification by ultrafiltration. *Journal of Membrane Science*, 2003. 215(1-2): p. 213-224.
120. Espinasse, B., P. Bacchin, and P. Aimar, On an experimental method to measure critical flux in ultrafiltration. *Desalination*, 2002. 146(1): p. 91-96.
121. Metsämuuronen, S., J. Howell, and M. Nyström, Critical flux in ultrafiltration of myoglobin and baker's yeast. *Journal of Membrane Science*, 2002. 196(1): p. 13-25.
122. Bacchin, P., P. Aimar, and R.W. Field, Critical and sustainable fluxes: theory, experiments and applications. *Journal of Membrane Science*, 2006. 281(1): p. 42-69.
123. Fane, A., Ultrafiltration: factors influencing flux and rejection. *Progress in filtration and separation*, 1986. 4: p. 101-179.
124. Song, L., A new model for the calculation of the limiting flux in ultrafiltration. *Journal of Membrane Science*, 1998. 144(1-2): p. 173-185.
125. Kozinski, A. and E. Lightfoot, Protein ultrafiltration: a general example of boundary layer filtration. *AIChE Journal*, 1972. 18(5): p. 1030-1040.
126. Wiley, D.E., C.J. Fell, and A.G. Fane, Optimisation of membrane module design for brackish water desalination. *Desalination*, 1985. 52(3): p. 249-265.
127. Van den Berg, G., I. Racz, and C. Smolders, Mass transfer coefficients in cross-flow ultrafiltration. *Journal of Membrane Science*, 1989. 47(1-2): p. 25-51.
128. Bartlett, M., Chemical cleaning of fouled membrane systems. *Doctoral Dissertation, Chemical Engineering Department, University of Bath*, 1998.
129. Aydiner, C., A novel approach based on distinction of actual and pseudo resistances in membrane fouling: "Pseudo resistance" concept and its implementation in nanofiltration of single solutions. *Journal of Membrane Science*, 2010. 361(1-2): p. 96-112.
130. Chang, E.-E., S.-Y. Yang, C.-P. Huang, C.-H. Liang, and P.-C. Chiang, Assessing the fouling mechanisms of high-pressure nanofiltration membrane using the modified Hermia model and the resistance-in-series model. *Separation and Purification Technology*, 2011. 79(3): p. 329-336.
131. Leberknight, J., B. Wielenga, A. Lee-Jewett, and T.J. Menkhaus, Recovery of high value protein from a corn ethanol process by ultrafiltration and an exploration of the associated membrane fouling. *Journal of Membrane Science*, 2011. 366(1): p. 405-412.
132. Cassano, A., L. Donato, and E. Drioli, Ultrafiltration of kiwifruit juice: operating parameters, juice quality and membrane fouling. *Journal of Food Engineering*, 2007. 79(2): p. 613-621.
133. Dictionary, O.E., Oxford English dictionary online. 2008: Oxford University Press, Oxford, UK http://www. oed. com.

134. Fane, A. and C. Fell, A review of fouling and fouling control in ultrafiltration. *Desalination*, 1987. 62: p. 117-136.
135. Liu, C., S. Caothien, J. Hayes, T. Caothuy, T. Otoyo, and T. Ogawa, Membrane chemical cleaning: from art to science. *Pall Corporation, Port Washington, NY*, 2001. 11050.
136. Liu, C., S. Caothien, J. Hayes, T. Caothuy, T. Otoyo, and T. Ogawa, Membrane chemical cleaning: from art to science. *HOTwater*, 2001. 4: p. 1–25.
137. Sahachaiyunta, P., T. Koo, and R. Sheikholeslami, Effect of several inorganic species on silica fouling in RO membranes. *Desalination*, 2002. 144(1-3): p. 373-378.
138. Goosen, M., S. Sablani, H. Al-Hinai, S. Al-Obeidani, R. Al-Belushi, and D. Jackson, Fouling of reverse osmosis and ultrafiltration membranes: a critical review. *Separation science and technology*, 2005. 39(10): p. 2261-2297.
139. Simoes, M., L.C. Simoes, and M.J. Vieira, A review of current and emergent biofilm control strategies. *Lwt-Food Science and Technology*, 2010. 43(4): p. 573-583.
140. Flemming, H., G. Schaule, and R. McDonough, How do performance parameters respond to initial biofouling on separation membranes. *Vom Wasser*, 1993. 80: p. 177-186.
141. Flemming, H. and G. Schaule, Biofouling on membranes-a microbiological approach. *Desalination*, 1988. 70(1-3): p. 95-119.
142. Aimar, P. and P. Bacchin, Slow colloidal aggregation and membrane fouling. *Journal of Membrane Science*, 2010. 360(1): p. 70-76.
143. Fane, A., Ultrafiltration of suspensions. *Journal of Membrane Science*, 1984. 20(3): p. 249-259.
144. Crozes, G., C. Anselme, and J. Mallevialle, Effect of adsorption of organic matter on fouling of ultrafiltration membranes. *Journal of Membrane Science*, 1993. 84(1-2): p. 61-77.
145. Sinnott, R., J. Coulson, and J. Richardson, Coulson & Richardson's chemical engineering: Chemical engineering design. 2005: Gulf Professional Publishing.
146. Bhattacharjee, C. and P. Bhattacharya, Flux decline analysis in ultrafiltration of kraft black liquor. *Journal of Membrane Science*, 1993. 82(1): p. 1-14.
147. Hermans, P. and H. Bredée, Principles of the mathematical treatment of constant-pressure filtration. *J. Soc. Chem. Ind*, 1936. 55: p. 1-4.
148. Shirato, M., T. Aragaki, and E. Iritani, Blocking filtration laws for filtration of power-law non-Newtonian fluids. *Journal of Chemical Engineering of Japan*, 1979. 12(2): p. 162-164.
149. Hermia, J., Constant pressure blocking filtration laws-application to power-law non-Newtonian fluids. *Chemical Engineering Research and Design*, 1982. 60(a): p. 183-187.
150. Tracey, E.M. and R.H. Davis, Protein fouling of track-etched polycarbonate microfiltration membranes. *Journal of colloid and interface science*, 1994. 167(1): p. 104-116.

151. Fane, A., C. Fell, and K. Kim, The effect of surfactant pretreatment on the ultrafiltration of proteins. *Desalination*, 1985. 53(1): p. 37-55.
152. Cherkasov, A., S. Tsareva, and A. Polotsky, Selective properties of ultrafiltration membranes from the standpoint of concentration polarization and adsorption phenomena. *Journal of Membrane Science*, 1995. 104(1): p. 157-164.
153. Nabe, A., E. Staude, and G. Belfort, Surface modification of polysulfone ultrafiltration membranes and fouling by BSA solutions. *Journal of Membrane Science*, 1997. 133(1): p. 57-72.
154. Silverstein, T.P., The real reason why oil and water don't mix. *Journal of chemical education*, 1998. 75(1): p. 116.
155. Lee, H., G. Amy, J. Cho, Y. Yoon, S.-H. Moon, and I.S. Kim, Cleaning strategies for flux recovery of an ultrafiltration membrane fouled by natural organic matter. *Water research*, 2001. 35(14): p. 3301-3308.
156. Kim, K., K. Lee, K. Cho, and C. Park, Surface modification of polysulfone ultrafiltration membrane by oxygen plasma treatment. *Journal of Membrane Science*, 2002. 199(1): p. 135-145.
157. Susanto, H., Y. Feng, and M. Ulbricht, Fouling behavior of aqueous solutions of polyphenolic compounds during ultrafiltration. *Journal of Food Engineering*, 2009. 91(2): p. 333-340.
158. Zhang, W., M. Wahlgren, and B. Sivik, Membrane characterization by the contact angle technique: II. Characterization of UF-membranes and comparison between the captive bubble and sessile drop as methods to obtain water contact angles. *Desalination*, 1989. 72(3): p. 263-273.
159. Cassie, A. and S. Baxter, Wettability of porous surfaces. *Transactions of the Faraday Society*, 1944. 40: p. 546-551.
160. Wenzel, R.N., Resistance of solid surfaces to wetting by water. *Industrial & Engineering Chemistry*, 1936. 28(8): p. 988-994.
161. Oatley, D.L., L. Llenas, R. Pérez, P.M. Williams, X. Martínez-Lladó, and M. Rovira, Review of the dielectric properties of nanofiltration membranes and verification of the single oriented layer approximation. *Advances in colloid and interface science*, 2012. 173: p. 1-11.
162. Chan, R. and V. Chen, Characterization of protein fouling on membranes: opportunities and challenges. *Journal of Membrane Science*, 2004. 242(1): p. 169-188.
163. Hunter, R.J., Zeta potential in colloid science: principles and applications. Vol. 8. 1981: Academic press London.
164. Nyström, M., M. Lindström, and E. Matthiasson, Streaming potential as a tool in the characterization of ultrafiltration membranes. *Colloids and surfaces*, 1989. 36(3): p. 297-312.
165. Nyström, M., A. Pihlajamäki, and N. Ehsani, Characterization of ultrafiltration membranes by simultaneous streaming potential and flux measurements. *Journal of Membrane Science*, 1994. 87(3): p. 245-256.

166. Molina, C., L. Victoria, A. Arenas, and J.A. Ibáñez, Streaming potential and surface charge density of microporous membranes with pore diameter in the range of thickness. *Journal of Membrane Science*, 1999. 163(2): p. 239-255.
167. Kim, K., A. Fane, M. Nystrom, A. Pihlajamaki, W. Bowen, and H. Mukhtar, Evaluation of electroosmosis and streaming potential for measurement of electric charges of polymeric membranes. *Journal of Membrane Science*, 1996. 116(2): p. 149-159.
168. Weis, A., M. Bird, M. Nyström, and C. Wright, The influence of morphology, hydrophobicity and charge upon the long-term performance of ultrafiltration membranes fouled with spent sulphite liquor*. *Desalination*, 2005. 175(1): p. 73-85.
169. Vainshtein, P. and C. Gutfinger, On electroviscous effects in microchannels. *Journal of Micromechanics and Microengineering*, 2002. 12(3): p. 252.
170. Huisman, I., G. Trägårdh, C. Trägårdh, and A. Pihlajamäki, Determining the zeta-potential of ceramic microfiltration membranes using the electroviscous effect. *Journal of Membrane Science*, 1998. 147(2): p. 187-194.
171. Levine, S., J. Marriott, G. Neale, and N. Epstein, Theory of electrokinetic flow in fine cylindrical capillaries at high zeta-potentials. *Journal of colloid and interface science*, 1975. 52(1): p. 136-149.
172. Huisman, I.H., B. Dutrê, K.M. Persson, and G. Trägårdh, Water permeability in ultrafiltration and microfiltration: Viscous and electroviscous effects. *Desalination*, 1997. 113(1): p. 95-103.
173. Jones, S., The application of enganced fluid dynamic gauging as a fouling sensor for pressure driven membrane separatiosn in the food industry. *Doctoral Thesis, Chemical Engineering Department, University of Bath*, 2012.
174. Bowen, W.R., T.A. Doneva, and H. Yin, Atomic force microscopy studies of membrane--solute interactions (fouling). *Desalination*, 2002. 146(1-3): p. 97-102.
175. Bowen, W.R., T.A. Doneva, and J.A.G. Stoton, Protein deposition during cross-flow membrane filtration: AFM studies and flux loss. *Colloids and Surfaces B: Biointerfaces*, 2003. 27(2-3): p. 103-113.
176. Evans, P.J., Membrane-solute-cleaning agent interaction during the ultrafiltration of black tea liquor. *Doctoral Thesis, Chemical Engineering Department, University of Bath*, 2008.
177. Ducker, W.A., T.J. Senden, and R.M. Pashley, Direct measurement of colloidal forces using an atomic force microscope. *Nature*, 1991. 353(6341): p. 239-241.
178. Bowen, W., N. Hilal, R. Lovitt, A. Sharif, and P. Williams, Atomic force microscope studies of membranes: force measurement and imaging in electrolyte solutions. *Journal of Membrane Science*, 1997. 126(1): p. 77-89.
179. Bowen, W.R., N. Hilal, R.W. Lovitt, and C.J. Wright, Direct measurement of interactions between adsorbed protein layers using an atomic force microscope. *Journal of colloid and interface science*, 1998. 197(2): p. 348-352.
180. Kim, K., A. Fane, M. Nyström, and A. Pihlajamaki, Chemical and electrical characterization of virgin and protein-fouled polycarbonate track-etched

membranes by FTIR and streaming-potential measurements. *Journal of Membrane Science*, 1997. 134(2): p. 199-208.

181. Rabiller-Baudry, M., M. Le Maux, B. Chaufer, and L. Begoin, Characterisation of cleaned and fouled membrane by ATR—FTIR and EDX analysis coupled with SEM: application to UF of skimmed milk with a PES membrane. *Desalination*, 2002. 146(1): p. 123-128.
182. Pihlajamäki, A., P. Väisänen, and M. Nyström, Characterization of clean and fouled polymeric ultrafiltration membranes by Fourier transform IR spectroscopy–attenuated total reflection. *Colloids and Surfaces A: Physicochemical and Engineering Aspects*, 1998. 138(2): p. 323-333.
183. Harrick, N.J., Internal reflection spectroscopy. 1967: Harrick Scientific Corp.
184. Väisänen, P., M. Bird, and M. Nyström, Treatment of UF membranes with simple and formulated cleaning agents. *Food and Bioproducts Processing*, 2002. 80(2): p. 98-108.
185. Nyström, M., P. Aimar, S. Luque, M. Kulovaara, and S. Metsämuuronen, Fractionation of model proteins using their physiochemical properties. *Colloids and Surfaces A: Physicochemical and Engineering Aspects*, 1998. 138(2): p. 185-205.
186. Chaufer, B., M. Rabiller-Baudry, A. Bouguen, J.P. Labbé, and A. Quémerais, Spectroscopic characterization of zirconia coated by polymers with amine groups. *Langmuir*, 2000. 16(4): p. 1852-1860.
187. Trägårdh, G., Membrane cleaning. *Desalination*, 1989. 71(3): p. 325-335.
188. Qaisrani, T. and W. Samhaber, Impact of gas bubbling and backflushing on fouling control and membrane cleaning. *Desalination*, 2011. 266(1): p. 154-161.
189. Head, L.E. and M.R. Bird, Backwashing of tubular ceramic microfilters fouled with milk protein isolate feeds. *Journal of Food Process Engineering*, 2013. 36(2): p. 228-240.
190. Maartens, A., E. Jacobs, and P. Swart, UF of pulp and paper effluent: membrane fouling-prevention and cleaning. *Journal of Membrane Science*, 2002. 209(1): p. 81-92.
191. Bowen, W.R. and H.A. Sabuni, Electrically enhanced membrane filtration at low cross-flow velocities. *Industrial & Engineering Chemistry Research*, 1991. 30(7): p. 1573-1579.
192. Lin, J.C.-T., D.-J. Lee, and C. Huang, Membrane fouling mitigation: membrane cleaning. *Separation Science and Technology*, 2010. 45(7): p. 858-872.
193. Shorrock, C. and M. Bird, Membrane cleaning: chemically enhanced removal of deposits formed during yeast cell harvesting. *Food and Bioproducts Processing*, 1998. 76(1): p. 30-38.
194. Chen, J.P., S. Kim, and Y. Ting, Optimization of membrane physical and chemical cleaning by a statistically designed approach. *Journal of Membrane Science*, 2003. 219(1): p. 27-45.
195. Scott, K., Handbook of industrial membranes. 1995: Elsevier.
196. Romney, A., CIP: cleaning in place. 1990: Society of Dairy Technology.

197. Plett, E.A. Cleaning of fouled surfaces. in *Fouling and Cleaning in Food Processing*. 1985: Dept. of Food Science, Madison, WI.
198. Weis, A. and M. Bird, The influence of multiple fouling and cleaning cycles upon the membrane processing of lignosulphonates. *Food and Bioproducts Processing*, 2001. 79(3): p. 184-187.
199. Zhu, H. and M. Nyström, Cleaning results characterized by flux, streaming potential and FTIR measurements. *Colloids and Surfaces A: Physicochemical and Engineering Aspects*, 1998. 138(2-3): p. 309-321.
200. Rana, D. and T. Matsuura, Surface Modifications for Antifouling Membranes. *Chemical Reviews*, 2010. 110(4): p. 2448-2471.
201. Desai, T.A., D.J. Hansford, L. Leoni, M. Essenpreis, and M. Ferrari, Nanoporous anti-fouling silicon membranes for biosensor applications. *Biosensors and Bioelectronics*, 2000. 15(9): p. 453-462.
202. Adams, R., C. Carson, J. Ward, R. Tannenbaum, and W. Koros, Metal organic framework mixed matrix membranes for gas separations. *Microporous and Mesoporous Materials*, 2010. 131(1): p. 13-20.
203. Chou, W.L., D.G. Yu, and M.C. Yang, The preparation and characterization of silver-loading cellulose acetate hollow fiber membrane for water treatment. *Polymers for Advanced Technologies*, 2005. 16(8): p. 600-607.
204. Rajesh, S., P. Maheswari, S. Senthilkumar, A. Jayalakshmi, and D. Mohan, Preparation and characterisation of poly (amide-imide) incorporated cellulose acetate membranes for polymer enhanced ultrafiltration of metal ions. *Chemical Engineering Journal*, 2011. 171(1): p. 33-44.
205. Ulbricht, M. and G. Belfort, Surface modification of ultrafiltration membranes by low temperature plasma II. Graft polymerization onto polyacrylonitrile and polysulfone. *Journal of Membrane Science*, 1996. 111(2): p. 193-215.
206. Mok, S., D. Worsfold, A. Fouda, and T. Matsuura, Surface modification of polyethersulfone hollow-fiber membranes by γ-ray irradiation. *Journal of Applied Polymer Science*, 1994. 51(1): p. 193-199.
207. Pieracci, J., D.W. Wood, J.V. Crivello, and G. Belfort, UV-assisted graft polymerization of N-vinyl-2-pyrrolidinone onto poly (ether sulfone) ultrafiltration membranes: comparison of dip versus immersion modification techniques. *Chemistry of materials*, 2000. 12(8): p. 2123-2133.
208. Nie, F.-Q., Z.-K. Xu, X.-J. Huang, P. Ye, and J. Wu, Acrylonitrile-based copolymer membranes containing reactive groups: surface modification by the immobilization of poly (ethylene glycol) for improving antifouling property and biocompatibility. *Langmuir*, 2003. 19(23): p. 9889-9895.
209. Wavhal, D. and E. Fisher, Hydrophilic modification of polyethersulfone membranes by low temperature plasma-induced graft polymerization. *Journal of Membrane Science*, 2002. 209(1): p. 255-269.
210. Gancarz, I., J. Bryjak, M. Bryjak, G. Poźniak, and W. Tylus, Plasma modified polymers as a support for enzyme immobilization 1.: Allyl alcohol plasma. *European polymer journal*, 2003. 39(8): p. 1615-1622.

211. Gancarz, I., J. Bryjak, G. Poźniak, and W. Tylus, Plasma modified polymers as a support for enzyme immobilization II. Amines plasma. *European polymer journal*, 2003. 39(11): p. 2217-2224.
212. Gancarz, I., G. Poźniak, and M. Bryjak, Modification of polysulfone membranes 1. CO_2 plasma treatment. *European polymer journal*, 1999. 35(8): p. 1419-1428.
213. Gancarz, I., G. Poźniak, and M. Bryjak, Modification of polysulfone membranes: 3. Effect of nitrogen plasma. *European polymer journal*, 2000. 36(8): p. 1563-1569.
214. Kang, M.S., B. Chun, and S.S. Kim, Surface modification of polypropylene membrane by low-temperature plasma treatment. *Journal of Applied Polymer Science*, 2001. 81(6): p. 1555-1566.
215. Lohokare, H., S. Kumbharkar, Y. Bhole, and U. Kharul, Surface modification of polyacrylonitrile based ultrafiltration membrane. *Journal of Applied Polymer Science*, 2006. 101(6): p. 4378-4385.
216. Qiao, X., Z. Zhang, and Z. Ping, Hydrophilic modification of ultrafiltration membranes and their application in Salvia Miltiorrhiza decoction. *Separation and Purification Technology*, 2007. 56(3): p. 265-269.
217. Reddy, A. and H.R. Patel, Chemically treated polyethersulfone/polyacrylonitrile blend ultrafiltration membranes for better fouling resistance. *Desalination*, 2008. 221(1): p. 318-323.
218. Ma, X., Q. Sun, Y. Su, Y. Wang, and Z. Jiang, Antifouling property improvement of poly (vinyl butyral) ultrafiltration membranes through acid treatment. *Separation and Purification Technology*, 2007. 54(2): p. 220-226.
219. Wei, X., Z. Wang, J. Wang, and S. Wang, A novel method of surface modification to polysulfone ultrafiltration membrane by preadsorption of citric acid or sodium bisulfite. *Membrane Water Treatment*, 2012. 3(1): p. 35-49.
220. Bhanushali, D., S. Kloos, C. Kurth, and D. Bhattacharyya, Performance of solvent-resistant membranes for non-aqueous systems: solvent permeation results and modeling. *Journal of Membrane Science*, 2001. 189(1): p. 1-21.
221. Ratetea.net. Which countries produce the most tea? 2010 [cited 2010 09/12/10]; Available from: http://ratetea.net/region.php.
222. geocurrents.info. Annual per capita tea consumption. 2009 [cited 2014 04/06].
223. Jain, N.K., Global advances in tea science. 1999: Aravali Books International.
224. Balentine, D.A. Manufacturing and chemistry of tea. in *ACS Symposium Series*. 1992: ACS Publications.
225. Stahl, W.H., The chemistry of tea and tea manufacturing. *Advances in food research*, 1962. 11: p. 201-262.
226. Bhattacharyya, N., S. Seth, B. Tudu, P. Tamuly, A. Jana, D. Ghosh, R. Bandyopadhyay, and M. Bhuyan, Monitoring of black tea fermentation process using electronic nose. *Journal of Food Engineering*, 2007. 80(4): p. 1146-1156.
227. Astill, C., M.R. Birch, C. Dacombe, P.G. Humphrey, and P.T. Martin, Factors affecting the caffeine and polyphenol contents of black and green tea infusions. *Journal of agricultural and food chemistry*, 2001. 49(11): p. 5340-5347.

228. Cabrera, C., R. Giménez, and M. López, Determination of tea components with antioxidant activity. *J. Agric. Food Chem*, 2003. 51(15): p. 4427-4435.
229. Balentine, D., S. Wiseman, and L. Bouwens, The chemistry of tea flavonoids. *Critical Reviews in Food Science and Nutrition*, 1997. 37(8): p. 693-704.
230. Xiamen. Chemical composition of fresh tea shoot. 2001 [cited 2010 10/12/10]; Chemical composition of fresh tea leaves]. Available from: http://www.fmltea.com/Teainfo/tea-chemistry%20.htm.
231. Rao, L. and V. Sharma, A Thought on the Biological Activities of Black Tea. *Critical Reviews in Food Science and Nutrition*, 2009. 49(5): p. 379-404.
232. Khan, N. and H. Mukhtar, Tea polyphenols for health promotion. *Life Sciences*, 2007. 81(7): p. 519-533.
233. Jöbstl, E., J. O'Connell, J. Fairclough, and M. Williamson, Molecular model for astringency produced by polyphenol/protein interactions. *Biomacromolecules*, 2004. 5(3): p. 942-949.
234. Noble, A., Astringency and bitterness of flavonoid phenols. *ACS Publications*, 2002: p. 192-201.
235. Finger, A., In-vitro studies on the effect of polyphenol oxidase and peroxidase on the formation of polyphenolic black tea constituents. *Journal of the Science of Food and Agriculture*, 1994. 66(3): p. 293-305.
236. Lunder, T. Catechins of green tea: antioxidant activity. 1992.
237. Graham, H., The polyphenols of tea–Biochemistry and significance–a Review. *XVIe Journées Internationales Groupe Polyphénols and The Royal Society of Chemistry, Lisbon*, 1992: p. 32–43.
238. Charlton, A., A. Davis, D. Jones, J. Lewis, A. Davies, E. Haslam, and M. Williamson, The self-association of the black tea polyphenol theaflavin and its complexation with caffeine. *Journal of the Chemical Society, Perkin Transactions 2*, 2000. 2000(2): p. 317-322.
239. Liang, Y. and Y. Xu, Effect of pH on cream particle formation and solids extraction yield of black tea. *Food Chemistry*, 2001. 74(2): p. 155-160.
240. Sanderson, G.W., A.S. Ranadive, L.S. Eisenburg, F.J. Farrell, R. Simons, C.H. Manley, and P. Coggon, Contribution of polyphenolic compounds to the taste of tea. 1976, ACS Publications.
241. Obanda, M., P.O. Owuor, R. Mang'oka, and M.M. Kavoi, Changes in thearubigin fractions and theaflavin levels due to variations in processing conditions and their influence on black tea liquor brightness and total colour. *Food chemistry*, 2004. 85(2): p. 163-173.
242. Drynan, J.W., M.N. Clifford, J. Obuchowicz, and N. Kuhnert, The chemistry of low molecular weight black tea polyphenols. *Natural product reports*, 2010. 27(3): p. 417-462.
243. Kuhnert, N., J.W. Drynan, J. Obuchowicz, M.N. Clifford, and M. Witt, Mass spectrometric characterization of black tea thearubigins leading to an oxidative cascade hypothesis for thearubigin formation. *Rapid Communications in Mass Spectrometry*, 2010. 24(23): p. 3387-3404.

244. Scharbert, S., N. Holzmann, and T. Hofmann, Identification of the astringent taste compounds in black tea infusions by combining instrumental analysis and human bioresponse. *Journal of agricultural and food chemistry*, 2004. 52(11): p. 3498-3508.
245. Yokogoshi, H., Y. Kato, Y.M. Sagesaka, T. Takihara-Matsuura, T. Kakuda, and N. Takeuchi, Reduction effect of theanine on blood pressure and brain 5-hydroxyindoles in spontaneously hypertensive rats. *Bioscience, biotechnology, and biochemistry*, 1995. 59(4): p. 615.
246. Kakuda, T., A. Nozawa, T. Unno, N. Okamura, and O. Okai, Inhibiting effects of theanine on caffeine stimulation evaluated by EEG in the rat. *Bioscience, biotechnology, and biochemistry*, 2000. 64(2): p. 287-293.
247. Tolstoguzov, V., Thermodynamic aspects of biopolymer functionality in biological systems, foods, and beverages. *Critical reviews in biotechnology*, 2002. 22(2): p. 89-174.
248. Siebert, K., A. Carrasco, and P. Lynn, Formation of Protein- Polyphenol Haze in Beverages. *J. Agric. Food Chem*, 1996. 44(8): p. 1997-2005.
249. Andrews, T. and B. Ballment, The function of the small subunits of ribulose bisphosphate carboxylase-oxygenase. *Journal of Biological Chemistry*, 1983. 258(12): p. 7514-7518.
250. Jobstl, E., J. Fairclough, A. Davies, and M. Williamson, Creaming in black tea. *J. Agric. Food Chem*, 2005. 53(20): p. 7997-8002.
251. Liang, Y., J. Lu, and L. Zhang, Comparative study of cream in infusions of black tea and green tea. *International Journal of Food Science & Technology*, 2002. 37(6): p. 627-634.
252. Martin, R., T.H. Lilley, N.A. Bailey, C.P. Falshaw, E. Haslam, D. Magnolato, and M.J. Begley, Polyphenol–caffeine complexation. *Journal of the Chemical Society, Chemical Communications*, 1986(2): p. 105-106.
253. Charlton, A., N. Baxter, M. Khan, A. Moir, E. Haslam, A. Davies, and M. Williamson, Polyphenol/peptide binding and precipitation. *J. Agric. Food Chem*, 2002. 50(6): p. 1593-1601.
254. Papadopoulou, A. and R. Frazier, Characterization of protein-polyphenol interactions. *Trends in Food Science & Technology*, 2004. 15(3-4): p. 186-190.
255. Siebert, K.J., Effects of protein-polyphenol interactions on beverage haze, stabilization, and analysis. *Journal of agricultural and food chemistry*, 1999. 47(2): p. 353-362.
256. Siebert, K.J., Haze formation in beverages. *LWT-Food Science and Technology*, 2006. 39(9): p. 987-994.
257. Harbowy, M.E., D.A. Balentine, A.P. Davies, and Y. Cai, Tea chemistry. *Critical reviews in plant sciences*, 1997. 16(5): p. 415-480.
258. Chao, Y.C. and B.H. Chiang, Cream formation in a semifermented tea. *Journal of the Science of Food and Agriculture*, 1999. 79(13): p. 1767-1774.

259. Tanizawa, Y., T. Abe, and K. Yamada, Black tea stain formed on the surface of teacups and pots. Part 1-Study on the chemical composition and structure. *Food Chemistry*, 2007. 103(1): p. 1-7.
260. Yamada, K., T. Abe, and Y. Tanizawa, Black tea stain formed on the surface of teacups and pots. Part 2-Study of the structure change caused by aging and calcium addition. *Food Chemistry*, 2007. 103(1): p. 8-14.
261. Liang, Y. and Y. Xu, Effect of extraction temperature on cream and extractability of black tea [Camellia sinensis (L.) O. Kuntze]. *International Journal of Food Science & Technology*, 2003. 38(1): p. 37-45.
262. Boadi, D. and R. Neufeld, Encapsulation of tannase for the hydrolysis of tea tannins. *Enzyme and Microbial Technology*, 2001. 28(7): p. 590-595.
263. McMurrough, I., R. Kelly, J. Byrne, and M. O'Brien, Effect of the removal of sensitive proteins and proanthocyanidins on the colloidal stability of lager beer. *Journal of the American Society of Brewing Chemists*, 1992. 50(2): p. 67-76.
264. Borneman, Z., V. Gökmen, and H. Nijhuis, Selective removal of polyphenols and brown colour in apple juices using PES/PVP membranes in a single-ultrafiltration process. *Journal of Membrane Science*, 1997. 134(2): p. 191-197.
265. Cassano, A., E. Drioli, G. Galaverna, R. Marchelli, G. Di Silvestro, and P. Cagnasso, Clarification and concentration of citrus and carrot juices by integrated membrane processes. *Journal of Food Engineering*, 2003. 57(2): p. 153-163.
266. Cassano, A., M. Marchio, and E. Drioli, Clarification of blood orange juice by ultrafiltration: analyses of operating parameters, membrane fouling and juice quality. *Desalination*, 2007. 212(1-3): p. 15-27.
267. Prodanov, M., I. Garrido, V. Vacas, R. Lebrón-Aguilar, M. Dueñas, C. Gómez-Cordovés, and B. Bartolomé, Ultrafiltration as alternative purification procedure for the characterization of low and high molecular-mass phenolics from almond skins. *Analytica chimica acta*, 2008. 609(2): p. 241-251.
268. Bartlett, M., M. Bird, and J. Howell, An experimental study for the development of a qualitative membrane cleaning model. *Journal of Membrane Science*, 1995. 105(1-2): p. 147-157.
269. Weis, A., M.R. Bird, and M. Nyström, The chemical cleaning of polymeric UF membranes fouled with spent sulphite liquor over multiple operational cycles. *Journal of Membrane Science*, 2003. 216(1-2): p. 67-79.
270. Pusch, W. and G. Mossa, Influence of pressure and/or pressure differential on membrane permeability. *Desalination*, 1977. 24(1): p. 39-53.
271. Persson, K., V. Gekas, and G. Trägårdh, Study of membrane compaction and its influence on ultrafiltration water permeability. *Journal of Membrane Science*, 1995. 100(2): p. 155-162.
272. Susanto, H. and M. Ulbricht, Characteristics, performance and stability of polyethersulfone ultrafiltration membranes prepared by phase separation method using different macromolecular additives. *Journal of Membrane Science*, 2009. 327(1): p. 125-135.

273. Bradford, M., A rapid and sensitive method for the quantitation of microgram quantities of protein utilizing the principle of protein-dye binding. *Anal Biochem*, 1976. 72(1-2): p. 248-254.
274. Singleton, V. and J.A. Rossi, Colorimetry of total phenolics with phosphomolybdic-phosphotungstic acid reagents. *American journal of Enology and Viticulture*, 1965. 16(3): p. 144-158.
275. de Bruijn, J. and R. Bórquez, Analysis of the fouling mechanisms during cross-flow ultrafiltration of apple juice. *LWT-Food Science and Technology*, 2006. 39(8): p. 861-871.
276. Dizechi, M. and E. Marschall, Viscosity of some binary and ternary liquid mixtures. *Journal of Chemical and Engineering Data*, 1982. 27(3): p. 358-363.
277. Ariza, M. and J. Benavente, Streaming potential along the surface of polysulfone membranes: a comparative study between two different experimental systems and determination of electrokinetic and adsorption parameters. *Journal of Membrane Science*, 2001. 190(1): p. 119-132.
278. Möckel, D., E. Staude, M. Dal-Cin, K. Darcovich, and M. Guiver, Tangential flow streaming potential measurements: hydrodynamic cell characterization and zeta potentials of carboxylated polysulfone membranes. *Journal of Membrane Science*, 1998. 145(2): p. 211-222.
279. Belfer, S., R. Fainchtain, Y. Purinson, and O. Kedem, Surface characterization by FTIR-ATR spectroscopy of polyethersulfone membranes-unmodified, modified and protein fouled. *Journal of Membrane Science*, 2000. 172(1): p. 113-124.
280. Oldani, M. and G. Schock, Characterization of ultrafiltration membranes by infrared spectroscopy, ESCA, and contact angle measurements. *Journal of Membrane Science*, 1989. 43(2-3): p. 243-258.
281. Fontyn, M., K. van't Riet, and B. Bijsterbosch, Surface spectroscopic studies of pristine and fouled membranes part II. Method development and adsorption mechanism. *Colloids and surfaces*, 1991. 54: p. 349-362.
282. Sims, C.A., J.S. Eastridge, and R.P. Bates, Changes in phenols, color, and sensory characteristics of muscadine wines by pre-and post-fermentation additions of PVPP, casein, and gelatin. *American journal of Enology and Viticulture*, 1995. 46(2): p. 155-158.
283. Mitchell, A.E., Y.J. Hong, J.C. May, C.A. Wright, and C.W. Bamforth, A Comparison of Polyvinylpolypyrrolidone (PVPP), Silica Xerogel and a Polyvinylpyrrolidone (PVP)–Silica Co-Product for Their Ability to Remove Polyphenols from Beer. *Journal of the Institute of Brewing*, 2005. 111(1): p. 20-25.
284. Han, M.-J. and S.-T. Nam, Thermodynamic and rheological variation in polysulfone solution by PVP and its effect in the preparation of phase inversion membrane. *Journal of Membrane Science*, 2002. 202(1): p. 55-61.
285. Koga, S., T. Yakushiji, M. Matsuda, K.-i. Yamamoto, and K. Sakai, Functional-group analysis of polyvinylpyrrolidone on the inner surface of hollow-fiber

dialysis membranes, by near-field infrared microspectroscopy. *Journal of Membrane Science*, 2010. 355(1): p. 208-213.

286. Miyano, T., T. Matsuura, D. Carlsson, and S. Sourirajan, Retention of polyvinylpyrrolidone swelling agent in the poly (ether p-phenylenesulfone) ultrafiltration membrane. *Journal of Applied Polymer Science*, 1990. 41(1-2): p. 407-417.
287. Lindau, J., A. Jönsson, and R. Wimmerstedt, The influence of a low-molecular hydrophobic solute on the flux of polysulphone ultrafiltration membranes with different cut-off. *Journal of Membrane Science*, 1995. 106(1-2): p. 9-16.
288. Al Malek, S., A. Seman, D. Johnson, and N. Hilal, Formation and characterization of polyethersulfone membranes using different concentrations of polyvinylpyrrolidone. *Desalination*, 2012. 288: p. 31-39.
289. Holt, J.K., H.G. Park, Y. Wang, M. Stadermann, A.B. Artyukhin, C.P. Grigoropoulos, A. Noy, and O. Bakajin, Fast mass transport through sub-2-nanometer carbon nanotubes. *Science*, 2006. 312(5776): p. 1034-1037.
290. Majumder, M., N. Chopra, R. Andrews, and B.J. Hinds, Nanoscale hydrodynamics: Enhanced flow in carbon nanotubes. *Nature*, 2005. 438(7064): p. 44-44.
291. Majumder, M., N. Chopra, and B.J. Hinds, Mass transport through carbon nanotube membranes in three different regimes: Ionic diffusion and gas and liquid flow. *ACS nano*, 2011. 5(5): p. 3867-3877.
292. Mattia, D. and F. Calabrò, Explaining high flow rate of water in carbon nanotubes via solid–liquid molecular interactions. *Microfluidics and Nanofluidics*, 2012: p. 1-6.
293. Mattia, D. and Y. Gogotsi, Review: static and dynamic behavior of liquids inside carbon nanotubes. *Microfluidics and Nanofluidics*, 2008. 5(3): p. 289-305.
294. Qin, X., Q. Yuan, Y. Zhao, S. Xie, and Z. Liu, Measurement of the rate of water translocation through carbon nanotubes. *Nano letters*, 2011. 11(5): p. 2173.
295. Zettlemoyer, A., Hydrophobic surfaces. *Journal of colloid and interface science*, 1968. 28(3): p. 343-369.
296. Weisenhorn, A.L., M. Khorsandi, S. Kasas, V. Gotzos, and H.-J. Butt, Deformation and height anomaly of soft surfaces studied with an AFM. *Nanotechnology*, 1993. 4(2): p. 106.
297. Heffernan, R., A. Semião, P. Desmond, H. Cao, A. Safari, O. Habimana, and E. Casey, Disinfection of a polyamide nanofiltration membrane using ethanol. *Journal of Membrane Science*, 2013. 448: p. 170-179.
298. Yang, X., A. Livingston, and L. Freitas dos Santos, Experimental observations of nanofiltration with organic solvents. *Journal of Membrane Science*, 2001. 190(1): p. 45-55.
299. Tsui, E.M. and M. Cheryan, Characteristics of nanofiltration membranes in aqueous ethanol. *Journal of Membrane Science*, 2004. 237(1): p. 61-69.

300. JPK. Determining the elastic modulus of biological samples using atomic force microscopy. 02-09-13; 1-9]. Available from: http://usa.jpk.com/index.download.5fb2f841667674176fd945e65f073bad.
301. Laligant, A., E. Dumay, C. Casas Valencia, J.L. Cuq, and J.C. Cheftel, Surface hydrophobicity and aggregation of. beta.-lactoglobulin heated near neutral pH. *Journal of agricultural and food chemistry*, 1991. 39(12): p. 2147-2155.
302. Grinberg, N., R. Blanco, D. Yarmush, and B. Karger, Protein aggregation in high-performance liquid chromatography: hydrophobic interaction chromatography of. beta.-lactoglobulin A. *Analytical chemistry*, 1989. 61(6): p. 514-520.
303. Foley, G., Membrane Filtration: A Problem Solving Approach with MATLAB®. 2013: Cambridge University Press.
304. Opong, W.S. and A.L. Zydney, Hydraulic permeability of protein layers deposited during ultrafiltration. *Journal of colloid and interface science*, 1991. 142(1): p. 41-60.
305. Huisman, I.H., P. Prádanos, and A. Hernández, The effect of protein–protein and protein–membrane interactions on membrane fouling in ultrafiltration. *Journal of Membrane Science*, 2000. 179(1): p. 79-90.
306. McDonogh, R., H. Bauser, N. Stroh, and H. Chmiel, Concentration polarisation and adsorption effects in cross-flow ultrafiltration of proteins. *Desalination*, 1990. 79(2): p. 217-231.
307. Maruyama, T., S. Katoh, M. Nakajima, H. Nabetani, T.P. Abbott, A. Shono, and K. Satoh, FT-IR analysis of BSA fouled on ultrafiltration and microfiltration membranes. *Journal of Membrane Science*, 2001. 192(1): p. 201-207.
308. Salgın, S., U. Salgın, and S. Bahadır, Zeta Potentials and Isoelectric Points of Biomolecules: The Effects of Ion Types and Ionic Strengths. *Int. J. Electrochem. Sci*, 2012. 7: p. 12404-12414.
309. Palecek, S.P. and A.L. Zydney, Intermolecular electrostatic interactions and their effect on flux and protein deposition during protein filtration. *Biotechnology progress*, 1994. 10(2): p. 207-213.
310. Fane, A., C. Fell, and A. Waters, The relationship between membrane surface pore characteristics and flux for ultrafiltration membranes. *Journal of Membrane Science*, 1981. 9(3): p. 245-262.
311. Jones, S.A., A. Pihlajamäki, and M. Bird, The role of synthetic membrane pre-treatment in influencing filtration performance over multiple operational cycles. *Separation Science and Technology*, 2012. 47(8): p. 1119-1128.
312. Khokhar, S. and S. Magnusdottir, Total phenol, catechin, and caffeine contents of teas commonly consumed in the United Kingdom. *Journal of agricultural and food chemistry*, 2002. 50(3): p. 565-570.
313. Lakenbrink, C., S. Lapczynski, B. Maiwald, and U.H. Engelhardt, Flavonoids and other polyphenols in consumer brews of tea and other caffeinated beverages. *Journal of agricultural and food chemistry*, 2000. 48(7): p. 2848-2852.

314. Yao, L., N. Caffin, B. D'arcy, Y. Jiang, J. Shi, R. Singanusong, X. Liu, N. Datta, Y. Kakuda, and Y. Xu, Seasonal variations of phenolic compounds in Australia-grown tea (Camellia sinensis). *Journal of agricultural and food chemistry*, 2005. 53(16): p. 6477-6483.
315. Chandini, S.K., L.J. Rao, and R. Subramanian, Membrane Clarification of Black Tea Extracts. *Food and Bioprocess Technology*, 2012: p. 1-18.
316. Balentine, D.A., S.A. Wiseman, and L.C. Bouwens, The chemistry of tea flavonoids. *Critical Reviews in Food Science & Nutrition*, 1997. 37(8): p. 693-704.
317. Menet, M.-C., S. Sang, C.S. Yang, C.-T. Ho, and R.T. Rosen, Analysis of theaflavins and thearubigins from black tea extract by MALDI-TOF mass spectrometry. *Journal of agricultural and food chemistry*, 2004. 52(9): p. 2455-2461.
318. Yuan, W. and A.L. Zydney, Humic acid fouling during microfiltration. *Journal of Membrane Science*, 1999. 157(1): p. 1-12.
319. Howell, J.A., Sub-critical flux operation of microfiltration. *Journal of Membrane Science*, 1995. 107(1): p. 165-171.
320. Jönsson, C. and A.-S. Jönsson, Influence of the membrane material on the adsorptive fouling of ultrafiltration membranes. *Journal of Membrane Science*, 1995. 108(1): p. 79-87.
321. Palacio, L., J. Calvo, P. Pradanos, A. Hernandez, P. Väisänen, and M. Nyström, Contact angles and external protein adsorption onto UF membranes. *Journal of Membrane Science*, 1999. 152(2): p. 189-201.
322. Gaffney, S.H., R. Martin, T.H. Lilley, E. Haslam, and D. Magnolato, The association of polyphenols with caffeine and α-and β-cyclodextrin in aqueous media. *Journal of the Chemical Society, Chemical Communications*, 1986(2): p. 107-109.
323. Martinez, S., L. Valek, Ž. Petrović, M. Metikoš-Huković, and J. Piljac, Catechin antioxidant action at various pH studied by cyclic voltammetry and PM3 semi-empirical calculations. *Journal of electroanalytical chemistry*, 2005. 584(2): p. 92-99.
324. Gordin, R., Certain aspects of the Thrombotest method for the control of anticoagulant therapy. *Scandinavian Journal of Clinical & Laboratory Investigation*, 1960. 12(3): p. 329-332.
325. Brans, G., C. Schroen, R. Van der Sman, and R. Boom, Membrane fractionation of milk: state of the art and challenges. *Journal of Membrane Science*, 2004. 243(1): p. 263-272.
326. Visvanathan, C. and R. Ben Aim, Application of an electric field for the reduction of particle and colloidal membrane fouling in crossflow microfiltration. *Separation Science and Technology*, 1989. 24(5-6): p. 383-398.
327. Blanpain, P., J. Hermia, and M. Lenoel, Mechanisms governing permeate flux and protein rejection in the microfiltration of beer with a cyclopore membrane. *Journal of Membrane Science*, 1993. 84(1): p. 37-51.

328. Penders, M.H., D.P. Jones, D. Needham, and E.G. Pelan, Mechanistic study of equilibrium and kinetic behaviour of tea cream formation. *Food hydrocolloids*, 1998. 12(1): p. 9-15.
329. Weast, R.C., M.J. Astle, and W.H. Beyer, CRC handbook of chemistry and physics. Vol. 1989. 1988: CRC press Boca Raton, FL.
330. Colorbasics. CIE 1931 Color Space. 2005 [cited 2010 28.10.2010]; Available from: http://www.colorbasics.com/CIESystem/.

Appendix A: Experimental calibrations and reference properties

A1: M-10 pressure transducer calibration

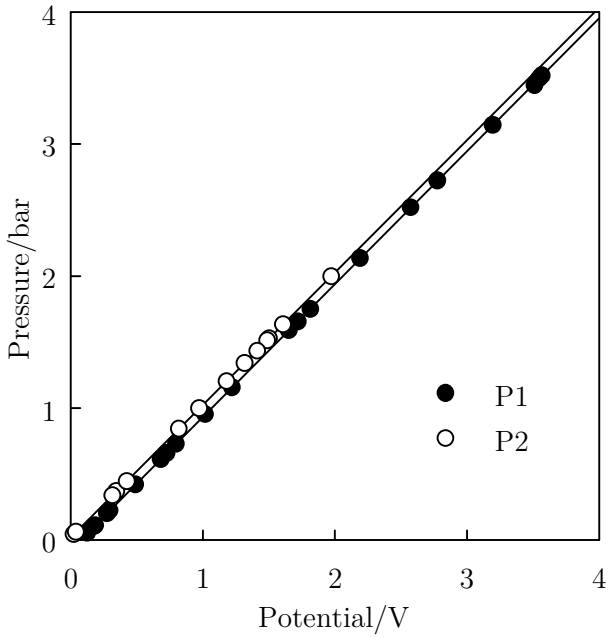

Figure A-1 – Sample calibration data for M-10 pressure transducers

TMP was calculated from pressure measurements using the following equation – an average of the converted potentials based on the linear fits for each transducer.

$$TMP = \frac{P_1 + P_2}{2} = \frac{(0.9931V_1 + 0.0734) + (0.9971V_2 - 0.0199)}{2}$$

A2: M-10 rotameter calibration

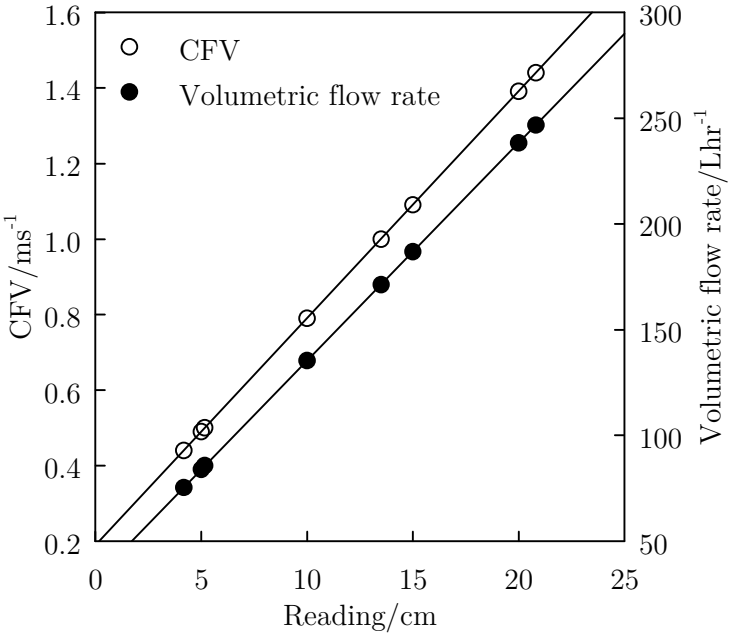

Figure A-2 - Rotameter calibration chart

A3: M-10 module/rig dimensions and materials

Table A-1 – M-10 module/rig properties

Dimension	*Value*	*Unit*
Channel length	0.135	m
Channel width	0.017	m
Channel height	0.0007	m
Number of channels	4	
Total channel volume	6.4×10^{-6}	m^3
Total module volume	5.7×10^{-5}	m^3
Effective hydraulic diameter	0.0013	m
Channel cross-sectional area	1.19×10^{-5}	m^2
Filtration area	0.0336	m^2
Filtration system dead volume	0.7	m^3

A4: Dead-end cell pressure gauge calibration

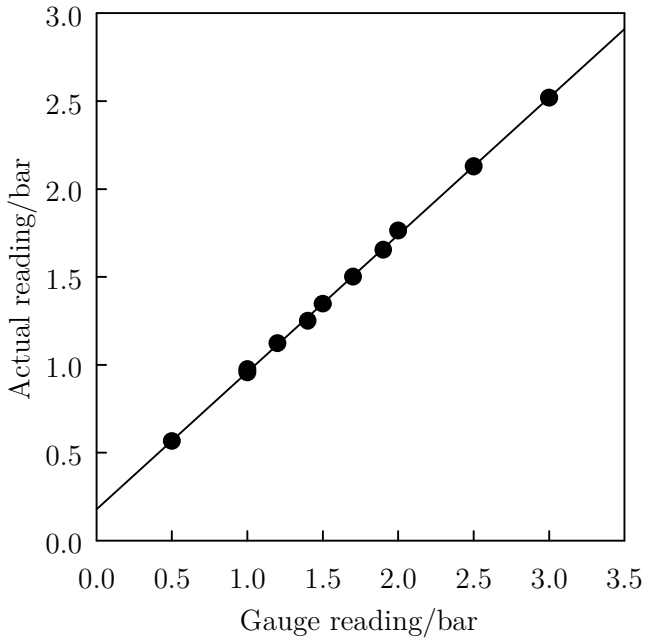

Figure A-3 - Gauge calibration for dead end cell/pre-treatment apparatus pressure gauge

A5: Gallic acid equivalents calibration (total polyphenols assay)

Table A-2 - Example absorbance data for gallic acid standards at 765 nm

Acid conc./ μgmL^{-1}	*Absorbance 1*	*Absorbance 2*	*Absorbance 3*	*Absorbance 4*	*Absorbance average*	*Absorbance standard deviation*
0	0.058 0.057	0.057 0.056	0.054 0.052	0.052 0.053	0.054	0.002
10	0.185	0.182	0.184	0.189	0.185	0.002
20	0.309	0.302	0.310	0.303	0.306	0.004
25	0.373	0.369	0.373	0.370	0.371	0.002
30	0.411	0.446	0.43	0.425	0.428	0.014
40	0.535	0.534	0.535	0.532	0.534	0.001
50	0.647	0.658	0.656	0.657	0.654	0.005
Sample #1	0.486	0.471	0.462	0.481	0.475	0.011
Sample #2	0.213	0.216	0.218	0.209	0.214	0.003

A straight line graph of absorbance vs. gallic acid concentration was obtained as shown in Figure A-4 with the line equation providing the necessary parameters for conversion. Diluted tea samples were compared against this curve to gain diluted total polyphenols concentration. A rejection coefficient based on the difference between retentate and permeate samples was then obtained.

$$[TPP]_{sample\ \#1} = \frac{Abs - 0.064}{0.012} = \frac{(0.475) - 0.065}{0.012} = 34.51\ \mu gmL^{-1}$$

$$[TPP]_{sample\ \#2} = \frac{Abs - 0.064}{0.012} = \frac{(0.214) - 0.065}{0.012} = 12.60\ \mu gmL^{-1}$$

Assuming sample #1 is a retentate sample and sample #2 is a permeate sample, an apparent rejection coefficient was calculated as follows:

$$R_{app,TPP} = 1 - \frac{c_{sample\ \#2}}{c_{sample\ \#1}} = 1 - \frac{12.60}{34.51} = 0.635$$

Error was estimated by dividing the standard deviation by the average across 4 readings to give a fractional area, then multiplying this factor by the final concentration reading for each sample. Error for the rejection was taken as the root mean square of the sample concentration errors.

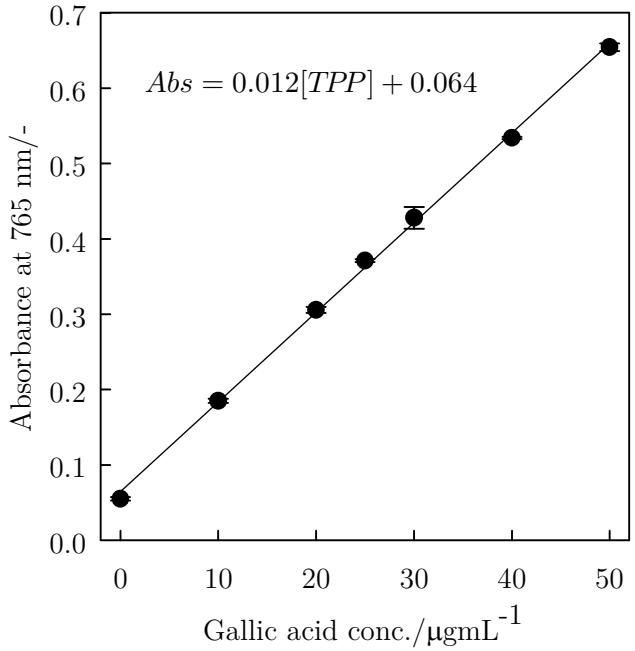

Figure A-4 - Calibration curve for total polyphenols quantification

A6: Absolute polyphenols concentration

The total proportion of polyphenols was calculated first by determining the solids concentration in samples after dilution with ACN, and further by water.

$$c_{dilute} = c_{tea\backslash tea+ACN} + c_{tea+ACN\backslash tea+ACN+water}$$

$$c_{dilute} = \frac{c(wt.\%)_{tea} \times 10(mgmL^{-1}) \times 1.8(mL)_{tea}}{1.8(mL)_{tea} + 1(mL)_{ACN}} \times \frac{0.1(mL)_{tea+ACN}}{0.1(mL)_{tea+ACN} + 4.9(mL)_{tea+ACN+water}}$$

For a 1.0 wt.% reconstitute:

$$c_{dilute} = \frac{(1) \times 10 \times 1.8}{1.8 + 0.2} \times \frac{0.1}{0.1 + 4.9} = 9 \times 0.02 = 0.18\ mgmL^{-1}$$

Total polyphenols fraction (y_{TP}) of total solids could then be calculated from a 1.0 wt.% tea sample with measured absorbance of 0.6259 ± 0.0040 (meaning a dilute concentration of 46.8 µgmL^{-1} polyphenols determined from standard curves) as follows:

$$y_{TP=} = \frac{c_{polyphenols,dilute}}{c_{solids,dilute}} = \frac{(0.0468)}{(0.18)} = 0.26$$

Further, total residual solids mass fraction (all non-polyphenols) could be calculated by way of a simple mass balance of total solids and total polyphenols mass fractions:

$$y_{TS} = y_{TP} + y_{TRS}$$

$$y_{TRS} = y_{TS} - y_{TP} = (1.0) - (0.26) = 0.74$$

A6: Sodium hydroxide pH

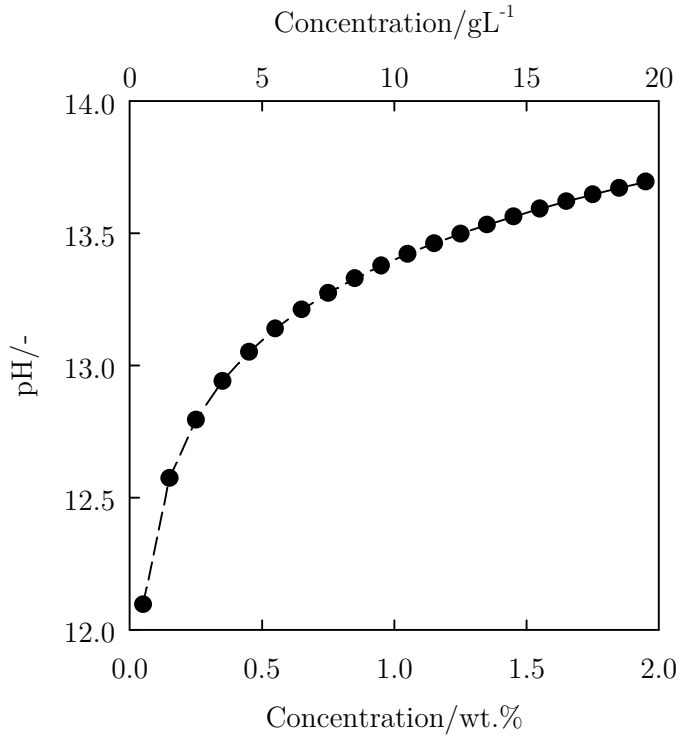

Figure A-5 - pH of sodium hydroxide solutions

A7: Tea viscosity - Unilever spray-dried reconstitute

Viscosity was measured using a Routine Viscometer (Cannon-Fenske, State College, PA, USA). An average of 10 time measurements were made before averaging and calculation of dynamic viscosity. Conversion of dynamic to kinematic viscosity (division by solution density) was made by assuming densities equivalent to water for a given temperature.

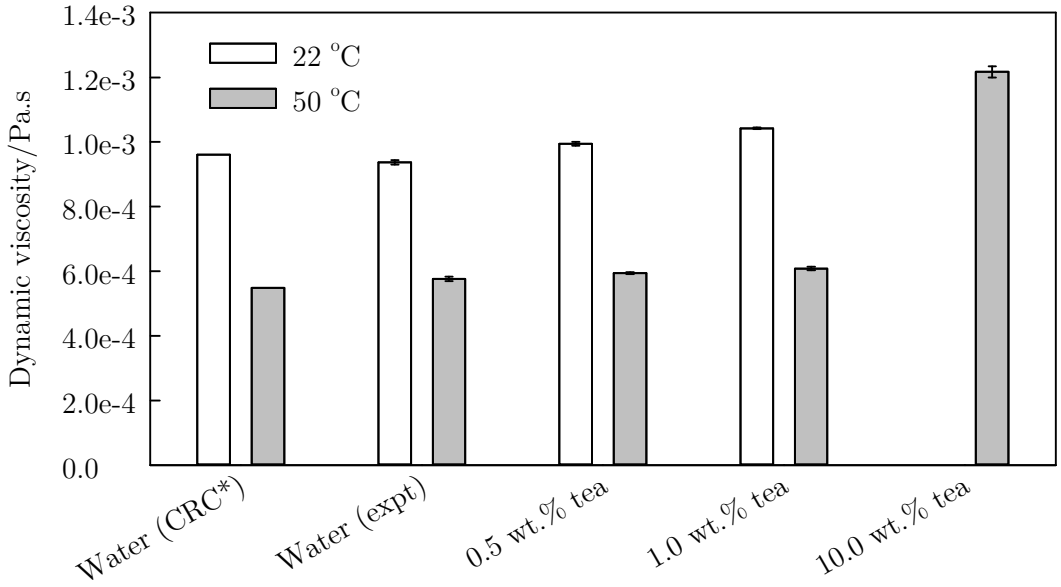

Figure A-6 – Dynamic viscosity comparisons of water (*from literature [329]) and water (determined experimentally) with tea reconstitute at various concentrations

A8: CWS tea characterisation methodology

Finlays tea was a Kenyan cold water soluble (CWS) tea powder. The powder is produced upon spray drying of extracted tea and is reconstituted as described in 4.2.3.2. The tea powder is cold-water soluble meaning it has been passed through an ambient centrifugation operation with the soluble concentrate stream being the target stream for such tea products.

A8.1: Tea solids and refractive index

In order to consistently dilute tea at point of filtration, refractive index (RI) was measured (in terms of °Brix) for 1.0 to 10.0 wt.% tea solutions. The data did not fit an exact linear trend accurately and was thus divided into three linear regions as shown in Figure A-7 - Refractive index variation with concentration

(straight line equations in the form $RI = m[C] + c$ for the regions are shown to the right of the figure).

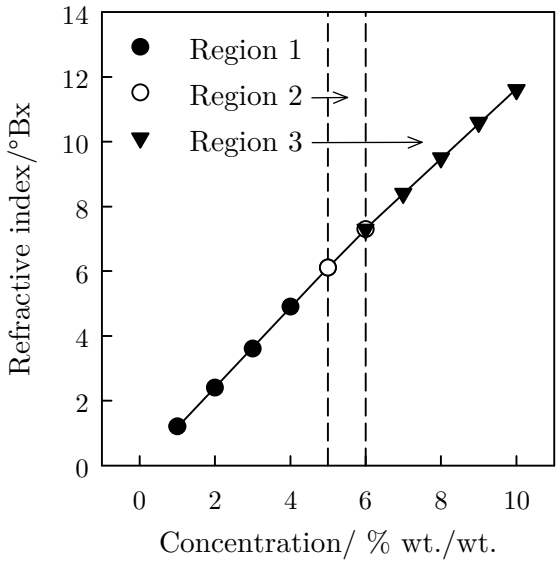

Region 1: $RI = 1.23[C] - 0.05$

Region 2: $RI = 1.20[C] + 0.10$

Region 3: $RI = 1.08[C] + 0.84$

Figure A-7 - Refractive index variation with concentration

A8.2: Dilution of tea samples

Upon conversion of RI to $[C]$, necessary dilutions were taken place to make 100 mL of 'simulated RTD tea beverage' using the following calculations (all volumes V are mL, all concentrations are wt.%)

$$V_{tea,concentrate} = \frac{V_{tea,final} \times [C]_{tea,final}}{[C]_{tea,concentrate}} = \frac{(100) \times (0.3)}{[C]_{tea,concentrate}}$$

$$V_{acid,0.3wt\%} = 1.0$$

$$V_{water} = 100 - V_{tea,concentrate} - 1.0$$

A8.3. Viscosity

Kinematic viscosity was measured for 1.0 – 10.0 wt.% tea at 25 °C using a standard viscometer (constant $= 8.018 \times 10^{-3}$) and converted to dynamic viscosity by division of the density (taken to be that of water).

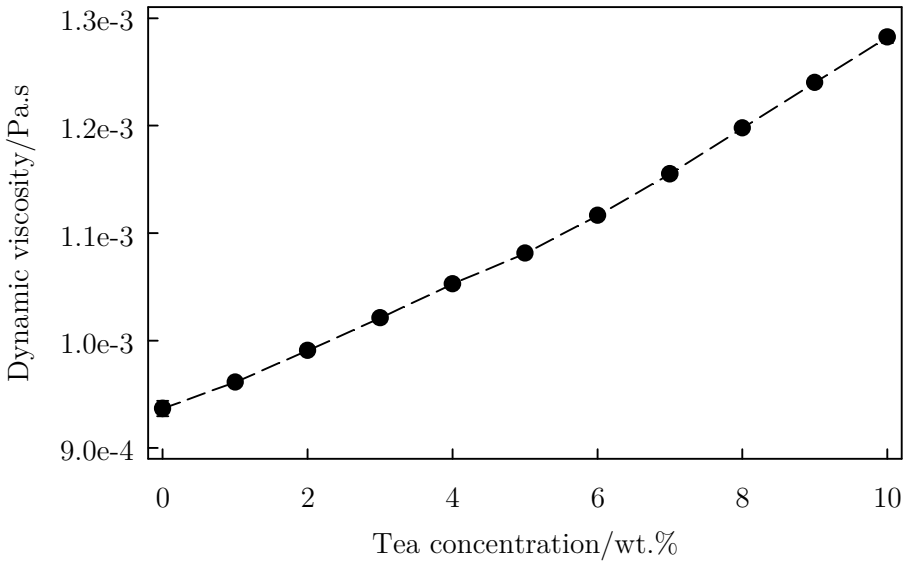

Figure A-8 - Dynamic viscosity of reconstituted Finlays CWS tea at various concentrations

A linear trend was observed with increasing concentration as shown in Figure A-8. An r^2 of 0.9936 resulted from the fit: $\mu = 3.55 \times 10^{-5}[C] + 9.15 \times 10^{-4}$ (μ is the dynamic viscosity in Pa.s). Knowledge of the viscosity allowed calculation of specific resistances at various points during the filtration as shown in Chapter 4.

A8.4: Total polyphenols

Figure A-9 shows the absorbance of gallic acid standards and tea using the Folin and Ciocalteu assay. GA standards were made in the range 0 to 0.05 $mgmL^{-1}$. A linear trend was observed with the equation: $Abs_{595nm} = 11.767[C_{phenolics,dilute}] + 0.0606$ and determination coefficient of 0.9917 shown in Figure A-9a. Figure A-9b shows the absorbance of tea at various concentrations. The graph shows non-linearity at higher concentrations and the overall trend fits a second order polynomial, not a linear trend. This suggests that at high concentrations, there is optical interference when measuring the absorbance at 595 nm, probably arising from the noticeably deeper (greener) colour of assayed samples at high concentration compared to the low end concentration and standards.

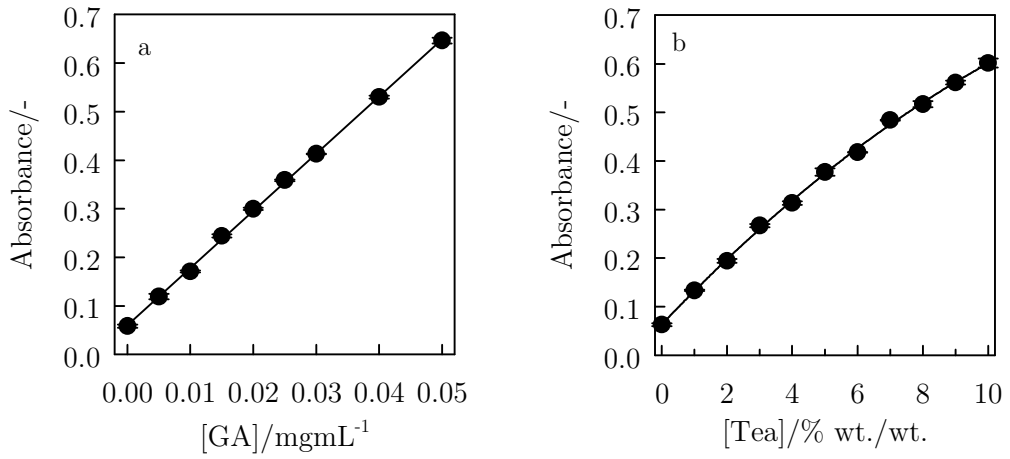

Figure A-9 - (a) Gallic acid standard curve. (b) Tea absorbance at various dilutions

For this reason, when conversion of tea absorbance to fraction of polyphenols was carried out, the ratio of polyphenols to total solids changed. A correction to the calibration was thus made based on the sample with, theoretically, the lowest interference i.e. 1.0 wt.% dilution. The discrepancy is shown in Figure A-10a.

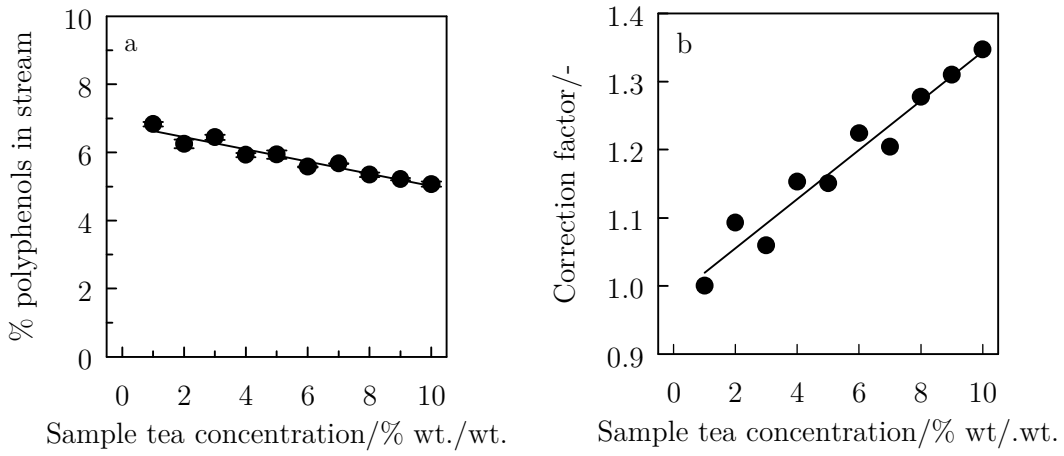

Figure A-10 - (a) Discrepancy in polyphenols fraction due to interference. (b) Correction factor for absorbance interference

By taking the ratio of the calculated sample polyphenol fraction to the 1.0 wt.% fraction, a correction factor φ was expressed so as to standardise the absorbance conversion process. φ has been expressed as a function of concentration by the equation $\varphi = 0.0361[C_{concentrate}] + 0.983$, plotted in Figure A-10b. The error in polyphenol fraction must also be adjusted accordingly. Multiplication of φ by the apparent concentration gives the corrected concentration. The correction factor is only valid for samples between 1.0 and 10.0 wt.%. Using the explained methodology, the proportion of total phenols in the unfiltered tea was found to be 6.8% ± 0.1%.

A9: Colour measurement and CIE Lab parameter derivation

L^*, a^* and b^* are derived parameters which give an indication of the colour of an object/substance. They are derived from spectra data based on the CIE 1931 *XYZ* colourspace. They represent perceptually uniform colour measures by linearisation of the nonlinear *XYZ* scale [330]. The approximation is designed to mimic human vision and thus provides a useful measure with respect to consumer perception of food products such as black tea. The *XYZ* scale is divided into tristimulus representing red, green and blue respectively which are derived from the differing response of three types of cone cells in the human eye. These cells are stimulated over different wavelength ranges; the absorbance spectra responses for these are shown in Figure A-11.

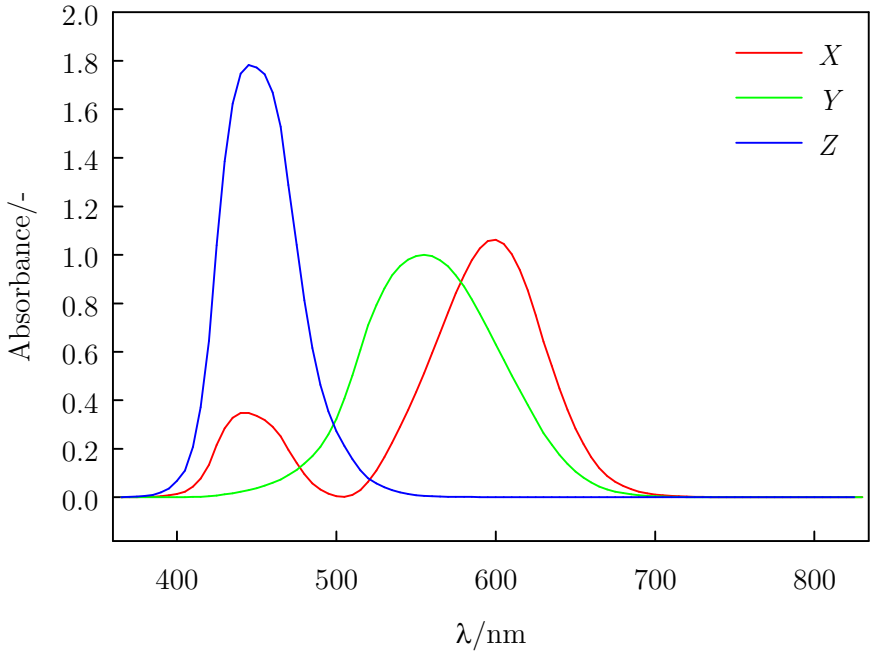

Figure A-11 – Colour matching functions for *XYZ* tristimulus spectra (CIE 1931)

XYZ values can be calculated by determining the area under the curve produced by the product of the spectral distribution ($I(\lambda)$) for a given colour and the colour matching function ($\bar{x}(\lambda)$) over the visible spectrum using the following formulae:

$$X = \int_{380}^{780} I(\lambda)\bar{x}(\lambda)d\lambda$$

$$Y = \int_{380}^{780} I(\lambda)\bar{y}(\lambda)d\lambda$$

$$Z = \int_{380}^{780} I(\lambda)\bar{z}(\lambda)d\lambda$$

In which λ is the monochromatic light wavelength equivalent. To finally calculate the CIE Lab coordinates, the following formulae are used incorporating the *XYZ* values

determined previously, and reference white point values (X_n, Y_n, Z_n) (normalised colour matching functions).

$$L^* = 116 f\left(\frac{Y}{Y_n}\right) - 16$$

$$a^* = 500\left[f\left(\frac{X}{X_n}\right) - f\left(\frac{Y}{Y_n}\right)\right]$$

$$b^* = 200\left[f\left(\frac{Y}{Y_n}\right) - f\left(\frac{Z}{Z_n}\right)\right]$$

where:

$$f(t) = \begin{cases} if\ t > \left(\frac{6}{29}\right)^3,\ t^{\frac{1}{3}} \\ otherwise, \frac{1}{3}\left(\frac{29}{6}\right)^2 t + \frac{4}{29} \end{cases}$$

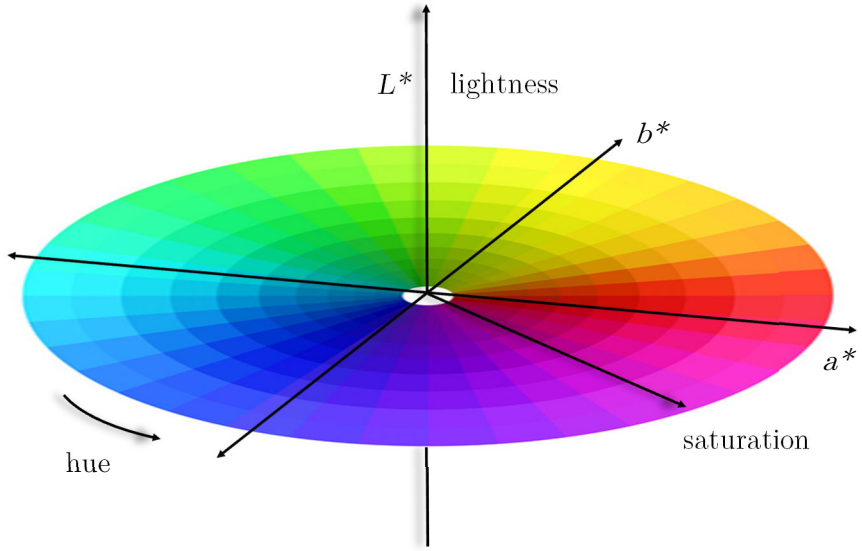

Figure A-12 - CIE Lab colourspace representation and colour-related definitions

Appendix B: Statistical methods

Statistical tests were implemented on data sets using a combination of MS Excel (typically for analytical calculations, normal probability plots and t-tests) and SigmaPlot for more complex tests (normality and non-parametric tests).

Descriptive and frequentist statistics

B1: Mean of repeat experiments

$$\bar{x} = \frac{\sum_{i=1}^{n} x_n}{n}$$

B2: Standard deviation of the mean

$$\sigma(x) = \frac{1}{n}\sqrt{\sum_{i=1}^{n}(x_i - \overline{x})^2}$$

B3: Data normality test (Shapiro-Wilk test)
The Shapiro-Wilk test was implemented for analysis of data sets prior to inferential statistical analysis. The test refers to the null hypothesis that the data set being tested is normally distributed and is rejected if the W value obtained using the following formula is below a pre-set value (set at $p < 0.05$ in this instance).

$$W = \frac{\left(\sum_{i=1}^{n} a_i x_{(i)}\right)^2}{\sum_{i=1}^{n}(x_i - \bar{x})^2}$$

Where $\bar{x}$ is the sample mean and a_i are the Shapiro-Wilk coefficients that are defined as follows:

$$(a_1, \ldots, a_n) = \frac{m^T V^{-1}}{(m^T V^{-1} V^{-1} m)^{\frac{1}{2}}}$$

where $m = (m_1, \ldots, m_n)^T$ and $m_1, \ldots, m_n$ are the expected order statistics from normally distributed random variables. V is the relevant covariance matrix of $m_1, \ldots, m_n$.

B4: Normal probability plots
As a verification of the Shapiro-Wilk test, the normal probability plot allows for a visual verification as to the goodness of fit of the data set compared to a uniformly normally distributed set of variables. Such plots are shown in Figure B-1 for AFM data. The plots are generated by comparing the expected normal values generated from the cumulative distribution function of the data set to the data itself with respect to the data's z-score.

As shown in the plots, significant deviation at the positive and negative tails is evident, verifying that data must be treated as non-normal when utilising further inferential tests.

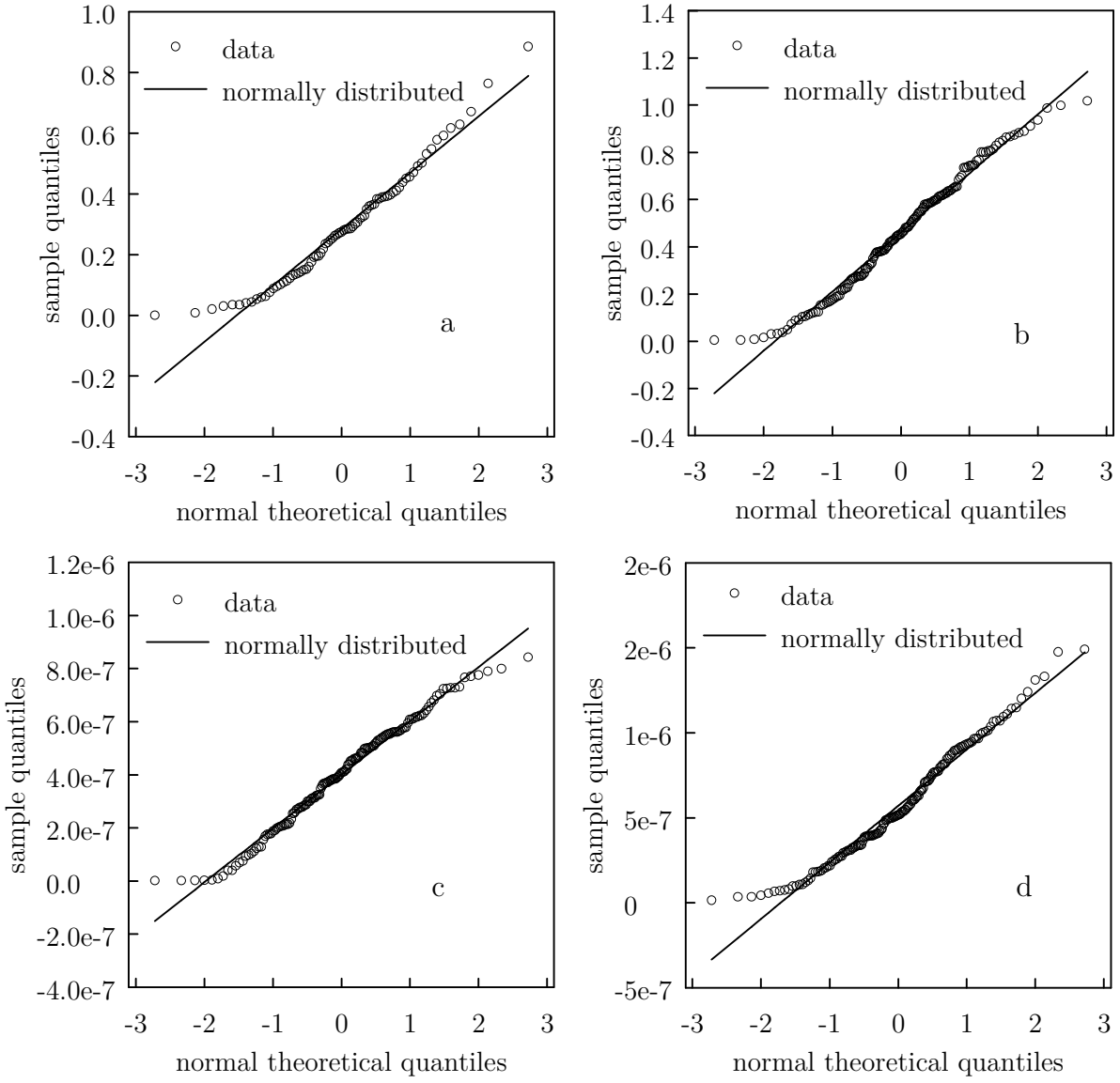

Figure B-1 - Normality probability plots of AFM data relating to PS50 membranes, (a) adhesive force untreated membrane, (b) adhesive force treated membranes, (c) work of adhesion on untreated membrane, and (d) work of adhesion on treated membrane.

Inferential statistics

B5: Normally distributed sample data (Student's t-test)

The t-test was used as a means to test significance between two groups of data. The formula below is for a two-tailed, independent test i.e. between two groups of normally distributed data with unequal variance in which the values have no dependency on one another (untied). Typically the test was used to ascertain a significant difference between a control membrane and a modified membrane. The general null hypothesis used for the test is that the means of the samples do not vary i.e. H_0; $\bar{x}_1 = \bar{x}_2$. In order for the null hypothesis to be rejected, the calculated t value must be greater than the critical t value. The calculated t value (t_{calc}) can be determined as follows:

$$t_{calc} = \frac{\bar{x}_1 - \bar{x}_2}{\sqrt{\frac{S_1}{n_1} - \frac{S_2}{n_2}}}$$

Where S is sample variance and n is sample frequency. The critical t value (t_{crit}) is obtained by consulting a t distribution table. These tables contain columns of t_{crit} values for given significance levels e.g. 95%, 99%, 99.9% confidence (usually expressed as p values; 0.05, 0.01, 0.001 respectively). The specific value is selected based on the combined degrees of freedom (df) of the sample sets, calculated as follows:

$$df = (n_1 - 1) + (n_2 - 1)$$

For ease of calculation, the MS Excel t-test function was used to calculate a p value directly from two columns of data, in order to save manual calculation and referral to tables. This was implemented using the following input:

```
=TTEST(A1:A12,B1:B12,2,3)
```

Where A1:A12 is the control sample, and B1:B12 is the test sample. 2 refers to the number of tails (two-tailed distribution), and 3 is a qualifier instructing Excel that the test is for two samples and variances are unequal (heteroscedasticity).

B6: Non-parametric sample data (Mann-Whitney U test)

The described test was used when data normality tested negative meaning a t-test was not applicable.

Two sample populations are displayed and ranked as shown in Table B-2. Both or either one of the populations have shown non-normality according to the Shapiro-Wilk test. The statistical significance is to be tested against the null hypothesis, '*there is no difference between sample 1 and sample 2*'.

Table B-1 - Sample data sets for Mann-Whitney U test

	Sample set 1			*Sample set 2*	
n_{x_1}	*result*	*rank*	n_{x_2}	*result*	*rank*
1	3	3	1	9	11
2	4	4	2	7	9
3	2	1.5	3	5	5.5
4	6	7.5	4	10	12
5	2	1.5	5	6	7.5
6	5	5.5	6	8	10
median	3.5		*median*	7.5	

First the rank totals for each sample set are calculated, and the larger total is labelled T_X, as follows:

$$T = \sum_{i=1}^{n} r_{n_x} \qquad T_1 = 23, \qquad T_2 = T_X = 55$$

Where r_{n_x} is a given rank of one sample element. Second, the total number of samples in each set is calculated, in this instance, $n = 6$ for both set 1 and set 2 and express as $N_1 = 6$ and $N_2 = 6$. Label the set which received the T_X label, with N_X. Finally, use the formula below to calculate the U *value* for the samples sets:

$$U = N_1 \times N_2 + N_X \times \frac{N_X+1}{2} - T_X = 2$$

To assess the result, comparison of the obtained U value must be compared to a table of critical values. Tables are of the form:

Table B-2 - Demonstration of critical U value table layout

N_1 / N_2	x	$x+1$	$x+2$	$x+n$
x	$U_{x,x}$	$U_{x+1,x}$	$U_{x+2,x}$	$U_{x+n,x}$
$x+1$	$U_{x,x+1}$	$U_{x+1,x+1}$	$U_{x+2,x+1}$	$U_{x+n,x+1}$
$x+2$	$U_{x,x+2}$	$U_{x+1,x+2}$	$U_{x+2,x+2}$	$U_{x+n,x+2}$
$x+n$	$U_{x,x+n}$	$U_{x+1,x+n}$	$U_{x+2,x+n}$	$U_{x+n,x+n}$

Table B-3 - U values for $p = 0.05$

N_1 / N_2	*5*	*6*	*7*	*8*
5	2	3	5	6
6	3	5	6	8
7	5	6	8	10
8	6	8	10	13

There are different tables relating to various levels of significance ($p = 0.05$, $p = 0.01$, $p = 0.001$). If the obtained U value is equal to or less than the critical table value, the degree of significance that the table values represent apply to the data set comparison being performed. For the example data sets, the tabulated U value is 5 compared to the calculated value of 2. The procedure is a two-tailed non-directional confirmation that

the difference is unlikely to be due to chance with 95% confidence (i.e. the null hypothesis can be rejected).

Appendix C: Sample calculations

C1: Flux

Flux was calculated using equation 3-1 as follows:

$$J_t = \frac{m_{t+\Delta t} - m_t}{\rho A \Delta t} = \frac{(0.060) - (0.020)}{(988.01)(3.36 \times 10^{-2})(20)} = 6.02 \times 10^{-5}\ ms^{-1}$$

$$= 216.9\ Lm^{-2}hr^{-1}$$

Terminal flux (or flux at any given time) was produced from repeated experiments. Average and standard deviation were used as measure and error accordingly

C2: Resistance and flux correction

Resistance was calculated using equation 3-2 as follows:

$$R = \frac{\Delta P}{\mu J} = \frac{(200000)}{(9.52 \times 10^{-4})(6.02 \times 10^{-5})} = 3.49\ \times 10^{12}\ m^{-1}$$

C3: Relative flux

Relative flux was used for comparison of any membrane flux recorded at any point during fouling, cleaning or following pre-treatment by dividing by the original virgin PWF as follows:

$$J_{rel} = \frac{J}{J_{PWF,virgin}} = \frac{273.4}{216.9} = 1.26$$

This calculation enabled relative flux for single experiment flux comparisons as well as comparison between equivalent points during different experiments.

C4: Reynolds number

Reynolds number was calculated to gauge the flow regime. First the hydraulic diameter was calculated based on dimensions shown in Figure C-1 as follows:

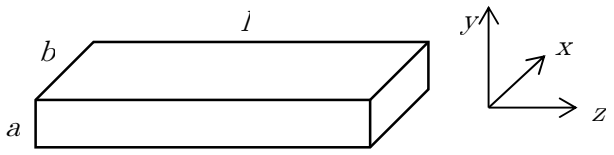

Figure C-1 - Dimensional definitions for M-10 module channels

$$d_h = \frac{2ab}{a+b} = \frac{2 \times (0.0007) \times (0.017)}{(0.0007) \times (0.0017)} = 0.0013\ m$$

Where d_h if the effective channel hydraulic diameter, a is channel height and b channel width

The velocity in the channel is calculated from the volumetric flow:

$$u = \frac{Q}{abN} = \frac{(2 \times 10^{-5})}{(0.0007) \times (0.017) \times (4)} = 0.42\ ms^{-1}$$

Where u is velocity in the channels, Q is volumetric flow rate and N is the number of channels.

Finally the Reynolds number is calculated as shown below:

$$Re = \frac{\rho u d_h}{\mu} = \frac{(988.01) \times (0.42) \times (0.0013)}{9.52 \times 10^{-4}} = 567$$

Where Re is Reynolds number, ρ is fluid density and μ is fluid viscosity.

C5: Maximum velocity in channels and shear stress

Typically the flow in channels had calculated Reynolds numbers in a laminar flow regime (< 2300). They have thus been assumed to observe parabolic velocity profiles across the channel width. In this instance, the maximum velocity in the channel can be calculated from the flow rate/CFV assuming the CFV is equal to the effective channel velocity i.e. $CFV = u_{effective}$ meaning that:

$$Q = Au_{effective} = abu_{effective}$$

Furthermore, the velocity component in the z direction at any position in the channel is expressed as:

$$u_z(y) = u_{max}\left[1 - \left(\frac{y}{a}\right)^2\right]$$

Where u_{max} is the maximum velocity. This is integrated across the channel height, a, (assuming a uniform profile over the channel width, b) to give the volumetric flow rate as follows:

$$Q = u_{max} b \int_0^a 1 - \left(\frac{y}{a}\right)^2 dy = \frac{2}{3} abu_{max}$$

Therefore:

$abV_{effective} = \frac{2}{3} abu_{max}$ meaning $u_{effective} = \frac{2}{3} u_{max}$

For various CFV values, the parabolic velocity profiles can now be drawn as shown in Figure C-2.

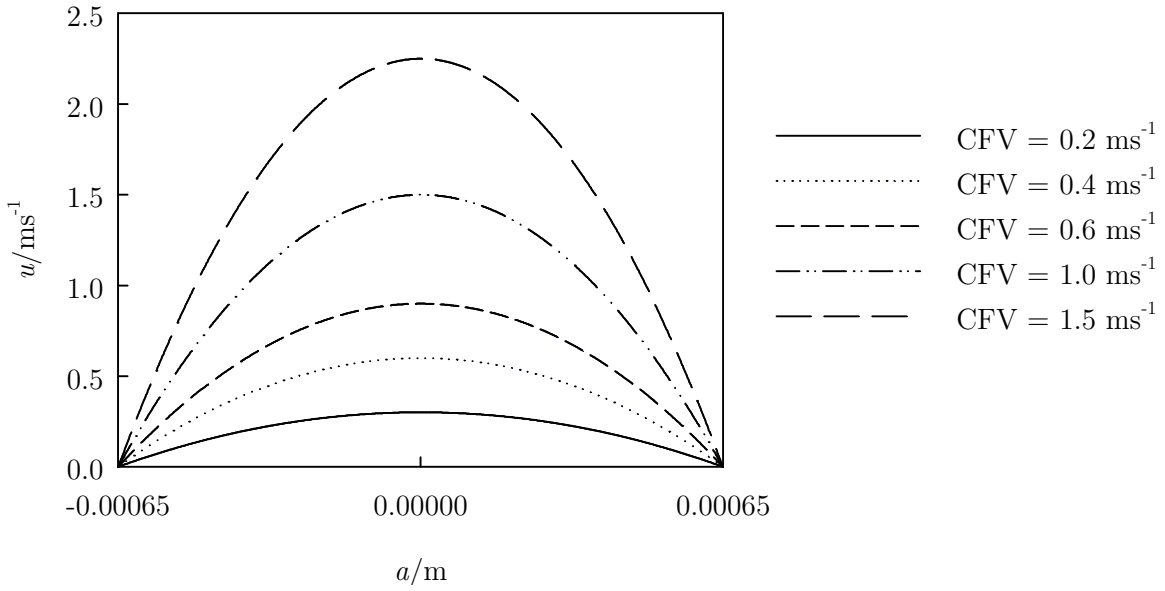

Figure C-2 - Velocity profiles for various CFVs

Further to this, the shear stress acting on the membrane surface can also be calculated using the centre of the channel as the reference plane such that $y = a/2$ (channel half height), as follows:

$$u_z(y) = u_{max}\ \left[1 - \left(\frac{2y}{a}\right)^2\right]$$

$$\frac{du_z}{dy} = u_{max}\left(\frac{-4y}{a^2}\right)2 = \frac{-8u_{max}y}{a^2}$$

$$for\ y = \frac{a}{2}, \qquad \frac{du_z}{dy} = \frac{-4u_{max}y}{a}$$

Finally, an expression for the shear stress at the wall can now be given as:

$$\tau = \mu\frac{du_z}{dy} = \frac{-4u_{max}y}{a}$$

Since fluid viscosity and CFV were varied during experimentation, shear stresses for the most common viscosities are displayed in Figure C-3 below.

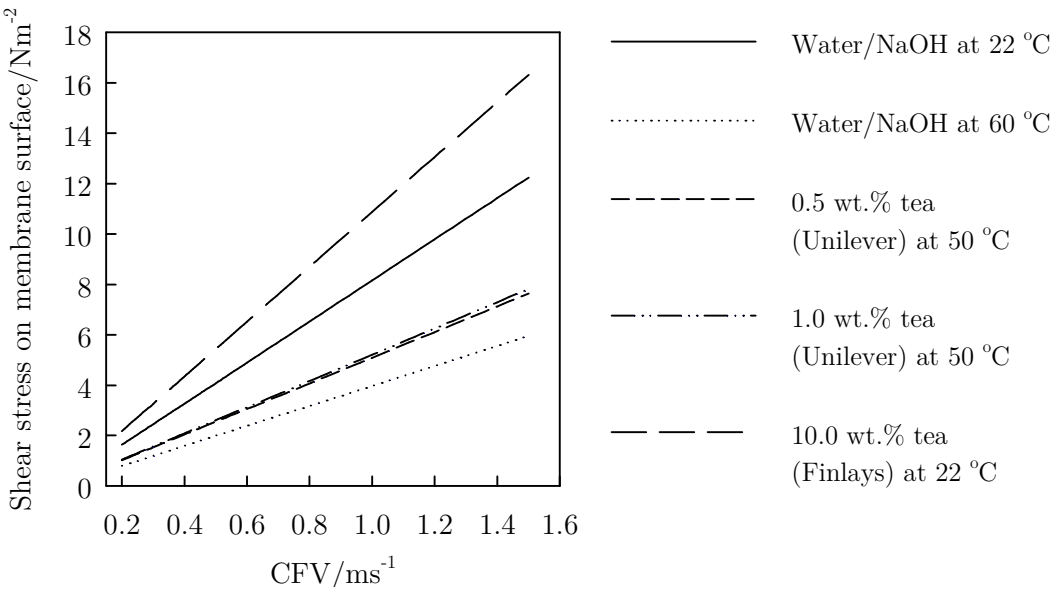

Figure C-3 – Calculated shear stress for various fluid, concentration and temperature combinations at various CFVs

C6: Relative Hansen solubility parameter

Relative solubility of polymers and solvents was calculated by way of the equation displayed in section 2.2.3. The example here is for gauging the solubility of PVP in pure ethanol where subscript p denotes polymer (PVP) and *sol* denotes solvent (ethanol).

$$r_a{}^2 = 4\left(\delta_{d_p} - \delta_{d_{sol}}\right)^2 + \left(\delta_{p_p} - \delta_{p_{sol}}\right)^2 + \left(\delta_{h_p} - \delta_{h_{sol}}\right)^2$$

$$= 4(17.5 - 15.8)^2 + (8 - 8.8)^2 + (15 - 19.4)^2$$

$$= 5.6\ MPa^{0.5}$$

C7: ζ potential

Streaming current measurements were made through the pores. A given streaming current was produced at certain TMPs through the pores. The correlation between these was linear (see Figure C-4) so as to allow the finite differential in the Helmholtz-Smoluchowski equation to be ascertained. From this, and with input of the electrolyte conductivity, viscosity, dielectric constant of water, and permittivity of a vacuum, a value for the apparent ζ potential through the membrane pores could be made.

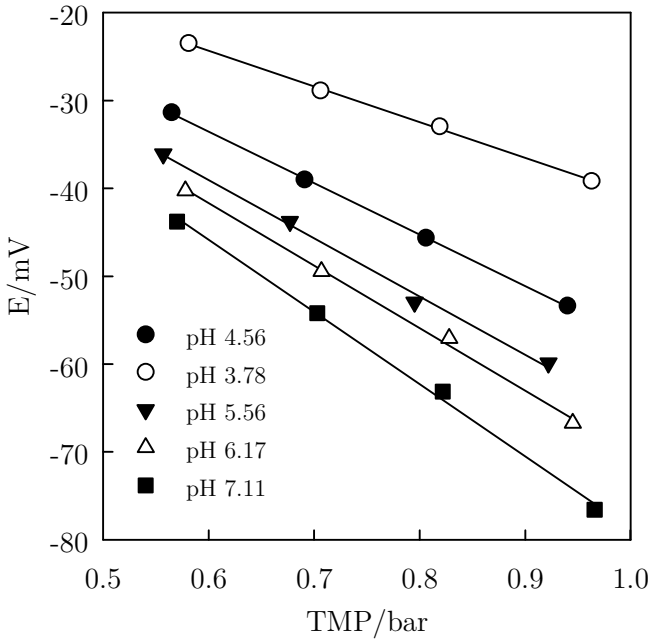

Figure C-4 - Raw streaming current data plotted versus TMP (data for untreated PS50 membrane)

Table C-1 - Calculated apparent ζ potentials from streaming current/pressure gradient data

pH/-	*Slope/mVbar^{-1}*	*ζ potential/mV*
4.56	*-58.37*	*-11.69*
3.78	*-40.65*	*-10.02*
5.56	*-66.36*	*-12.58*
6.17	*-71.22*	*-13.43*
7.11	*-82.27*	*-15.63*

$$\zeta = \frac{\Delta E}{\Delta P}\frac{\mu k}{\varepsilon_0 \varepsilon_r} = (-58.37) \times \frac{(0.8904) \times (155.539)}{(78.4) \times (8.854)} = -11.69\ mV$$

Where $\Delta E/\Delta P$ is the slope, μ is solution viscosity, k is conductivity, ε_0 is the permittivity of a vacuum, and ε_r is the dielectric constant of water.

C8: Elasticity

Elasticity was measured from AFM probe data using the Hertz model (see equation below). By subtraction of the force calculated from deformation of the cantilever (δ) from the total distance moved by the motor in the downwards direction (z), the degree of indentation (δ) can be calculated (see Figure C-5). With knowledge of the total force applied, the Hertz model can be rearranged for elastic modulus (E) considering a parabolic tip i.e. a sphere (or curvature) of known radius (r_c) and assuming the deformation is isotropic and linearly elastic (Poisson ratio, $\nu = 0.5$).

$$F = \frac{4\sqrt{r_c}}{3}\frac{E}{(1-\nu)^2}\delta^{3/2} \rightarrow E = \frac{3}{4\sqrt{r_c}}\frac{F(1-\nu)^2}{\delta^{3/2}}$$

$$= \frac{3}{4\sqrt{8.49\times10^{-6}}}\frac{(1.5\times10^{-6})(1-(0.5))^2}{(4.1\times10^{-9})^{3/2}}$$

$$= 0.52\ GPa$$

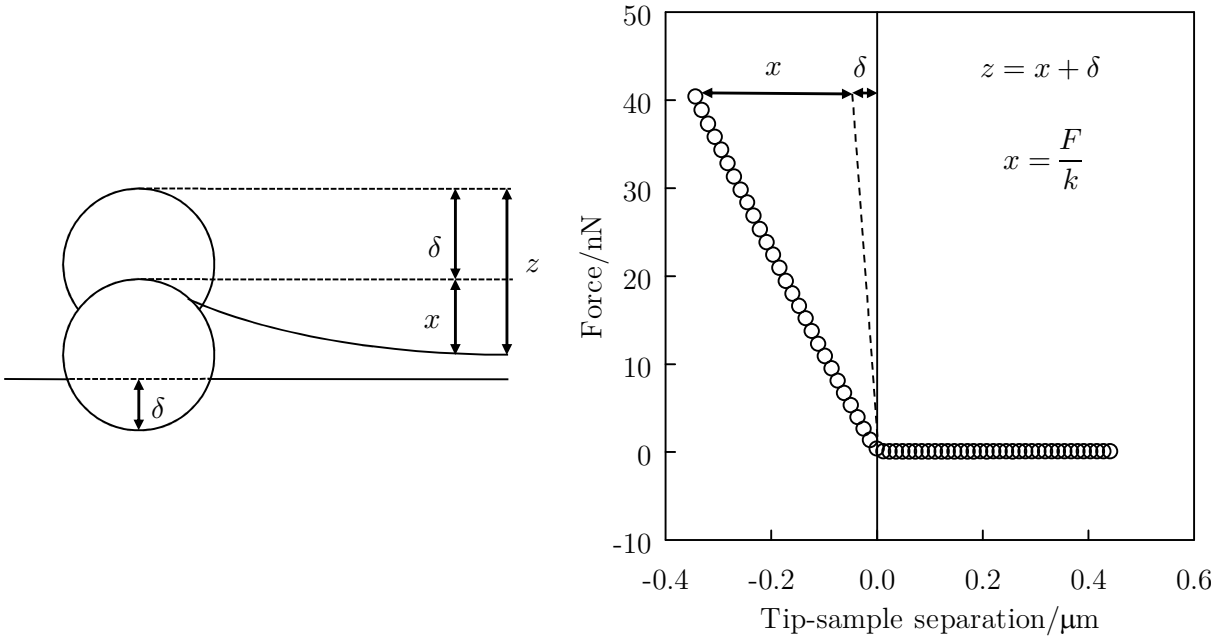

Figure C-5 - (left) definition of distances for elasticity calculation, (right) sample data and graphical representation of distances

C9: Pore size and porosity

Pressures were selected for the porosimeter measurements which related to pore diameters using the Washburn equation (see below). Mercury was the non-wetting liquid used for intrusion into the membranes (contact angle $\theta = 130°$).

$$P = -\frac{4\gamma cos\theta}{d_p} \rightarrow d_p = -\frac{4\gamma cos\theta}{\mathrm{P}} = (1.45\times10^{-4}) \times \frac{4\times(0.485)\times\cos(130)}{22056} = 8.2\ nm$$

Porosity was calculated by the accumulation of volumes of reach pressure/pore size increment (void space) and expressed as a fraction of the total sample volume:

$$\phi = \frac{V_V}{V_T} = \frac{\sum_{i=1}^{n} V_n}{V_T}$$

Where V_n is each volume increment for the given pressures.

C10: Dry weight and solids rejection coefficient

Table D-2 - Dry weight example data

Sample i.d.	*Tube #*	*Tube/g*	*Tube + wet mass/g*	*Tube + dry mass/g*	*Conc./wt%*	*Average conc. and S.D./wt.%*
Feed	**1**	5.2719	13.2079	5.3074	0.445	0.442 ± 0.007
Feed	**2**	5.3255	13.5711	5.3625	0.446	
Feed	**3**	5.3275	13.7196	5.3641	0.434	
Perm	**1**	5.2962	13.5303	5.3747	0.944	0.949 ± 0.005
Perm	**2**	5.2937	13.7187	5.3749	0.954	
Perm	**3**	5.3215	13.846	5.4032	0.949	

After dry weight data was obtained, rejection coefficient for total solids could be calculated as follows:

$$R_{app,TS} = 1 - \frac{c_{sample\ perm}}{c_{sample\ feed}} = 1 - \frac{0.442}{0.949} = 0.534$$

Error was estimated by calculation of the root mean square of the fractional errors and multiplied by the derived rejection coefficient.

Appendix D: Models

D1: Specific cake resistance

Below is a simple MATLAB code sample used to generate data and a plot of inverse volume differential as a function of total volume filtered. The plots were used for determination of specific cake resistance in section 5.8.3.

```
% BSA dead end
t = [20 40 60 80........]; % data string
Vf=[7.68 13.38 18.04 22.20  ......]; % data string
dtdVf=diff(t)./diff(Vf);
Vfm=Vf(1:end-1)+diff(Vf)/2;
plot(Vfm,dtdVf,'ok')
xlabel('V_f ( mL )'); ylabel ('\Delta / \DeltaV_f (s/mL)')
```

D2: Pore blocking model algorithm

The following MATLAB function file was written to determine the best fit of the various pore blocking mechanisms of cross flow filtrations as explained in 4.5.2.1

```
function Yest = BlockingLaws(Yest);
format shortE

prompt = 'Enter value for blocking law mechanism\n(n = 0, 1, 3/2, 2
for cake, intermediate, standard or complete - ';
result = input(prompt);

b = result;
t = [0:20:18000];

filename2 = uigetfile('*.txt');
Ymeas = importdata(filename2);

Jlim = mean(Ymeas(851:1:901));

%Ymeas(1) in data string should be scaled initial relative flux of
the membrane at filtration (rel. to filtration temperature)%
[Y0]=deal(Ymeas(1));

plot(t(1:5:end),Ymeas(1:5:end),'--
rs','LineWidth',2,'MarkerEdgeColor','k','MarkerFaceColor','g','Marke
rSize',5);
hold on;

%optimisation using fminunc function%
h = plot(t,Ymeas,'b','linewidth',2);
minERR = Inf;
opts = optimset('fminunc');
opts.LargeScale = 'off';
```

```
Xest = fminunc(@(X)objfun(X),[0],opts);
Xest = num2cell(Xest);

if result == 0
    fprintf('Cake filtration mechanism selected (n = 0)\n')
end
if result == 1
    fprintf('Intermediate pore blocking mechanism selected (n =
1)\n')
end
if result == 3/2
    fprintf('Standard pore blocking mechanism selected (n = 3/2)\n')
end
if result == 2
    fprintf('Complete pore blocking mechanism selected (n = 2)\n')
end

[K] = deal(Xest{:});
          function ERR = objfun(X)
              X = num2cell(X);
              [K] = deal(X{:});
                                [t,Yest] = ode45(@(t,Y)[(-K*(1/(Y(1)^(b-
2)))*(Y(1)-Jlim))],[0:20:18000],Y0);
              ERR = sum((Ymeas(:)- Yest(:)).^2);
              if ERR < minERR
                  minERR = ERR;
                  for n = 1; set(h(n),'Ydata',Yest(:,n));
                  end
                  drawnow;
              end;

          end


Jlim;
SSresid = minERR;
SStotal = (length(Yest)-1)*var(Yest);
Rsq = 1-(SSresid/SStotal);

D=[b,Jlim,K,SSresid,Rsq];
fprintf('\n')
disp('            b    Jlim         K            SSresid      Rsq')
disp(' ');
disp(D)

end
```

D3: Cassie-Baxter model for analysis of wetting

The Cassie-Baxter model was used to show that changes seen to the measured contact angle could be an effect of changing surface morphology (a physical effect). Using the PS50 membrane as an example, the Cassie-Baxter contact angle i.e. the apparent contact angle for an untreated surface, is used to calculate the true contact angle of the material based on the degree of contact between liquid and homogeneous i.e. porous surface. This was achieved by estimating the surface porosity of the membrane from flux data via the Hagen-Poiseuille model, with the assumptions that the tortuosity is approximately 0.5 ($\tau = 0.5$), the membrane thickness is 140 μm, and the uniform average pore size is 50 nm. Surface porosity was thus calculated as follows:

$$\varepsilon = \frac{32\Delta x \tau \mu}{d_p^2}\frac{J}{\Delta P} = \frac{32(150 \times 10^{-6})(0.5)(0.009)}{(50 \times 10^{-9})} \times (3.1 \times 10^{-10}) = 0.246$$

Using this value, the apparent contact angle, or Cassie-Baxter contact angle in this instance (θ_{CB}) can be used to calculate the true contact angle (θ_t) using the equation below:

$$cos(\theta_{CB}) = (1 - \varepsilon)(cos(\theta_t) + 1) - 1$$

For an untreated membrane surface which displays $\theta_{CB} = 62°$, the true contact θ_t is found to be 20°. To appreciate how the effects of surface porosity, which given the drastic flux increases would imply porosity increased, a range of theoretical porosity values were inputted into the above equation. The model shows that a modification in porosity between 0.25 and 0.31 would be sufficient to up-modify the apparent contact angle of the membrane. Although most values are based on assumptions, the model gave a strong insight into showing that relatively minor changes in surface porosity can influence the apparent contact angles to the amount which is shown by experimental data.

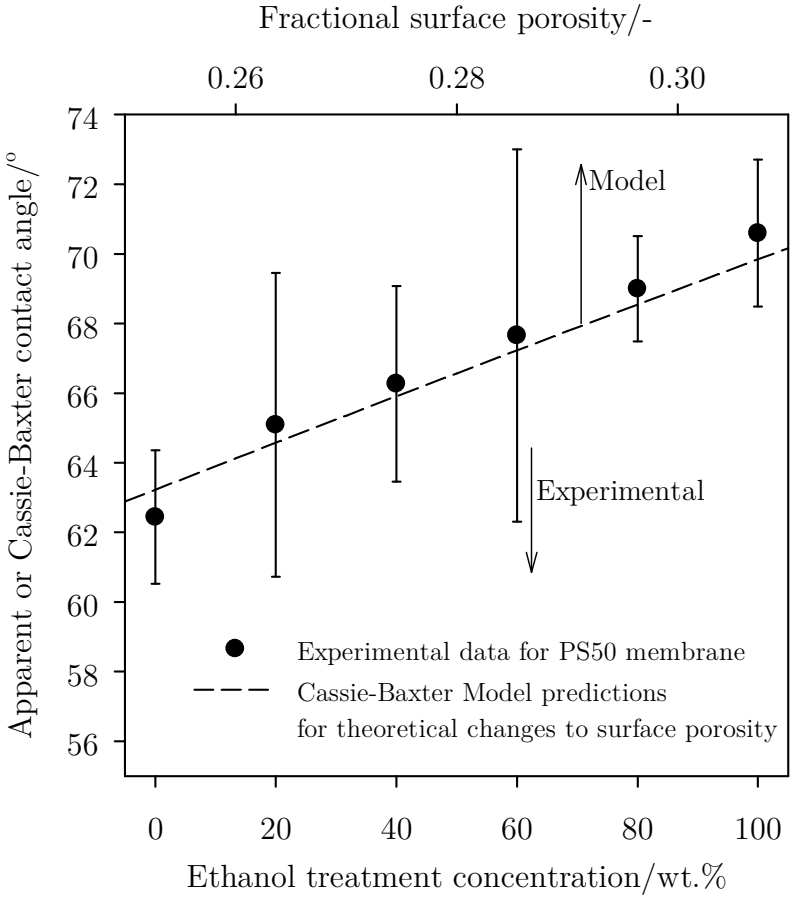

Figure D-3 – Cassie-Baxter model prediction of apparent contact angle on surface as a function of surface porosity compare to experimental data for treatment at varied alcohol concentration